# ΑΡΙΣΤΟΤΕΛΕΙΟ ΠΑΝΕΠΙΣΤΗΜΙΟ ΘΕΣΣΑΛΟΝΙΚΗΣ

## ΔΙΑΤΜΗΜΑΤΙΚΟ
## ΠΡΟΓΡΑΜΜΑ ΜΕΤΑΠΤΥΧΙΑΚΩΝ ΣΠΟΥΔΩΝ

**‘Οικολογική ποιότητα και διαχείριση υδάτων σε επίπεδο λεκάνης απορροής’**

**ΤΜΗΜΑΤΩΝ**
**ΒΙΟΛΟΓΙΑΣ, ΓΕΩΛΟΓΙΑΣ και ΠΟΛΙΤΙΚΩΝ ΜΗΧΑΝΙΚΩΝ**

**ΠΕΡΙΒΟΛΙΩΤΗ ΤΡΙΑΝΤΑΦΥΛΛΙΑ-ΜΑΡΙΑ**
**ΒΙΟΛΟΓΟΣ**

«Παρακολούθηση παραμέτρων οικολογικής ποιότητας της Λίμνης Κορώνειας μέσω εκτεταμένης χρονοσειράς πολυφασματικών δορυφορικών εικόνων και ανάπτυξης εξειδικευμένου λογισμικού»

**ΜΕΤΑΠΤΥΧΙΑΚΗ ΔΙΑΤΡΙΒΗ ΕΙΔΙΚΕΥΣΗΣ**

**ΘΕΣΣΑΛΟΝΙΚΗ 2016**

# ARISTOTLE UNIVERSITY OF THESSALONIKI

## INTERDISCIPLINARY
## POSTGRADUATE MASTER PROGRAM

**'Ecological water quality and management at a river basin level'**

**BY THE SCHOOLS OF**
**BIOLOGY, GEOLOGY and CIVIL ENGINEERING**

**PERIVOLIOTI TRIANTAFYLLIA-MARIA**
**BSc in BIOLOGY**

«Monitoring water quality parameters of Lake Koronia by means of long time-series multispectral satellite images and by the development of specialized software»

**MASTER DISSERTATION THESIS**

**THESSALONIKI 2016**

**<u>Τριμελής Εξεταστική Επιτροπή/Examining Committee</u>:**

**1) Antonios Mouratidis,** Lecturer, Aristotle University of Thessaloniki, Department of Physical & Environmental Geography, ***Supervisor,***

**2) Dimitra Bobori,** Assistant Professor, Aristotle University of Thessaloniki, Department of Zoology,

**3) Georgia Doxani,** Research Fellow, European Space Agency

**Acknowledgements**

The very first person I would like to thank, with the deepest appreciation and the most honor that I feel, being one of his students, is my supervisor Antonios Mouratidis, Lecturer, Aristotle University of Thessaloniki, School of Geology, Department of Physical & Environmental Geography. His scientific support, encouragement and guidance were very important for the composition of the present Master Thesis.

The second person who had a great impact on the scientific and technical support of the present study, is Dimitra Bobori, Assistant Professor, Aristotle University of Thessaloniki, School of Biology, Department of Zoology. I thank her for all the valuable time and the vast knowledge that I have gained.

My special thanks, also, go to Georgia Doxani, Research Fellow, European Space Agency. I greatly appreciate her help, time and support in applying satellite image atmospheric corrections. I will always remember her guidance and encouragement every time we met to discuss further steps in image pre-processing.

I acknowledge, also, Maria Lazaridou, Department of Zoology Emiritus Professor, for her unconditional continuous support.

My great appreciation and true thanks is for Management Authority of Lakes Koronia-Volvi that supported me financially for the realization of the *in situ* measurements. I also thank the European Space Agency for the provision of the satellite data , after the submission of a proposal (ID: 31068).

My deepest thanks and appreciation are for Dimitrios Terzopoulos; his support from the first step through to the last step of my research was remarkable. I will always remember his guidance, encouragement and continuous follow up.

I am grateful for all the academic staff members of the Interdisciplinary Postgraduate Study Program (IPSP) 'Ecological water quality and management at a river basin level' for offering me their scientific and technical experiences.

Also, I would like to thank Olga Petriki and Athina Patsia for their valuable help during the field work in the lake. I am and will always be grateful for the sincere support and kind spirit of my classmates and my dear and true friends.

Last, but very far from least, I would like to thank my family for their help and forbearance.

# Contents

**Περίληψη**

Τα υδάτινα σώματα γλυκού νερού υπόκεινται σε ανθρώπινες παρεμβάσεις και δραστηριότητες παγκοσμίως. Ως εκ τούτου, η ποιότητα και η σύστασή τους βρίσκεται υπό διαρκή μεταβολή. Τα λιμναία οικοσυστήματα βρίσκονται υπό πίεση, καθώς αποτελούν αποδέκτες μεγάλων ποσοτήτων αποβλήτων της βιομηχανικής και γεωργικής δραστηριότητας. Μάλιστα, η ποιότητα του νερού ορισμένων λιμνών ανά τον κόσμο επηρεάζεται σε τέτοιον βαθμό, ώστε καθίσταται αδύνατον να αποκατασταθεί. Στην Ευρώπη, με στόχο την άμβλυνση των επιπτώσεων υποβάθμισης των επιφανειακών και υπογείων υδάτων, έχει εκδοθεί η Οδηγία-Πλαίσιο 2000/60/ΕΚ. Ο στόχος της είναι η προστασία των επιφανειακών υδάτων και η εξασφάλιση, ότι δεν θα ακολουθήσει περαιτέρω υποβάθμιση της ποιότητας των υδάτων, καθώς και της δομής και της λειτουργίας των υδάτινων οικοσυστημάτων.

Με στόχο τον καθορισμό της οικολογικής κατάστασης, τα βιολογικά, φύσικο-χημικά και υδρομορφολογικά Ποιοτικά Στοιχεία (Quality Elements – QE) πρέπει να παρακολουθούνται και να αξιολογούνται. Σε πολλές περιπτώσεις δεν υπάρχουν, ή είναι εξαιρετικά περιορισμένα, δεδομένα σχετικά με την ποιότητα των λιμναίων υδάτων. Οι διαθέσιμες βάσεις δεδομένων *in situ* μετρήσεων συχνά αναφέρονται σε σποραδικά συλλεχθέντα δεδομένα ή σε μετρίως τεκμηριωμένη και χωρίς συνοχή πληροφορία. Παρά ταύτα, ένα σημαντικό τμήμα της πληροφορίας αυτής έχει καταγραφεί στα ιστορικά αρχεία δορυφορικών δεδομένων, χωρίς, όμως, να έχει ανακτηθεί.

Οι τεχνικές της Τηλεπισκόπησης μπορούν να χρησιμοποιηθούν για τη χαρτογράφηση και παρακολούθηση των Ποιοτικών Στοιχείων λιμνών με στόχο την αναπαραγωγή της ιστορικής εξέλιξης των παραμέτρων ποιότητας των υδάτων, την ελάττωση κόστους και χρόνου, και την αντιμετώπιση προβλημάτων προσβασιμότητας στο πεδίο. Καθώς ορισμένα από τα Ποιοτικά Στοιχεία μπορούν να προσδιοριστούν με τεχνικές Τηλεπισκόπησης, οι τεχνολογίες Παρατήρησης της Γης είναι δυνατό να ενσωματωθούν στα προγράμματα παρακολούθησης, τα οποία ορίζει η Οδηγία, δεδομένου, ότι μπορεί να δειχθεί, ότι προσφέρουν τη δυνατότητα ανεξάρτητης αξιολόγησης Ποιοτικών Στοιχείων.

Η λίμνη Κορώνεια ανήκει στη λεκάνη απορροής της Μυγδονίας (Κεντρική Μακεδονία, Βόρεια Ελλάδα). Είναι ένας από τους πιο σημαντικούς υγροτόπους της συνθήκης Ramsar στην Ελλάδα και προστατεύεται ως περιοχή Natura 2000. Όμως, αντιμετωπίζει σημαντικά περιβαλλοντικά θέματα και προβλήματα διαχείρισης, όπως η μείωση της ποσότητας των υδάτων της, υποβάθμιση της ποιότητας, αύξηση αλατότητας και σχεδόν ολοκληρωτικό αφανισμό του οικοσυστήματος. Κατά το παρελθόν και τη διάρκεια ορισμένων περιόδων του έτους ξηραίνονταν σχεδόν ολοκληρωτικά. Ο όγκος νερού της λίμνης πλέον εξαρτάται κυρίως από τα κατακρημνίσματα. Ο όγκος, αλλά και η χωρική και χρονική ανάλυση των επιτόπου δεδομένων, τα οποία έχουν συλλεχθεί τις τελευταίες δεκαετίες είναι πολύ περιορισμένος.

Ο στόχος της παρούσας μελέτης ήταν η δημιουργία ενός πυκνού ιστορικού προφίλ της ποιότητας των υδάτων της λίμνης Κορώνειας ακολουθώντας μία προσέγγιση από

την οπτική γωνία της Τηλεπισκόπησης. Για τον σκοπό αυτόν πραγματοποιήθηκε μία προσπάθεια παρακολούθησης των Ποιοτικών Στοιχείων χρησιμοποιώντας αλγόριθμους, οι οποίοι έχουν αναπτυχθεί σε προηγούμενες μελέτες Συγκεκριμένα αφορούσαν τον προσδιορισμό της Θερμοκρασίας, του pH, της Διαφάνειας/του Βάθους Δίσκου Secchi (SDD), της Χλωροφύλλης *α* και της Αγωγιμότητας, με βάση πολυφασματικές δορυφορικές εικόνες από μία περίοδο 33 ετών, από το 1984 έως το 2016. Επιπλέον χαρτογραφήθηκε το Βάθος, καθώς και η κάλυψη της λίμνης από επιπλέουσα βλάστηση (Μακρόφυτα) και ανθίσεις Κυανοβακτηρίων. Τα δεδομένα, τα οποία χρησιμοποιήθηκαν, ήταν δορυφορικές εικόνες από τις δορυφορικές αποστολές Landsat-5/TM (Thematic Mapper), Landsat-7/ETM (Enhanced Thematic Mapper), Landsat-8/OLI (Operational Land Imager) και Landsat-8/TIRS (Thermal Infrared Sensor).

Εκτός από τη χαρτογράφηση της χρονικής και χωρικής εξέλιξης των παραμέτρων της ποιότητας των υδάτων της λίμνης Κορώνειας για τις περασμένες 3 δεκαετίες, τα αποτελέσματα αναμένεται να συμβάλουν και: (α) στον καθορισμό βέλτιστων διαδικασιών επεξεργασίας δορυφορικών εικόνων για την εκτίμηση Ποιοτικών Στοιχείων και διαδικασιών εξωτερικής βαθμονόμησης με βάση πολυφασματικές δορυφορικές εικόνες και *in situ* μετρήσεις, (β) στην αξιολόγηση της συσχέτισης μεταξύ Ποιοτικών Στοιχείων και φασματικών ζωνών των αποστολών Landsat, (γ) την ανάπτυξη διαδικασιών, οι οποίες θα συνδέσουν τα παρελθόντα δορυφορικά δεδομένα με πληροφορία σχετικά με την ποιότητα υδάτων από μελλοντικά δεδομένα της δορυφορικής αποστολής Sentinel-2, (δ) την ανάπτυξη εξειδικευμένου λογισμικού, το οποίο θα επιτρέπει την εξαγωγή τιμών Ποιοτικών Στοιχείων χρησιμοποιώντας δεδομένα των αποστολών Landsat και (ε) στην παρακολούθηση της εξέλιξης του συστήματος της λίμνης Κορώνειας.

Με βάση τα αποτελέσματα της ανάκτησης παραμέτρων ποιότητας της λίμνης Κορώνειας, διαπιστώθηκε ότι όλες οι παράμετροι είναι προσδιορίσιμες με τη χρήση της συγκεκριμένης μεθοδολογίας. Υπάρχει ντετερμινιστική σχέση μεταξύ ορισμένων παραμέτρων (Θερμοκρασία, Βάθος Νερού, Κάλυψη λίμνης, Χλωροφύλλη *α*) και των οπτικών ιδιοτήτων του νερού. Αντιθέτως, ο προσδιορισμός κάποιων παραμέτρων (Βάθος Δίσκου Secchi, Αγωγιμότητα, pH) δεν στηρίζεται σε σαφή συσχέτιση, αλλά σε στατιστικές ερμηνείες, καθιστώντας τα αντίστοιχα μοντέλα αξιόπιστα για περιορισμένο χρονικό διάστημα. Γενικότερα, τα μοντέλα που χρησιμοποιήθηκαν συνέβαλλαν στο επιτυχή προσδιορισμό των τιμών ή/και της τάσης των παραμέτρων ποιότητας, ανεξαρτήτως ύπαρξης ντετερμινιστικής σχέσης.

Η λίμνη Κορώνεια χαρακτηρίζεται από συνεχόμενα μεταβαλλόμενες υδρολογικές συνθήκες, με συχνή ξήρανση και επαναπλήρωση της. Αυτό είχε ως αποτέλεσμα, τον μη δυνατό υπολογισμό των ποιοτικών παραμέτρων όταν οι σταθμοί δειγματοληψίας ήταν εκτός «μάσκας νερού» και τη μείωση της ακρίβειας των μετρήσεων λόγω επιδράσεων του πυθμένα. Για τη βελτίωση των αποτελεσμάτων προτείνεται η ανάπτυξη μοντέλων εξειδικευμένων για τη λίμνη Κορώνεια καθώς και η διεξαγωγή επίγειων μετρήσεων για

τον προσδιορισμό της ανακλαστικότητας, με σκοπό την καλύτερη διόρθωση ατμοσφαιρικών επιδράσεων

Καταλήγοντας, η χρήση δορυφορικών δεδομένων ενδείκνυται, καθώς η πρόσβαση σε αυτά είναι σχετικά εύκολη και πολλές φορές έχουν μηδενικό κόστος. Η εξαγωγή μεγάλου όγκου διαχρονικών δεδομένων για σημαντικές παραμέτρους (Θερμοκρασία, Δίσκος Secchi, Χλωροφύλλη *α*, pH, Αγωγιμότητα, Βάθος, Κάλυψη Λίμνης) είναι σχετικά εύκολη διαδικασία. Η Τηλεπισκόπηση μπορεί να παρέχει δεδομένα για χρονικές περιόδους όπου είναι αδύνατη η λήψη δεδομένων με άλλη μέθοδο.

**Abstract**

Water bodies are usually affected by human intervention and activities worldwide. As a result, their quality and composition get modified. Lake ecosystems are under pressure due to their use as recipients of huge quantities of waste discharges from industry and agriculture. Water quality of a number of lakes around the world is so impacted that it is unrecoverable by natural means of purification. In Europe, in order to alleviate the degradation of surface and ground waters, Water Framework Directive (WFD, 2000/60/EC) has been enforced. The aim of this WFD is the protection of surface waters and the ensuring that there shall be no further deterioration in water quality, structure and function of aquatic ecosystems.

Towards the definition of the ecological status, biological, physico-chemical and hydromorphological Quality Elements (QE) have to be monitored and assessed. In many cases, lake water quality data either do not exist or are very limited. Databases from *in situ* measurements often refer to sporadically collected data or to poorly documented, non-consistent information. Nevertheless, a substantial part of this "missing" information has been recorded in the historical archives of satellite imagery, but has never been retrieved.

Satellite remote sensing can be used to map and monitor lake QE, with the aim to reconstruct the historical evolution of water quality indicators, to reduce cost and time and to deal with problems of accessibility to the field. As some of the lake quality elements can be determined by remote sensing techniques, Earth Observation technologies may be integrated in the monitoring programs defined by the WFD, provided they can be demonstrated to independently assess QE.

Lake Koronia is part of Mygdonia basin (Central Macedonia, N. Greece). It is one of the most important Ramsar wetlands of Greece and it is protected as a Natura 2000 site. However, it faces serious environmental issues and water management problems, such as decreasing water levels, deterioration of water quality, water salinization and almost extinction of the ecosystem. In the past, during some time periods throughout the year, it was almost dry. Its water depends mainly on precipitation. As a result, the amount, but also the spatial and temporal resolution of in situ data that have been collected during the past decades is limited.

The purpose of this study was to create a dense historical water quality profile of lake Koronia, one of the most important Ramsar wetlands of Greece, following a remote sensing approach. In an effort of monitoring the QE, Water quality algorithms developed from previous studies were used. Namely, the determination of Water Temperature, pH, Transparency/Secchi Disk Depth (SDD), Chlorophyll *a* and Conductivity was carried out by using multispectral satellite images of a time period of 33 years, from 1984 to 2016. In addition, Water Depth, as well as the distribution of floating vegetation and cyanobacterial blooms were mapped. In addition, Water Depth, as well as the distribution of the floating vegetation (Macrophytes) and the cyanobacterial blooms was mapped. The data were images of Landsat-5/TM (Thematic Mapper), Landsat-7/ETM+

(Enhanced Thematic Mapper), Landsat-8/OLI (Operational Land Imager) and Landsat-8/TIRS (Thermal Infrared Sensor).

Apart from mapping the temporal and spatial water quality variability of lake Koronia for the past three decades, the results are expected to contribute to: (a) the definition of optimal image processing routines for QE estimation and external calibration procedures based on multispectral satellite images and in situ measurements, (b) the assessment of the correlation between QE and Landsat bands, (c) the establishment of procedures that shall allow the compatibility of past satellite information with water quality information derived from future Sentinel-2 data, (d) the development of special software that will allow the extraction of QE values using Landsat data and (e) the monitoring of the development of Lake Koronia.

Based on the results affiliated with the recovery quality parameters of lake Koronia, all parameters can be assessed using this methodology. There is a deterministic relationship between some parameters (Temperature, Water Depth, Lake Coverage, Chlorophyll *a*) and the optical properties of water. In contrast, the determination of some parameters (Secchi Disk Depth, Conductivity, pH) is not based on a clear relationship, but it may be valid for purely statistical reasons, making the respective models reliable for a limited time. In general, the models that were used in the present study, contributed to the successful determination of the values and/or trend of the quality parameters, regardless of the existence of a deterministic relationship.

Lake Koronia is characterized by continuously variable hydrological conditions, including frequent drying and refill. As a result, the calculation of the quality parameters was not possible when the sampling stations were not included in the water mask and the measurement accuracy was reduced due to the effects of the bottom. In order to improve the measurement accuracy, the development of specific models for Lake Koronia and the prosecution of surface reflectance measurements, for more accurate atmospheric correction is proposed.

In conclusion, the use of satellite data is encouraged, as they are relatively easy to access and have a very low cost. The extraction of large volumes of longitudinal data (Temperature, Secchi Disk Depth, Chlorophyll *a*, pH, Conductivity, Water Depth, Lake Coverage) is a relatively easy process. Earth Observation can be used for the data derivation that would not be possible using different methodology.

# 1. INTRODUCTION

## 1.1 Chapter overview

*This chapter is an introduction to the research work presented in this thesis. It includes the theoretical framework of lake water quality monitoring, according to Water Framework Directive 2000/60/EC, and introduces the contribution of Earth Observation techniques to lake monitoring. In addition, this chapter contains extensive material on satellite programs and sensor characteristics and introduces the reader to the nature and properties of digital image data in remote sensing. Finally, it presents an overview of the significance and the scope of the present research study.*

## 1.2 The importance of water

Water is one of the most important natural resources for mankind and covers about 70% of the Earth's surface. Almost 97% of the global water supply is saline and is located in the oceans; only a very small amount is found in saline lakes (Figure 1). The remaining volume of water (3%) is 'freshwater', as it contains less than 1000 mg/l of dissolved solids, mainly salt (McMichael, 2014 [url2]) .

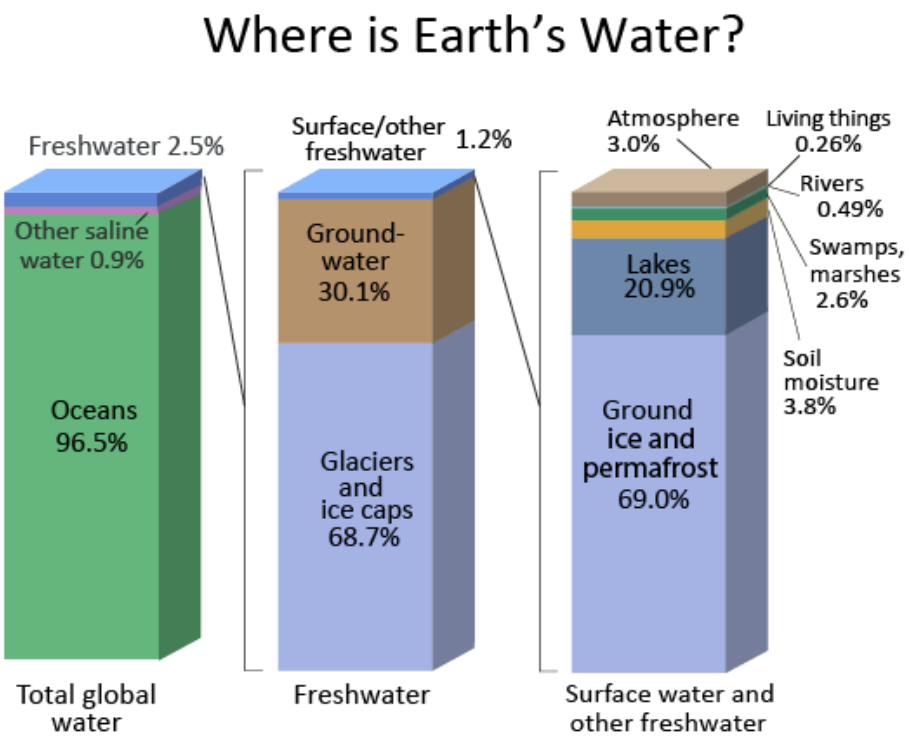


**Figure 1.** Distribution of Earth's water resources. Numbers are rounded percent summations and may not add to 100. (Igor Shiklomanov's chapter 'World fresh water resources' in Peter H. Gleick,1993, Water in crisis: A guide to the World's Fresh Water Resources [url1])

Nowadays, freshwater quality is under pressure, because water bodies serve as recipients of huge quantities of waste discharges from land use and agriculture (Torbick

et al. 2013). Water can be considered polluted, when its quality or composition gets altered as a result of human activities, so as to become less suitable for uses, for which it would have otherwise been suitable, in its natural, unmodified state. Any physical, chemical or biological factor can be characterized as a pollutant, in case it causes aesthetic or functional effects on aquatic life, as well as on those who consume water (Goel 2011). The effects of water pollution can be summarized as follows (Harrison 2001):

- ✓ Degradation of aesthetic properties
- ✓ Increase of water temperature
- ✓ Decrease of dissolved oxygen concentration
- ✓ Toxic pollutants causing damage to aquatic or human life
- ✓ Endocrine disruption or changes in biodiversity (Sublethal toxicity)
- ✓ Disturbance of pH regime
- ✓ Eutrophication

Two types of water pollution can be distinguished: a) point sources and b) non-point sources. Point sources are pipes or channels, characterized by discrete flows of polluted water that enter a water body. Non-point sources, on the other hand, are connected to land use and refer to contributions that occur over a wide area – typically within a drainage basin.

In Greece, drainage basins are generally characterized by streams of intermittent flow, while significantly-sized lakes and rivers are predominantly located in the central and northern part of the country. Surface water resources serve drinking and irrigation purposes, hydroelectric power production, industrial uses, fisheries and recreation activities, while agricultural, municipal and industrial effluents have altered the surface water composition and restricted its use (Skoulikidis et al. 1998).

Even though Earth is not in a shortage of water overall, most countries will face problems due to water scarcity at local/regional level. The reason is that water resources are unevenly distributed, undervalued and mismanaged. In Europe, in order to alleviate the degradation of surface and ground waters, the Water Framework Directive (WFD, 2000/60/EC) has been published. The goal of the WFD is the expansion of water protection to all waters and the ensuring that there shall be no further degradation of freshwater ecosystem resources, functions and biodiversity.

### 1.3 **Legal Framework**

**Water Framework Directive 2000/60/EC**

Europe's Water Framework Directive 2000/60/EC (WFD) includes binding water protection measures within its legislative framework. WFD has brought about major changes in the protection and improvement of the quality of all surface and ground water in the European countries. The Official Journal of the European Communities published WFD in December 2000. All Member States had to incorporate the WFD into national law by the end of 2003.

The aim of WFD is to achieve:

- ✓ Good ecological and chemical status of all European surface (rivers, lakes, coastal, transitional) waters by 2015
- ✓ Good chemical and quantitative status of all European ground waters by 2015

WFD introduces a new and innovative approach to water management, namely:

- ✓ Cross-border co-operation between countries on water management
- ✓ Economic analysis of water use
- ✓ Introduction of River Basin Management on a Europe-wide scale
- ✓ Mitigating the effects of floods and droughts
- ✓ Promotion of sustainable water use, based on long-term protection of water resources, through specific measures for the progressive reduction and the cessation or phasing-out of discharges, emissions and losses of priority substances

The Directives, which were published before the WFD, were characterized mainly by technical criteria including emission limits. According to the WFD, the quality of a water body is assessed using ecological terms, insuring a complete environmental management.

In order to define the ecological quality of a water body, biological, physico-chemical and hydromorphological quality elements (QE) are assessed (Table 1).

**Table 1.** The qualitative elements for the lake ecological quality assessment (European Parliament Council 2000).

| Biological elements | Chemical and Physico-chemical elements supporting the Biological elements | Hydromorphological elements supporting the Biological elements | Specific pollutants |
|---|---|---|---|
| ✓ Abundance and composition of Aquatic flora<br>✓ Composition, abundance and biomass of Phytoplankton<br>✓ Composition and abundance of benthic Invertebrate fauna<br>✓ Composition, abundance and age structure of fish fauna | ✓ Thermal conditions<br>✓ Oxygenation conditions<br>✓ Acidification status<br>✓ Nutrient conditions<br>✓ Transparency<br>✓ Salinity | ✓ Hydrological regime<br>• quantity and dynamics of water flow<br>• residence time<br>• connection to the groundwater body<br>✓ Morphological conditions<br>• lake depth variation<br>• quantity, structure and substrate of the lake bed<br>• structure of the lake shore | ✓ Pollution by all priority substances identified as being discharged into the body of water<br>✓ Pollution by other substances identified as being discharged in significant quantities into the body of water |

Assessing the status of a water body includes several stages (Quevauviller et al. 2008):

- ✓ Use dependable indicators

- ✓ Determine the water body type applying System A or B
- ✓ Set reference conditions
- ✓ Agree on common principles for setting quality class boundaries. Through the Intercalibration Exercise, country members, sharing common types of waterbodies in order to classify the QE, use common numerical class boundaries, in accordance with the objectives of WFD.

The ecological quality is determined by the Ecological Quality Ratio (EQR). EQR is the quotient of the observed conditions to the reference conditions. The results have a range from value 0 to 1. Value 1 represents natural conditions, without anthropogenic pressure (reference conditions). Values close to 0 represent 'bad' conditions. In accordance with Annex V, ecological quality must be expressed to a color coded scale (Table 2).

**Table 2.** Gradients of five levels ecological quality (European Parliament Council 2000).

| Ecological status classification |
|---|
| High |
| Good |
| Moderate |
| Poor |
| Bad |

**Law 3199/2003**

In Greece, the institutional framework was adapted to WFD by replacing Law 1739/87 with Law 3199/2003. The latter has been further specialized with five Ministerial Decisions and a Presidential Decree (51/2007), which was passed to define measures and procedures for integrated protection and water management. According to Law 3199/2003:

- ✓ The fragmentation of responsibilities is amended by having a Central Water Service established in the Special Secretariat
- ✓ Cost recovery of water service is introduced, by considering environmental cost
- ✓ The definitions of Directive 2000/60/EC are incorporated without further references
- ✓ A National Water Commission is established
- ✓ A priority in the use of water resources as water is defined

According to Law 1739/87, Greece is divided into 14 water districts based on hydrological and hydrogeological characteristics (Figure 2). This division corresponds to administrative areas, based on drainage basins. In this context, the water districts of Greece are: 1) West Peloponnese, 2) North Peloponnese, 3) East Peloponnese, 4) West

Central Greece, 5) Epirus, 6) Attica, 7) East Central Greece and Evia, 8) Thessaly, 9) West Macedonia, 10) Central Macedonia 11) East Macedonia, 12) Thrace 13) Crete, 14) Aegean Islands

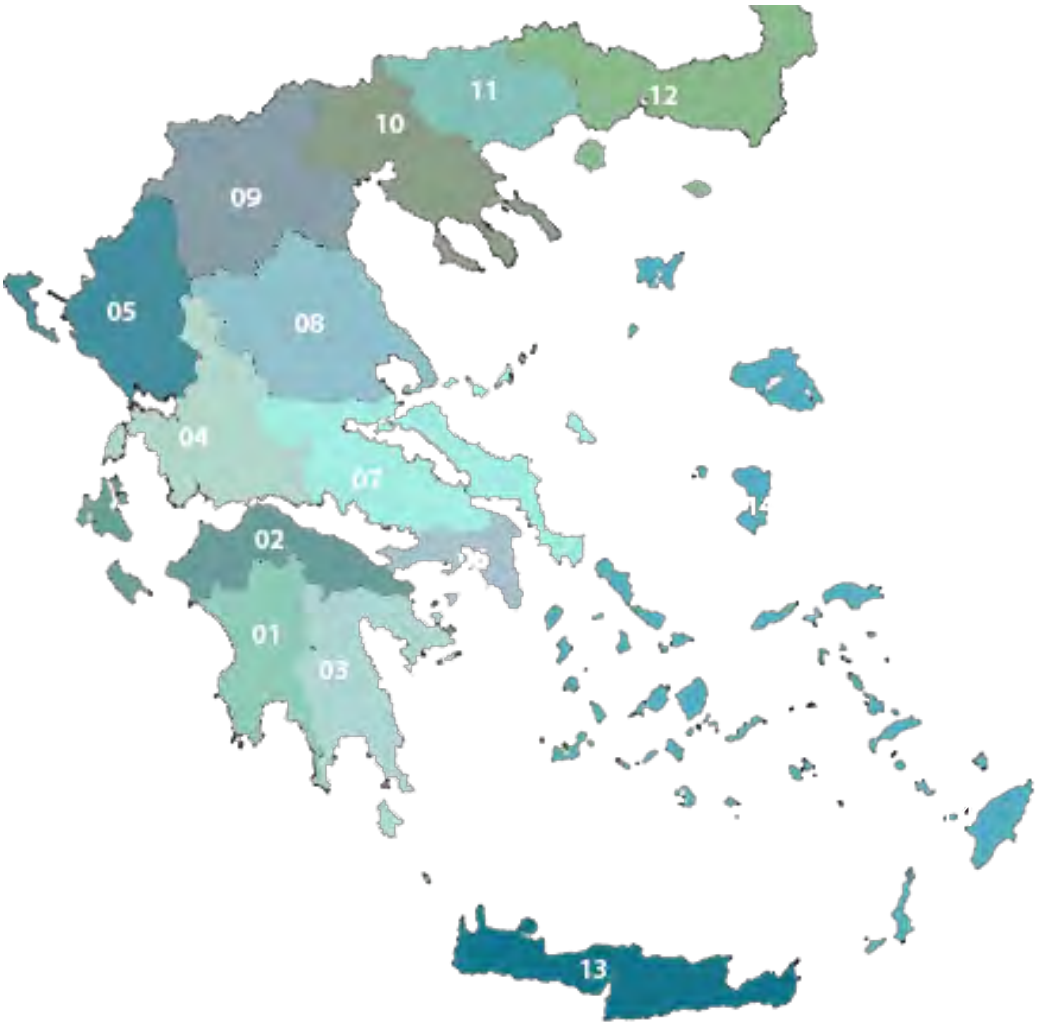


**Figure 2.** Water Districts of Greece [url3].

**Monitoring water quality**

WFD (Article 8) establishes the criteria for the monitoring of surface water, ground water quality and protected areas. Monitoring includes all water bodies; inland waters, transitional and coastal waters (up to one sea mile). Monitoring programs have to be accomplished in order to establish a coherent and comprehensive quality overview of all water bodies within each district. The monitoring programs had to be operational by 22 December 2006.

According to the WFD (Annex V), monitoring surface waters is necessary for:

i. The classification of water body status. Every Member State has to provide a map for each river basin district illustrating the classification of the ecological and chemical quality, using the five-color scale
ii. Supplementing and validating the Annex II risk assessment procedure

iii. The designing of effective future monitoring programs
iv. The assessment of long-term changes (naturally caused or resulting from anthropogenic activity) in natural conditions
v. Estimating pollutants, which are transferred across international boundaries
vi. Assessing changes in the status of those bodies identified as being at risk, in response to the application of measures for improvement or prevention of deterioration
vii. Identifying causes of water bodies failing to achieve good ecological quality, as well as for confirming the reason for failing
viii. Quantifying compliance with the standards of protected areas
ix. Assessing reference conditions (Annex II) for surface water bodies

According to WFD there are 3 types of monitoring:

- ✓ **Surveillance Monitoring**: This type of monitoring aims to assess long-term changes in natural conditions of a water body. Information will be provided for the efficient and effective design of future monitoring programs. Additionally, the results of such monitoring will be used for the assessment of long term changes, resulting from human activity, as well as for the validation of the impact assessment procedure (WFD, Annex II). Surveillance monitoring shall be carried out for each monitoring site for one year during the period covered by a river basin management plan for:
    i. parameters indicative of all biological quality elements
    ii. parameters indicative of all hydromorphological quality elements
    iii. parameters indicative of all general physico-chemical quality elements
    iv. priority list pollutants, which are discharged into the river basin or sub-basin and
    v. other pollutants discharged in significant quantities in the river basin or sub-basin

  In case the previous surveillance monitoring exercise reveals that the water body concerned reached good status and there is no evidence that the impact of human activity has changed (WFD, Annex II), it shall be carried out once every three river basin management plans.
- ✓ **Operational Monitoring**: The objective of operational monitoring is to establish the status of water bodies identified as being at risk of failing to achieve their environmental objectives. Also, it will be used to assess any changes in the status of such bodies, resulting from the programs of measures. This type of monitoring shall be carried out for all those water bodies which, on the basis of either the impact assessment carried out in accordance with WFD, Annex II or surveillance monitoring, are identified as being at risk of failing to meet their environmental objectives (Article 4) and for those into which priority list substances are discharged. In order to assess the impact of the pressures to which the water bodies are subject, Member States shall monitor as relevant:

i. parameters indicative of the biological quality element, or elements, most sensitive to the pressures to which the water bodies are subject,
ii. all priority substances discharged, and other pollutants discharged in significant quantities,
iii. parameters indicative of the hydromorphological quality element most sensitive to the pressure identified

- ✓ **Investigative Monitoring**: It is required when the cause for any exceedances is unknown. Investigative monitoring is performed, in case the objectives detailed in Article 4 for a water body are not likely to be achieved and operational monitoring has not already been used, in order to ascertain the causes. Also, this type of monitoring can be used in order to ascertain the magnitude and impacts of accidental pollution. The information of Investigative Monitoring will be useful for the establishment of a program of measures for the achievement of the environmental objectives and specific measures, which are necessary to solve the problems caused by accidental pollution.

Monitoring frequencies shall be chosen, so as to achieve an acceptable level of confidence and accuracy. The variability in parameters resulting from both natural and anthropogenic conditions should influence the monitoring frequency. Monitoring time shall be selected so as to minimize the impact of seasonal variation on the QE, ensuring that the results reflect changes caused by anthropogenic pressure.

### 1.4 **Monitoring of lake QE**

A lake [Etymology: *lacus* (Latin)] is a body of standing inland surface water (European Parliament Council 2000). Each lake is an irreproducible water body, with unique physical and chemical characteristics, which are related to the climatic, geomorphological and geochemical conditions of the drainage basin and the underlying aquifer.

Community policy referring to dangerous or hazardous substances in surface and ground waters of Europe's Member States was introduced almost thirty years ago by the directive on pollution resulting from discharges of certain dangerous substances (Council Directive 76/464/EEC, codified as 2006/11/EC) (Guidance document no.7, 2003). Several substances have been regulated in 'daughter' directives in the 1980s, by defining emission limits and quality objectives. The Directive 76/464/EEC was integrated into the Water Framework Directive 2000/60/EC and fully repealed in 2013.

Some of the most important elements for lake monitoring are the physico-chemical QE, the phytoplankton biomass and the chlorophyll $\alpha$ (Quevauville et al. 2008). Recently, the WFD has introduced the monitoring of biological QE in the programs of Member States. Figure 3 summarizes the quality elements that are selected by WFD for lake monitoring. In Annex I, the key features of each physico-chemical parameter of lakes are detailed.

Water quality monitoring programs, in many countries, are not designed based on data needs, but rather on available equipment and capacities. Consequently, the current monitoring status is 'monitoring for monitoring's sake' and 'data is rich but information is poor' (Azab 2012). Also, in many cases, access to water quality data is either inexistent or limited. Databases from *in situ* measurements often refer to sporadically collected data or to poorly documented, non-consistent information. *In situ* assessment methods are costly and time consuming, limiting the temporal frequency and spatial coverage of the QE (Torbick et al. 2013), resulting in inadequate coverage, in terms of temporal and spatial scales needed to address aquatic quality and public health concerns. Additionally, there is no widely accepted agreement on the monitoring methodology using field testing, resulting in a wide sampling variability owing to the personnel. Different institutes and researchers are involved in water quality monitoring in order to achieve their own objectives, independent of other related activities.

As some of the lake quality elements can be determined by remote sensing with a reasonable accuracy, remote sensing technologies may be integrated in the monitoring programs defined by the WFD, provided they can be demonstrated to independently assess Water Quality Parameters (Giardino et al. 2007). Remote sensing data may be used to determine the physical properties, assessing the patterns of distribution of water color. The designing of monitoring programs can also be improved by the use of satellite imagery, as it can indicate the best sampling locations.

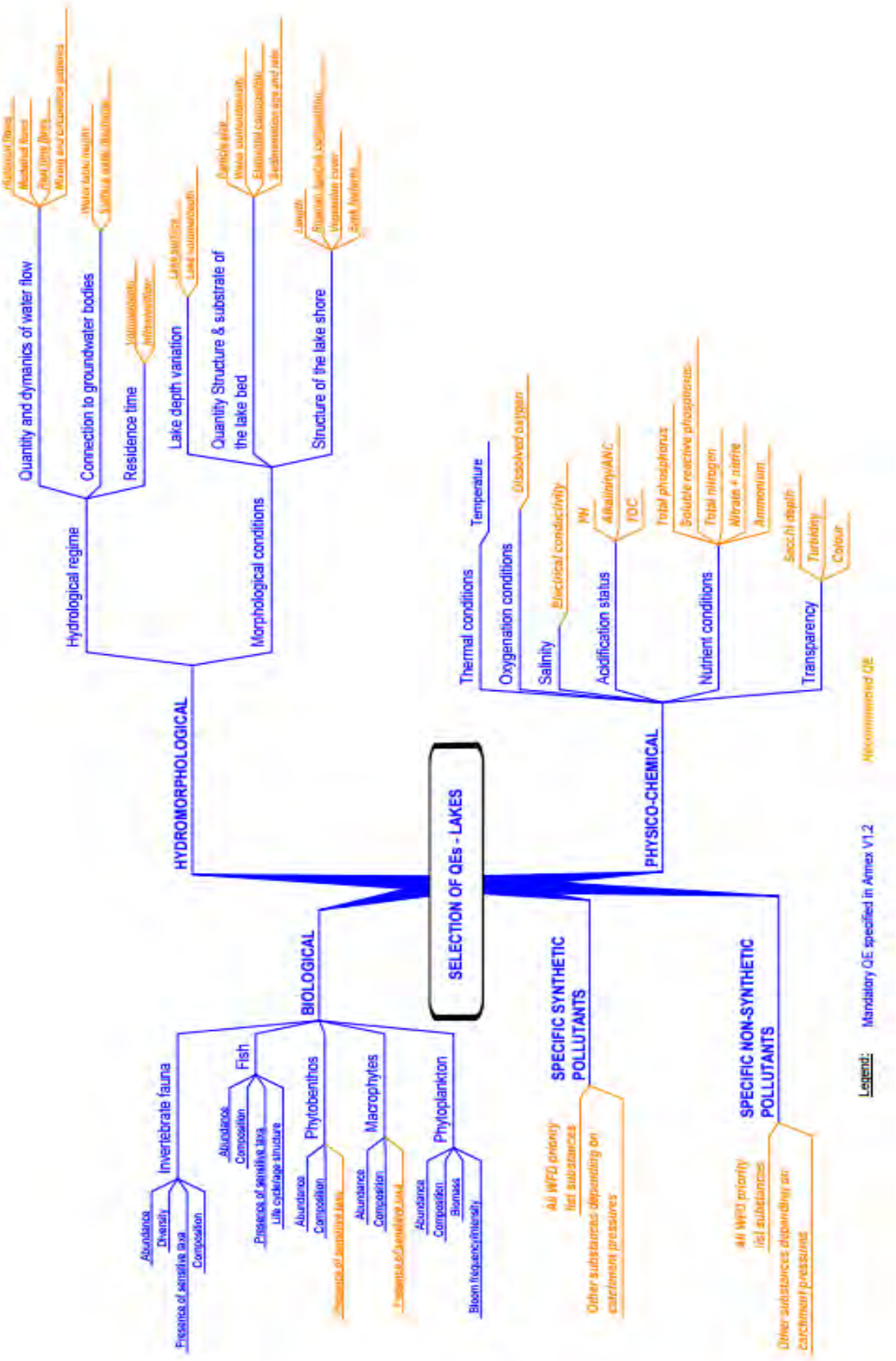


**Figure 3.** Selection of quality elements for lakes (Guidance document no.7, 2003).

## 1.5 **Earth Observation/Remote sensing**

According to Colwell (1966), the term “remote sensing” in its broad sense merely means “reconnaissance at a distance”.

Earth Observation (typically space-based, through the use of Satellites) is a particular field of Remote Sensing that includesthe gathering of information about physical, chemical, biological, geometrical properties of the Earth, all of whichcan be used for assessing the status and monitor changes of both the natural and cultural environment (Bakker et al. 2009).

Thus, in the context of Earth Observation, the definition of remote sensing can be modified as follows:

*Remote Sensing is the practice of deriving information about the Earth’s land and water surfaces using images (or data, in general) acquired from an overhead perspective, using electromagnetic radiation in one or more regions of the electromagnetic spectrum, reflected or emitted from the Earth’s surface* (Campbell 2002).

Near real-time environmental monitoring by adapting remote sensing techniques can be conducive to the more accurate detection of ecosystem threats (Rose et al. 2015).Therefore, the threat reduction and the management decisions will be accelerated.

Remote sensing has played an increasingly important role in detecting, mapping, understanding and predicting changes on the Earth’s surface, since the U.S. National Aeronautics and Space Administration (NASA) launched the Landsat-1 spacecraft in 1972 (Rose et al. 2015). Satellites are placed in constant orbits (up to 1 km either side of a nominal ground track) enabling systematic monitoring of rivers, lakes, wetlands, inland seas and floodplains (Vuglinskiy 2009).

According to Rose et al. (2015) Earth Observation has applications in:

- ✓ Assessing the spatial and temporal effects of climate on ecosystems
- ✓ Understanding, monitoring and predicting ecosystem response to multiple threats
- ✓ Controlling spatial and temporal dynamics of animal movements
- ✓ Assessing the agricultural and aquacultural expansion
- ✓ Maintaining ecologically functional and resilient populations of target species and ecosystem services
- ✓ Developing models of species distributions and abundances

The use of remote sensing for the environmental monitoring is advantageous due to (Bakker et al. 2009):

- ✓ High survey repeatability; high spatial resolution and frequent revisits
- ✓ Low cost; Satellite data are provided for free by many space agencies
- ✓ Data are acquired globally, using the same or similar sensor
- ✓ In the future, more data will be quantified using hyper spectral techniques
- ✓ Its attribute as a “multi-channel”; Multiple data can be assessed by a satellite image

Nevertheless, there are some limitations:

- ✓ The Earth's observation (typically) relates to a thin layer of the surface (Bakker et al. 2009)
- ✓ Cloud free and daylight conditions are usually necessary

**Remote sensing process**

A satellite image is the product of multiple effects and processes. In order to define the acquisition process of a satellite image, it is necessary to examine the interactions of electromagnetic radiation both in the atmosphere, as well as on the Earth's surface (Figure 4). The image is typically formed by a sensor, which records electromagnetic radiation emitted or reflected from Earth's surface. The solar radiation which reaches the atmosphere is scattered or attenuated. The remaining energy interacts (absorption, transmission, reflectance) with the objects and structures of the landscape. The interaction depends upon its wavelength. The reflected energy is also influenced by the atmosphere, before being recorded by a satellite sensor as incoming energy. The outcome of these interactions is ultimately recorded into an array of values – what is commonly known as an image.

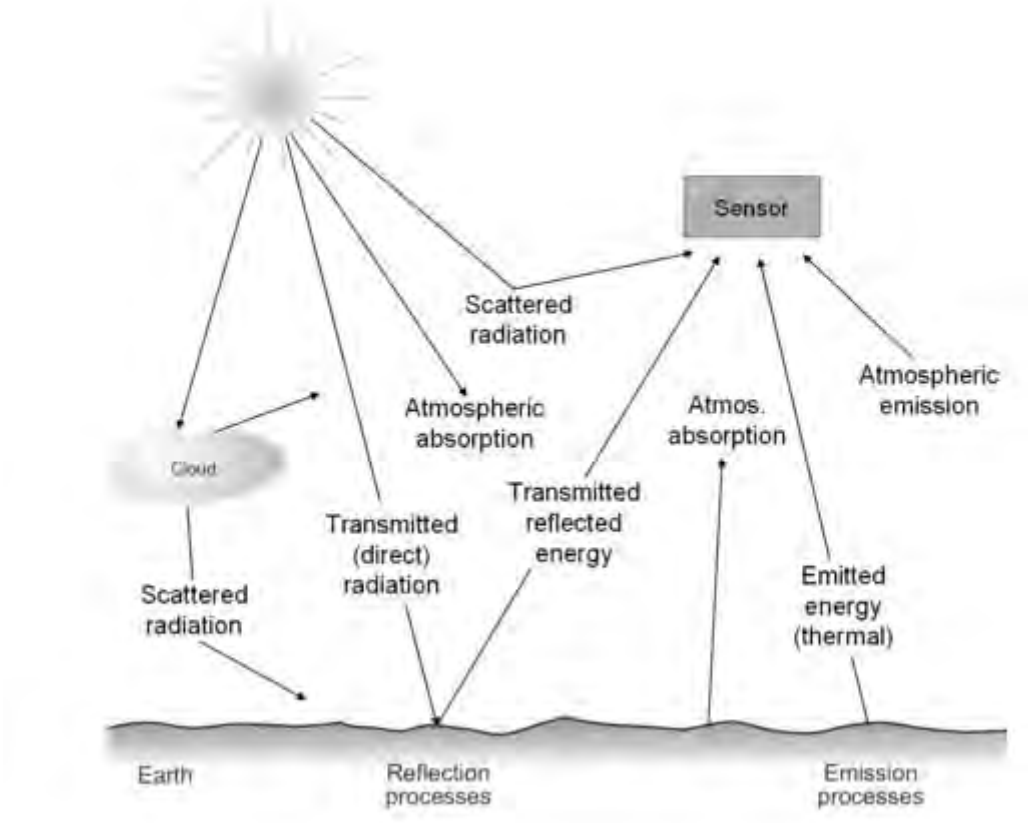


**Figure 4.** The acquisition process of a satellite image (Bakker et al. 2009).

**Remote sensing sensors**

Many types of platforms, such as unmanned airborne vehicles, manned aircrafts, satellites and space stations have been evaluated for remote sensing of the Earth, using techniques principally in the ultraviolet (UV), visible (VIS), infrared (IR), and microwave parts of the electromagnetic radiation spectrum (EMR spectrum) (Njoku 2014).

Satellites include one or more sensors. These sensors may vary in design and capabilities and can be grouped into two basic types: a) passive sensors and b) active sensors (Figure 5). The Sun, which is also referred to as natural radiation, is the main source of energy for passive sensors. Such instruments onboard satellites record the solar radiation, which is reflected or emitted from the Earth's surface. As a result they can only acquire data during daylight hours. Sensors receive energy, which is converted into electrical signals. These electrical signals are processed, stored, compressed, formatted and transmitted to ground stations. For example, photographic cameras, electro-optical sensors and thermal IR sensors can be characterized as passive sensors. However, thermal sensors can detect naturally emitted energy at any time of the day or night, as long as the amount of energy is large enough to be recorded.

Active sensors, such as Radar and LiDAR, emit energy towards a target and detect the amount of energy, which is backscattered/reflected back to satellite. Active sensors can gather information any time of the day or night, whereas Radar sensors can also "see" through clouds.

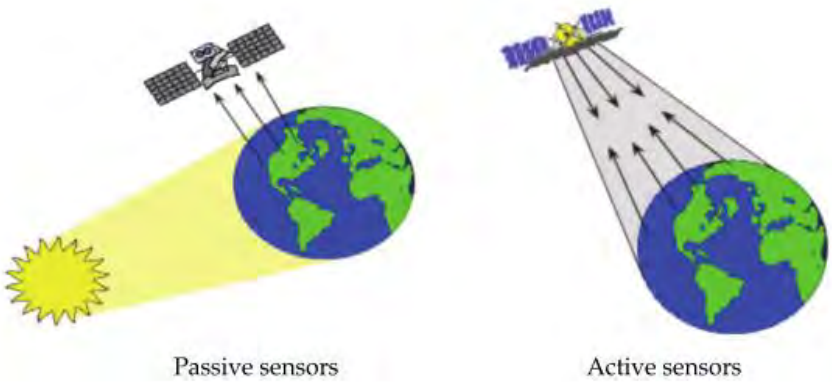


**Figure 5.** Active and passive sensors (Atazadeh 2011).

Satellite sensors record reflected energy in the form of brightness values, in order to image features on the Earth's surface (Younos & Parece 2015). Passive electro-optical imagery can be divided into three groups:

- ✓ **Panchromatic**: It consists of a single, grayscale spectral band, which enables maximum spatial resolution, as more light is available over the wide spectral range used.
- ✓ **Multispectral**: They consist of multiple, moderately-wide spectral range grayscale bands. Multispectral images have been proven useful for

discrimination, classification and analysis of objects, based on their spectral characteristics.

- ✓ **Hyperspectral**: It includes hundreds of narrow continuous spectral bands, which contribute to the improvement of object discrimination.

The spatial, spectral, radiometric and temporal resolution characterize the information collected by each sensor onboard a satellite. In particular:

- ✓ **Spatial resolution:** It is the ground surface area that can be displayed in one pixel on a satellite image
- ✓ **Spectral resolution:** It is defined as the number and width of spectral bands used by each satellite sensor
- ✓ **Radiometric resolution:** It is the capability of a sensor to display the differences, in terms of brightness values, on a satellite image. The number of value levels is related to the number of bits (e.g. an 8 bit image may display $2^8 = 256$ levels)
- ✓ **Temporal resolution:** It is the frequency, with which a satellite revisits the same area of the Earth's surface, with the same instrument and with the same viewing conditions (i.e. geometry and spatial resolution). The temporal resolution is related to the design of the satellite sensor, its orbit and the image acquisition strategy

**Electromagnetic radiation spectrum**

Satellite remote sensing concerns different ranges of the electromagnetic radiation spectrum (EMR spectrum) (Figure 6). Remote sensing, usually uses visible light, reflected and emitted infrared, as well as microwave radiation. The VIS and IR region of the electromagnetic spectrum includes wavelengths from 0,4 μm to 100 μm.

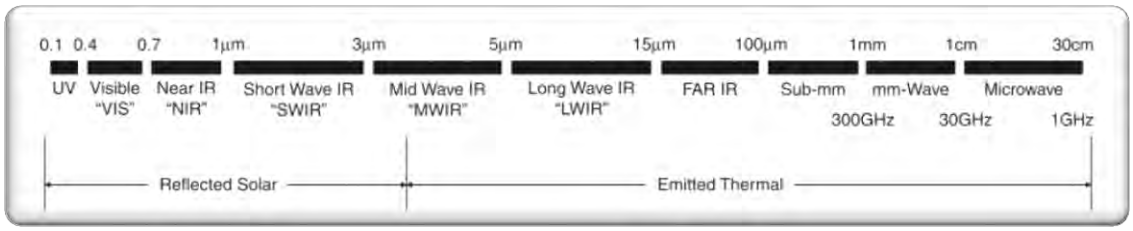


**Figure 6.** EMR spectrum from the ultraviolet to the microwave (Njoku 2014).

The term "spectral band" is used in order to describe a discrete interval of the electromagnetic spectrum. Sensors are able to measure responses within particular spectral bands in order to enable the detection of Earth's surface objects. The sensor's spectral bands are determined by the absorption characteristics of objects on the Earth surface, but also the consideration of atmospheric effects.

The region of the EMR spectrum that can be used for satellite remote sensing is very limited, because of the scattering, absorption and emission of radiation in the atmosphere. Figure 7 presents a typical atmospheric transmittance curve in those spectral regions that can be exploited with remote sensing techniques (Weng 2011).

The reflected energy from Earth's features can be used to distinguish the type of the Earth's land cover. Each type of land cover has unique properties of reflectance and absorption over different wavelengths. The term "spectral signature" is used in order to define the reflectance of radiation from one type of surface material, which varies over the range of wavelengths in the EMR spectrum.

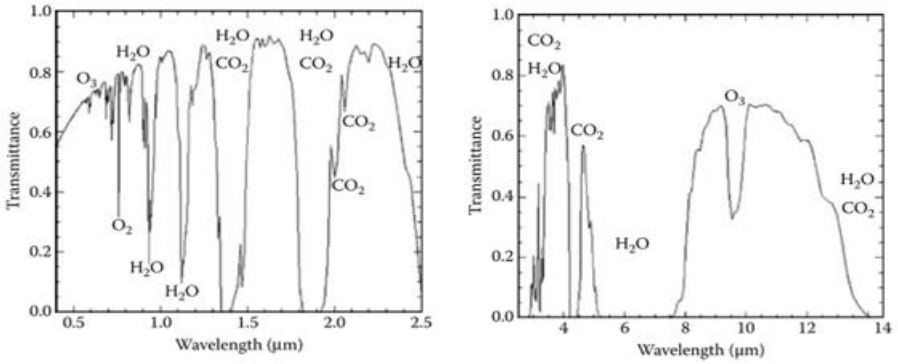


**Figure 7.** Atmospheric transmittance in the 0.4–2.5 μm and 3–14 μm regions (Weng 2011).

**Landsat satellites**

During the last few decades, environmental management has been greatly influenced by technological advances. Ecological sciences, coupled with advances in Geographical Information Systems (GIS), Digital Cartography and modeling, lead to an explosion of environmental applications. The Landsat satellite programme has played a major role in this context.

With over 40 years, the longest temporal record of space-based surface observations has been provided by Landsat satellites. Figure 8 shows the timeline of all Landsat satellite missions. Landsat-1 was launched in 1972 by the National Aeronautics and Space Administration (NASA), which developed the Earth Resources Technology Satellite (ERTS, later renamed Landsat). The U.S. Geological Survey (USGS) was given the archival responsibility to acquire and distribute these data at the new Earth Resources Observation System Data Center in Sioux Falls, South Dakota (Cohen & Goward 2004). Seven Landsat satellites have been launched since 1972. Landsat-5 and -6 were launched in 1984 and 1993 respectively, with Landsat-6 failing to achieve orbit. Landsat-7 was launched in 1999. On February 11$^{th}$ 2013, the launch of Landsat-8 took place, from Vandenberg Air Force Base, California. Landsat-8 was developed through the partnership between NASA and the Department of the Interior USGS (Irons & Loveland 2013). The Landsat-8/OLI exhibits a higher resolution wavelength coverage than the previous Landsat satellites, due to the addition of a new costal/aerosol band (0.43–0.45 μm) for detecting SS and chlorophyll in coastal regions and a new cirrus band (1.36–1.39 μm) for detecting clouds (Roy et al. 2014).

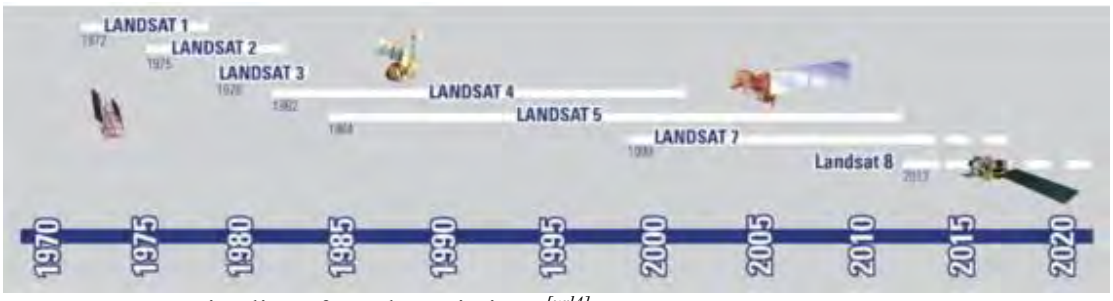


**Figure 8.** Timeline of Landsat missions *[url4]*.

Landsat data are useful for mapping and monitoring land cover and land surface biophysical and geophysical properties (Hansen & Loveland 2012, Wulder et al. 2012), but also hold potential for terrestrial data combination, biogeochemical cycling and land use forecasting applications (Nemani et al. 2009, Lewis et al. 2012, Sleeter et al. 2012). Landsat's applications are related to both scientific discovery, managing and monitoring resources for economic and environmental quality, public health and human well-being and national security (Roy et al. 2014).

Landsat data have several advantages for monitoring applications relying on multi-temporal data sets (Cohen & Goward 2004):

- ✓ Landsat series may offer the longest-running time series of systematically collected remote sensing data
- ✓ The spatial resolution of the images is suitable for the characterization of land cover and cover change associated with land management
- ✓ Landsat Thematic Mapper (TM) and the later Enhanced Thematic Mapper Plus (ETM+) acquire spectral measurements in visible, near-infrared (NIR), shortwave-infrared (SWIR)
- ✓ Large volumes of Landsat data can be processed and analyzed by new computer systems

**Sentinel-2**

Sentinel-2, the latest Earth Observation optical mission developed by the European Space Agency (ESA), is part of the Copernicus Program (former GMES/Global Monitoring for Environment and Security). It consists of two identical satellites, Sentinel-2A and Sentinel-2B, in order to achieve frequent revisits and high information availability, as they are planned to operate simultaneously. The launch of Sentinel-2A took place on 23 June 2015 on a Vega launcher. Sentinel-2B will be launched in mid-2016. Sentinel-2 provides improved continuity of Spot and Landsat missions, with improved revisit time, coverage area, spectral bands, swath width and radiometric and geometric image quality, meeting GMES needs for operational land and emergency services. Sentinel-2 mission is close to the Landsat local time and matches SPOT's, allowing the combination of Sentinel 2 images with past data, in order to build a long-term time data series of compatible data.

## 1.6 **Scope**

The objective of the present master thesis was to investigate the contribution of Earth Observation to water quality monitoring in accordance with the WFD, focusing on the possibility of measuring lake quality elements (or their variability) using satellite images. The kind of remote sensing to be discussed in the present study was devoted to observation of the Earth's water surfaces, by means of reflected or emitted electromagnetic energy.

Therefore, the methods of this master thesis were relevant to Earth Observation-Image processing, Cartography-GIS, Limnology- Lake Monitoring as per the WFD (*in situ* measurements), Data and Statistical analysis.

In particular, the aim of the study was to reconstruct/create a historical water quality parameter profile, by adopting a remote sensing approach. To this end, the goal was to monitor seven water quality elements using multispectral Landsat images from 1984 to 2016. Additionally, Sentinel-2 images were used, in order to highlight the performance and advantages/improvements of Sentinel-2 against previous satellites.

The results of this study were expected to contribute to the:

- ✓ Definition of optimal processing routines and external calibration procedures, in order to calculate lake water quality parameters, using multispectral satellite images
- ✓ Assessment of the correlation of water quality parameters with Landsat bands
- ✓ Mapping of the long-term temporal and spatial changes of water quality parameters from satellite imagery
- ✓ Development of specialized software that shall allow the extraction of QE values using Landsat data

The investigation took place over a Ramsar-protected ecosystem, Lake Koronia, which shall be described next.

## 2. STUDY AREA

### 2.1 Chapter overview

*This chapter deals with the description of the study area, including aspects of geology, climate and land use. Additionally, it presents the international, European and national protection status which is relevant to the wider area of Lakes Koronia-Volvi. The chapter concludes with the evolution of Lake Koronia during the last years.*

### 2.2 Location

Lake Koronia, also known as Lake of Lagadas or Lake Agiou Vasiliou, is located 30 km north-east from Thessaloniki, Central Macedonia, northern Greece (Figures 9-10) and belongs to Central Macedonia water district. It is part of the hydrologic basin of Mygdonia, an interrelated water resources system including Rechios River and Lake Volvi. The center of the study area is located at 40° 40'58" N, 23° 09'33" E and lies 75 m above sea level. Lake Koronia borders the Municipality of Lagadas and the Municipality of Volvi.

It is an elliptic-shaped, shallow, polymictic lake, with a surface of 29 $km^2$ . Koronia receives water via small streams and torrents, within a drainage area of about 780 $km^2$. The main streams that discharge into Lake Koronia are: Kavallari and Bogdanas (Northwest), Kolhiko and Analipsi (North) and Gerakarou (South).


**Figure 9.** Study area: Lake Koronia and Koronia sub-basin.

**Figure 10.** A current view of Lake Koronia (30/11/2015).

## 2.3 **Geology**

The main formations of Mygdonia basin are: shale, gneiss, amphibolite, thin layers of marble and granite. The formation of Mygdonia basin was the result of intense normal faulting, during the Mid-Paleogene period. The substrate of Mygdonia basin consists of two crystalline gneiss series: the deepest part of Kerdilliou series (East) and the upper layers of the Vertiskos formation (West). The gneiss appears in various combinations: gneiss with marble and amphibolite aggregates or combined with gneiss slate.

The plain part of the Koronia basin includes mostly loose sediments (Figure 11). The basement rocks of the Koronia Lake and Scholarion sub-basins consist of metamorphic rocks of the Paleozoic age Servo Macedonian massif (two mica gneisses, amphibolite), as well as of the Mesozoic age Circum Rhodope Belt (phyllites, quartzite, clay-schists, marbles and granites).

A more detailed geological description of Mygdonia basin has been carried out by Psilovikos (1977).


**Figure 11.** Geological map of the study area (Mylopoulos et al. 2007).

### 2.4 **Climate**

The climate of the wider area of Lake Koronia is transitional between Mediterranean and temperate. It has a large annual temperature range (> 20 $^0$C) and a relatively even distribution of rainfall compared to the rest of Greece. Annual precipitation during the last century ranged from 262-722 mm, while the mean annual value is 455.8 mm (Zalidis et al. 2004). The warmest and the driest months of the year are July and August. There are two precipitation peaks, one in December and a secondary one in June (Zalidis et al. 2004).

### 2.5 **Land use**

Agriculture is the main source of water consumption over Lake Koronia basin. The 68% of the basin, namely 238 km$^2$ are cultivated (Kolokytha 2014). Table 3 incudes the main cultivated areas in Koronia basin.

**Table 3.** Main crops and cultivated areas in Lake Koronia basin (Kolokytha 2014).

| | | NON- IRRIGATED CULTIVATIONS | | | | | IRRIGATED CULTIVATIONS | | | | | | | | |
|---|---|---|---|---|---|---|---|---|---|---|---|---|---|---|---|
| Municip. | Municipal sections | Wheat | Durum wheat | Barley | Oat | Rye | unflowe | Tobacc | Clover | Maize for animals | Maize | Hortocultural products | Olives | Grapes | Trees |
| Assiros | Assiros | 3200 | 1860 | 0 | 0 | 0 | 2100 | 0 | 280 | 0 | 0 | 50 | 200 | 40 | 235 |
| Egnatia | Evagelismos | 1400 | 20 | 330 | 0 | 0 | 0 | 0 | 500 | 0 | 0 | 185 | 0 | 90 | 335 |
| | Sxolari | 2000 | 100 | 100 | 0 | 50 | 1900 | 70 | 800 | 1700 | 1800 | 202 | 84 | 115 | 50 |
| Koronia | St. Vasilios | 3000 | 3000 | 300 | 0 | 100 | 1300 | 0 | 1750 | 200 | 150 | 24 | 50 | 25 | 105 |
| | Vasiloudi | 2600 | 1500 | 150 | 600 | 100 | 1350 | 0 | 180 | 100 | 60 | 71 | 0 | 40 | 100 |
| | Gerakarou | 1100 | 3000 | 250 | 300 | 115 | 3400 | 0 | 1400 | 500 | 0 | 80 | 70 | 37 | 48 |
| | Lagadikia | 830 | 1100 | 600 | 100 | 100 | 600 | 0 | 500 | 500 | 1300 | 50 | 56 | 100 | 21 |
| Lagada | Analipsi | 800 | 750 | 700 | 0 | 0 | 0 | 0 | 750 | 500 | 0 | 150 | 40 | 40 | 224 |
| | Iraklio | 1600 | 1200 | 515 | 0 | 0 | 700 | 0 | 1200 | 800 | 750 | 180 | 203 | 0 | 0 |
| | Kavalari | 1900 | 3100 | 1200 | 0 | 0 | 800 | 0 | 6000 | 2750 | 500 | 240 | 0 | 0 | 122 |
| | Kolhiko | 1500 | 1000 | 650 | 0 | 0 | 1600 | 0 | 500 | 1500 | 2000 | 1800 | 305 | 6 | 83 |
| | Lagada | 1800 | 4400 | 800 | 0 | 0 | 0 | 0 | 1700 | 2750 | 1450 | 613 | 60 | 100 | 238 |
| | Lagina | 400 | 1400 | 1300 | 0 | 0 | 0 | 0 | 800 | 120 | 90 | 0 | 24 | 0 | 10 |
| | Perivolaki | 250 | 750 | 500 | 0 | 0 | 12 | 0 | 2000 | 540 | 85 | 175 | 0 | 0 | 0 |
| | Chrisavgi | 1200 | 5100 | 1000 | 0 | 200 | 0 | 0 | 0 | 400 | 0 | 1 | 122 | 180 | 31 |
| Mygdonia | Liti | 2900 | 5400 | 1000 | 0 | 0 | 0 | 0 | 600 | 0 | 680 | 5 | 15 | 21 | 0 |
| | Drimos | 1500 | 16000 | 400 | 0 | 0 | 40 | 0 | 400 | 40 | 240 | 65 | 14 | 14 | 256 |
| | Melissohori | 1600 | 6580 | 600 | 0 | 0 | 120 | 0 | 10 | 0 | 150 | 0 | 13 | 6 | 70 |
| Total | | 29.580 | 56.260 | 10.395 | 1.200 | 665 | 13.922 | 70 | 19.370 | 12.400 | 9.285 | 3.891 | 1.256 | 832 | 1.928 |

Figure 12 gives a detailed description of land cover of Mygdonia, basin according to the last version of Corine Land Cover 2000 *[url9]*.

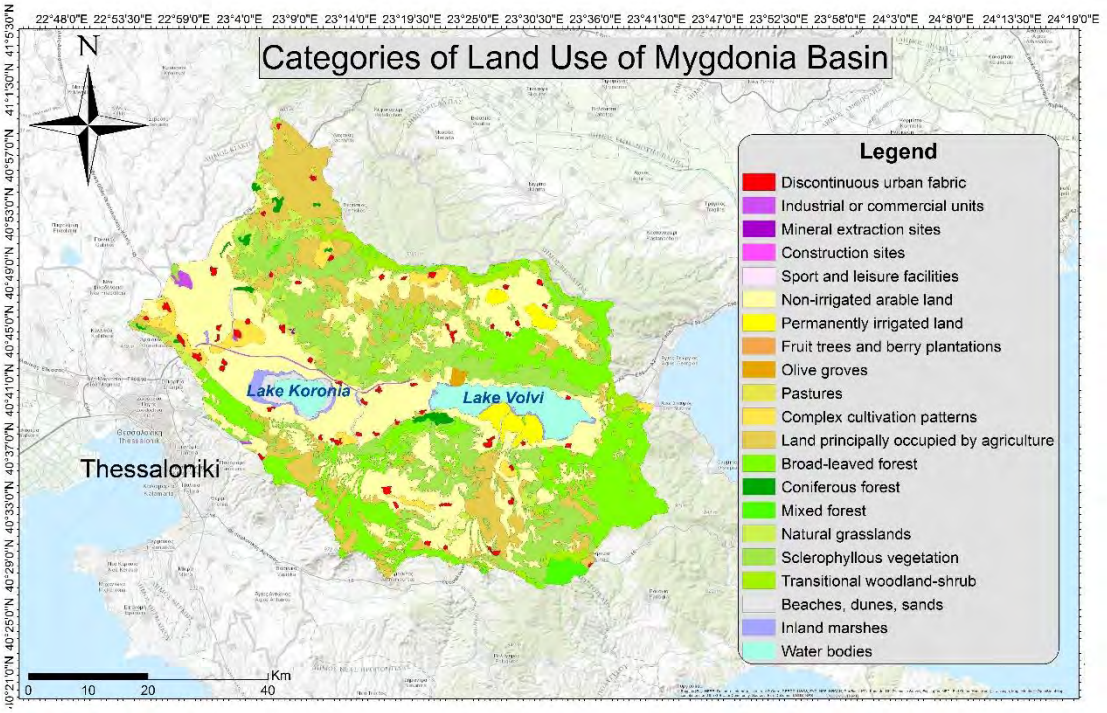


**Figure 12.** Categories of land cover of Mygdonia basin (Corine LandCover 2000).

## 2.6 **Protection status**

The wider area of Lakes Koronia-Volvi is under international, European and national protection status (Management Authority of Lakes Koronia-Volvi *[url10]*) (Figure 13):

- ✓ Wetland of International Importance under the Ramsar Convention, named 'Lakes Koronia–Volvi' (Code: 3GR005). The Ramsar Convention 'on the protection of wetlands of international importance' was ratified by Legislative

Decree 191/1974 (Government Gazette 350/A/11.20.1974) and amendments n. 1751/1988 (Government Gazette 26/A/9.2.1988) and n. 1950/1991 (Government Gazette 84/A/31.5.1991)

- ✓ Special Protection Area (Special Protected Area) under Directive 79/409/EEC (now 2009/147/EC) 'On the conservation of wild birds', with code GR1220009 'Lakes Volvi and Lagada and Rendina Straits'
- ✓ Site of Community Importance (Site of Community Importance - SCI, Network NATURA 2000) according to Directive 92/43/EEC "For the conservation of natural habitats and of wild fauna and flora" with code GR1220001 'Lakes Volvi and Lagada - Surrounding area'. Natura 2000 is the key instrument to protect biodiversity in the European Union. It is an ecological network of protected areas, set up to ensure the survival of Europe's most valuable species and habitats
- ✓ National Wetland Park of lakes Koronia-Volvi and Macedonian Tempe, as characterized by JMD 6919/2004 (Government Gazette 248/5.3.2004) and amending this JMD 39542/2008 (Government Gazette 441/9.10.2008)
- ✓ Wildlife Refuges: '"Lagada Lake", "Profitis- Nymfopetra", "Firth Richiou-Volvi", "Lakeside woods Platanon" (Government Gazette 398/B/1983)

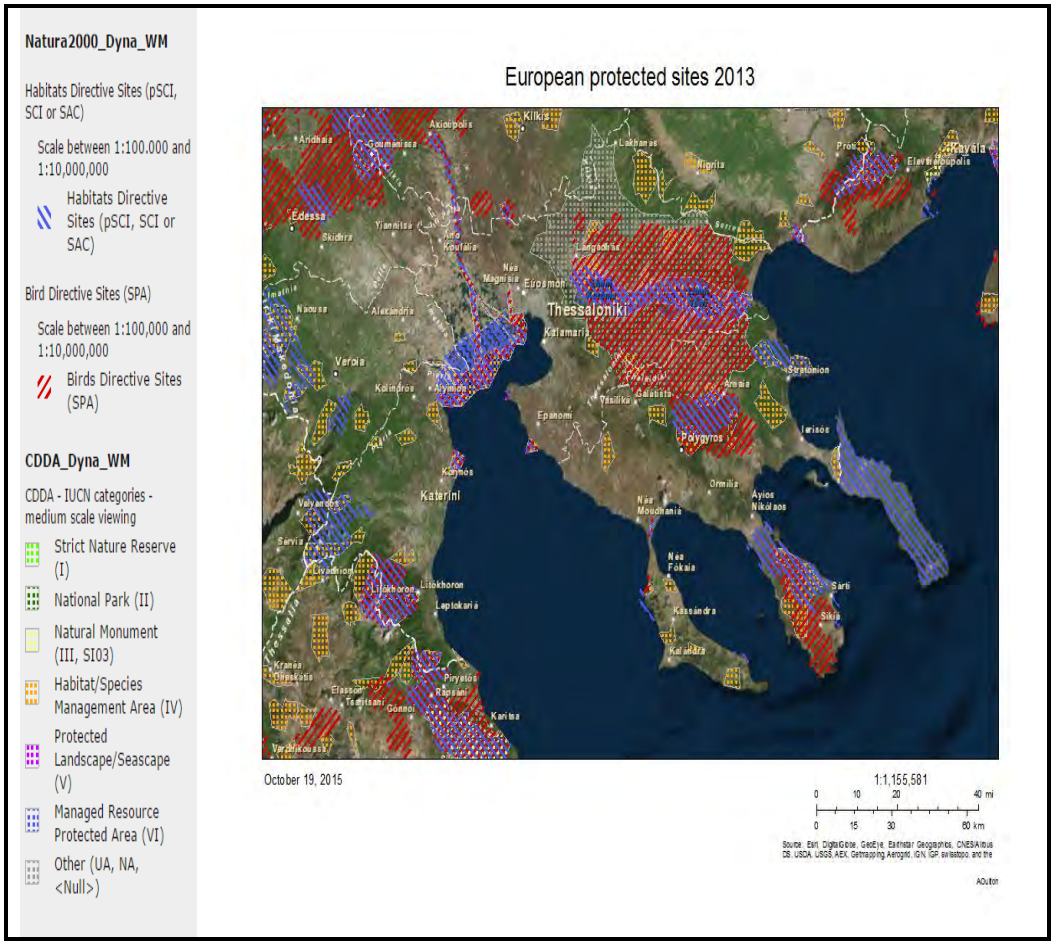


**Figure 13.** The protected sites of the study area, including Natura 2000 sites and nationally designated areas (CDDA) *[url13]*.

## 2.7 **Protection zones**

According to Joint Ministerial Decision 6919/2004 three protection zones have been distinguished (Figure 14) (Management Authority of Lakes Koronia-Volvi, [url10]):

- ✓ **ZONE A**: Zone A1 includes the forest of Apollonia, the bed and the mouth of the stream Melissourgos, the boundaries and the land areas of the forest. Zone A2 includes the bed and banks of the Richios river from lake Volvi to the Strymonic Gulf and part of the valley including hygrophilous and sclerophyllous scrub vegetation, rock formations, etc.
- ✓ **ZONE B**: The area between the settlements Evagelismos, Scholari, Agios Vasilios, Nymfopetra, Mikri and Megali Volvi, Rentina, Modio, Nea Madytos, Kokkalou, Loutra Volvis and Peristeronas and adjacent settlements Cavallari, Drakontio Analipsi, Profitis, Lagadikia, Stivos, Gerakarou, Vasiloudiou, Vaiochoriou, Stavrou, N. Apollonia and Plateia
- ✓ **ZONE C**: Area which abuts Zone B and reaches the boundaries of the Mygdonia Basin


**Figure 14.** The three protection zones of Mygdonia basin. Blue line: A Zone boundaries, Pink line: B Zone Boundaries, Green line: C Zone Boundaries (Management Authority Lakes Koronia-Volvi, [url10]).

## 2.8 **The evolution of Lake Koronia**

The water quality of Lake Koronia is monitored by Management Authority of Lakes Koronia-Volvi. The Management Authority of Lakes Koronia-Volvi was established in 2002 under Law 3044. Additionally, multiple individual researchers (Bobori 2001, Kaiserli et al. 2002, Mitraki et al. 2004, Petaloti et al. 2004, Michaloudi et al. 2009, Michaloudi et al. 2012, Moustaka-Gouni et al. 2012) have defined the features and assessed the QE of Lake Koronia, but for a limited temporal frequency and spatial coverage.This discontinuity of data is due to the difficult access to the lake, caused by small water quantities coupled with loose sediment. Also, restoration and management

plans have been proposed (Zalidis et al. 2004, Mylopoulos et al. 2007, Alexandridis et al. 2007).

Lake Koronia was once the 4th largest lake in Greece, but during the last years it has become a temporary lake. The ecosystem of Lake Koronia faces both qualitative and quantitative environmental problems. The quantitative problems include the progressive decline of the water level, from 8m (1960) to less than 1m by 2001 (Manakou et al. 2008). Based on previous studies the evolution of Lake Koronia can be summarized in the following stages:

- ✓ During the 1960s, Lake Koronia covered an area of approximately 50 $km^2$
- ✓ In the beginning of the 1970s, Lake Koronia covered an area of approximately 47 $km^2$ and the mean depth was 5 m (Tzionas et al. 2004)
- ✓ In the mid-1970s the lake occupied an area of 46,2$km^2$ with a maximum depth of about 4 m, 6 m and 8.5 m, in its western, central and eastern part respectively (Psilovikos 1977). In 1970, its surface area was 47 $km^2$ declining to 30$km^2$ in 1995 (Papakonstantinou & Katirtjoglou 1995). During the same period, water volume contracted from 150-200*$10^6$ $m^3$ to 30*106 $m^3$ (Papakonstantinou et al. 1996), and by 2001 it was <10*$10^6$ $m^3$
- ✓ At the end of 1980s, the water quantity was decreasing rapidly. In the period 1985-1995, a reduction of the maximum water depth by 3 m took place (from 4.5 m to 1.5 m) and the lake surface decreased to 30 $km^2$ (Kungolos et al. 1998)
- ✓ In 1995, the lake surface area was 30 $km^2$ and the maximum depth 1 m
- ✓ In the summer of 2002, Lake Koronia dried up. Intense rainfalls during the winter months resulted in the repletion of the lake
- ✓ Early in 2003 the lake started filling with water and the maximum depth was about 0.9 m. During the period from 2003 the lake depth was < 2 m and the lake dried up again in autumn 2009

The qualitative deterioration refers to the degradation of the water quality and the swift from the eutrophic to the hypertrophic state. According to Mourkides et al. (1978) Lake Koronia was eutrophic since as early as 1977. Lake Koronia has developed a progressive increase in trophic state associated with decreasing water level since the early 1990s (Mitraki et al. 2004). Currently, it has turned to hypertrophic. The lake status has gotten worse since the Macrophytes have disappeared and cyanobacteria have dominated the lake. According to Koussouris et al. (1992), Lake Koronia displayed the second highest chlorophyll $\alpha$ concentration (206 $mg/m^3$) and lowest transparency (Secchi disk) (0.2 m) of 14 Macedonian lakes. In August 1995, the rise in pH, coupled with high temperature and low water volume (max<1m), killed all fish in the lake (Bobori 2001). In August–September 2004, an extremely dense bloom of the haptophyte *P. parvum* was observed and caused a mass bird (thousands) and fish (hundreds) kill (Moustaka-Gouni et al. 2004).

The degradation of the lake's ecosystem is due to pollution and non-sustainable water management. The surface water of Koronia, as well as the groundwater cannot sustain the unsystematic economic growth of the area, resulting into water depletion, negative

water balance, environmental degradation and very serious economic problems (Mylopoulos et al. 2007). The negative water balance was caused not only by natural inflow reduction, but also by agricultural, industrial and urban sector overuse. Additionally, even though the aquifer has a poor communication with the lake, due to argillaceous layers that cover the lake's bottom, the decrease of its water level creates intense infiltration of run-off water resulting to a deficient amount of river water discharging in the lake (Tzimopoulos et al. 2005). Unlike the current status, according to Knight et al. (1999) the water balance in the sub-basin of Koronia was positive since 1985, with a surplus of $37*10^6$ $m^3$/year. Figure 15 summarizes the causes of Koronia's water level reduction.

In order to restrict the system degradation, two operational plans were created (Master Plan I & II). Master Plan I was filed in 1998 by the English Company Knight Piesold Ltd in collaboration with the Prefecture of Thessaloniki. Master Plan II was published in 2004 and constituted a revised version of Master Plan I, which needed substantial amendments. It was filed by the Aristotle University of Thessaloniki on behalf of the Prefecture of Thessaloniki, which was financed by the Cohesion Fund.

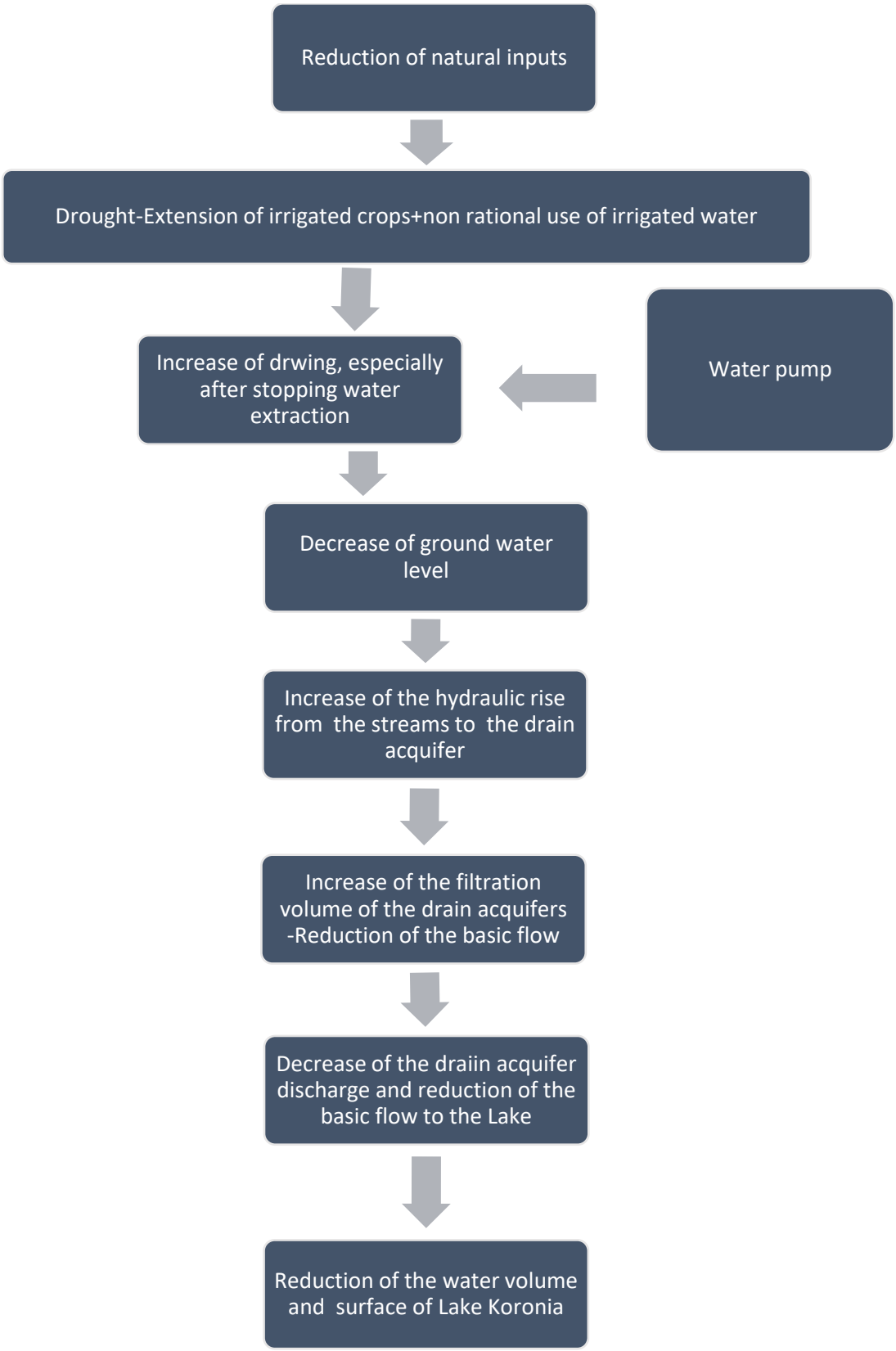


**Figure 15.** The causes of Koronia's water level reduction (Zalidis et al. 2004).

# 3. MATERIALS AND METHODOLOGY

## 3.1 **Chapter overview**

*This chapter is a brief overview of all data that were used, in order to compose the present Master thesis. It includes all the satellite images, the cartographic data and the equipment that were selected. In addition, it contains the software required for the data pre-processing and analysis, as well as a workflow guide for image-processing with respect to quantifying/mapping lake water QE.*

## 3.2 **Satellite images**

The following satellite data were identified as appropriate for the purposes of the present study:

- ✓ Landsat 4-5/TM (Thematic Mapper)
- ✓ Landsat-7/ETM (Enhanced Thematic Mapper)
- ✓ Landsat-8/OLI (Operational Land Imager)
- ✓ Landsat-8/TIRS (Thermal Infrared Sensor)
- ✓ Sentinel-2/MSI (Multi-Spectral Instrument)

Only two Landsat scenes are required to cover Lake Koronia (path/row: 184/32,183/32) (Figure 16).

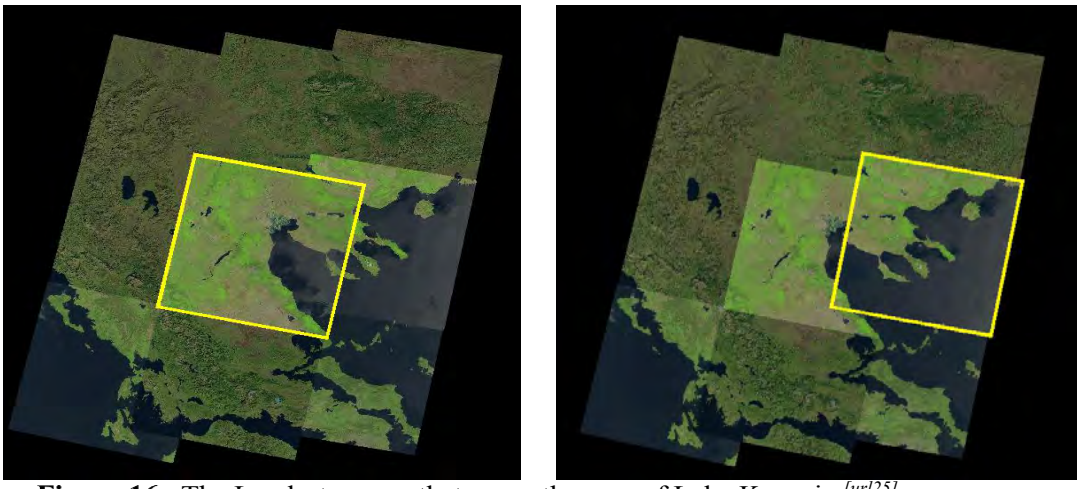

**Figure 16.** The Landsat scenes that cover the area of Lake Koronia [url25].

## 3.3 **Maps**

- ✓ Topographic maps at 1:50000 scale [Sheets: Thermi (1970,1982) and, Thessaloniki (1982)] of the Hellenic Military Geographical Service.

## 3.4 **Equipment**

For the purposes of the present study, the following equipment was necessary:

- ✓ Computer platforms, with Windows and Linux operating systems, including at least a 2 TB hard drive and 4GB of RAM
- ✓ GPS receiver, Garmin GPSMap76S
- ✓ Oxi 3205, WTW, D.O. meter
- ✓ pH 3110, WTW, pH meter
- ✓ Cond 3210, WTW, Conductivity meter

### 3.5 **Software**

The image selection and downloading was completed employing:

- ✓ EOLI-SA (Earth Observation Link-Stand Alone), European Space Agency (ESA)
- ✓ GloVis (Global Visualization Viewer), United States Geological Survey (USGS) Bulk download application *[url25]*, an easy-to-use tool for downloading large quantities of satellite imagery and geospatial data

In order to view, edit, create, and analyze geospatial data the following Geographical Information Systems were used:

- ✓ ArcGIS (ArcInfo version) and its main components ArcMap, ArcCatalog and ArcToolbox

The implementation of the atmospheric correction procedure was based on:

- ✓ LEDAPS 2.0 (standalone version), downloaded from ORNL DAAC, NASA *[url16]*. LEDAPS software ran on 32-bit Linux, Ubuntu 14.04.4 LTS. LEDAPS was originally developed in 2006 at National Aeronautics and Space Administration (NASA) Goddard Space Flight Center (GSFC) and the University of Maryland with funding from the NASA Terrestrial Ecosystems and Applied Sciences Programs
- ✓ L8SR 0.4.0 Version was downloaded from GitHub *[url18]* and ran on 32-bit Linux, Ubuntu 14.04.4 LTS.

For the satellite image processing the following programs were used:

- ✓ ENVI™
- ✓ ERDAS Imagine™
- ✓ Matlab R2015b
- ✓ SNAP Desktop

The composition of the algorithmic procedures and the final GUI was carried out using:

- ✓ Matlab R2015b

Additionally, the following software were utilized:

- ✓ Microsoft Office™ (Word, Excel, Powerpoint)
- ✓ Adobe Photoshop, a raster graphics editor
- ✓ Cygwin DLL, a large collection of GNU and Open Source tools which provide functionality similar to a Linux distribution on Windows
- ✓ Google Earth

### 3.6 **Workflow**

This section is intended as a workflow guide to image-processing with respect to quantifying/mapping lake water QE. The image processing procedures were developed for Lake Koronia, but with appropriate modifications to reflect local observation interests and pre-existing geographic information and other data sources these procedures should work equally well for other lakes.

The developed methodology requires the following steps (Figure 17):

1. Image selection: **Landsat-5/TM, -7/ETM+, -8/OLI** and **Sentinel-2** images were used
2. Image pre-processing
    a. **Radiometric calibration**: Convert DN of the selected images to TOA reflectance and surface reflectance, applying atmospheric correction
    b. Selection of the **Area of Interest** in order to reduce the file size of the Landsat image by removing unneeded data
    c. **Geometric correction**: Correct geolocation errors using *Ground Control Points* (GCPs) and *DEM*
    d. Create **water-only image** editing a guide (unsupervised classification lake map) for development of an open-water image
3. **Extraction of water quality parameters**: Water quality algorithms, mathematical equations which relate radiometric variables to the concentrations of water QE, developed from previous studies, were applied to radiometrically calibrated pixels of lake Koronia
4. **Satellite data calibration**: Use of an adequate database of *in situ* measurements for satellite data calibration

The results allow the mapping the temporal and spatial water QE variability of lake Koronia for the past three decades.

A large number of useful stand-alone functional modules were developed during the pre-processing and the QE calculation routine. These were almost exclusively serving the purpose of deriving data and information from satellite images and were composed in a straightforward manner, in order to synthesize a **specialized software** that will allow the extraction of QE values using Landsat data.

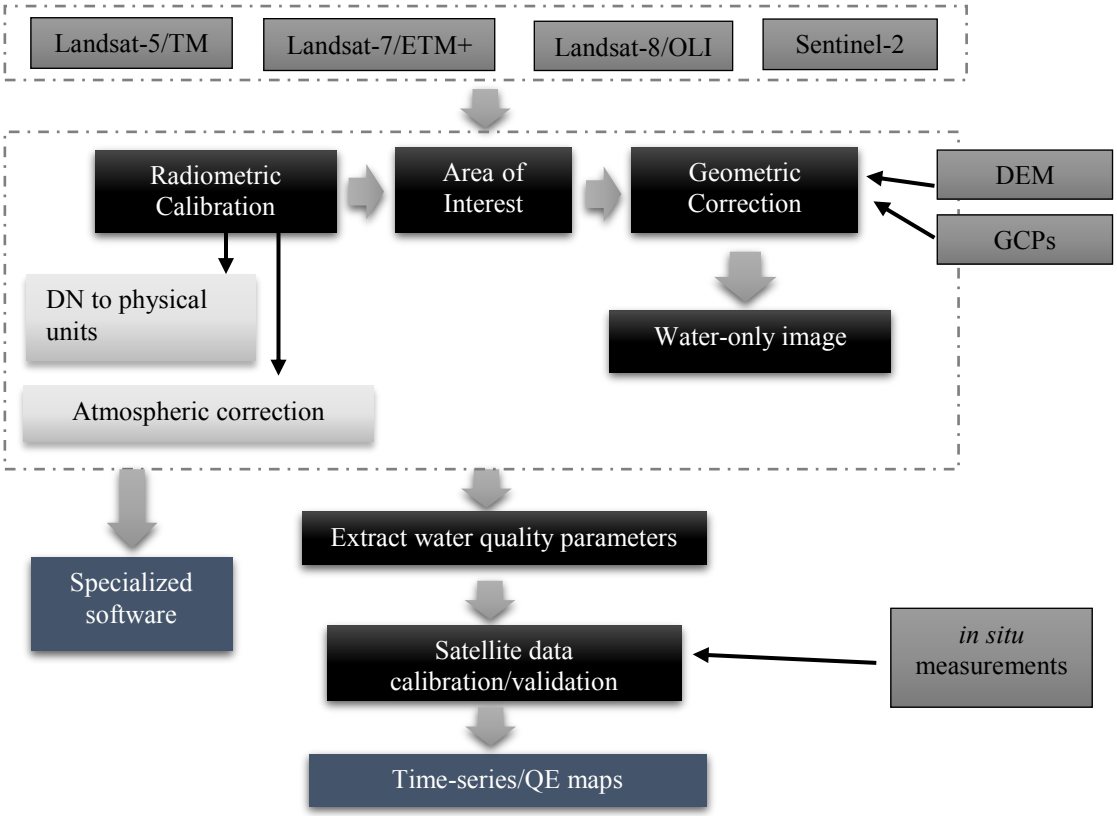


**Figure 17.** Workflow diagram of Landsat image processing and analysis steps.

# 4. DATA MINING

## 4.1 Chapter overview

*This chapter further discusses the spatial, spectral, radiometric, and temporal resolution characteristics of remotely sensed Landsat and Sentinel-2 data. It focuses on the method adopted for the selection of the appropriate satellite data, which will be used for the extraction of the water quality parameters.*

## 4.2 Satellite data

Due to spectral, spatial and temporal resolution (Table 4), the following satellite data were identified as appropriate for the purposes of the present study:

- ✓ Landsat 4-5/TM (Thematic Mapper)
- ✓ Landsat-7/ETM (Enhanced Thematic Mapper)
- ✓ Landsat-8/OLI (Operational Land Imager)
- ✓ Landsat-8/TIRS (Thermal Infrared Sensor)
- ✓ Sentinel-2/MSI (Multi-Spectral Instrument)

Landsat MSS (Multi Spectral Scanner) data were excluded, mainly due to inadequate spectral resolution (lack of blue band), as well as low spatial resolution.

Landsat TM images consist of seven spectral bands with a spatial resolution of 30 m for Bands 1 to 5 and 7. Spatial resolution for Band 6 (thermal infrared) is 120 m, but is resampled to 30 m pixels.

Landsat ETM+ images are characterized by eight spectral bands with a spatial resolution of 30 m for Bands 1 to 7. The resolution for Band 8 (panchromatic) is 15 m. All bands can collect one of two gain settings (high or low) for increased radiometric sensitivity and dynamic range, while Band 6 collects both high and low gain for all scenes. ETM+ Band 6 is acquired at 60 m resolution, but products are resampled to 30 m.

Landsat-8/OLI & TIRS images consist of nine spectral bands with a spatial resolution of 30 m for Bands 1 to 7 and 9. Band 1 (ultra-blue) can be used for coastal and aerosol studies. Band 9 is useful for cirrus cloud detection. The resolution for Band 8 (panchromatic) is 15 m. Thermal bands 10 and 11 are useful in providing more accurate surface temperatures and are collected at 100 m. TIRS bands are acquired at 100 m resolution, but are resampled to 30 m in delivered data product.

**Table 4.** The temporal, radiometric and spatial resolution of Landsat satellites.

| Satellite/Sensor | Spatial Resolution (m) | Spectral Resolution (μm) | Temporal Resolution (revisit in days) |
|---|---|---|---|
| Landsat 4-5/TM *[url1]* | 30*30<br>120*120 (TIR) | Band 1: 0.45 - 0.52<br>Band 2: 0.52 - 0.60<br>Band 3: 0.63 - 0.69<br>Band 4: 0.76 - 0.90<br>Band 5: 2.08 - 2.35<br>Band 6: 2.08 - 2.35<br>Band 7: 10.4 - 12.5 | 16 |
| Landsat 7/ETM+ *[url12]* | 15*15(Pan)<br>30*30<br>60*60 (TIR) | Band 1: 0.441 - 0.514<br>Band 2: 0.519 - 0.601<br>Band 3: 0.631 - 0.692<br>Band 4: 0.772 - 0.898<br>Band 5: 1.547 - 1.749<br>Band 6: 10.31 - 12.36<br>Band 7: 2.064 - 2.345<br>Band 8: 0.515 - 0.896 (Pan) | 16 |
| Landsat 8/OLI & Landsat-8/TIRS *[url12]* | 15*15 (panchromatic)<br>30*30 (visible, NIR,SWIR)<br>100*100 (thermal) | Band 1: 0.435 - 0.451<br>Band 2: 0.452 - 0.512<br>Band 3: 0.533 - 0.590<br>Band 4: 0.636 - 0.673<br>Band 5: 0.851 - 0.879<br>Band 6: 1.566 - 1.651<br>Band 7: 2.107 - 2.294<br>Band 8: 0.503 - 0.676<br>Band 9: 1.363 - 1.384<br>Band 10: 10.60 - 11.19 (TIRS)<br>Band 11: 11.50 - 12.51 (TIRS) | 16 |

The MSI sensor onboard Sentinel-2 records data in 13 spectral bands, ranging from the visible and near-infrared (VNIR) to the short-wave infrared (SWIR), with four at 10 m, six at 20 m and three at 60 m resolution (Table 5). It is characterized by narrower bands for improving identification of features, additional red channels for assessing vegetation and dedicated bands for improving atmospheric correction and detecting cirrus clouds.

Appropriate satellite data have been identified using EOLISA *[url24]* and USGS Global Visualization Viewer *[url25]*.Typically, only two Landsat scene is required to cover Lake Koronia (path/row: 184/32,183/32). EOLISA's satellite data was provided by ESA, after the submission of a proposal (ID:31068).

**Table 5.** The temporal, radiometric and spatial resolution of the Sentinel 2 mission.

| Satellite/Instrument | Spatial Resolution (m) | Central Wavelength (nm) | Bandwidth (nm) | Temporal Resolution (revisit in days) |
|---|---|---|---|---|
| Sentinel-2/MSI [url14] | 60 | Band 1: 443 | 20 | 5 days under the same viewing angles |
| | 10 | Band 2: 490 | 65 | |
| | 10 | Band 3: 560 | 35 | |
| | 10 | Band 4: 665 | 30 | |
| | 20 | Band 5: 705 | 15 | |
| | 20 | Band 6: 740 | 15 | |
| | 20 | Band 7: 783 | 20 | |
| | 10 | Band 8: 842 | 115 | |
| | 20 | Band 8a: 865 | 20 | |
| | 60 | Band 9: 945 | 20 | |
| | 60 | Band 10: 1375 | 30 | |
| | 20 | Band 11: 1610 | 90 | |
| | 20 | Band 12: 2190 | 180 | |

GloVis (Global Visualization Viewer) is a direct link from USGS online, allowing the image visualization (in *.jpeg format) before ordering the actual full data. Once a scene has been selected, it can be downloaded with or without processing in the same format (*.jpeg). Processed scenes were ordered and downloaded as compressed (zipped, *.zip) files at a later stage. Level 1 data, which include calibrated images of a specific standard - with corrected common errors, arising from problems with digitization, noise and transmission (Waxter 2014) - were selected. The corrections to the common errors in the digital data values are referred to as radiometric corrections. Multiple processed scenes were downloaded with the "Bulk Data Application" available through USGS.

Multispectral satellite images since 1984 that fulfilled the following criteria have been selected:

- ✓ Less than 70% overall cloud coverage
- ✓ Low cloud coverage over the study area
- ✓ Characterized as downloadable (USGS Global Visualization Viewer)

A total of 715 images were selected (Table 6), spanning the period from 1984 to 2016. Annex II includes an extended description of the selected images.

**Table 6.** The number of selected images per Landsat satellite.

| Satellite/Sensor | No. of images |
|---|---|
| **Landsat-5/TM** | 395 |
| **Landsat-7/ETM+ SLC ON** | 70 |
| **Landsat-7/ETM+ SLC OFF** | 181 |
| **Landsat-8/OLI** | 69 |
| **Total** | **715** |

In addition to the Landsat images, four Level 1C Sentinel 2 images were provided by ESA a few months before their official release (commissioning phase) on the Sentinels Scientific Data Hub (https://scihub.copernicus.eu) (Table 7). One Sentinel 2 scene was

selected to cover Lake Koronia . Figure 18 shows the Sentinel-2 image acquired on 16/11/2015.

**Table 7.** The selected Sentinel 2 images and their acquisition date.

| Product ID | Acquisition Date |
|---|---|
| S2A_OPER_MSI_L1C_TL_MTI__20150729T095149_A000519_T34TFK_N01.01 | 29/7/2015 |
| S2A_OPER_MSI_L1C_TL_MTI__20150818T094956_A000805_T34TFK_N01.03 | 18/8/2015 |
| S2A_OPER_MSI_L1C_TL_MTI__20150828T094933_A000948_T34TFK_N01.03 | 28/8/2015 |
| S2A_OPER_MSI_L1C_TL_SGS__20151116T112611_A002092_T34TFK_N01.05 | 16/11/2015 |

**Figure 18.** Sentinel-2 image (16/11/2015).

# 5. IMAGE PRE-PROCESSING

## 5.1 Chapter overview

*All image pre-processing routines that were utilized are presented in this chapter. This chapter contains the sections covering radiometric calibration, including a concise review of atmospheric correction algorithms LEDAPS and L8SR that are specific for Landsat images. It presents the methods for setting the area of interest plus performing geometric corrections. It also focuses on the classification algorithms that were used for the extraction of water features and concludes with examples of the water mask formation.*

## 5.2 Radiometric calibration

Sun is a source of energy emitting at a given rate of Joules/second, or Watts. The Sun energy radiates through space isotropically in an inverse square law fashion, so that at a given distance the sun's emission can be measured as the power emitted, divided by the surface area of a sphere at that distance (Richards & Jia 2006). This power density is referred to as *irradiance*, a property which describes the strength of any emitter of electromagnetic energy. In case the surface is perfectly smooth, then this amount of energy is scattered uniformly into the upper hemisphere. The term *radiance* [W/($m^2$ sr $\mu$m)] refers to the amount of power density scattered in a particular direction, which is defined by its density per solid angle, as equal amounts are scattered into equal cones of solid angle.

The radiance reaching the sensor passes through the optics, where a detector and a system of electronics, performs analogue-to-digital conversion. Satellite images consist of pixels. A pixel (short for "Picture Element"), can be defined as the smallest individual element of a picture represented on the screen. A pixel consists of an intensity value and a location address on a two dimensional image. Each pixel's intensity value represents the measured solar radiance in a particular wavelength band reflected from the surface. This value is the average value for the whole ground area, which is covered by the pixel.

Due to finite storage capacity, the data in remote sensing is in the form of digital numbers (DN). The radiance varies through a continuous range of values, which are recorded and digitized onboard the spacecraft. DNs don't indicate a direct measurement of Earth-leaving radiance, as they are the steps/quanta into which a range of physical values is divided. This 'quantization' results from the 'breaking down of a continuous range into a discrete number of steps'. The DN of a particular pixel is normally the average value for the whole ground area covered by the pixel. Each DN is stored with a finite number of bits. For example, Landsat TM and ETM+ products are delivered as 8-bit images (256 grey levels), while Landsat 8 products as 16-bit images (65.536 grey levels). The range of the bits determines the radiometric resolution of an image. In

general, the greater the number of quantization levels the greater the radiometric resolution.

For the detecting, measuring and monitoring of changes through time in Earth's surface condition, the ability to compare images from different dates and sites in different scenes is required. The DNs from each image must be calibrated to common reference values. The raw data values recorded by the sensors vary over time or/and between scenes (Furby & Campbell 2001). The image normalization process removes time- and scene-dependent effects in remotely sensed data. Acquisition conditions are not consistent, due to the presence of differences in atmospheric absorption and scattering, sensor-target illumination geometry, and sensor calibration.

The basic premise in using remote sensing data for change detection is that changes in Earth's surface must result in changes in radiance values. These changes in radiance due to surface change must be large with respect to radiance changes caused by other factors (Ingram et al. 1981, Singh 1989). These factors consist of:

a) differences in atmospheric conditions,
b) differences in Sun angle and
c) differences in soil moisture

When satellite images collected over a long time period are to be compared, it is necessary to convert the radiance values recorded by the sensor into reflectance factors in order to eliminate the effects of variable irradiance over the seasons of the year. *Reflectance* is the dimensionless ratio of the irradiance and the radiant emittance of an object (Mather 2004). It is independent of irradiance, as it is a ratio. Following the law of energy conservation, the value of the reflectance is in the inclusive interval 0 to 1. The use of reflectance instead of radiance has the following advantages:

- ✓ The cosine effect of different solar zenith angles due to the time difference between image acquisitions is removed. It compensates for different values of the exoatmospheric solar irradiances arising from spectral band differences

At first, only Landsat images, which were acquired within one day of *in situ* data collection, were radiometrically calibrated. Two different methods of radiometric calibration were used with those images:

a) By conversion to top-of-atmosphere (TOA) reflectance from digital numbers (DN), without atmospheric correction. *TOA reflectance* is the reflectance measured by a space-based sensor flying higher than the Earth's atmosphere. This conversion resulted in the reduction of variability between images. Converting raw digital numbers (DN) in the images to the exoatmospheric or top-of-atmosphere reflectance (TOA) removes the effects of differences in illumination geometry (Collett et al.1997, Mahiny & Turner 2007).
b) By conversion to surface reflectance from digital numbers (DN) followed by atmospheric correction, via Landsat Ecosystem Disturbance Adaptive Processing System (LEDAPS) and L8SR, for the determination of surface

reflectance. Surface reflectance was estimated in order to distinguish the aerosol signals from the measured exoatmospheric reflectance.

Whichever of these two methods yielded better results with respect to the data derived from *in situ* measurements, was used in all the remaining images, in order to obtain a time-series.

### 5.2.1 Conversion of DNs to Physical Units

In order to detect and quantify changes on the Earth's surface, satellite sensors must provide calibrated and consistent measurements. For a better comparison of the data between images taken from different acquisition dates and by different sensors, Digital Numbers (DNs) from image data were converted to spectral radiance ($L_\lambda$) and top-of-atmosphere (TOA) reflectance ($\rho_P$). Also temperature was estimated from all Landsat images using the respective thermal bands. For Landsat TM and ETM+ data conversion, the process described by Chander & Markham (2003) was followed, while Landsat 8 DNs were rescaled, adopting the procedures described by Zanter (2015).

***Conversion to Radiance***

**Landsat-5/TM and Landsat-7/ETM+**

The conversion of DNs to radiance is the fundamental step in setting a common radiometric scale for all Landsat images. The conversion from Calibrated Digital Numbers ($Q_{cal}$) to at - sensor spectral radiance ($L_\lambda$) can be performed using the following equation:

$$L_\lambda = \left(\frac{LMAX_\lambda - LMIN_\lambda}{Q_{cal\,max}}\right) Q_{cal} + LMIN_\lambda$$

where ($\boldsymbol{L_\lambda}$) spectral radiance at the sensor's aperture, in W/(m$^2$ sr $\mu$m)
($\boldsymbol{Q_{cal}}$) quantized calibrated pixel value in DNs
($\boldsymbol{Q_{cal\,max}}$) maximum quantized calibrated pixel value (DN = 255) corresponding to ($LMAX_\lambda$)
($\boldsymbol{Q_{cal\,min}}$) minimum quantized calibrated pixel value (DN = 0) corresponding to ($LMIN_\lambda$)
($\boldsymbol{LMAX_\lambda}$) spectral radiance that is scaled to ($Q_{cal\,max}$), in W/(m$^2$ sr $\mu$m)
($\boldsymbol{LMIN_\lambda}$) spectral radiance that is scaled to ($Q_{cal\,min}$), in W/(m$^2$ sr $\mu$m)

**Landsat-8/OLI**

The Calibrated Digital Numbers ($Q_{cal}$) were converted to spectral radiance using the radiance scaling factors, which were provided in the metadata file of each Landsat image:

$$L_\lambda = M_L \cdot Q_{cal} + A_L$$

where ($\boldsymbol{L_\lambda}$) spectral radiance at the sensor's aperture, in W/(m$^2$ sr $\mu$m)

($M_L$) radiance multiplicative scaling factor for the band (RADIANCE_MULT_BAND from the metadata file)
($A_L$) radiance additive scaling factor for the band (RADIANCE_ADD_BAND from the metadata)
($Q_{cal}$) quantized calibrated pixel value in DNs

***Radiance to TOA reflectance***

**Landsat-5/TM and Landsat-7/ETM+**

The data were normalized to TOA reflectance using the following approach:

$$\rho_P = \frac{\pi \cdot L_\lambda \cdot d^2}{ESUN_\lambda \cdot \cos \vartheta_s}$$

where ($\rho_P$) planetary reflectance (unitless)
($L_\lambda$) spectral radiance at the sensor's aperture
($d$) Earth-sun distance in astronomical units
($ESUN_\lambda$) mean solar exoatmospheric irradiances W/(m$^2$ sr $\mu$m)
($\vartheta_s$) solar zenith angle in degrees

The $d$ values per day were downloaded from NASA [url20] . The solar zenith angle $\vartheta_s$ is the angle between the zenith and the center of the sun's disk. The elevation of the sun (solar elevation angle) and solar zenith angle are complementary. As a result, the determination of solar zenith angle $\vartheta_s$ was achieved using the values of sun elevation from each Landsat image metafile.

Table 8 summarizes the values of solar exoatmospheric spectral irradiances that were used for Landsat TM and ETM+ data calibration.

**Table 8.** The values of solar exoatmospheric spectral irradiances, which were used for data calibration, per Landsat mission.

| Band | Solar Exoatmospheric Irradiances W/(m$^2$ sr $\mu$m) | |
|---|---|---|
| | **Landsat TM** (Chander & Markham 2003) | **Landsat ETM+** [url21] |
| 1 | 1957 | 1970 |
| 2 | 1825 | 1842 |
| 3 | 1557 | 1547 |
| 4 | 1033 | 1044 |
| 5 | 214.9 | 225.7 |
| 7 | 80.72 | 82.06 |
| 8 | | 1369 |

**Landsat-8/OLI**

$ESUN_\lambda$ values have not been provided for Landsat 8 data - Landsat 8 adopted two independent National Institute for Standards and Technology (NIST) traceable radiance and reflectance calibration methods. The coefficients that are necessary for the

conversion are provided by the metadata files. The following equation was used to convert Level 1 DN values to TOA reflectance:

$$\rho\lambda' = M_\rho \cdot Q_{cal} + A_\rho$$

where ($\boldsymbol{\rho\lambda'}$) TOA planetary spectral reflectance (without correction for solar angle)
($\boldsymbol{M_\rho}$) reflectance multiplicative scaling factor for the band (REFLECTANCEW_MULT_BAND from the metadata file)
($\boldsymbol{A_\rho}$) reflectance additive scaling factor for the band (REFLECTANCE_ADD_BAND from the metadata file)
($\boldsymbol{Q_{cal}}$) quantized calibrated pixel value in DNs

The true TOA reflectance was calculated using the equation:

$$\rho_\lambda = \frac{\rho\lambda'}{\sin\vartheta}$$

where ($\boldsymbol{\rho_\lambda}$) TOA planetary reflectance (unitless)
($\boldsymbol{\vartheta}$) solar elevation angle

The solar elevation angle was provided from the metadata file of each Landsat 8 image.

**Sentinel-2**

The Sentinel-2 images (Level 1C) products were already standard products of TOA reflectance. Reflectance is converted into integer values, in order to preserve the dynamic of the data by applying a fixed coefficient (1000 by default). As a result there was no need for radiometric calibration.

The numeric digital counts of each pixel image $(i, j)$ and each spectral band are converted to TOA reflectance $(\rho)$. This conversion takes into account the equivalent extra-terrestrial solar spectrum, the incoming solar direction defined by its zenith angle for each pixel of the image and the absolute calibration of the instrument MSI. The conversion equation is *[url28]*:

$$\rho_\kappa(i,j) = \frac{\pi \cdot CN_{k,NTDI}(i,j)}{A_{k,NTDI} \cdot E_S \cdot d(t) \cdot \cos(\vartheta_s(i,j))}$$

where $\boldsymbol{(CN_{k,NTDI})}$ is the equalized numeric digital count of the pixel $(i, j)$ with NDTI, the number of Sentinel-2 TDI lines
($\boldsymbol{E_S}$) is the equivalent extra-terrestrial solar spectrum and depends on the spectral response of the Sentinel-2 bands
($\boldsymbol{d(t)}$) is the correction for the Earth-sun distance variation. It utilizes the inverse square law of irradiance, under which, the intensity of the light radiating from a point source is inversely proportional to the square of the distance from the source.

$$d(t) = \frac{1}{(1 - 0.01673 \cdot \cos(0.0172 \cdot (t - 2)))^2}$$

where $(\boldsymbol{t})$ is the Julian Day corresponding to the acquisition date

***Landsat Thermal Band / at-satellite Temperatures***

**Landsat-5/TM and Landsat-7/ETM+**

Effective at-satellite temperature was calculated using spectral radiance of thermal band from Landsat images. The effective at-satellite temperature of the imaged Earth surface assumes unity of emissivity (Chander & Markham 2003). The effective at-satellite temperature was computed as follows:

$$T = \frac{K2}{\ln(\frac{K1}{L_\lambda} + 1)}$$

where $(\boldsymbol{T})$ effective at-satellite temperature, in Kelvin
$(\boldsymbol{K1})$ calibration constant 1, in W/(m$^2$ sr $\mu$m)
$(\boldsymbol{K2})$ calibration constant 2, in Kelvin
$(\boldsymbol{L_\lambda})$ spectral radiance at the sensor's aperture

Table 9 summarizes the calibration constants, which were used for Landsat TM and ETM+ thermal band calibration. For Landsat 8 the constant values were provided from the metadata file (K1_CONSTANT_BAND and K2_CONSTANT_BAND)

**Table 9.** Landsat TM and ETM+ thermal band calibration constants.

| | Reference | K1 [W/(m$^2$ sr µm)] | K2 (Kelvin) |
|---|---|---|---|
| **Landsat-5/TM** | Chander & Markham 2003 | 607.76 | 1260.56 |
| **Landsat-7/ETM+** | *[url21]* | 666.09 | 1260.56 |

**Landsat-8/OLI**

TIRS band data can be converted from spectral radiance to brightness temperature using the thermal constants provided in the metadata file (USGS 2016):

$$T = \frac{K2}{\ln(\frac{K1}{L_\lambda} + 1)}$$

where $(\boldsymbol{T})$ At-satellite brightness temperature (K)
$(\boldsymbol{K1})$ Band-specific thermal conversion constant from the metadata (K1_CONSTANT_BAND_x, where x is the thermal band number)
$(\boldsymbol{K2})$ Band-specific thermal conversion constant from the metadata (K2_CONSTANT_BAND_x, where x is the thermal band number)
$(\boldsymbol{L_\lambda})$ TOA spectral radiance (Watts/(m$^2$*srad*µm))

### 5.2.2 Atmospheric correction

Earth's atmosphere mainly consists of carbon dioxide, water vapor and ozone. These elements interact with the electromagnetic radiation.

- ✓ Carbon dioxide is uniformly mixed up to about 100 km in Earth's atmosphere (Elachi & Zyl 2006). It interacts with electromagnetic radiation in the infrared region (4.3-15 μm) of the EMR spectrum. Carbon dioxide is responsible for the cooling of the mesosphere as it emits radiation.
- ✓ Water vapor is related with the cloud formation, precipitation, and energy transfer in the form of latent heat. Water vapor concentration varies spatially and temporally. Clouds scatter and, to some extent, absorb electromagnetic radiation in the visible and near-IR (NIR) regions up to 3 μm of the EMR spectrum.
- ✓ Ozone is located at 20-50 km altitude, and its distribution varies. It absorbs ultraviolet radiation and causes a shortwave cutoff of the Earth's transmission at 0.3 μm or shorter.

Additionally, Earth's atmosphere includes a number of other minor constituents, which play a major role in the atmosphere chemistry. Figure 19 shows the absorption of the main atmosphere components along a vertical atmosphere path in the spectral region from 1 to 16 μm of the EMR spectrum.

In remote sensing, the particles, which are suspended in the atmosphere are called "aerosol" (Njoku 2014). These particles are atmospheric dust particles of radii between 0.1 and 10 μm. Clouds of liquid and solid water include particles of size varying between 1 and 100 μm. They may be produced naturally (volcanoes, desert winds, breaking waves) or by human activities (fossil fuel and agricultural burning and altering of the natural land surface cover). The amount and the type of aerosol amount and type vary spatially and temporally in Earth's atmosphere. Particles are located in the lowest few kilometers and scatter radiation in the visible and near- to mid-IR regions of the EMR spectrum. Aerosols scatter more than 90 % of the visible light, whereas nearly 70% of Earth's surface is dark water (Njoku 2014). As a result particles tend to cool down Earth, by making it more reflective.

There are a number of applications of remote sensing, which can be successful, without applying atmospheric correction, such as classification and mapping. In these procedures, the magnitude of the difference, the direction and the sign of the difference is not important, as nothing is gained by correcting radiance values for atmospheric effects (Rollin et al. 1985). However in remote sensing some procedures are used to measure physical attributes of the Earth's surface and, as a result, accurate radiometry is necessary, providing results that are free from the effects of the atmosphere. Usually, the atmosphere effects have to be removed from satellite data when (Rollin et al. 1985):

- ✓ absolute values of the Earth's surface radiance must be calculated
- ✓ relatively small differences at the surface are to be interpreted against a large atmospheric component

✓ multi-temporal data are to be compared

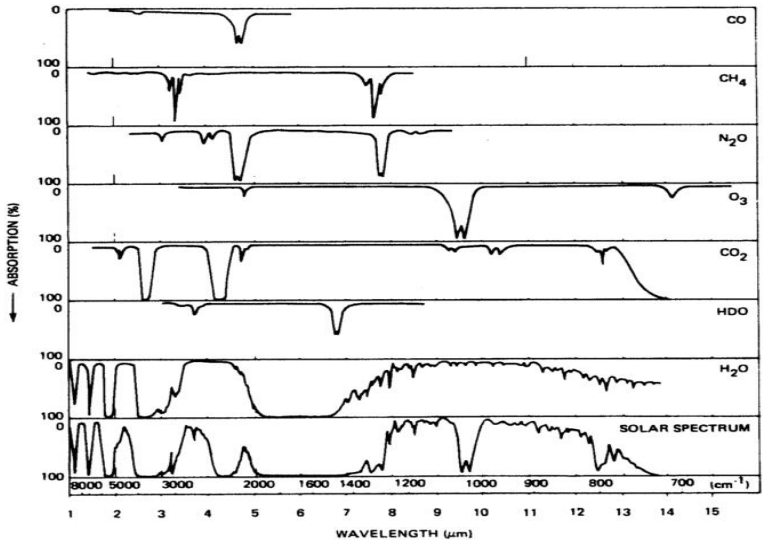


**Figure 19.** Absorption along a vertical atmosphere path by a variety of constituents in the spectral region from 1 to 16 μm (Shaw 1970, Elachi & Zyl 2006).

In the present study, atmospheric corrections were applied to the Landsat images, using the Landsat Ecosystem Disturbance Adaptive Processing System (LEDAPS). More specifically, Landsat-5/TM and -7/ETM+ GeoTIFF images (Level 1 products) were atmospherically corrected using LEDAPS Calibration, Reflectance, Atmospheric Correction Preprocessing Code, Version 2.0 (Masek et al. 2013). The atmospheric corrections were based on the Second Simulation of a Satellite Signal in the Solar Spectrum 6S (Vermote et al. 1997, Kotchenova et al. 2006,) radiative-transfer model used by the Moderate Resolution Imaging Spectroradiometer (MODIS) Land Science Team.

Landsat ETM+ files with extensions '*MTL.txt' or '*.met' and Landsat metadata with extensions '*_WO', and '*MTL.txt' were read by LEDAPS. It produces top-of-atmosphere (TOA) reflectance from digital numbers (DN) and applies atmospheric corrections to generate a surface-reflectance product.

It consists of six modules to execute the following three key steps:

1) Convert Digital Numbers to TOA reflectance
2) Detect pixels containing clouds based on TOA reflectance
3) Convert to surface reflectance from TOA reflectance and auxiliary datasets

The LEDAPS modules that was used is described below, and the overall processing flow that had been presented in Figure 20.

**Module 1 Parameter** – "lndpm" parses the Landsat metadata file and creates the necessary input files that will be used by the following LEDAPS modules.

**Module 2 Calibration** – "lndcal" module calibrates Landsat data from DN to TOA reflectance. Additionally, for the thermal band, DN are calibrated to brightness temperature.

**Module 3 Cloud Shadow Mask** —"lndcsm" is used for the production of a cloud mask based on a pre-2004 C translation of an Interactive Data Language (IDL) Automated Cloud Cover Assessment (ACCA) algorithm.

**Module 4 Surface Reflectance** —"lndsr" computes the surface-reflectance for the Landsat reflectance bands and creates a quality mask for fill, dark dense vegetation (DDV), snow and land/water data.

**Module 5 Surface Reflectance Based Mask** —"lndsrbm" is used for the detection and the creation of cloud, cloud shadow, and adjacent clouds masks using a surface-reflectance based algorithm.

**Module 6 Append** —"lndapp" appends the thermal brightness temperature band, which had been calculated by "lndcal" module, to the surface-reflectance output product.

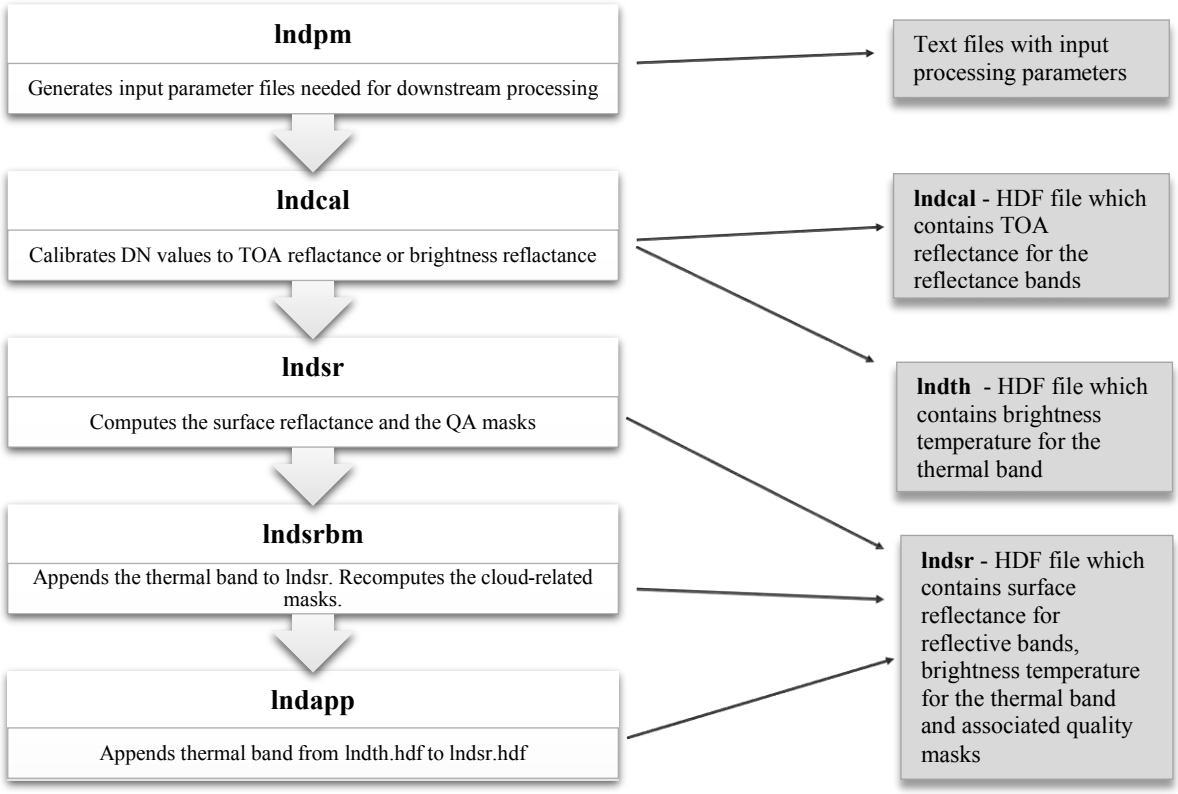


**Figure 20.** LEDAPS Calibration, Reflectance, Atmospheric Correction Preprocessing Code processing flow.

These modules build upon each other by using output from one as input to another, as well as by incorporating auxiliary datasets. LEDAPS utilizes external inputs from:

- ✓ National Centers for Environmental Prediction (NCEP) meteorological reanalysis data,
- ✓ NASA GSFC Ozone Monitoring Instrument (OMI),
- ✓ NASA GSFC Meteor-3 and Nimbus-7 Total Ozone Mapping Spectrometer (TOMS),
- ✓ National Oceanic and Atmospheric Administration (NOAA) Television and Infrared Observation Satellite (TIROS) Operational Vertical Sounder (TOVS), and

- ✓ Global Climate Model (GCM) DEM.

The daily external inputs are needed for the acquisition date of the desired Landsat scene. LEDAPS auxiliary files from 1980 to 2014 were downloaded from USGS *[url17]*. In cases where TOMS data are not available (for example, 1994–96), TOVS data were used. Scripts developed at USGS EROS are used to download the inputs, sort the files by years, save them to subdirectories, and reformat them into Hierarchical Data Format (HDF).

Landsat-8/OLI GeoTIFF images were atmospherically corrected using L8SR *[url18]* algorithm. This method currently uses the scene center for the sun angle calculation and then hardcodes the view zenith angle to 0. The solar zenith and view zenith angles are used for calculations as part of the atmospheric correction. This algorithm differs from the LEDAPS algorithm used by USGS to process Landsat 4–5 TM and Landsat 7 ETM+ Level 1 products to Surface Reflectance (Table 10). Landsat OLI products were converted to the ESPA, in order to import the data to the L8SR application.

**Table 10.** Differences between Landsat-5/TM, -7/ETM+ and Landsat-8/OLI Surface reflectance algorithms.

| Parameter | LEDAPS | L8SR |
|---|---|---|
| (Original) research grant | NASA GSFC, MEaSUREs, (Masek) | NASA GSFC |
| Global coverage | Yes | Yes |
| TOA | Visible (1-5,7) + Brightness temp (6) bands | Visible (1-7, 9) +Thermal (10-11) bands |
| SR | Visible (1-5,7) bands | Visible (1-7) bands (OLI/TIRS only) |
| Radiative transfer model | 6S | Internal algorithm |
| Thermal correction level | TOA only | TOA only |
| Thermal band units | Kelvin | Kelvin |
| Pressure | NCEP Grid | Surface pressure is calculated internally based on the elevation |
| Water vapor | NCEP Grid | MODIS CMA |
| Air temperature | NCEP Grid | MODIS CMA |
| DEM | Global Climate Model DEM | Global Climate Model DEM |
| Ozone | MOI/TOMS | MODIS CMG Coarse resolution ozone |
| AOT | Correlation between chlorophyll absorption and bound water absorption of scene | MODIS CMA |
| Sun angle | Scene center from input metadata | Scene center from input metadata |
| View zenith angle | From input metadata | Hard coded to 0 |
| Undesirable zenith angle correction | N/A | SR not processed when solar zenith angle >76 degrees |
| Pan band processed? | No | No |
| XML metadata? | Yes | Yes |
| Brightness temperature calculated | Yes (Bands 6 TM/ETM+) | Yes (Bands 10 &11 TIRS) |
| Cloud mask | CFmask | CFmask |
| Data format | INT16 | INT16 |
| Fill values | -9999 | -9999 |
| QA bands | Cloud | Cloud |
| | Adjacent cloud | Adjacent cloud |
| | Cloud shadow | Cloud shadow |
| | DDV | Aerosols |
| | Fill | Cirrus |
| | Land water | |
| | Snow | |
| | Atmospheric opacity | |

### 5.3 **Area of interest**

All Landsat images were cropped, setting as Area of Interest (AOI) a small area surrounding Lake Koronia. The selected AOI had to fulfill the following criteria:

- ✓ Small spatial subset and file size, facilitating further processing
- ✓ Include the maximum extent of Lake Koronia, regardless of the presence of water in each image

The initial dimension of 7308*6944 pixel was restricted to 403*269 pixels (Figure 21). More specifically, the spatial subset, which was isolated for further processing, included the samples 1141-1544 and the lines 2075-2344 of the Landsat images.

**Figure 21.** An example of cropping a Landsat TM image (LT51830322008091ESA00) to the AOI. The initial dimension of 7308*6944 pixels was restricted to 403*269 pixels.

### 5.4 **Geometric correction**

Geometric distortions are defined as the deviations between the image coordinates and the ideal ones, which correspond to the terrain and would be projected by using an ideal sensor and conditions. These geometric distortions vary considerably with different factors, such as the platform, the sensor, and the associated scanner (Table 11). Geometric distortions make the image non-planimetric and as a consequence a geometric correction procedure must be performed (Jensen 1996), in order to maximize its usefulness for information extraction. The correction of this distortion is necessary, as it repositions the pixels from their original position in the data array into a specified reference grid (Schowengerdt 2007). Orthorectification is a form of pixel by pixel geometric correction that takes into account the relief of the terrain. It is used for the correction of geometric distortion due to topography. This procedure requires a Digital Elevation Model (DEM), as every pixel's location should be adjusted for topographic relief displacement.

**Table 11.** Description of error sources for the two categories, the observer and the observed, with different sub-categories (Weng 2011).

| Category | Subcategory | Description of error sources |
|---|---|---|
| **The observer or the acquisition system** | Platform | Variation of the movement |
| | | Variation in the platform attitude |
| | Measuring instrument | Time variations or drift; clock synchronicity |
| | Sensor | Variations in sensor mechanics |
| | | Lens distortions |
| | | Viewing angles |
| **The observed** | Atmosphere | Refraction and turbulence |
| | Map | Geoid to ellipsoid, ellipsoid to map |
| | Earth | Curvature, rotation, topographic effect |

Three steps, known as warping (Wolberg 1990) should be followed:

- ✓ **Selection of the appropriate mathematical distortion model**. The suitable method of geometric correction should be selected considering the type of geometric distortion as well as the available reference data.
- ✓ **Coordinate transformation interpolation and resampling**

Once the suitable transformation model $f$ is found, it is used to correct the distorted image coordinates $(x, y)$ to the reference coordinates $(x_{ref,}y_{ref})$.

$$(x, y) = f(x_{ref}, y_{ref})$$

The coordinates $(x, y)$, in general, will not be integer values and as a result a new pixel must be "created" between the existing using an interpolation method, known as resampling. The output of the resampling procedure is a corrected image, in which each $(x_{ref,}y_{ref})$ location of a new, empty array is filled with the pixel calculated at $(x, y)$ in the distorted image. This mapping from $(x, y)$ to the reference coordinates $(x_{ref,}y_{ref})$ avoids overlapping pixels and locations that have no assigned pixels in the corrected image (Schowengerdt 2007). Resampling can be defined as a convolution of the distorted image with a moving window function, as in spatial filtering (Schowengerdt 2007). There are three resampling methods:

- ✓ **Nearest neighbor (or zero-order interpolation):** This is the simplest method of resampling. It uses the value of the pixel in the untransformed image that is closest to the reference coordinates. As a result, geometric discontinuities on the order of plus or minus one-half pixel are produced in the corrected image (Schowengerdt 2007). This method is fast and ensures that the pixel values in the corrected image are real, as they are copied from the initial image. Nearest neighbor resampling method causes a rather blocky effect, as some pixel values are repeated (Mather 2004).
- ✓ **Bilinear interpolation:** This method uses the four pixels that surround the point $(x, y)$ in order to recalculate the value of the output pixel. Usually, bilinear interpolation is implemented by first convolving the input image along its rows, creating new columns in the resampled image and then along the new columns to create new, resampled rows, with a triangle weighting

function in both directions (Schowengerdt 2007). It is an averaging process, resulting a smoother output image. If the point $(x, y)$ is coincident with any the four pixel centers in the initial image, the method breaks down (Mather 2004).

- ✓ **Bicubic interpolation (second-order):** The bicubic interpolation process is based on the fitting of two third-degree polynomials to the region surrounding the point $(x, y)$. It tends to give a more natural-looking image without the blockiness of the nearest neighbor or the over-smoothing of the bilinear method. Bicubic interpolation can be accomplished using either Lagrange polynomials, cubic splines, or a cubic convolution algorithm. The values of the 16 nearest pixel in the initial image are used to estimate the value at $(x_{ref,}y_{ref})$ on the corrected image. Bicubic interpolation is more complicated than either the nearest neighbor or the bilinear methods, but gives a more natural-looking result (Mather 2004).

For the present study, as mentioned in Chapter 4.2, Landsat Level 1T products, in map projection UTM, Zone 34N and datum WGS84, were used. Precision and terrain correction have been applied to these products. This procedure provides radiometric and geodetic accuracy to the image by combining ground control points while employing a Digital Elevation Model (DEM) for topographic displacement. The image quality and the accuracy, number and distribution of Ground Control Points (GCPs) influence the product's geodetic accuracy. The GCPs points used for Level 1T correction are currently based on the Global Land Survey (GLS) reference database. This reference database has being revised using Landsat OLI data within the GCP improvement plan. The elevation data used for relief displacement of the L1T products consist of Shuttle Radar Topography Mission (SRTM), National Elevation Dataset (NED), Canadian Digital Elevation Data (CDED), Digital Terrain Elevation Data (DTED), Global 30 Arc-Second Elevation (GTOPO30) and Greenland Ice Mapping Project (GIMP) source DEMs. However, geometric distortions (geolocation errors of up to several kilometers) were identified in some of the available Landsat images (Figure 22).

**Figure 22.** An example of geometric distortion. The procedure of selecting the AOI has initially failed, due to an error of the original image geocoding by several km. Such errors have been corrected, via orthorectification of the original image.

The GCPs that were used for the orthorectification of these images were available from Mouratidis et al. (2010). GCPs were in geographic coordinates (WGS84). In order to apply corrections due to topography, a processed SRTM 90m (Data Version 4.1) DEM was downloaded from CGIAR-CSI *[url19]*. The coordinates of the DEM's center point were 42.50N (Latitude) and 22.50E (Longitude). The downloaded data were in ARC GRID, ARC ASCII and GeoTIFF format, in decimal degrees and datum WGS84.

The GCPs were collected in 2008 (Mouratidis et al. 2010). With the intention of limiting errors caused by GCPs change over time, two Landsat TM images (path:183/184), that were acquired in 2008 were selected (Table 12). The selected images had no cloud coverage.

**Table 12.** The characteristics of the Landsat TM images that were orthorectified, using the GCPs available from Mouratidis et al. (2010).

| Image ID | Path | Acquisition Date |
|---|---|---|
| **LT51830322008123ESA00** | 183 | 2/5/2008 |
| **LT51840322008242ESA00** | 184 | 29/8/2008 |

Erdas Imagine 2014 was used for the orthorectification procedure. The GCPs were selected taking into consideration the following characteristics:

- ✓ High contrast in the selected images
- ✓ Small feature size
- ✓ Easy identification (road intersections, river features, corners of agricultural fields)
- ✓ Optimal distribution across Mygdonia basin

To obtain good accuracy of geometric correction, GCPs were distributed equally in the image (Figure 23). The process was repeated, until the accuracy was less than 0.5 pixel (15m). Table 13 summarizes the number of the selected GCPs per image and the Control Point Error (X, Y and Total). The corrected images were resampled using bilinear interpolation.

**Table 13.** The number of the selected GCPs per Landsat TM image and the accuracy of the orthorectification process.

| Image ID | No. of GCPs | CPE* (X) (m) | CPE* (Y) (m) | CPE* (Total) (m) |
|---|---|---|---|---|
| **LT51830322008123ESA00** | 20 | 9.4669 | 9.8765 | 9.8765 |
| **LT51840322008242ESA00** | 18 | 9.5503 | 2.7985 | 9.9519 |

*Control Point Error

(a)

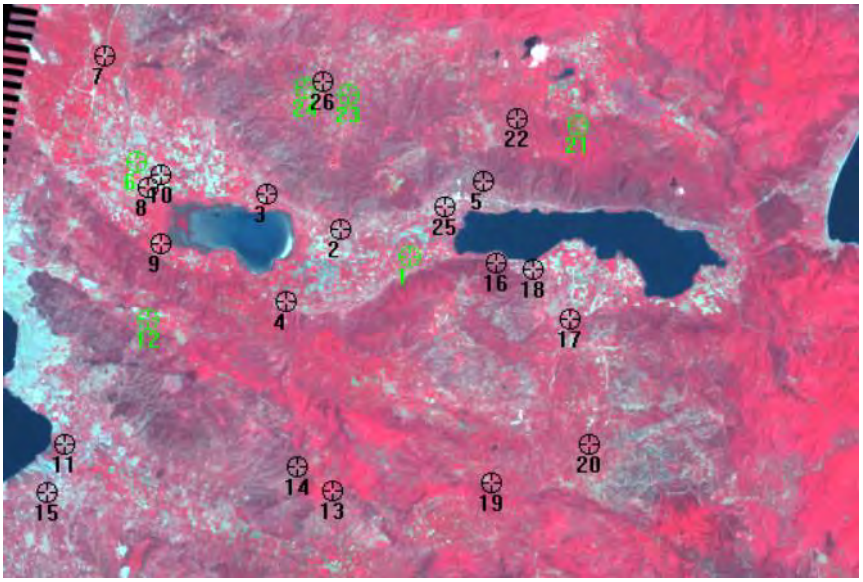


(b)

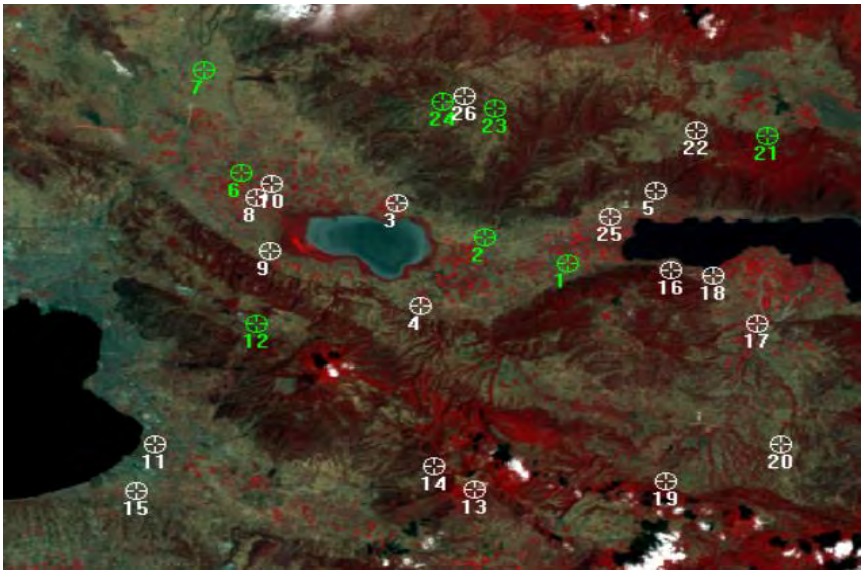


**Figure 23.** The distribution of GCPs on the Landsat images: a) LT51830322008123ESA00 image, b) LT51840322008242ESA00 image. The green GCPs were not used for the image orthorectification.

These two orthorectified Landsat TM images were used as base images to the image co-registration process of the distorted images. Image co-registration is defined as the geometrical aligning of two or more images to integrate or fuse corresponding pixels that represent the same objects. The automatic image to image registration was carried out using ENVI 4.8. The selected warp band, as well as the master band, for image to image co-registration was the red band. The automatic image to image co-registration tool uses area-based matching to acquire tie points. This matching method compares the pixel values of patches of two or more images and determines conjugate image locations based on similarity in those pixel value patterns. The results of area-based matching largely depend upon the quality of the approximate relationship between the base image and the warp image. The following parameters were set:

- ✓ **Number of Tie Points:** The number of tie points was specified. The recommended value 25 was selected.

- ✓ **Search Window Size:** The size of the search window, in square pixels, was defined. It is a subset of the image, within which a smaller area is scanned, in order to determine a topographic feature match for tie point placement. The Search Window Size must be larger than the Moving Window Size. If a large value is used, there is a greater chance of finding the conjugate point, but the process takes more processing time. However, setting an excessively large value may cause false matches, as more similar points exist in a wider area. The default value 81 was used.
- ✓ **Moving Window Size:** The Moving Window scans the image subset area determined be the Search Window Size, in order to match topographic features of the two images. For a 10 m or higher resolution image, a range of 9-15 square pixels should be used. The value 12 was used.
- ✓ **Area Chip Size:** Area Chip Size is the image chip size that was used to extract tie points. The default size 128*128 was used.
- ✓ **Minimum Correlation:** It is the minimum correlation coefficient required in order to consider an object as a tie point. The larger Moving Window Size, the smaller value of Minimum Correlation is used. The 0.8 value was set to this field.
- ✓ **Point Oversampling:** The number of tie points that was collected from a single image chip was specified. The value 1 was used.
- ✓ **Interest Operator:** The Forstner operator was applied to the image to image co-registration. This method obtains and analyzes the gray scale gradient matrix between one pixel and its adjacent pixels.

Given a reference map projection or a reference image, which is either geometrically correct or regarded as a geometric basis of a set of images, the main task of geometric operations is to establish a deformation model between the input image and the reference and then to rectify or co-register the input image to the reference, in order to generate an output image. Polynomial warping, which is one of the most important and commonly used geometric transformation for remotely sensed image data, was applied. The polynomial degree that was applied was dependent on the number of the GCPs, where the number of GCPs was larger than the $(\text{degree} + 1)^2$. The geometric transformation includes two major steps:

1. Establish the polynomial deformation model. This is usually done using ground control points (GCPs).
2. Image resampling based on the deformation model. This includes resampling image pixel positions (coordinates) and DNs.

The nearest neighbor resampling method was applied to the corrected image.

### 5.5 **Water-only image**

In order to get useful data from the lake water itself, the measured pixel should not contain anything else than water, but close to the shoreline the ‘water’ pixels usually contain land. The same kind of problems may occur because of islets in the lakes.

Another similar effect is caused by the water vegetation reaching the surface or bottom of the lake. Several methods have been evaluated for delineating water bodies and for the enhancement of their presence in satellite images. Usually, these methods make use of (Paris 1992):

- ✓ Reflected solar radiation
- ✓ Emitted thermal radiation
- ✓ Active microwave emission

According to the number of image bands used, there are two procedures for the extraction of water features (Xu 2006): a) single band and b) multi-band methods. Generally, a single band method involves the use of a single band from a multispectral satellite image (Rundquist et al. 1987). For the water body extraction, a threshold for the band is set. However, this may lead to an over- or under-estimation of the water body and the extracted information often contains shadow noise (Xu 2006). Multi-band methods use a combination of multiple bands for separating water bodies from terrestrial features. Signature differences between water and other surface features can be determined by analyzing the signature difference among different bands. Water extraction is achieved using logic statements. Alternatively, a band ratio of two bands can be used. One band uses visible wavelengths and is divided by another one, usually a NIR band.

Water-only images were created in order to remove unneeded data and differentiate water from land areas. Additionally, water-only images were used for the creation of pixel level condition maps of the Lake. The isolation of the area of Lake Koronia, which was covered with water, was performed using the Normalized Difference Water Index (NDWI) (McFeeters 1996). In order to extract a water-only image from each AOI Landsat image, from 1984 to 2016, a function was developed in MATLAB R2015b. Figure 24 summarizes the process that was followed for the extraction of Lake Koronia from the Landsat images. Firstly, NDWI was calculated using the following equation (McFeeters 1996):

$$NDWI = (GREEN - NIR)/(GREEN + NIR)$$

where **GREEN** is the band that includes reflected green light and **NIR** is the reflected near-infrared radiation.

NDWI has an advantage as it is characterized by:

- ✓ the maximization of water reflectance, using green band
- ✓ the minimization of low NIR reflectance by water
- ✓ high reflectance of NIR by vegetation and soil features

As a consequence, NDWI has positive values for water features and zero or negative values for vegetation and soil.

Since the optical properties of Lake Koronia vary temporally and spatially, the water extraction cannot be based on one standard cut-off value. Unsupervised classification, k-means, was performed to the NDWI Landsat-5/TM,-7/ETM+ (SLC ON) and -8/OLI

images to distinguish water from land. Two classes were specified, one for the land area and one for the water features. In order to avoid the isolation of water features that are not included in Lake Koronia, a neighbor expansion method was followed. A clearly recognizable pixel of Lake Koronia that was consistently covered with water during the period 1984 - 2016 was selected. The class that included the selected pixel was characterized as the water class. Once the water class was identified, the class of the adjacent 8 pixels was checked. In case the adjacent pixels belonged to the water class, the class of the adjacent pixels, which had not been checked previously, was determined. Every time a neighboring pixel is found to belong to the class, it is included in the mask and a new "expansion wave" begins from this pixel. If one pixel did not belong to the water class, the pixels that surround it would not be checked. The process finished and the mask was created when there was no pixel, the neighboring pixels of which belonged to the water class. As the water class pixels had been identified, they were used as a binary mask to remove unneeded areas from the AOI Landsat image. The value of the pixels included in water mask was set at 255, while the value of the excluded pixels had 0 value.

From the above description, it is relatively easy and intuitive to infer that the computational complexity of the process is non-polynomial, which means, merely, that the computational load becomes disproportionately more cumbersome as the expected number of total pixels increases, even slightly. For this reason, the process of creating a mask for every image took a large amount of time. An alternative version of the algorithm examines neighboring areas instead of neighboring pixels, in order to speed up the process at the cost of a small tolerance for including a few pixels not contained in the water class.

Both supervised and unsupervised classification procedures are frequently applied for identifying and classifying water features in images. A supervised maximum-likelihood classification was used by Kingsford et al. (1997) to map wetlands on Landsat MSS imagery. However, supervised methods require a priori knowledge about the number of classes and the spectral signature attributed to each class in the scene. Unsupervised classification based on “isodata” (Iterative Self-Organizing Data Analysis Technique) or “k-mean” clustering is often used to generate spectral signatures of each class (Kloiber et al. 2002, Olmanson et al. 2008, Reis and Yilmaz 2008). The created water mask did not include cloud shadows, haze or other distortions (Figure 25).

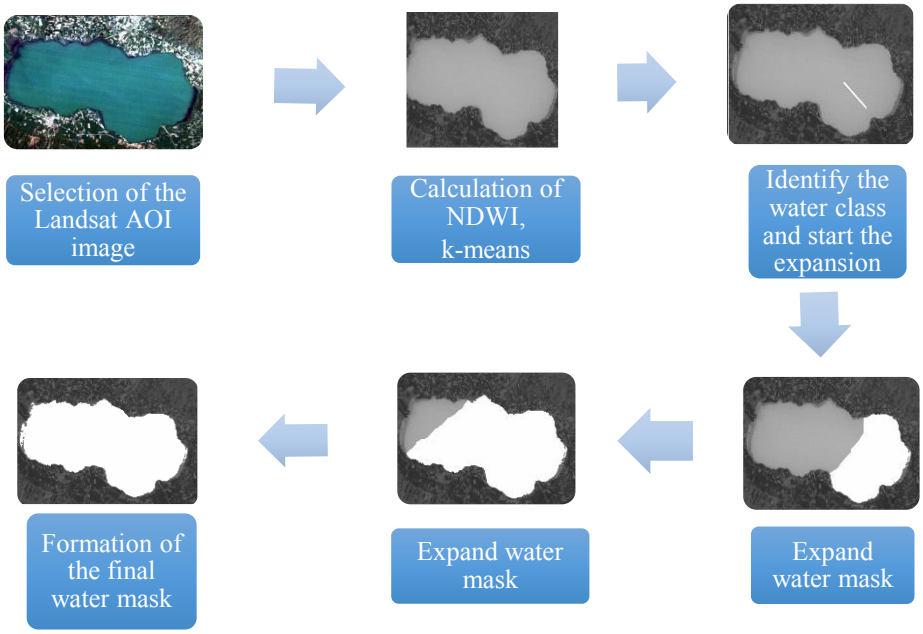


**Figure 24.** The steps that were followed for the creation of a water mask. In this example a Landsat TM image (LT51840321984128ESA00) was used. The value of the pixels included in water mask was set at 255.

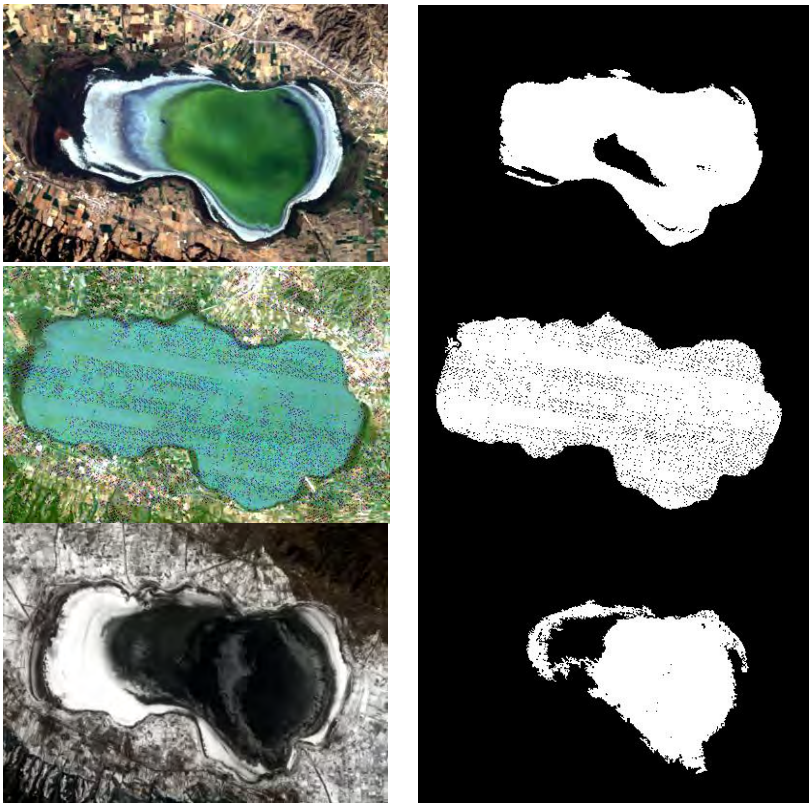

a) Algae coverage

b) Noisy data

c) Cloud coverage

**Figure 25.** The water mask formation in case of a) algae coverage, b) noisy data and c) cloud coverage.

The neighbor expansion method described earlier was modified to accommodate the separation between land and water when using Landsat-7/ETM+ SLC OFF images. The

image pixels were divided in two categories, valid and invalid (erroneous due to observation gaps). Unsupervised classification in two classes followed, using the k-means method for the valid pixels. Three special positions were chosen to assist the process. The initial pixel position, chosen as the northernmost discernible pixel position to be seen as clearly inside the lake, the lake pixel position, defined as a pixel that is always inside the lake, chosen to be as close to the lake's geometric center (centroid) as possible, and the limit pixel position, chosen as the southernmost discernible pixel position to be seen as clearly inside the lake. In case the lake or the initial pixel positions would contain an invalid pixel, the next pixel southwards was checked recursively, until a position with a valid pixel was attained, thus providing valid initial and lake pixel positions.

After classification, the lake pixel position was used to determine the lake class. Starting off from the initial pixel, the aforementioned "expansion wave" technique was used to select the pixels belonging to the lake class (Figure 26). Because gaps confine this expansion wave, the initial pixel position was followed southwards, until the next gap, and over that, tracing the first pixel position belonging to the next area between gaps and triggering a new expansion wave. This process repeated for all lake strips between gaps and ceased when the southward search extended beyond the row of the limiting pixel position. It should be noted that for the consideration of the initial and limit pixel assisting positions, many images were examined and an average lake shape and morphology was considered.

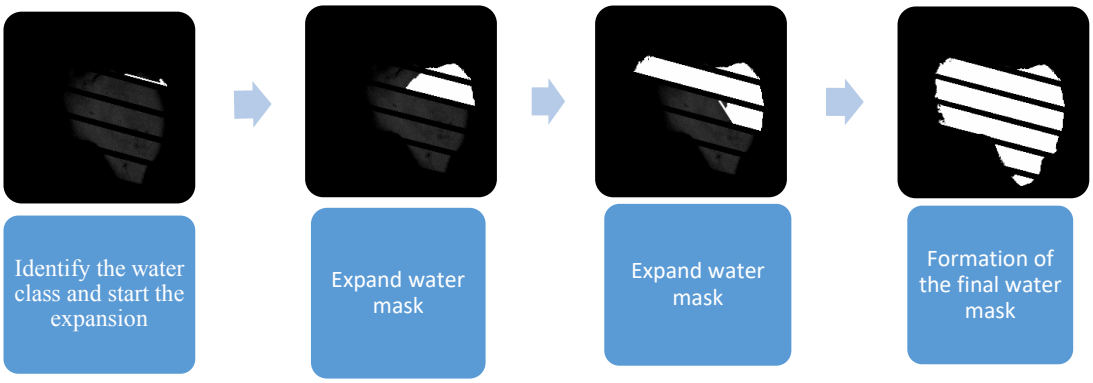


**Figure 26.** The expansion steps that were followed for the creation of a water mask of a Landsat-7/ETM+ SLC OFF image.

For purposes of comparison, the Quality Assessment (QA) bands of the Landsat Surface Reflectance High Level Data Products were used. The water pixels over the area of the lake have been isolated to these products using a different algorithmic procedure by USGS. According to the algorithmic procedure used to derive these products, after studying the open source code of some of the implemented functions *[url23]*, the water isolation criteria were found to be the following:

$$(NDVI < 0.01)\ \boldsymbol{AND}\ (Refl_{NIR} < 0.11)$$
OR
$$(0 < NDVI < 0.1)\ \boldsymbol{AND}\ (Refl_{NIR} < 0.05)$$

Satisfaction of the above criteria leads to characterization of a pixel as a clear water pixel, mentioned as "Zhe's water test" in the original code.

**Sentinel-2**

The NDWI index for Sentinel-2 can be calculated using the following equation (Du et al. 2016):

$$NDWI = \frac{\rho_3 - \rho_8}{\rho_3 + \rho_8}$$

where $(\boldsymbol{\rho_3, \rho_8})$ is the TOA reflectance of the Band 3 (Green band) and Band 8 (NIR band)

Band 3 and 8 have a spatial resolution of 10 m and as a result the NDWI image has also a spatial resolution of 10 m. In order to create the water-only image the neighbor expansion method, evaluated for Landsat-5/TM, -7/ETM+, -8/OLI was used (Figure 27).

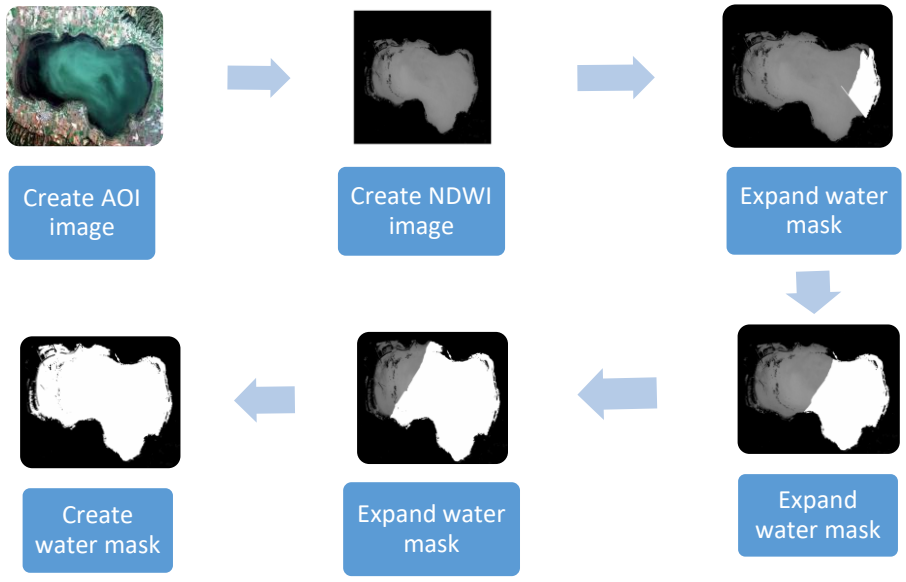


**Figure 27.** The steps that were followed for the creation of a water mask for Sentinel-2 images (Example:16/11/2015).

# 6. *IN SITU* MEASUREMENTS

## 6.1 Chapter overview

*This chapter aims to present the in situ sampling strategy that was adopted for accurate field measurements of QE and adequate spatial coverage of Koronia. In addition to the in situ measurements, it includes information about the in situ data that were provided by Management Authority of Lakes Koronia-Volvi.*

## 6.2 Field work

*In situ* measurements were carried out at three sampling stations in Lake Koronia, on 30 November, 2015. The *in situ* data collection was simultaneous with Landsat 8 overpass. The coordinates of the sampling points (Table 14) were determined using GPS receiver, Garmin GPSMap76S. In order to reduce the geolocation error, the coordinates were determined three times per sampling point and the average value was considered. The distribution of *in situ* sampling points is given in Figures 28-29. Two sampling stations were located at medium depth points and one sampling station was located over the deepest point of Lake Koronia. The location of the sampling stations was selected taking into account an adequate spatial coverage of Lake Koronia.

**Table 14.** The coordinates (Lat/Lon, WGS 84) of the three sampling stations, where *in situ* measurements were carried out on 30 November 2015, in Lake Koronia.

| Sampling Station | Label | | Longitude | Latitude |
|---|---|---|---|---|
| *Station1* | Medium Depth Point 1 (Station 1) | 1 | 023$^{O}$09.079' | 40$^{O}$41.051' |
| | | 2 | 023$^{O}$09.079' | 40$^{O}$41.046' |
| | | 3 | 023$^{O}$09.080' | 40$^{O}$41.049' |
| | | **Average** | **023$^{O}$09.079'** | **40$^{O}$41.049'** |
| *Station 2* | Medium Depth Point 2 (Station 2) | 1 | 023$^{O}$07.509' | 40$^{O}$41.491' |
| | | 2 | 023$^{O}$07.503' | 40$^{O}$41.494' |
| | | 3 | 023$^{O}$07.595' | 40$^{O}$41.496' |
| | | **Average** | **023$^{O}$07.506'** | **40$^{O}$41.493'** |
| *Station 3* | Deep Point (DP) | 1 | 023$^{O}$11.079' | 40$^{O}$40.680' |
| | | 2 | 023$^{O}$11.104' | 40$^{O}$40.681' |
| | | 3 | 023$^{O}$11.106' | 40$^{O}$40.681' |
| | | **Average** | **023$^{O}$11.096'** | **40$^{O}$40.681'** |

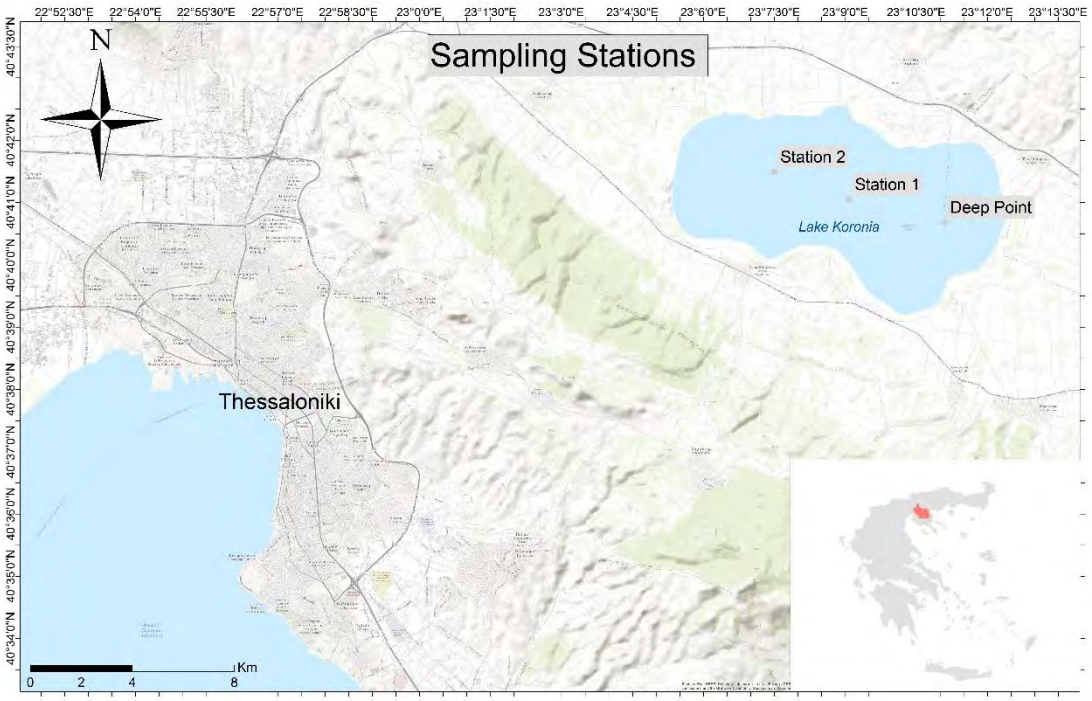


**Figure 28.** The location of *in situ* sampling points in Lake Koronia. The sampling was carried out on 30 November, 2015.

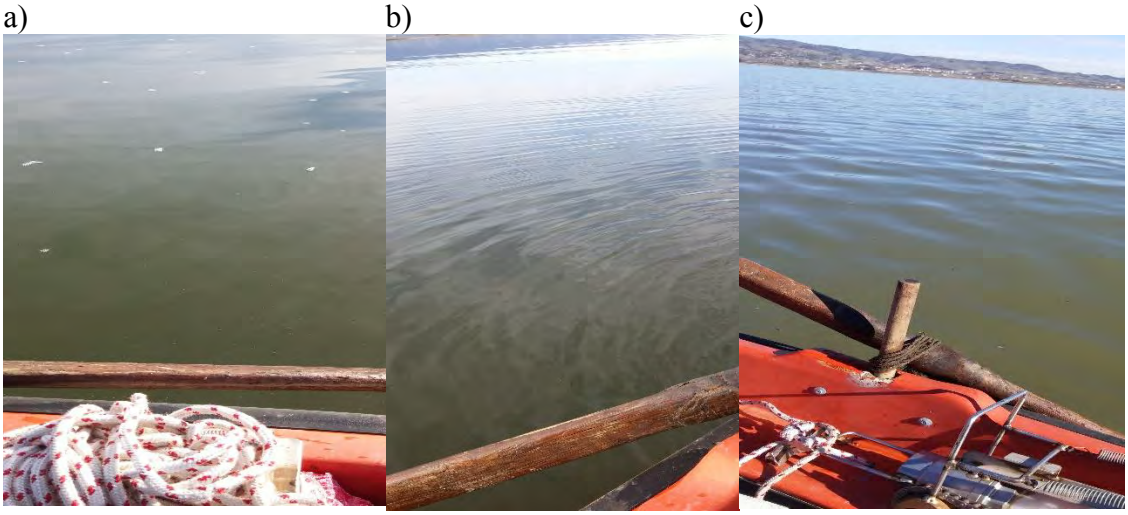


**Figure 29.** Photographs of the three sampling stations: a) Station 1, b) Station 2, c) DP.

Field measurements of Conductivity (μS/cm), Salinity (ppt), Dissolved Oxygen (D.O.) (mg/l), Temperature (°C) and pH were carried out at the three sampling stations, on 30 November, 2015.

Oxi 3205, WTW, Dissolved Oxygen (D.O.) meter, including integrated temperature sensor, was used to perform D.O. and Water Temperature measurements from the upper layer of the surface. After the D.O. sensor was connected to the meter, the meter with the sensor was checked and calibrated. The D.O. sensor was immersed in the upper layer of the water surface. The display of the stable measured value was considered.

pH measurements were estimated using pH 3110, WTW. The pH combination electrode was connected to the meter. The current water temperature was measured. The

meter and the combination electrode were calibrated. The pH combination was immersed in the upper layer of the water surface and the stable measured value was recorded.

Conductivity and Salinity measurements were performed using Cond 3210, WTW. The conductivity measurement cell was connected to the measurement instrument and the measuring cell and cell constant setting were checked. The conductivity measuring cell was immersed in the upper layer of the water surface and the stable measured value was recorded.

Table 15 summarizes the measuring accuracy of Oxi 3205, pH 3110 and Cond 3210 that were used for the field measurements, on 30 November, 2015.

**Table 15.** The measuring accuracy of the equipment that was used for the field QE measurements at Lake Koronia, on 30 November, 2015.

| | **QE/range*** | **Accuracy** | **Temperature of the test sample** |
|---|---|---|---|
| PpH 3110, WTW | -2.0…+20.0 | ±0.1 | +15 ºC…+15 ºC |
| | -2.00…+20.00 | ±0.01 | +15 ºC…+15 ºC |
| | -2.000…+19.999 | ±0.005 | +15 ºC…+15 ºC |
| Oxi 3205,WTW | | ±0.5% of measured value at ambient temperature | +5 ºC…+30 ºC |
| *Temperature sensor* | | ± 0.1 | |
| Cond 3210, WTW *Conductivity* | | ± 0.5% | |
| *Salinity* | | ± 0.1 | +5 ºC…+25 ºC |
| | | ± 0.2 | +25 ºC…+30 ºC |

*The accuracy values specified here apply exclusively to the meter.

Also, at every sampling station, water samples were collected from the upper layer of the water surface, and were filtered through a membrane filter (0.45 pore size). The filtered water sample of each sampling station was poured into a separate vessel (120 ml). These samples were transposed to the laboratory of the Management Authority of Lakes Koronia-Volvi, which is located in Nea Apollonia. The filtered water samples were used for the determination of the concentration of $N\text{-}NO_2$, $N\text{-}NO_3$, $N\text{-}NH_4$, $P\text{-}PO_4$ and Total Nitrogen (TN) (mg/l). For the measurement of $N\text{-}NO_3$ concentration, the Nitrate Cell Test N2/25 Method (173730) was utilized. The method that was adopted was analogous to DIN 38405 D9. In sulfuric and phosphoric solution, nitrate ions reacted with 2,6-dimethylphenol to form 4-nitro,2,6-dimethyphenol, which was determined photometrically. The measuring range of the Nitrate Cell Test N2/25 is 0.5-25.0 mg/l $N\text{-}NO_3$. The standard deviation of the method is ±0.13 mg/l $N\text{-}NO_3$ and the confidence interval is ±0.3 mg/l $N\text{-}NO_3$.

Ammonium Cell Test (114739) was used for the determination of $N\text{-}NH_4$ concentration. The method that was followed was analogous to EPA 350.1, A.P.H.A 4500-$NH_3$ F, ISO 7150-1 and DIN 38406-5. Generally, $N\text{-}NH_4$ occurs partly in the form

of ammonium ions and partly as ammonia. A pH dependent equilibrium exists between the two forms. In strongly alkaline solution ammonium nitrogen is present almost entirely as ammonia, which reacts with hypochlorite ions to form monochloramine. This in turn reacts with a substituted phenol to form a blue indophenol derivative that was determined photometrically. Due to the intrinsic yellow coloration of the reagent blank, the measurement solution was yellow-green to green color. The measuring range of the Ammonium Cell Test is 0.010-2.000 mg/l $N\text{-}NH_4$.The standard deviation of the method is ±0.0146 mg/l $N\text{-}NH_4$ and the confidence interval is ±0.035 mg/l $N\text{-}NH_4$.In order to determine $P\text{-}PO_4$ concentration, Phosphate Cell Test P6/25 (173705) was used. The method that was adopted was analogous EPA 365.2+3, APHA 4500-P E and DIN EN ISO 6878. In sulfuric solution orthophosphate ions reacted with molybdate ions to form molybdophosphoric acid. Ascorbic acid reduced this to phosphomolybdenum blue that was determined photometrically. The measuring range of the Phosphate Cell Test is 0.05-5.00 mg/l $P\text{-}PO_4$. The standard deviation of the method is ±0.023 mg/l $P\text{-}PO_4$ and the confidence interval is ±0.05 mg/l $P\text{-}PO_4$.Total Nitrogen Cell Test (114537) was used for the determination of TN concentration (mg/l). The digestion is analogous to DIN EN ISO 11905-1. Organic and inorganic nitrogen compounds were transformed into nitrate according to Koroleff's method by treatment with oxidizing agent in a thermoreactor. In concentrated sulfuric acid, this nitrate reacted with a benzoic acid derivative to form a red nitro compound that was determined photometrically. The measuring range of Total Nitrogen Cell Test (114537) is 0.5-15.0 mg/l TN. The standard deviation of the method is ±0.14 mg/l TN and the confidence interval is ±0.3 mg/l TN.

### 6.3 **Data provided by Management Authority of Lakes Koronia-Volvi**

In addition to the *in situ* measurements that were carried out on 30 November 2015, *in situ* data of the studied parameters (D.O., Temperature, pH, Conductivity, $P\text{-}PO_4$, $N\text{-}NH_4$, $N\text{-}NO_2$, $N\text{-}NO_3$) were provided by the Management Authority of Lakes Koronia-Volvi. Data of $BOD_5$ and Turbidity measurements were, also, provided. The QE D.O., Temperature, pH, Conductivity, $BOD_5$, Turbidity are measured monthly, as well as nutrients such as $P\text{-}PO_4$, $N\text{-}NH_4$, $N\text{-}NO_2$, $N\text{-}NO_3$ are measured three times a year. These parameters are monitored from two sampling stations (Figure 30) (if/when these sites are covered with water) and as a consequence there is an adequate database of *in situ* measurements that can be used for satellite data calibration.

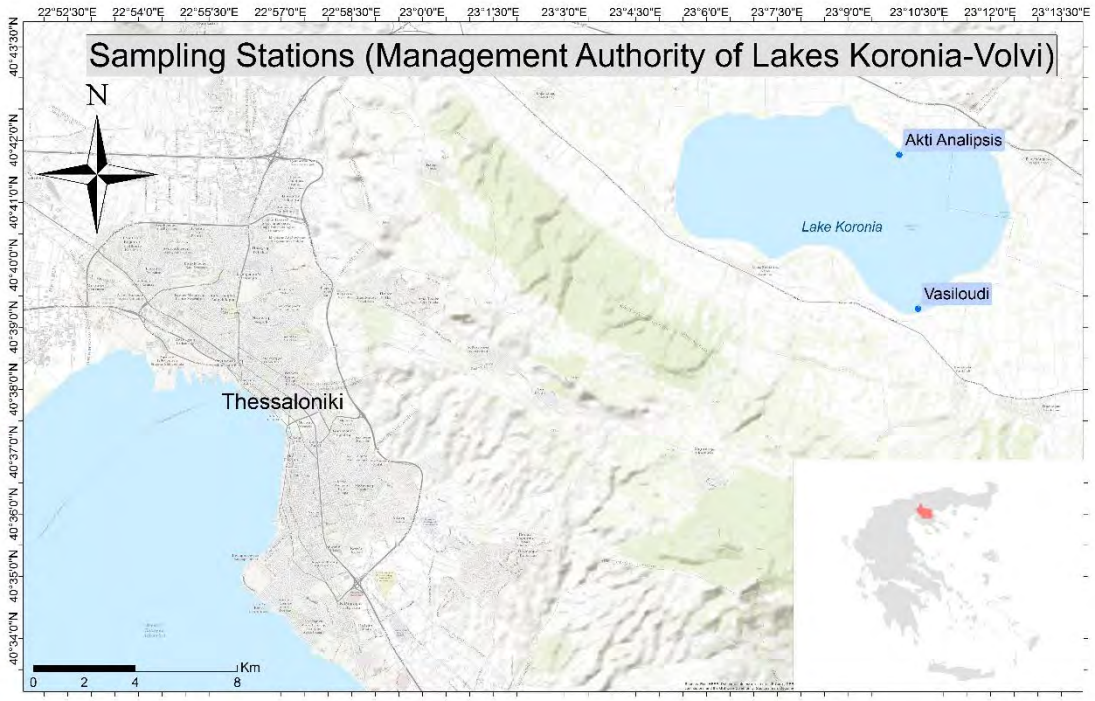


**Figure 30.** The sampling stations of *in situ* measurements provided by Data Management Authorities of Lakes Koronia-Volvi.

The *in situ* data, which were provided, cover a period between 27/4/2009 and 2/11/2014. Table 16 summarizes the methods and the equipment that had been used by the Management Authority of Lakes Koronia-Volvi for the QE measurements, during the period 2009-2014.

The provided *in situ* data, which were collected within ±1 day of a Landsat image acquisition, were selected (Table 17). According to Kloiber et al. (2002), field data collected within one day of the satellite overpass yielded the best calibrations, while the larger number of field measurements with the longer time window offsets some of the loss of correlation. If the *in situ* measurements are sparse, the larger number of field observations with longer time window improve the calibration of the satellite data (Olmanson et al. 2008).

In case of absence of *in situ* measurements of the QE, data available from publications were used (Michaloudi et al. 2009, Michaloudi et al. 2012, Moustaka-Gouni et al. 2012). Michaloudi et al. (2009) and Michaloudi et al. (2012) present the values of physical and chemical parameters in water samples from the deepest point of Lake Koronia during the period from March 2003 to December 2004. Moustaka-Gouni et al. (2012) present phytoplankton data that were collected in years 2003-2007 and 2009-2011.

**Table 16.** The methods and the equipment that had been used by the Management Authority of Lakes Koronia-Volvi for the QE measurements, during the periods 2009-2012 and 2013-2014.

| **2009 - 2012** | | **2013 - 2014** | |
|---|---|---|---|
| QE | Method/Equipment | QE | Method/Equipment |
| D.O. (mg/l) | Multi-Parameter TROLL 9500 | D.O. (mg/l) | Oxi 3205, WTW |
| Water Temperature (ºC) | Multi-Parameter TROLL 9500 | Water Temperature (ºC) | Oxi 3205, WTW |
| Conductivity (μS/cm) | Multi-Parameter TROLL 9500 | Conductivity (μS/cm) | Cond 3210, WTW |
| pH | Multi-Parameter TROLL 9500 | pH | PH 3110, WTW |
| Turbidity (FNU) | Multi-Parameter TROLL 9500 | Turbidity (FNU) | |
| $P\text{-}PO_4$ (mg/l) | A.P.H.A. 1985 | $P\text{-}PO_4$ (mg/l) | Phosphate Cell Test P6/25 (173705) |
| $N\text{-}NH_4$ (mg/l) | A.P.H.A. 1985 | $N\text{-}NH_4$ (mg/l) | Ammonium Cell Test (114739) |
| $N\text{-}NO_2$ (mg/l) | A.P.H.A. 1985 | $N\text{-}NO_2$ (mg/l) | |
| $N\text{-}NO_3$ (mg/l) | A.P.H.A. 1985 | $N\text{-}NO_3$ (mg/l) | Nitrate Cell Test N2/25 Method (173730) |
| $BOD_5$ (mg/l) | Dilution method | $BOD_5$ (mg/l) | Dilution method |

**Table 17.** The dates of the selected *in situ* measurements, which were carried out by the Management Authority of Lakes Koronia-Volvi and the corresponding Landsat image acquisition dates.

| **Akti Analipsis** | | | **Vasiloudi** | | |
|---|---|---|---|---|---|
| Date of field measurements | Satellite overpass | Satellite/Instrument | Date of field measurements | Satellite overpass | Satellite/ Instrument |
| 21/4/2010* | 22/4/2010 | Landsat 5/TM | 21/4/2010* | 22/4/2010 | Landsat 5/TM |
| 23/8/2011* | 23/8/2011 & 22/8/2011 | Landsat 7/ETM+ & Landsat 5/TM | 12/6/2012* | 13/6/2012 | Landsat 7/ETM+ |
| 12/6/2012 | 13/6/2012 | Landsat 7/ETM+ | | | |
| 9/8/2012 | 8/8/2012 | Landsat 5/TM | | | |
| 23/5/2013** | 23/5/2013 | Landsat 8/OLI | | | |
| 11/7/2013** | 11/7/2013 & 10/7/2013 | Landsat 7/ETM+ & Landsat 8/OLI | | | |

*The QE $BOD_5$ (mg/l), $N\text{-}NO_2$ (mg/l), $N\text{-}NO_3$ (mg/l), $P\text{-}PO_4$ (mg/l), $N\text{-}NH_4$ (mg/l) had not been measured.

**The QE $N\text{-}NO_2$ (mg/l), $N\text{-}NO_3$ (mg/l), $P\text{-}PO_4$ (mg/l), $N\text{-}NH_4$ (mg/l) had not been measured.

# 7. WATER QUALITY PARAMETERS EXTRACTION FROM MULTISPECTRAL SATELLITE DATA

## 7.1 Chapter overview

*This chapter lays the theory and methodology needed to relate lake water quality parameters to remote sensing measurements. Hereby presented is a review of the optical properties of lake water, how variations in optics will influence remote sensing measurements and how variations in lake water quality parameters will in turn influence the optical properties. Practical information on the measurement of water quality parameters using remote sensing techniques are also provided.*

## 7.2 Optical properties of pure water

Pure water is a chemically pure substance that consists of water molecules occurring under the natural conditions (Wozniak & Dera 2007). The most common structure of the water molecule is $H_2{}^{16}O$. Additionally, its isotopic variants are $H_2{}^{18}O$, $H_2{}^{17}O$, and $HD^{16}O$ (ratio: 2:0.4:0.3) (Wozniak & Dera 2007).

Each isotope is characterized by unique dynamic, electric, and magnetic properties and the way that it absorbs electromagnetic differs from the spectra of other variants and spectra of $H_2{}^{16}O$ water molecules (Barret & Mansell 1960, Eisenberg & Kauzmann 1969, Greenwood & Earnshaw 1997, Janca et al. 2003, Chaplin 2006). This is due to the fact that the isotopes are characterized by different geometrical structures, characteristic dimensions and mass. The transitions between these different energy states result in the absorption of photons of different wavelengths, which increase as the molecular mass does so.

These differences do not significantly affect the total coefficient of radiation absorption of the pure liquid water, as the overall concentration of $H_2{}^{16}O$ is generally more than a thousand times greater than the concentration the isotopic variants.

Pure water scattering is inversely proportional to wavelength. Pure water displays a backscatter, which emanates to a great extent from multiple molecular scattering and shifts the color towards shorter wavelengths. The transitions between the vibrational-rotational energy states in water molecules result in the strong absorption of NIR by water molecules. Additionally, it acts as a monochromator for blue light absorbing it selectively (Jerlov 1976) and the light absorption increases above 550 nm. Generally, the absorption at 700 nm has been used as reference value to classify inland waters. Figure 31 shows the electromagnetic waves absorption spectra of liquid water over the complete spectral range.

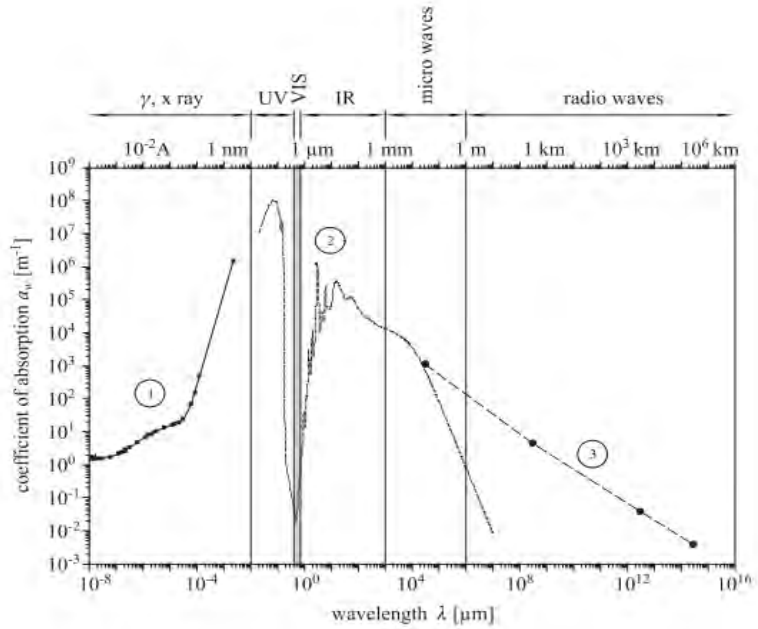


**Figure 31.** Electromagnetic waves absorption spectra of liquid water over the complete spectral range, from high-energy quanta γ (l ≈ 10−4 Å) to long radio waves (l ≈ 3 × 105 km). (1) Relationship among the radiation absorption coefficient of pure water and the wavelength for γ-radiation, X-radiation, and high-energy UV photons (2) same relationship for pure water in the UV- short radiowave range (3) the same relationship for oceanic salt water in the microwave-longwave (l ≈ 3 × 105 km) region (Wozniak & Dera 2007).

## 7.3 **Optical properties of lake water**

Inland natural waters are complex physical–chemical–biological systems, including living and non-living materials that may be present in aqueous solutions or in aqueous suspensions (Younos & Parece 2015). Lake water is not pure, as it contains numerous dissolved mineral salts and organic substances, suspensions of solid organic and inorganic particles, including various live microorganisms, and also gas bubbles and oil droplets. The components of the water participate directly in the interactions with solar radiation in that they absorb or scatter photons. Also, they may participate in diverse geochemical and biological functions, for example, in photosynthesis, which regulates the circulation of matter in these ecosystems, and affects the concentrations of most of the optically active components of water. Four components of aquatic ecosystems are the major cause of light absorption in natural waters (Kirk 2013):

a) Water,
b) Photosynthetic biota (phytoplankton and Macrophytes),
c) Tripton, and
d) Dissolved pigments

The color of inland waters is influenced by scattering and absorption processes as well as emission by the water column and of reflectance by the substrate. The color of surface waters varies because of the content of particulate and dissolved substances that absorb and scatter light, penetrating the water surface. At any wavelength, lake water

has a total absorption coefficient, which is the sum of the absorption coefficients of all the light-absorbing components, at that wavelength.

Remote sensing sensors measure the *water leaving radiance* ($L_u$), which is the upwelling radiance emerging from the water surface, as well as the radiance derived from scattering processes in the atmosphere (Figure 32).

The estimation of water quality derived from remote sensing measurements is based on water quality parameters that have an effect on water-leaving radiance. The absorption and scattering properties of the medium are described by its *inherent optical properties* (IOPs). These properties of the of the underwater light field are independent of the ambient light field. The IOPs of the water are independent of the intensity and geometry of the incoming radiation and vary in relation to the concentration of the dissolved and suspended materials. The IOPs of lake water follow Beer's Law; the absorption and the scattering coefficients are proportional to the concentrations of different components in the water.

Remote sensing reflectance ($RR$) is the ratio is the ratio of upwelling radiance ($L_u$) leaving a water body to downwelling irradiance ($Ed$) impinging on the water body. It is relatively independent of illumination and has often been approximated as an empirical function of two of the water IOPs (Kirk 1994, Lindell et al. 1999):

$$RR(\lambda) = \frac{L_u(\lambda)}{Ed(\lambda)} = \frac{0.083 \cdot b_b(\lambda)}{a(\lambda)} + bb(\lambda)$$

where $\boldsymbol{b_b(\lambda)}$ is the backscattering coefficient, which describes the probability of a photon being scattered
$\boldsymbol{a(\lambda)}$ is the absorption coefficient, which describes the probability of a photon being absorbed
$\boldsymbol{\lambda}$ is the wavelength

It is assumed that the IOPs are temporally constant over a relatively short sampling interval (Lindell et al. 1999).

Consequently:

- ✓ The more light scattered up towards the water, the greater the radiance and reflectance.
- ✓ The greater the absorption, the lower the radiance and reflectance.

This is the basis for determining the concentrations of the different components in natural waters by measurements of the inherent optical properties and thus, for a mechanistic approach in remote sensing.

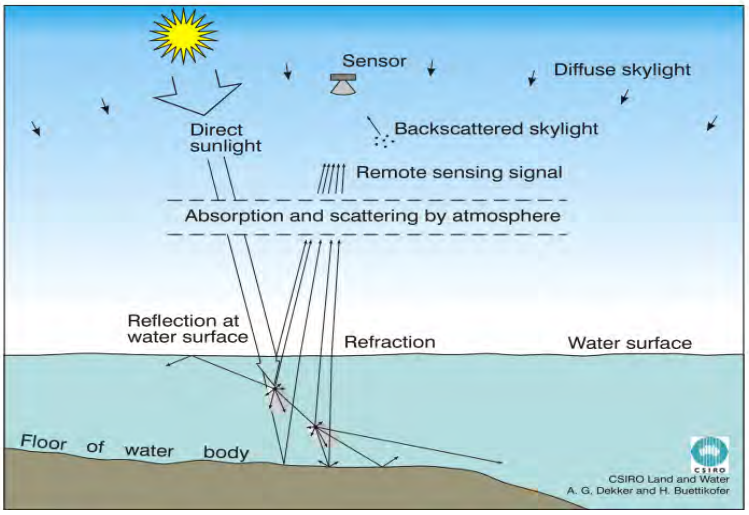


**Figure 32.** The processes that contribute to the signal as measured by a remote sensor in an optically shallow water, where the substrate has a significant effect on the water leaving radiance at the water surface (Dekker et al. 2001).

Multiple individual researchers have estimated water quality properties of oceanic waters using remote sensing. In this case, the measured spectral reflectance depends on (Dekker 1993):

a. The absorption by algal pigments, detritus and low concentrations of (aquatic) humus at short wavelengths and by pure water at long wavelengths
b. The scattering by water molecules at short wavelengths and Raman scattering at intermediate wavelengths. Raman scattering occurs when photons are scattered by excitation, with the scattered photons having a frequency different from that of the incident photons.
c. Fluorescence caused by humus at shorter and algal pigments at longer optical wavelengths.

Lake monitoring is more complex than monitoring of oceanic waters, as non-linear relations between QE and reflection occur. Comparing inland water optical properties with oceanic waters, the following have been noted (Dekker 1993):

a. Backscattering (≤1000 times greater than backscattering of the clearest oceanic waters) from particles (the main scattering factor)
b. High concentrations of humus and suspended inorganic matter absorb at short visible wavelengths. Large portions of humus may have an allochthonous source. Suspended inorganic material occur in great concentration due to local riverine inputs and resuspension processes
c. Absorption at orange to red wavelengths of algal pigments; this effect cannot be remotely sensed in oceans, due to the much stronger absorption by water than the absorption by the low concentration of algal pigments
d. Water molecule scattering, Raman scattering and fluorescence by aquatic humus and algal pigments have a decreased contribution

Additionally :

e. The size distribution spectra of inorganic particulate material may differ significantly from that found in the oceans
f. Greater concentrations of organic detrital material may be present from different sources
g. The upper optical depths of the water column are vertically stratified, and stratification often occurs with the biomass maximum in the first optical depth

**Optical water types**

The transmittance of solar radiation by natural waters varies greatly and it is helpful to have some broad indication of the optical 'behavior' of the water without having to fully specify all the IOPs. According to Jerlov (1976) oceanic waters can be classified in three types (I,II,III), based on spectral transmittance of downward irradiance at high solar altitudes (Figure 33). Additionally, he has recognized nine types of coastal water, in order of decreasing transmittance coastal water have divided into nine types (1-9). This classification is based on the fact that the shape of the volume scattering function of surface water is relatively constant among different oceanic regions. Jerlov's measurements were carried out using broad-band color filters and the curved obtained with modern submersible spectroradiometers are in some cases in poor agreement with his.

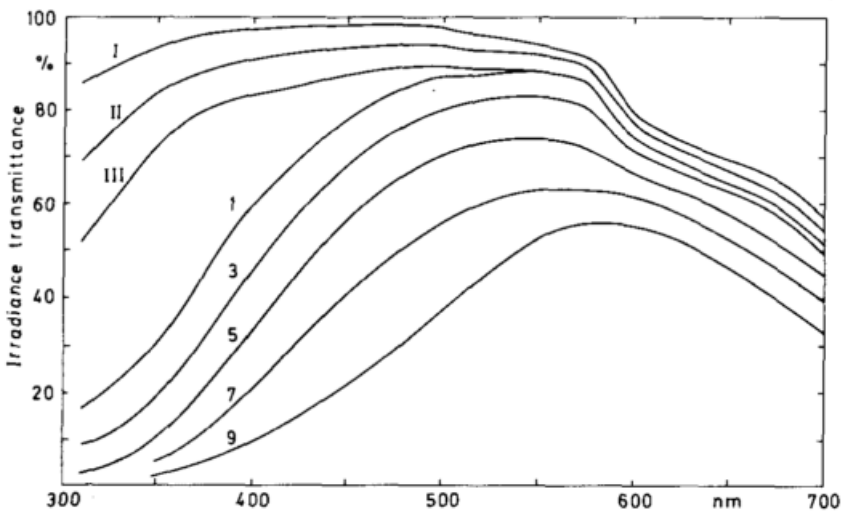


**Figure 33.** Transmittance per meter of downward irradiance in the surface layer for optical water types. Oceanic types I, II, III and coastal types 1,3,5,7,9 (Jerlov 1976).

Smith & Baker (1978), on the basis of their measurements of the spectral variation in several types of ocean waters, have concluded that in regions away from terrigenous influences, the attenuation (apart from that due to water) is mainly due to the phytoplankton and various pigmented detrital products. As a result, the total content of chlorophyll-like pigments provides a sufficient basis for optical classification, since on the basis of the pigment content, the curve of the vertical attenuation coefficient for irradiance against wavelength can be calculated. The classification of the ocean into 'Case l' and 'Case 2' waters, put forward by Morel & Prieur (1977), and further refined

by Gordon & Morel (1983), has been found useful in remote sensing for water monitoring. Case 1 waters are those for which phytoplankton and their derivative products (organic detritus and dissolved yellow color, arising by zooplankton grazing, or natural decay of the algal cells) play a dominant role in determining the optical properties of the ocean. They range from oligotrophic to eutrophic status. Case 2 waters are those for which an important or dominant contribution to the optical properties comes from re-suspended sediments from the continental shelf, or from particles and/or dissolved color in river run-off or urban/industrial discharge.

- ✓ An optical classification applicable mainly to inland waters was proposed by Kirk (1980). This classification was based on measurements of the absorption spectra of the soluble and particulate fractions from Australian water bodies. **Type G**: Gilvin, at all wavelengths in the photosynthetic range, absorbs light more strongly than the particulate fraction.
- ✓ **Type GA**: Gilvin absorbs more strongly than the particulate fraction throughout the shorter wavelength part of the spectrum, but the absorption coefficients of the particulate fraction exceed those of the soluble fraction at the red end of the spectrum due to the presence of substantial levels of algal chlorophyll.
- ✓ **Type T:** The particulate fraction, consisting mainly of tripton, absorbs light more strongly than the soluble fraction at all wavelengths. Mainly turbid waters with large amounts of suspended silt particles are included in this category.
- ✓ **Type GT:** Absorption by the soluble and particulate fractions is roughly comparable throughout the photosynthetic range
- ✓ **Type W:** Water bodies that are non-productive, free of silt and dissolved color are included in this group. For example, most oceanic, and some coastal, waters may be categorized as type W, as water itself is the dominant light absorber.
- ✓ **Type WG:** Waters may be classified as WG, in case the gilvin absorption at the blue end of the spectrum can be roughly similar in magnitude to the water absorption at the red end. Estuarine and the more colored coastal waters can be characterized as type WG.

Inland waters can change from one optical type to another. For example, heavy rain in the basin with consequent soil erosion could quickly change a type G water (gilvin dominated) to a type T water (tripton dominated). Nevertheless, some water bodies have water of a particular type most of the time. For instance, shallow, wind-exposed lakes with unconsolidated sediments are likely to be of type T all the time. Marine waters are, apart from the effects of the yearly phytoplankton cycle (in non-tropical areas), generally constant in their optical properties.

## 7.4 **General methodology**

According to Morel & Gordon (1980) there are three different approaches to measure water QE using spectral radiance:

*The empirical method*

The empirical approach is based on the calculation of a statistical relation between the water constituent concentrations and the radiance that is measured by the sensor. According to this approach, remote sensing data is related by regression analysis to the *in situ* measurements of QE. Extensive field work needs to be carried out, as *in situ* samples have to be collected simultaneously or near simultaneously with the overpass of the sensor. Multiple algorithms for estimating water quality parameters have been proposed, starting from a simple linear regression between reflectance and water constituent concentrations to non-linear multiple regressions between a combination of band ratios and the concentrations.

The advantage of using this approach is that the algorithms are straightforward and easy to use. However, false results may occur while performing this method, because a causal relationship does not necessarily exist between the parameters studied (Hogenboom & Dekker 1999). The empirical method is based on bivariate or multivariate regressions between remote sensing measurements and *in situ* measurements of QE. This method is the least scientifically supported because (Dekker & Seyhan 1988):

- ✓ The QE measured may not fully represent those which influence water color
- ✓ It is necessary to qualify the statistical relationships
- ✓ Not all statistical relationships are fully understood
- ✓ There is much to investigate for the influence of water parameters on the underwater light field

While ocean water color remote sensing is relatively mature, both empirical and semi-analytical algorithms for inland water quality may suffer from several limitations: retrieval of information is often on only a single water quality constituent, specific sensor applicability, the requirement for ongoing coincident *in situ* data for parameterization, and limited transferability across different inland water optical types, time and concentration ranges (Malthus et al. 2013).

*The semi-empirical method*

The semi-empirical method is used when spectral characteristics of the studied QE are more or less accurately known. This information may be used for the statistical analysis, which is focused on well-chosen spectral areas and appropriate bands or combinations of bands are used as correlates. Quantitatively, the coefficients only apply to the data set at hand so each application must be individually calibrated. The semi-empirical method is commonly chosen.

*The analytical method*

This method uses the inherent and apparent optical properties of water, in order to model the reflectance and vice versa. An in-water model is developed to measure the remote sensing data and retrieve the QE concentrations. Water QE are related to the bulk inherent optical properties via the specific inherent optical properties and are expressed in their specific absorption and backscatter coefficients. Subsequently, a suite of analytical methods can be used to optimally retrieve the water constituents or parameters from the remotely sensed.

There are few standardized techniques for analyzing water quality from satellites. The relationships developed to monitor water quality in lakes within semi-empirical approaches are often site dependent and can be only applied to those images from which relationships are derived. Well-calibrated and validated spectral inversion procedures are instead applicable to every site acquired over the selected waterbody, giving the opportunity to assess water quality independently from ground measurements. The procedure is also transferable to other systems, for which the optical characterization of the waterbody is known.

The optimal wavelength used to measure a water QE depends on the substance being measured, its concentration, and the sensor characteristics (Ritchie et al. 2003). The main factors, which affect water quality of a water body are turbidity, algae (i.e., chlorophylls, carotenoids), physico-chemical parameters (i.e., nutrients, pesticides, metals), dissolved organic matter (DOM), thermal releases, aquatic vascular plants, pathogens, and oils. Suspended sediments, algae, DOM, oils, aquatic vascular plants, and thermal releases change the energy spectra of reflected solar and/or emitting thermal radiation from surface waters which can be measured using remote sensing techniques. Most chemicals and pathogens do not change the spectral or thermal properties of surface waters, so they can only be inferred indirectly from measurements of other water quality parameters affected by them (Ritchie et al. 2003).

Digital values of a certain 'water' pixel may be affected by different factors (Lindell et al. 1999):

- ✓ The type of substances present in the water. The presence of different substances in the water results in different spectral responses
- ✓ The depth at which the substances are located. The spectral signature of a certain substance, especially for bottom cover, is strongly related to the water depth of that substance. The intensity of the response signal is decreasing with increasing depth, and also the hue and saturation dimensions may also be affected
- ✓ The atmosphere can affect the incoming signal significantly, as small amounts of water vapor in the atmosphere could cause dramatic effects on the estimation of water QE. In order to correct this effect, atmospheric correction models could be applied. Good quality field data are, therefore, necessary for the correction. Even availability of field measurements on the atmospheric parameters may not be

sufficient as the spatial variations in the aerosol content of the atmosphere could cause interpretation errors.

- ✓ In all of the European countries the seasonal effects on the water quality and thus the satellite response is prominent. Not only does the development of the algal population change the spectral character of the water mass, but also the Sun's angle and the different air masses associated with different seasons, affect the spectral response patterns
- ✓ The weather conditions affect the satellite signal, sometimes predictably. These distortions are not easily corrected, in case there are no available field measurements

### 7.5 **Satellite measurements**

The methodology that was followed in the present study is generally based on the application of an empirical or statistical approach for remote sensing data analysis. Water quality algorithms, mathematical equations which relate radiometric variables to the concentrations of water QE, developed from previous studies, were applied to radiometrically calibrated pixels of Lake Koronia. Namely, algorithms and procedures for the estimation of **Water Temperature** (Ritchie et al. 1990, National Aeronautics and Space Administration 1999, Giardino et al. 2001, Chander & Markham 2003, Wloczyk et al. 2006,Lamaro et al. 2013, Zanter 2015), **Secchi Disk Depth** (Dekker & Peters 1993, Jassby et al. 1999, Lindell et al. 1999, Giardino et al. 2001, Kloiber et al. 2002, Dewidar et al. 2005, Swift et al. 2006, Wang et al. 2006, Fuller & Minnerick 2007, Olmanson et al. 2008, Torbick et al. 2013, Butt & Nazeer 2015), **Chlorophyll *a*** (Ritchie et al. 1990, Mittenzwey et al. 1992, Lindell et al. 1999, Giardino et al. 2001, Brivio et al. 2001, Ma & Dai 2005, Han & Jordan 2005, Wang et al. 2006, Fuller & Minnerick 2007, Azab 2012, Torbick et al. 2013, Danbara 2014, Waxter 2014, Butt & Nazeer 2015, Theologou et al. 2015), **pH** (Khattab & Merkel 2014, Theologou et al. 2015, Mushtaq & Nee Lala 2016), **Water Depth** (Lyzenga 1978, Lyzenga & Polcyn 1979, Philpot 1989, Stumpf et al. 2003, Smith & Sandwell 2004, Dewidar et al. 2005, Doxani et al. 2012, Tang & Pradhan 2015, Pattanaik et al. 2015), **Lake Coverage** (Li & Liu 2002, Fyfe 2003, Williams et al. 2003, Cho 2007, Ma et al. 2008, Ji et al. 2009, Younos & Parece 2015, Oyama et al. 2015), **Conductivity** (Khattab & Merkel 2014, Theologou et al. 2015, Mushtaq & Nee Lala 2016), **TN** and **TP** (Chen & Quan 2012, Theologou et al. 2015), **$NO_2$** and **$NO_3$** (Khattab & Merkel 2014), **$PO_4$** (Khattab & Merkel 2014, Mushtaq & Nee Lala 2016), **Salinity** (Dewidar et al. 2005), **Dissolved Oxygen** (Theologou et al. 2015, Mushtaq & Nee Lala 2016) and **$NH_4$** (Theologou et al. 2015) were adopted. Generally, these algorithms estimate QE by statistically modeling relations between combinations of spectral bands and measured water quality variables. Band combinations may use DNs, radiance or reflectance as inputs. These algorithms were applied to Lake Koronia images which were acquired within one day of *in situ* data collection. The QE estimation using reflectance values was carried out twice, once using

TOA reflectance and once using surface reflectance produced by LEDAPS (Chapter 5.2).The deviation of these satellite measurements from the *in situ* data was determined, in order to define which algorithms provide easy implementation and high accuracy for the estimation of QE of Lake Koronia, as well as to specify the suitable radiometric calibration. Whichever of these algorithms yielded results that are in closer matchto data derived from *in situ* measurements, was used in all the remaining images, in order to obtain a timeline of Lake Koronia. Timelines of seven QE elements (**Water Temperature, Conductivity, pH, Secchi Disk Depth, Chlorophyll *a*, Lake Coverage, Water Depth)** were created, as the corresponding procedures yielded the results with low deviation from the *in situ* data. The procedures and the algorithms that were used for the estimation of these seven QE are described in the following sub-Chapters.

### 7.5.1 Temperature

A punctual value of lake temperature is related with the difference between the income and loss of heat. Temperature is an important parameter to be measured in water quality and ecological studies, as its distribution over time provides information about the lake thermal cycle. Also, it affects many biological and chemical processes of the ecosystem. The biological activities may be affected by water temperature changes, caused by anthropogenic pressure (thermal pollution). Remote sensing gives the opportunity for mapping the absolute temperatures and for providing information about thermal releases. Quantitative estimates of surface water temperature inform for interpreting outputs from mathematical models of thermal plumes (Ritchie et al. 2003). These inputs are useful for the development of management plans, in order to reduce the effect of man-made thermal releases.

According to Baban (1993a), surface temperature depends on the altitude and the volume 'surface area and depth', as a linear regression has shown that altitude and volume yield an explanation of variance of 82% and 77% respectively.

Energy exchange processes (sensible and latent heat flux and long wave radiation) between water body and atmosphere are located within a thin boundary layer, affecting the surface skin. This layer causes the difference between the radiometric temperature measurement and the water temperature (Ewing & McAlister 1960, McAlister & McLeish 1969, Paulson & Parker 1972). Due to evaporative cooling, sensible heat flux and long wave radiation, the surface skin is usually some tenths of a degree cooler than the temperature of the underlying water column (Schneider & Mauser 1996). Surface water temperature, as well as the skin effect, pronounce daily amplitude. There are three major limitations in using satellite measurements of lake temperature:

a) Poor resolution for lake monitoring purposes. For example, the Landsat IR sensor (120 m) is inferior to the other channels (30 m).
b) Atmospheric water vapor absorbs radiation. Thus the accuracy of the satellite derived lake surface temperature depends upon the quality of the atmospheric correction procedure. Sensors mounting two channels in the thermal infrared

wavelength range represent a prime temperature data source due to the simple atmospheric correction utilizing the so called "Split Window Technique". Satellite sensors carrying only one thermal band, such as Landsat TM, required the modelling of the thermal radiation transfer through the atmosphere to correct for the atmosphere affecting satellite signal. These models are complicated and time consuming and require additional meteorological data.

c) Infrared radiation from the water originates from the first micrometers below the water surface, because it does not propagate in water. Due to the evaporation cooling, sensible heat flux and long-wave radiation, the surface skin temperature is usually some tenths of a degree cooler than the temperature of the underlying water column. Direct comparisons of remotely sensed surface temperature measurements with bulk water temperature measurements requires knowledge of this temperature differences. Moreover, the wind effect should be taken into account: high wind speed may reduce the amplitude of the temperature difference between surface skin and bulk water temperature (Schneider & Mauser 1996)

According to Schott (1989), the measured thermal radiance is the sum of the following components:

$$L_\lambda = (\varepsilon_\lambda L_{w\lambda} + r_\lambda L_{\downarrow\lambda})T_\lambda + L_{\uparrow\lambda}$$

where ($\boldsymbol{\varepsilon_\lambda}$) emissivity of the water
($\boldsymbol{L_{w\lambda}}$) long wave radiation from the water surface
($\boldsymbol{r_\lambda}$) reflectivity of water
($\boldsymbol{L_{\downarrow\lambda}}$) downward long wave atmospheric radiation
($\boldsymbol{T_\lambda}$) transmissivity of the atmosphere
($\boldsymbol{L_{\uparrow\lambda}}$) upward long wave atmospheric radiation

In details:

- ✓ *Thermal radiation emitted by the water surface*: Longwave radiation emitted by lake water is reduced due to the atmospheric transmittance and emissivity of the water. Water vapor reduces the transmissivity of the atmosphere. Additionally, humid air masses affect the estimation of temperature using remote sensing techniques. The thermal radiation emitted by the water surface depends upon the emissivity of the water. This emissivity value was calculated as a weighted mean according to tabulated numbers published by Masuda et al. (1988).
- ✓ *Thermal radiation emitted by the atmosphere*: The atmosphere not only absorbs, but it also emits thermal radiation according to its own temperature and emissivity. This fraction of the satellite measured thermal radiation does not contain any information concerning the water surface.
- ✓ *Reflected atmospheric radiation***:** Longwave atmospheric radiation reflected at the water surface constitutes the third component of the sensor measured

signal. This fraction is small in comparison to the other components due to the high emissivity of the water surface.

Landsat-5/TM Band 6 allows to map the surface temperature and the surface radiation budget (Dekker & Peters 1993). Landsat-7/ETM+ has a unique thermal band (band 6) divided into two: low gain band (B6L) and high gain band (B6H), with a spectral resolution from 10.4 to 12.5 lm and a spatial resolution of 60 m covering a surface of 3.600 $m^2$ per pixel (0.36 ha). The Landsat-7/ETM+ thermal Band 6 data files refer to the gain settings of which the band is acquired. Band 6 is acquired in both high and low gain, the gain settings are provided as two separate band files (Band 61 or 6L, Band 62 or 6H). Band 6L provides an expanded dynamic range and lower radiometric resolution (sensitivity), with less saturation at high Digital Number (DN) values. Band 6H has higher radiometric resolution (sensitivity), although it has a more restricted dynamic range. Landsat-8/TIRS measures land surface temperature in two thermal bands, using a technology that applies quantum physics to detect heat. TIRS uses Quantum Well Infrared Photodetectors (QWIPs) to detect long wavelengths of light emitted by the Earth whose intensity depends on surface temperature. The QWIPs that TIRS uses are sensitive to two thermal infrared wavelength bands, helping it separate the temperature of the Earth's surface from that of the atmosphere. The two TIRS bands were selected to enable the atmospheric correction of the thermal data using split-window surface temperature retrieval algorithms *[url22]*. The use of two separate, relatively narrow, thermal bands has been shown to minimize the error in the retrieval of surface reflectance (Caselles et al. 1998).

The water Temperature, in the present study, was estimated applying the methods described in Chapter 5.2.

### 7.5.2 Secchi Disk Depth (SDD)

The SDD is an important optical characteristic of water related to water quality. Secchi disk is widely used for obtaining water transparency, because of its simplicity. Transparency represents the depth (m) at which the difference of luminosity between the Secchi disk and the vertically diffused light from the water is within the reach of the distinct vision of a human eye. SDD is an important optical characteristic of water which has to be monitored in order to determine and manage water quality. SDD may be wrongly identified with Total Suspended Matter which includes organic and inorganic particulates suspended in the water column.

According to Duntley (1952), the attenuation of the contrast of the submerged object along an inclined path of sight can be measured using the following equation:

$$C_R = C_0 e^{-(a+K\cos\vartheta)R}$$

where $(\boldsymbol{C_0})$ the inherent contrast of the object against its background
$(\boldsymbol{C_R})$ its apparent contrast as seen by an observer at some distance
$(\boldsymbol{R})$ the length of the path of sight

$(\boldsymbol{a}, \boldsymbol{K})$ the attenuation coefficients

Observation downward along a vertical path reduces the equation to:

$$C_R = C_0 e^{-(\alpha+K)R}$$

which is specific for Secchi disk observation.

A Secchi disk "reading" should therefore be simply a record of the object distance for the condition of the liminal visual detection. It should be the value of $R$ in equation above for a value of $C_R$ equal to liminal visual contrast. Blackwell (1946) has described the liminal visual contrast for circular targets in the air. Tyler (1960) suggested that if the irradiance $H$ is measured at two depths in a water body, then the parameter K can be determined using the relationship:

$$H_{Z1} = H_{Z2} e^{-K\Delta Z}$$

For instance, if $H_0$ is the is the irradiance incoming the water surface, the irradiance on Secchi disk at water depth Z will be:

$$H_Z(-) = H_0 e^{-KZ}$$

The radiant emittance for the Secchi disk will be $H_0\,(-)r$ where $r$ is its measured reflectance. The radiant emittance of the water at the depth of the Secchi disk will be $H_Z(+)$ which can be obtained from the reflectance factor $H_Z(+)/H_0\,(-)$ for water.

An observer does not see the full radiant emittance of an object since he can collect only that radiant flux that enters the solid angle defined by the pupil of his eye. If the directional reflectance characteristic is assumed for both the target and the water background, then the inherent contrast of an object can be determined as follows:

$$C_0 = \frac{H_Z(-) \cdot \frac{r}{\pi} - 0.02 \cdot \frac{H_Z(-)}{\pi}}{0.02 \cdot \frac{H_Z(-)}{\pi}} = \frac{r - 0.02}{0.02}$$

where $(\boldsymbol{r})$ the reflectance of the object

$(\boldsymbol{\pi})$ simply indicates that both target and background are assumed to be Lambert emitters

To determine $C_0$ it is necessary to assume a reflectance for the Secchi disk because none is given. For convenience a reflectance of 82% is assumed. $C_0$ is therefore

$$C_o = \frac{0.82 - 0.02}{0.02} = 40$$

As a result applying these numbers:

$$(\alpha + K) = \frac{8.69}{Z_{SD}}$$

where $(\boldsymbol{\alpha, K})$ coefficients in the above equation will of course be the average values for the water column through which the Secchi disk is observed

The coefficient $\alpha$ increases with the absorption coefficient and the total scattering coefficient and,in a stable field, $K$ increases with the absorption coefficient and the back-scattering coefficient.

The following problems associated with the Secchi disk measurements must be taken into consideration (Tyler 1968):

- ✓ The image of Secchi disk is fragmented by refraction effects caused by motion of water surface
- ✓ The reflected light of water surface tends to reduce the visibility of the Secchi disk, in case the observation is above the water surface
- ✓ Field conditions are exerting an undue influence on the measurement of SDD
- ✓ Secchi disk must be concerned as an instrument that may give the average values of $\alpha, K$ and these only in the upper water layer, where the highest concentration of contamination is generally observed

Remote sensing has widely been used for measuring water transparency. SDD can be determined in a wavelength range 520–600 nm. At this range the effects of yellow are negligible (Jerlov 1976) and there is a minimum in absorption by phytoplankton (Shifrin 1988).

The estimation of SDD of Lake Koronia using Landsat images was performed using the equation (Giardino et al. 2001):

$$\text{SDD} = 8.01 \cdot \rho_{blue}/\rho_{green} - 8.27$$

where $(\boldsymbol{\rho_{blue}, \rho_{green}})$ the reflectance of blue, green bands

### 7.5.3 Chlorophyll *α* (Chl*α)*

In eukaryotic plants, photosynthesis is carried out by chloroplasts, the most well-known members of the great class of related and interconvertible organelles known as plastids. The chloroplasts include the pigments that capture the light, the electron carriers that use the absorbed energy to generate reducing power in the form of NADPH2 and biochemical energy in the form of ATP, and the enzymes that use the NADPH2 and the ATP to convert $CO_2$ and water to carbohydrate. Attached to the chloroplasts is an array of particles 30 to 40 nm in diameter, known as phycobilisomes and consisting mainly of biliprotein molecules. The task of collecting light energy from the underwater light field is carried out by the photosynthetic pigments whose structures are such that they efficiently absorb light in different parts of the 400 to 700 nm range. There are three chemically distinct types of photosynthetic pigment: the chlorophylls, the carotenoids

and the biliproteins. Chlorophylls are cyclic tetrapyrrole compounds with a magnesium atom chelated at the center of the ring system. All photosynthetic plants contain chlorophyll *a* (or *a2*), and most classes of plant contain, in addition, either chlorophyll *b* (or *b2*), or one or more of the chlorophyll *cs*, or chlorophyll *d*. Chl*α* normally constitutes most of the chlorophyll present.

The Soret peak corresponds to excitation of the Chl*α* molecule to the upper singlet state. This is very unstable and decays to the lower excited singlet state in about $10^{-12}$ seconds by a radiationless transition. The excited molecule can now revert to the ground state by emission of a photon – the phenomenon of fluorescence (Figure 34). Since the energy change is about the same as that accompanying excitation of a molecule from the ground state to the lower excited singlet state, the main chlorophyll fluorescence peak is in the red region. There is an additional smaller peak in the emission spectrum at about 720 to 730 nm, corresponding to photons emitted as the Chl*α* molecules undergo transition from the lowest vibrational sublevel of the lower excited state to the first excited vibrational sublevel of the ground state. The emitted photons are at longer wavelength because the energy change is somewhat smaller. Absorption is very low, but not zero, in the middle, green, region of the spectrum, hence the green color of these pigments.

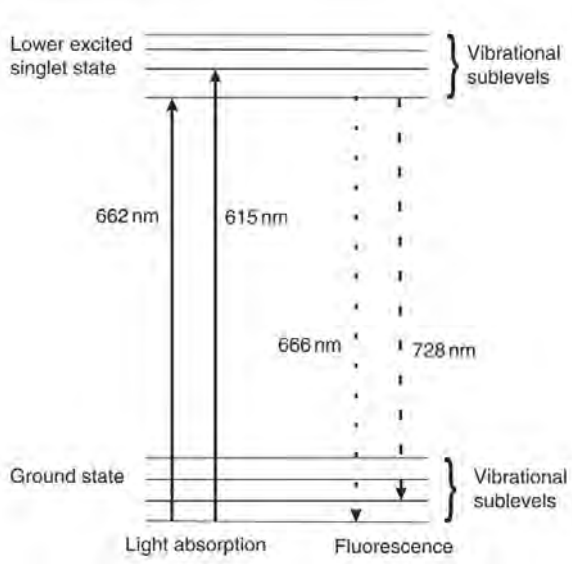


**Figure 34.** Energy level diagram indicating the vibrational sublevels of the ground state and the lower excited singlet state of Chl*α* (Nobel 1991). Solid vertical lines indicate absorption of a photon by Chlα dissolved in diethyl ether: dashed lines represent the transitions corresponding to emission of a photon in fluorescence (Kirk 2013).

The mineral and detrital particles, mainly, are responsible for the scattering in most natural waters (Kirk 2013). Algal cells have a scattering phase function that is strongly peaked at small forward angles, (Stramski & Morel 1990) but the back- scattering ratio (the proportion of the total scattering that is in a backwards direction, $\vartheta > 90°$) is much lower (0.0001–0.004) for the living cells (Bricaud et al. 1983, Stramski & Morel 1990) than for the mineral and detrital particles (~0.019). This is due to (Bricaud et al. 1983) the low refractive index (relative to water) of the algal cells (1.015–1.075) (Jerlov 1976).

The backscattering ratio is greater in the small (picoplankton) cells, such as cyanobacteria, than in the larger eukaryotic cells (Stramski & Morel 1990).

In shallow, eutrophic to hypereutrophic lakes, the dynamics of phytoplankton are complex and difficult to predict. Although, in order to limit the lake eutrophication, the Chl*α* monitoring is necessary (Carlson 1977).

Remote sensing has been used by multiple researchers for measuring Chl*α* concentrations spatially and temporally. Empirical relationships between radiance/reflectance in narrow bands or band ratios and Chl*α* have been used for Chl*α* estimation. *In situ* measurements (Schalles et al.1997) show spectra with increasing reflectance with increased Chl*α* concentration across most wavelengths but areas of decreased reflectance in the spectral absorption region for Chl*α* (675 -680 nm) (Figure 35). According to Ma & Dai (2005), the Landsat bands, which exhibit the most correlative coefficients between reflectivity and Chl*α* concentration, lie in the range 540 to 557 nm, 666 to 693 nm and 820 to 840 nm.

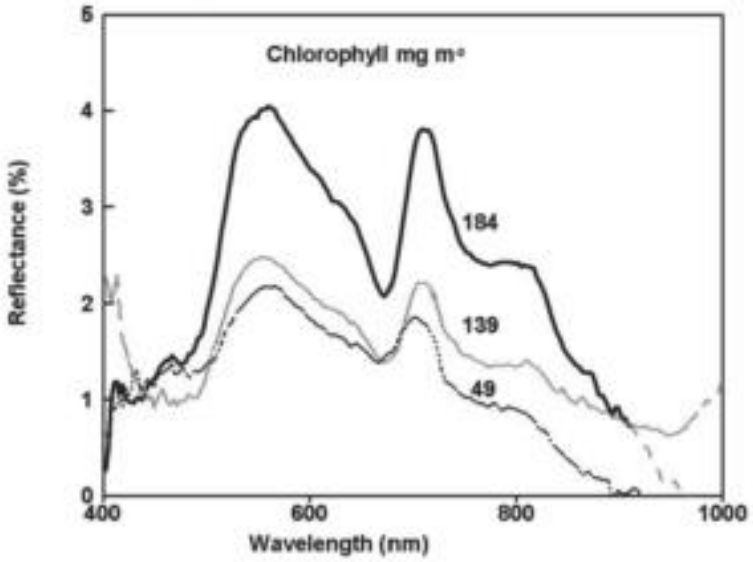


**Figure 35.** Relationship between reflectance and wavelength for different Chl*α* concentrations (Ritchie et al. 2003).

In turbid lake waters, related with high Total Suspended Matter concentration, the discrimination of chlorophyll using remote sensing techniques is very difficult (Dekker & Peters 1993), due to the dominance of the spectral signal from the Total Suspended Matter. According to Gitelson et al. (1994), there is a linear relationship between Chl*α* and the difference between the emergent energy in the primarily chlorophyll scattering range (700 to 705 nm) and the primarily Chl*α* absorption range (675 to 680 nm). This linear relationship is reported even if there are high TSM concentrations (Figure 36).

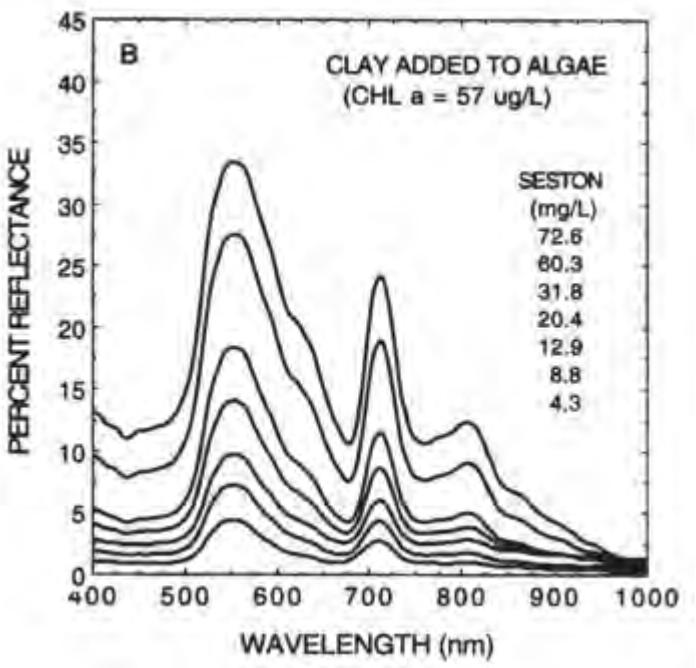


**Figure 36.** Relative contributions of chlorophyll and suspended sediment to a reflectance spectra of surface water (Schalles et al.1997).

According to Vahtmae et al. (2006) and Kutser et al. (2006), the spectral signatures of cyanobacterial blooms are similar to those of different benthic habitats. Benthic habitat mapping can be applied when no blooms have been formed at the lake's surface. The monitoring of cyanobacterial blooms in shallow lakes is very complicated or impossible. The recognition of bloom-forming phytoplankton at a species level is based on their reflectance spectra. This requires the determination of unique spectral signatures of the different algal species and sensors that are capable of detecting these spectral differences. High concentrations of Colored Dissolved Organic Matter and Suspended Solids may mask the spectral features that characterize certain phytoplankton species or their groups. The mapping of phytoplankton bloom distribution and the determination of Chl*α* concentration, using remote sensing techniques, are obstructed due to:

- ✓ The phytoplankton variation by orders of magnitude within one pixel
- ✓ The vertical distribution of some phytoplankton species in the water column. In this case, the re-design of *in situ* sampling strategies, in order to obtain results that are more suitable from a remote sensing point of view, may be needed (Kutser 2009)
- ✓ The variation of Chl*α* concentration in a cyanobacterial bloom (Kutser 2004). Yacobi et al. (1995) found that chlorophyll concentration varied by 300% on two sides of the boat while studying a *Protoperidinium sp*. bloom in Lake Kinnert. This raises questions about using a single point measurement in calibration of satellite data
- ✓ The limitations by the varying fluorescence efficiencies of different phytoplankton populations and changes in water absorption, which reduce the available light

- ✓ The re-absorption of the fluoresced light by Chl$\alpha$, resulting in a decrease of the emitted signal. This happens when the Chl$\alpha$ concentration increases above 10–15 mg/m$^3$ (Kishino et al. 1986)
- ✓ The difficulty of studying the vertical distribution of cyanobacteria when the sub-surface layer is not very thick or when surface scum occurs (Hajdu et al. 2007). According to Kutser et al. (2008), the vertical structure of the distribution of cyanobacterial biomass in the water column has serious impacts on both absolute values and the shape of reflectance spectra. The development of remote sensing algorithms and methods requires knowledge about the vertical distribution of cyanobacteria
- ✓ Kutser (2004) has shown that the depth of penetration may be just centimetres in dense cyanobacterial blooms. In such a case, the surface sample is sufficiently representative of the biomass that remote sensing sensors are detecting

The limitations described above lead to the assumption that water samples from a single depth are appropriate for the calibration of remote sensing data and, conversely, the Chl$\alpha$ concentration estimate obtained from remote sensing data is valid for the whole mixed layer. Modelling results for the Baltic Sea conditions (Kutser et al., 2006) indicated that the Chl$\alpha$ concentration has to be higher than 8-10 mg/m$^3$ before the phycocyanin absorption feature becomes detectable.

For the purpose of this experiment, both the Chl$\alpha$ concentration (mg/m$^3$) and the phytoplanktonic coverage of Lake Koronia were determined.

For the remote sensing measurements of Chl$\alpha$ concentration (mg/m$^3$) the following equation was used (Brivio et al. 2001):

$$\ln(Chla) = 0.52 \cdot \ln(\rho_{blue}) - 0.79 \cdot \ln(\rho_{green})$$

where ($\boldsymbol{\rho_{blue}}$, $\boldsymbol{\rho_{green}}$) the reflectance of blue, green bands

### 7.5.4 Lake Coverage

The aquatic vegetation and Cyanobacterial bloom distribution assessment has been undertaken via aerial photography, which is labor intensive and somewhat subjective, making small changes over time harder to detect. The use of advanced satellite or airborne remote sensor technology provides an opportunity to undertake a more cost-effective, objective monitoring of the lake condition, in support of catchment management activities.

Aquatic vegetation and Cyanobacterial blooms have an important role in the maintenance of healthy lake functioning. These parameters are partly influenced by sedimentation and nutrient loading, two factors influenced by catchment processes, and, hence, the health of the aquatic vegetation and phytoplankton is a link to the broader catchment management. The mapping of the distribution and change of these parameters over time may provide catchment managers with information that can be used in the

ongoing assessment of lake health. In the present study, in addition to the estimation of the Chl$\alpha$ concentration of Lake Koronia, the distribution of aquatic vegetation and Cyanobacterial blooms was mapped.

Aquatic plants provide food to aquatic organisms, serve as nursery habitats, help reduce shoreline erosion and influence the supply of oxygen in water. However, fast growing aquatic plants, especially free-floating or floating-leaved plants of inland water bodies, can become invasive by outcompeting native species. Information on aquatic vegetation distribution, composition, and abundance is widely used as an indicator of aquatic environmental quality; and the improved mapping capability for those plants will enhance the ability to assess underwater habitat changes. Remote sensing of benthic aquatic plants, however, is limited to the visible wavelengths where light penetrates the water column and can be reflected back to a sensor (Fyfe et al. 2003).

The boundary between the various classes of emergent, floating, floating-leaved and submerged vegetation, whose biomass in unit area have significant differences, is not distinct, as these communities merge into one another (Ma et al. 2008). At depths (and wavelengths) where radiation penetrates to the bottom, the latter component includes bottom reflectance, volume reflectance from the water column, and reflectance from the water surface (Wezernak & Lyzenga 1975).

Lake Koronia pixels were divided into four zones: the floating vegetation, submerged vegetation, lake water and the Cyanobacterial bloom zones. In the case of lake Koronia, for the separation of aquatic Macrophytes and Cyanobacterial blooms, as well as clear water, a three-step process was followed. The separation was carried out following the Floating Algae Index (FAI) modification presented in (Oyama et al. 2015), in which it was demonstrated that lower FAI values correspond to water and higher values are indicative of vegetation.

$$FAI = R_{rc,B4} - \left[R_{rc,B5} + (R_{rc,B5} - R_{rc,B3}) \cdot \frac{(\lambda_{B4} - \lambda_{B3})}{(\lambda_{B5} - \lambda_{B3)}}\right]$$

where ($\boldsymbol{\lambda_{Bi}}$) is the center wavelength for the *i*th band of Landsat-5

K-means classification was initially performed in order to separate pixel values in two classes. The pixels in the class with higher FAI values were classified as vegetation. Afterwards, floating vegetation was distinguished from SAV using a blue/green band ratio, as shown in (Cho 2007), in which, since the presence of vegetation in water alters the relationship between depth and reflectance in blue and green bands, it was experimentally shown that a ratio between bands 1 and 2 provided the highest degree of correlation with vegetation cover in shallow waters. As a result, vegetation pixels were further separated in two classes using k-means classification. Lower Blue/Green reflectance ratio pixel values were classified as SAV and higher values as floating vegetation.

Finally, the separation of floating vegetation in Cyanobacterial blooms and aquatic Macrophytes was carried out using an $NDWI_{4,5}$ index proposed in (Oyama et al. 2015), in which it was shown that an optimal $NDWI_{4,5}$ threshold value for the given experimental data was around 0.63. This value was concluded to accurately detect aquatic Macrophytes when their concentration in the lake exceeds 10%.

$$NDWI_{4,5} = \frac{(\rho_{NIR} - \rho_{SWIR})}{(\rho_{NIR} + \rho_{SWIR})}$$

where $(\boldsymbol{\rho_{NIR}, \rho_{SWIR}})$ the reflectance of NIR, SWIR bands

Consequently, the floating vegetation pixels were, once again, separated in two classes using k-means classification with respect to $NDWI_{4,5}$ values. The class with larger values corresponds to cyanobacterial blooms, whereas the class with the lower values corresponds to aquatic Macrophytes.

The overall separation in four classes (water, SAV, aquatic Macrophytes and cyanobacterial blooms) was depicted in bitmap images of the lake using suitable colors for each class as a vegetation map. A complete record was therefore created, resulting in one vegetation map per satellite image.

### 7.5.5 pH

DOM (Dissolved Organic Matter) fluorescence and absorbance measurements are sensitive to changes in the environmental conditions of the water (Spencer et al. 2007). Senesi (1990) studied these environmental conditions with respect to fulvic acids and fluorescence and included temperature, pH, metal ions, solvent interactions and other solutes. An increase in fluorescence intensity of DOM with increasing pH over the range of 1 to 10–11, with a decrease at pH 12 was observed by Patel-Sorrentino et al. (2002). Spectral shifts are also observed in response to changing pH. Mobed et al. (1996) observed a red shift, in fluorescence intensity maxima, with increasing pH at long wavelengths (~390nm) and a similar red shift at shorter wavelengths (~320nm) in soil derived humic substances. In aquatic derived DOM, shorter wavelength fluorescence peaks have been observed to blue shift with increasing pH (Mobed et al. 1996). According to Spencer et al. (2007) the spectrometric properties of freshwater samples are sensitive to pH. In freshwater ecosystems, DOC alters water color (Williamson et al. 1999) and increases acidity (lowers pH). As a result, there appears to be potential for the measurement of pH using remote sensing techniques as it effects the properties of fluorescent water components.

In order to measure the pH of Lake Koronia the following equation was used (Khattab & Merkel 2014):

$$pH = 9.738 - 0.084 DN_{SWIR}$$

where $(\boldsymbol{DN_{SWIR}})$ the DN of SWIR band

### 7.5.6 Conductivity

Conductivity is a measure of a solution's ability to conduct electricity. Unlike pH which represents the concentration of H+ ion only, conductivity measures the concentrations of all active ions present in the solution. In many cases, conductivity is linked directly to the Total Dissolved Solids (TDS) concentration and pH. Generally, the greater the ion concentration, the greater the value of conductivity. These ions all have the electrical unit charges shown by their symbols, but they move at different velocities (mobilities) through the solution, so they contribute differently to the conductivity. The conventional mobility of an ion depends on the charge and radius of the solvated ion and the viscosity of the medium. In aqueous solutions, there is only about 1.5 V of practical working potential—a relatively short range when one recalls that the electrochemical series extends over about 4.5 V. This is because the dielectric constant is so much lower in non-aqueous than in aqueous solutions and therefore the Coulombic attraction between ions of opposite sign is higher in the former solutions, so that there is a greater tendency to "stick together". Consequently, conductivity effects vicariously the water reflected energy as it is the sum of the contribution of all the ions present in a solution and as a result it can be measured using remote sensing techniques.

In order to measure the conductivity of Lake Koronia, the following equation was used (Mushtaq et al. 2016):

$$EC = 92183\mathrm{e}^{-34.7\rho_{red}}$$

where ($\boldsymbol{\rho_{red}}$) the reflectance of red band

### 7.5.7 Water Depth

Remote sensing is useful for mapping lake bathymetry and depends on the electromagnetic energy's varying degree of water penetration at different wavelengths. *In situ* measurements do not provide the desired mapping accuracy, as they are based on a limited number of sampled points. Some methods include using ship-borne underwater dragging sonar to record returned sounding signals in a fixed time interval for extensive water depth measurements (Li et al. 2004). Although, this approach can accurately depict the underwater terrain and has widely been used for marine engineering design, its high cost makes it less accessible.

Turbidity, phytoplankton cells, Total Suspended Matter (TSM) and CDOM may affect the depth of penetration and limit the range over which optical data may be used to estimate depth, scattering scatter, absorbing light and increasing attenuation. The material in the water column influences the amount of absorption and scattering of radiation. This effect, which varies with wavelength, is represented by the coefficient of water attenuation and this property is important when considering the effect of depth on the amount of radiation returning to the sensor (Bierwirth et al. 1993). In addition, the spectral properties of lake water may be affected by recent precipitation, wind velocity,

depth attenuation and bottom reflectance. Runoff may cause an increase of TSM concentration to water bodies resulting in a change in the spectral signature. Waves and currents resulting from wind also cause variations in spectral signature (Hathout 1985). Some other factors like the Sun's angle, azimuth, height of platform as well as scatter; absorption and refraction of the atmosphere might affect the characteristics of the returned electromagnetic waves.

Several models, differing in their structures and constructions, have been evaluated for mapping water depth:

- ✓ **Models based on the transmission equation of electromagnetic radiation in water.** A theoretical model is used for computing water depth measuring the optical parameters within the water column. These models, however, require a complex estimation for a number of water column reflectance parameters, some of which can be very difficult to obtain and are not widely used in practical water depth mapping .
- ✓ **Empirical models based on the statistical relationship between pixel values and field-measured water depth.** They do not require reflectance parameters of the water column and are simplistic in their development; therefore, they are widely applied in many case studies. These models are created for specific water bodies and the assumption about the existence of correlations between in-situ water depth and remote sensing data may not hold. This may result to less desirable estimations and the derived models less transferable.
- ✓ **Theoretical and statistical models by simplifying the former through the use of statistical regression to estimate the photochemical parameters.** These methods use bottom-albedo based single-band models and multi-band ratio models.

Due to the eminent difference in attenuation percentage of visible light in the three different color bands, Stumpf et al. (2003) proposed a model that utilizes the ratio of the reflectance logarithms as a factor that correlates even more strongly with depth than the reflectance itself. As such, the original log-linear model proposed earlier is transformed to:

$$Z = m_1 \frac{\ln(nR_w(\lambda_i))}{\ln(nR_w(\lambda_i))} - m_0$$

where $(\boldsymbol{m_1})$ is a tunable constant to scale the ratio to depth,
$(\boldsymbol{n})$ is a fixed constant for all areas,
$(\boldsymbol{m_0})$ is the offset for a depth of 0 m (Z=0)

The derivation of the above model can be found in (Stumpf et al. 2003). The value of n is chosen suitably, in order to assure that the logarithmic values will be positive for

any calculation involved and that the model captures a linear correlation with depth. Usually, the band ratios favored are blue/green, or blue/red.

The ratio used to study the bathymetric characteristics of lake Koronia was blue/red. Suitable reflectance logarithm ratio values were calculated for the pixels of the water area of the lake using satellite data recorded on (22/5/1986) and a digital elevation model of the bottom created from maps of the Hellenic Military Geographical Service (HMGS) from the '70s. The map depicted in Figure 37 depicts the DEM of the bottom of the lake. This DEM was used along with the mask created using the NDWI algorithm mentioned in Chapter 5.5 , in order to get the average altitude of the pixels of the shore of the lake. This value was taken as the mean altitude of the surface of the lake. The depth of every pixel was derived as the difference between its altitude and the lake level altitude. A linear model was fitted in value pairs of reflectance logarithm ratios and depths and the model parameters were recorded. The model was applied on the same satellite image to map the reliability of the model with respect to the original depths. The errors were found to lie within reasonable ranges, in comparison to, for example (Tang & Pradhan 2015).

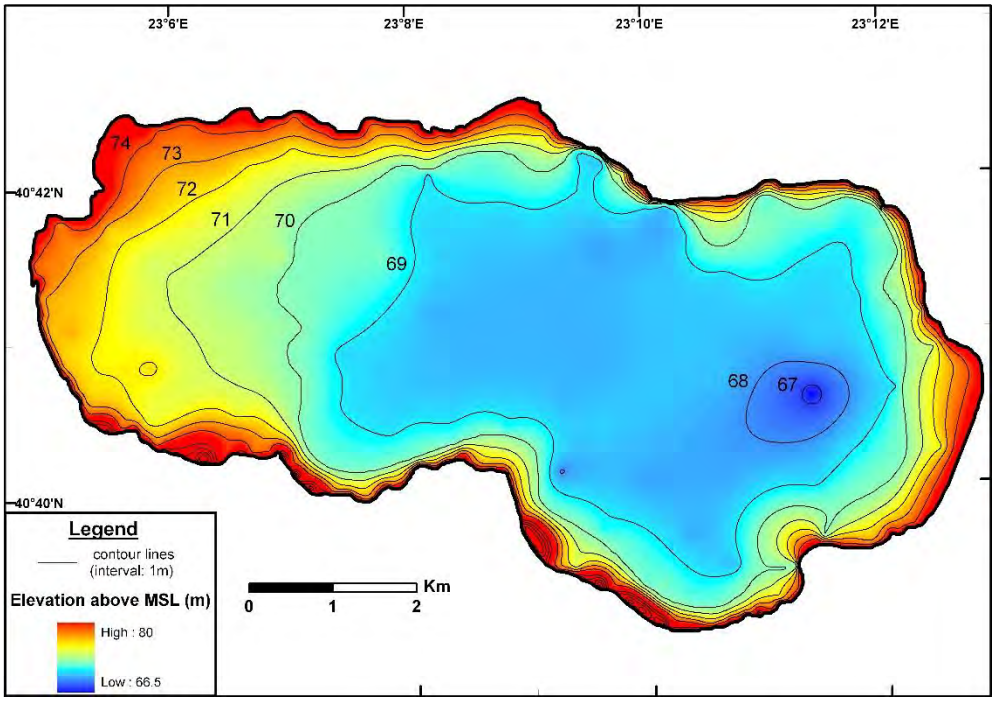


**Figure 37.** Digital elevation model of the lake Koronia bottom (Mouratidis et al. 2010).

# 8. DEVELOPMENT OF SPECIALIZED SOFTWARE FOR THE WATER QE ESTIMATION

## 8.1 Chapter overview

*The application of some of the more complicated algorithms necessitated the use of specialized software. Within the scope of this study, the acquisition of the results was carried out by programming suitable code within the MATLAB development environment. One of the products of this process was a unified processing environment presented as a Graphical User Interface (GUI), providing users with access to the algorithms implemented in the present study. The development was a two-step procedure. The first step involved the composition of the algorithms and the second step was concerned with designing the aforementioned graphical interface. The ultimate purpose of this attempt is to provide a standalone software gadget to facilitate the use of satellite images for the estimation of water quality parameters over water bodies. The specific capabilities of the tool are outlined in this chapter.*

*The idea behind the composition of the software lay in the fact that a large number of useful stand-alone functional modules were to be developed during the calculation phase, almost exclusively serving the purpose of deriving data and information from satellite images. Using the tools in a combined way would provide a user with a convenient chain of basic satellite image editing and data mining procedures. Furthermore, since the development was totally customized, the various modules implementing the algorithms were able to be fine-tuned to a desired extent, providing, on occasion, small pieces of functionality that may elude some of the currently available specialized software packages.*

## 8.2 Algorithms and functionality

Most of the algorithmic procedures have been composed in a straightforward manner, in separate modules as stand-alone functions, in order to hide the intricate details from the composition of the final GUI end product. Some of the more complicated algorithms require access to the lower-level functions composed in advance. In this way, a small function library was built to provide functionality to the GUI. The basic functionality of the final applet is briefly outlined below.

- ✓ Import and view multiple GeoTIFF files with pixel coordinate information
- ✓ View true-color images using RGB band information
- ✓ Create, export and import water body masks from multiple separate image areas (water bodies) using NDWI classification, according to the procedure described in Chapter 5.5

- ✓ Calculate and view grayscale indexed images of complex formulas using multiple bands from an image
- ✓ Create time-series plots of calculated parameters
- ✓ Perform bathymetric log-ratio model fit using external DEM file
- ✓ Classify aquatic vegetation in SAV, Macrophytes and cyanobacterial blooms
- ✓ Create colormaps of temperature or other water quality parameters using custom colors
- ✓ Fit various parametric models of band values over pointwise *in situ* data

The applet provides the functionality through a graphical multiple-window interface, with a main figure containing the basic controls. Each different function of the applet typically creates a separate window to either perform the requested procedure or view the results.

### 8.3 **Advantages and comparison with previous software**

Multiple specialized pieces of software have been developed, in order to process data derived from specific instruments or different instruments working at a specific part of the EMR spectrum. However, only few software have been tailored to a data analysis protocol. Using a multitude of software/tools for data analysis may result in errors, as they have to be consistent with each other. Also, maintenance and data analysis is time consuming, as is training of non specialist users. As a result, one single integrating tool would be much more efficient. Some of the most important tools specific for aquatic environments are, for example, WASI (Gege 2004) for modeling and analyzing optical *in situ* measurements in aquatic environments and WASI-2D (Gege 2014) for quantitative analysis of multi- and hyperspectral data from oceanic, coastal and inland waters and BOMBER (Giardino et al. 2012) for estimating water quality and bottom properties from remote sensing images.

WASI (Water colour Simulator) (Gege 2004) is a Windows-based, sensor-independent spectra generator and spectra analyzer, which was developed for forward and inverse calculation of the main types of spectra in aquatic medium. The implemented models are associated with measurements in deep water. It supports eight, commonly measured types of spectra:

- ✓ Downwelling Irradiance above and below the water surface
- ✓ Upwelling Radiance above and below the surface
- ✓ Remote Sensing Reflectance above and below the surface
- ✓ Irradiance Reflectance
- ✓ Specular Reflectance at the water surface
- ✓ Absorption
- ✓ Attenuation
- ✓ Bottom Reflectance

Up to 25 parameters can be determined by WASI, while all model constants and input spectra can be changed easily for adaptation to a specific region.

WASI-2D (Gege 2014) is an image processing module, which has been implemented into the WASI, developed for quantitative analysis of multi- and hyperspectral data from oceanic, coastal and inland waters. The input files are atmospherically corrected images from airborne sensors and satellite instruments. Users can process data in various formats and units, derived from different sensors and associated with the optical properties of the studied water body. Image analysis can be done by inverse modelling using established analytical models. The models of WASI-2D account for Coloured Dissolved Organic Matter, detritus, phytoplankton (six classes) and two spectrally different types of suspended matter, while the sea floor reflectance is specified as sum of up to six substrate types.

BOMBER (Bio-Optical Model Based tool for Estimating water quality and bottom properties from Remote sensing images) (Giardino et al. 2012) is a software package, which is specific for optically deep and shallow waters, for retrieval of the optical properties of water column and bottom from remote sensing data. BOMBER runs as an add-on tool for the ENVI+IDL software and it is available upon request. Users are able to set the appropriate model type, to import and export the necessary files and to set all the variables associated with the model parameterization and inversion. Input data are atmospherically corrected images with reflectance values. BOMBER can be used for the creation of chlorophyll, suspended particulate matter, Coloured Dissolved Organic Matter absorption maps and, in case of shallow waters, bottom depth and distributions of up to three different types of substrate can be defined.

This GUI product, which was developed in the present study, is an application for processing the common types of spectra that are measured by Landsat and similar satellites and extracting lake quality parameters. The algorithmic procedures were originally developed for application in Lake Koronia, but due to their general design, they can also be used for other lakes. The supported spectrum types are irradiance, DNs and reflectance. The basic steps of image processing, described in sub-Chapter 8.2, can be accomplished within a few minutes. Users are able to import a large number of GeoTIFF multispectral images (as single images or as image stacks) and apply all the appropriate methods for assessing water quality parameters. All GeoTIFF images can be viewed as true-color images and include pixel coordinate information. The GUI product includes well documented calculation steps and gives the opportunity of automated, graphical visualization of results and output data. The GUI product can be easily used by non-specialist researchers in Earth Observation from Space and data processing techniques. As a result, these tools can be widely used by lake management agencies and researchers.

## 8.4 **Interface**

Fundamental programming practices dictate that the interface to any functionality library has to be as user-friendly as possible. That rule alone is enough to guide the interface designing process, in order to create a functional GUI without information

congestion and optical disturbances. Much effort was spent to make the GUI interface as user-friendly as possible. For the composition of the GUI in the present study, care was taken to achieve the following guidelines:

- ✓ Simplistic appearance, with controls spatially grouped in sections of specific functionality
- ✓ A main menu controls the basic input functionality
- ✓ Detailed control of each distinct function is separated in different windows in order to avoid an overcrowded main figure
- ✓ Intermediate or end results can be viewed in separate windows and saved in filesProcess-specific functionality is packed in right-click context menus

Since most options in the different pop-up windows of the GUI are intuitive, not every detail is described in this sub-Chapter. A few screenshots are shown henceforth (Figures 35-36), as taken during the development phase. These correspond to a prototype, which, however, is coherent to the appearance of the final product. The screenshots are from various phases of the data processing carried out in the present study. The basic elements that are included in the GUI product are the following (Figures 39-40):

1 Drop-down menu; for importing GeoTIFF files as single images or as image stacks.

2 Drop-down menu; for importing water mask as Matlab file (*.mat). The menu items for the visualization and deletion of the calculated or the imported water mask.

3 Listbox; for the visualization of the imported GeoTIFF files.

4 Listbox; for the visualization of the available band of each GeoTIFF file.

5 Right -click menu; for specifying the range of the EM spectrum of each band.

6 Menu; for the calculation and the visualization of NDWI image, using the equation described in Chapter 5.5.

7 Band Math menu;,a flexible image processing tool. Band Math dialog can be used to define bands or files used as input and to calculate the desired QE. Users can enter mathematical expressions for the calculation of lake QE. All variables in the expression must be named according to the format "$b_n$", i.e. the variables in the expression that represent input bands must begin with the character "b", followed by a numeric character (n) ranging from 1 to 12. Table 18 shows the correspondence between the band names used in Band Math and the range of the EMR spectrum. Each expression is applied on a simple pixel-by-pixel basis. Therefore, the input bands (to which an expression is applied) must all have the same spatial dimensions. The calculated image has the same dimension as the input bands. Figure 38 depicts Band Math processing that adds three bands.

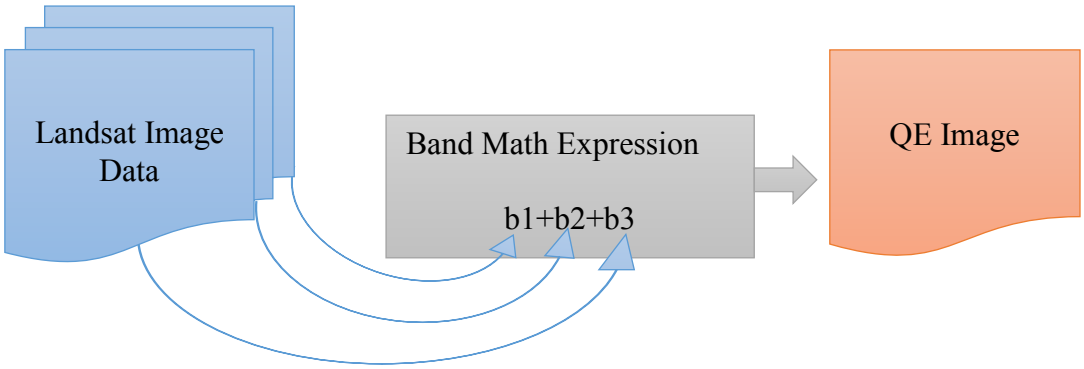


**Figure 38.** An example of Band Math processing.

**Table 18.** The band names used in Band Math of GUI product corresponding range of the EM spectrum.

| Band Name | Range Of EM Spectrum |
|---|---|
| **b1** | Blue |
| **b2** | Green |
| **b3** | Red |
| **b4** | NIR |
| **b5** | SWIR_1 |
| **b6** | SWIR_2 |
| **b7** | Thermal |
| **b8** | Coastal_Aerosol |
| **b9** | TIRS_1 |
| **b10** | TIRS_2 |
| **b11** | Cirrus |
| **b12** | Panchromatic |

8 View Visible Image menu; for manual assignment and visualization of an RGB combination. Users can select the band name, which will be assigned to the red channel, then repeat the procedures, in order to make the green and blue channel selections.

9 Figure window; for the visualization of the NDWI image. It also contains information about the displayed data at the current cursor location.

10 Right-click menu; for the creation of water mask. This tool can be used for the creation of water body masks from multiple separate water bodies. The algorithm that is used for the mask calculation is described in Chapter 5.5. Water masks can be exported as Matlab files (*.mat).

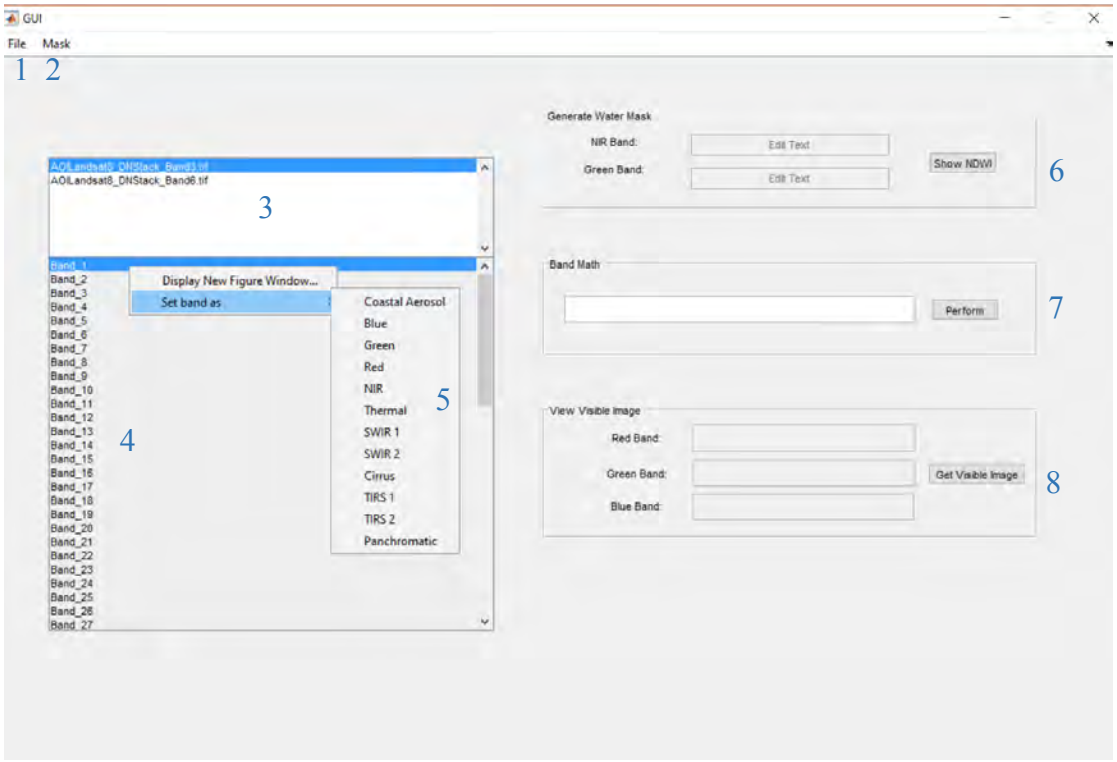


**Figure 39.** Screenshot of the software interface, during the development phase.

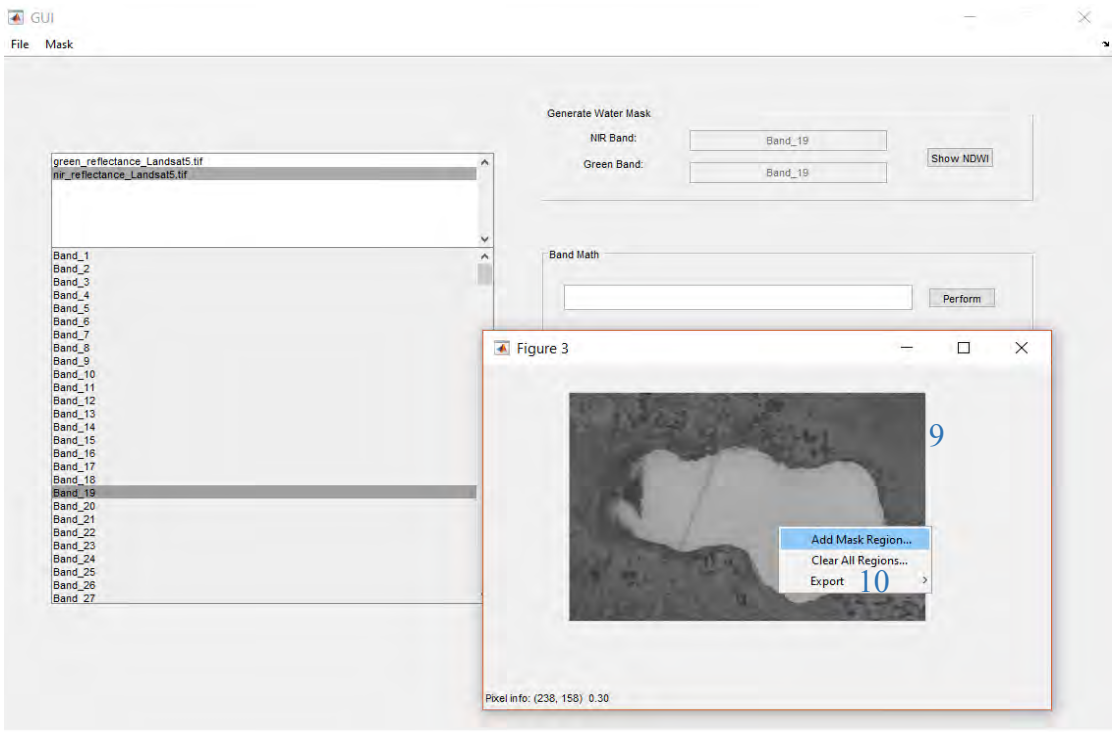


**Figure 40.** Screenshot from the mask creation procedure.

## 9. RESULTS - DISCUSSION

### 9.1 *In Situ* Parameters

The values of the hydromorphological and physicochemical parameters, measured on 30 November, 2015 at three sampling stations are given in Table 19. No significant deviations were observed between the values at the three sampling stations for most of the parameters. This could be attributed to the relatively intense weather conditions at the time of the sampling, which were characterized by relatively strong winds and water currents, causing significant relocations of large water masses, thus smoothing out the parameter variations over the lake area.

The Lake Koronia water showed a slightly to fairly alkaline character with pH values ranging from 8.52-8.54.

The hypersaturated conditions observed may be attributed to water mixing and turbulence, as well as to significant primary production and biogenic aeration.

High conductivity values were recorded at the three sampling stations, ranging from 3700-3380 μS/cm. High conductivity values were also found in previous studies (Bobori 2001, Petaloti et al. 2004) indicating that the waters were rich in electrolytes.

**Table 19.** Physical and chemical composition of *in situ* water samples (Station 1, Station 2, MD) from Lake Koronia on 30 November 2015.

| | | Sampling Station | | |
|---|---|---|---|---|
| **Parameters** | **Units** | **Station 1** | **Station 2** | **DP** |
| pH | | 8.54 | 8.54 | 8.52 |
| Conductivity | μS/cm | 3370 | 3370 | 3380 |
| Dissolved Oxygen | mg/l | 10.2 | 10.5 | 9.9 |
| Temperature | °C | 11.1 | 11.1 | 11.3 |
| Electrical resistance | Ω | 297 | 297 | 295 |
| Water Depth | m | 2.3 | 2.1 | 2.2 |
| Salinity | ppt | 1.7 | 1.7 | 1.7 |
| $N\text{-}NO_2$ | mg/l | 0.025 | 0.024 | 0.035 |
| $N\text{-}NO_3$ | mg/l | 0.2 | 0.06 | 0.21 |
| $N\text{-}NH_4$ | mg/l | 0.033 | 0.05 | 0.072 |
| $P\text{-}PO_4$ | mg/l | 0.05 | 0.05 | 0.06 |
| TN | mg/l | 1.2 | 1.4 | 1.7 |

## 9.2 **Mask Derivation Algorithm**

Figure 41 provides a juxtaposition of a number of Landsat Surface Reflectance High Level Data Product water masks of Lake Koronia, downloaded from the EarthExplorer site (http://earthexplorer.usgs.gov/) of USGS and the calculated masks using the NDWI values with the algorithm described in Chapter 5.5. In most occasions, the two masks have a high degree of similarity (measured as the percentage of pixels of the mask from the NDWI algorithm that coincide with the corresponding water pixels from the downloaded QA bands). The primary reason that the land-water separation algorithm was necessary is because of the limited temporal availability of official land-water masks, as in some cases the water mask of Lake Koronia was not calculated. Another important reason was that the QA bands of the Surface Reflectance High Level Data Products contained pixels that were diffused in the end-product, making it impossible to designate a usable connected water surface body for further calculations. Thus, it was deemed more suitable to reconstruct an algorithm and use the QA bands for validation.

In a few cases, the QA bands appear to identify much fewer water pixels than the algorithm implemented in this study. The explanation lies in the different water separation criteria used. Although it is difficult to argue about which one is more reliable, the NDWI index appears to be widely accepted as accurate and highly specific (Sahu 2014, Ji et al. 2009) and was preferred in this study.

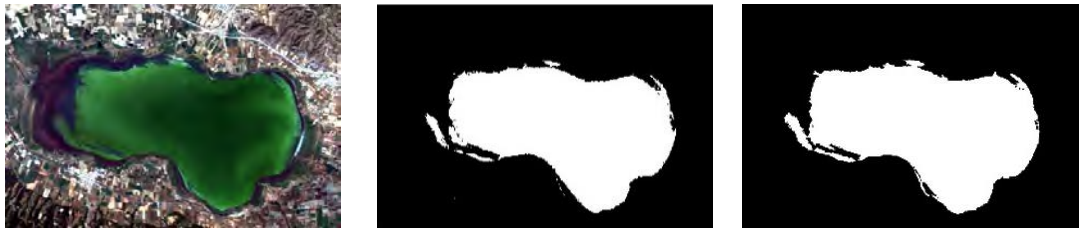

29/5/2006 (Landsat-5/TM) ~96.3% Identical

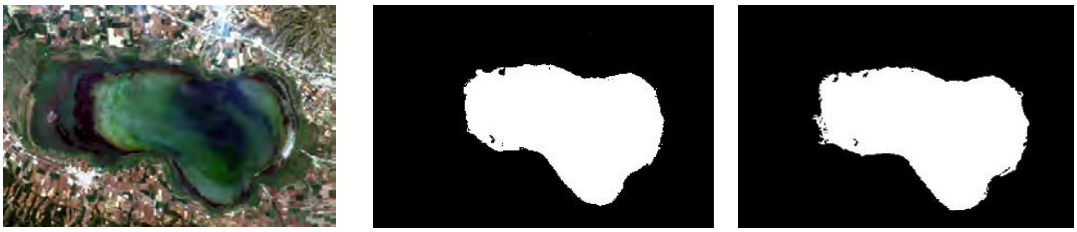

9/6/2010 (Landsat-5/TM) ~93.1% Identical

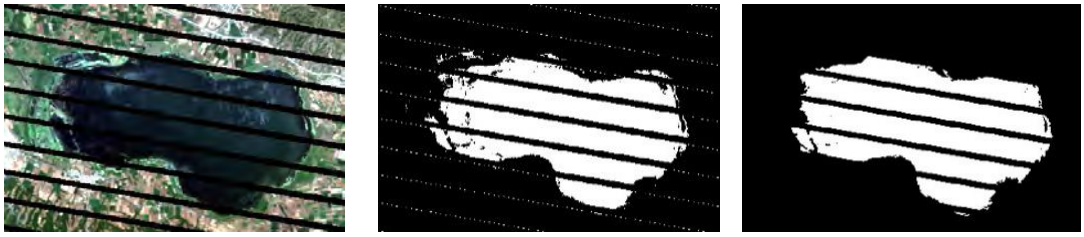

22/6/2015 (Landsat-7/ETM+ SLC OFF) ~93.6% Identical

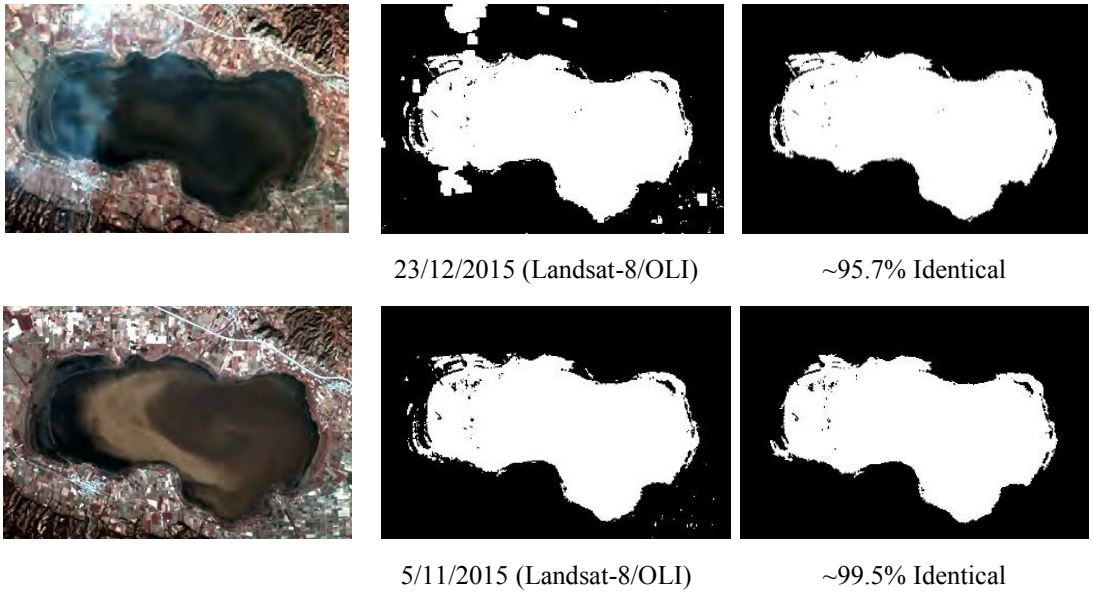


**Figure 41.** A comparison of the natural color Landsat images (left column) Landsat Surface Reflectance High Level Data Product water masks of Lake Koronia, downloaded from the EarthExplorer, USGS (middle column) and the evaluated masks using the method described in Chapter 5.5 (right column).

At this point, it ought to be stressed that a significant number of satellite images appear to exhibit a relatively high percentage of cloud coverage over Lake Koronia, which has been verified in the following results to interfere with the calculations, often severely degrading the accuracy of the estimated parameters. Thus, the satellite-derived results presented henceforth occasionally exhibit extreme deviations when compared against *in situ* data.

### 9.3 Satellite data validation using *in situ* measurements

Table 20 shows the *in situ* data recorded on 30 November 2015. These values appear to have large deviations from the corresponding parameter values calculated from the Landsat-8 satellite image of the same day. This was, in part, expected, due to the very prominent cloud artifact coverage of the image during the day of overpass. Apart from that, it was impossible to calculate temperature data because the TIRS instrument of the Landsat-8 satellite was not functional during that time period. On Sunday, November 1, 2015, the Thermal Infrared Sensor (TIRS) experienced an anomalous condition related to the instrument's ability to accurately measure the location of the Scene Select Mechanism (SSM). The anomaly caused the upper bits of the encoder counts in the ancillary data to be corrupt, resulting in the TIRS bands becoming misregistered by approximately 500 meters (18 pixels) *[url22]*.

**Table 20.** Comparison between *in situ* and satellite-derived data for pH and conductivity

| Parameters | Units | Sampling Station | | | | | |
|---|---|---|---|---|---|---|---|
| | | Station 1 | | Station 2 | | DP | |
| | | *In situ* | Satellite measurements | *In situ* | Satellite measurements | *In situ* | Satellite measurements |
| pH | | 8.54 | 5.4 | 8.54 | 5.8 | 8.52 | 5.81 |
| Conductivity | (μS/cm) | 3370 | 0.304 | 3370 | 1.505 | 3380 | 1.533 |

As mentioned in Chapter 7.5, the Landsat images, which were simultaneous with the available *in situ* data, were also processed using the LEDAPS and L8SR algorithm, in order to obtain surface reflectance values. The results from these images exhibited strong discordance to the *in situ* data and, consequently, were not employed, rather all calculations were carried out using standard TOA reflectance.

Figure 42 depicts the temperature variations over the two sampling stations, Akti Analipsis and Vasiloudi in pairs of time-series from *in situ* data, provided by Management Authority of Lakes Koronia-Volvi, and data derived from suitable radiometric calibration of the thermal bands of the corresponding Landsat satellites. The satellite-derived values were calculated as 3x3 averages over the stations' matching pixels.

First of all, it is important to note that the time-series pairs do not span the exact same periods, that is, for most of the available data series. This was due to the fact that there was a shortage of *in situ* data with respect to the sampling stations. The only significant match between *in situ* and satellite-derived temperature values occurred for the sampling station of Akti Analipsis when using thermal band reflectance data from Landsat-5/TM thermal and Landsat-7/ETM+VCID-2 bands. There appears to be a significant systematic difference between VCID-1 and VCID-2 bands when used to extract temperature values. VCID-1 provides an expanded dynamic range and lower radiometric resolution (sensitivity), with less saturation at high Digital Number values, while VCID-2 has higher radiometric resolution (sensitivity) although it has a more restricted dynamic range *[url26]*. This may explain the more significant match between *in situ* and VCID-2 than the match between *in situ* data and VCID-1. The irregular (negative) values in the figures for the cases of Landsat-7 are attributed to the cases where the sampling station pixels are at a location with invalid satellite data, due to the Landsat-7 SLC malfunction. Although, according to Lamaro et al. (2013) Landsat-7/ ETM+ thermal band 6 Low Gain is suitable for estimation of water surface temperature, because its range is greater and it is not saturated.

The mismatch between the time-series values of Landsat-8 and the *in situ* data could be because of stray light. Since the launch of Landsat 8 in 2013, thermal energy from outside the normal field of view (stray light) has affected the data collected in TIRS Bands 10 and 11 *[url27]*. This stray light increases the reported temperature by up to four degrees Kelvin (K) in Band 10 and up to eight K in Band 11. This can vary throughout

each scene and depends upon radiance outside the instrument field of view, which users cannot correct in the Landsat Level 1 data product. Band 11 is significantly more contaminated by stray light than Band 10. It is recommended that users refrain from using Band 11 data in quantitative analysis including use of Band 11 in split-window surface temperature retrieval algorithms *[url27]*.

The mismatch between the time-series values could also be because of the particularities of the sampling station locations. These locations are very close to the shore, where heavy vegetation is often found, which, along with the muddy bottom of the very shallow waters, might be distorting the optical properties of water and, in turn, the parameters extracted from satellite images, in this case, temperature. In a number of cases, the lake water level is also very low, and the parameter values over the station pixels practically refer to dry land, causing the irregularities on the charts.

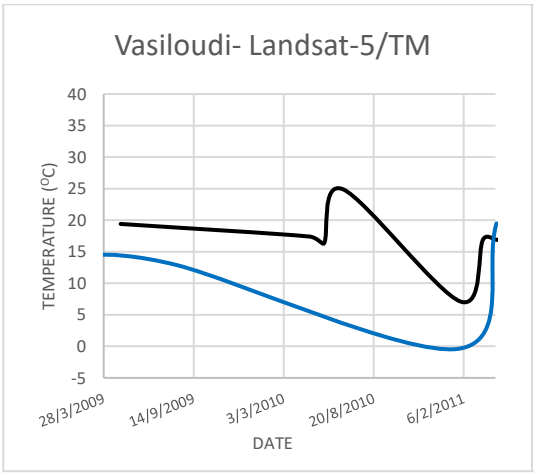


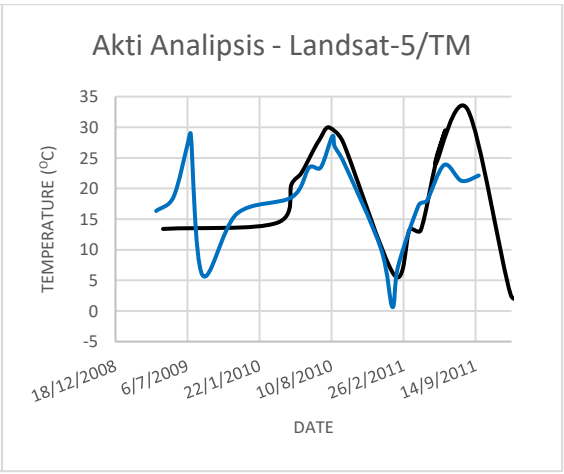


There were no available *in situ* data

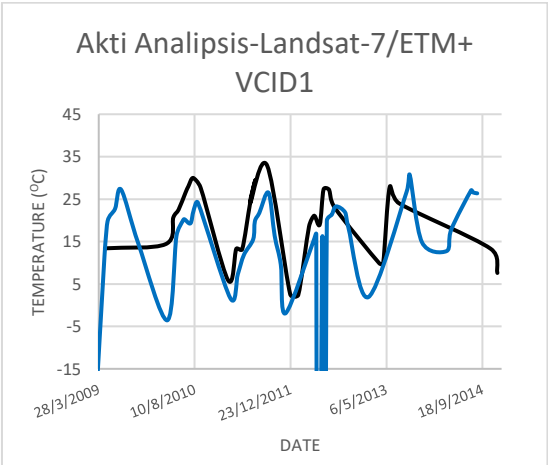

There were no available *in situ* data

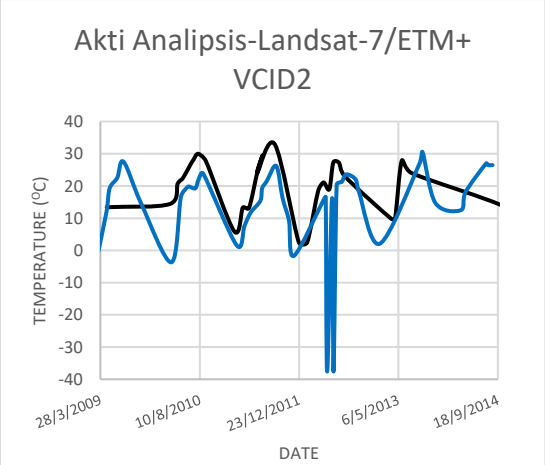


There were no available *in situ* data

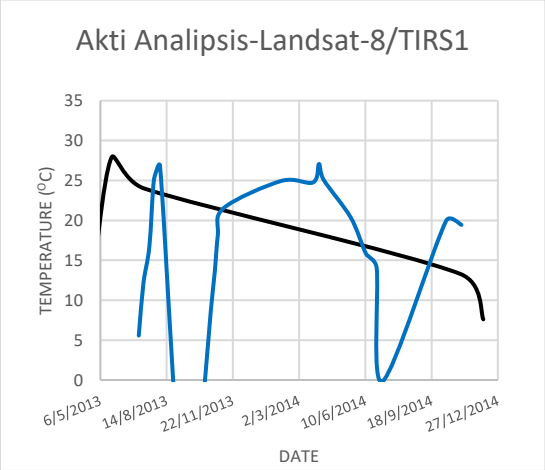


There were no available *in situ* data

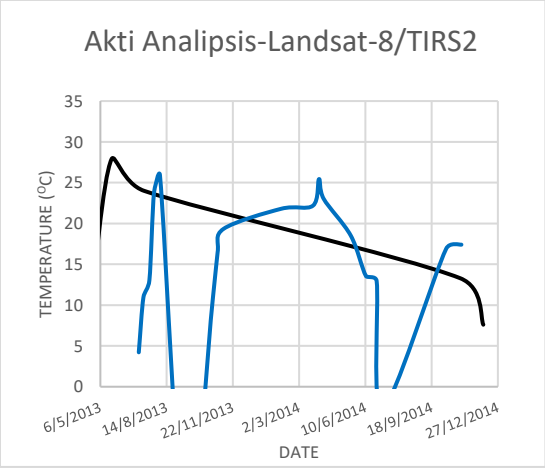


**Figure 42.** Water Temperature variations over the two sampling stations (Vasiloudi, Akti Analipsis) in pairs of time-series (2009-2014) from *in situ* data and data derived from suitable radiometric calibration of the thermal bands of the Landsat satellites. Landsat-5/TM time-series adequately follows *in situ* data. Landsat-7/ETM+ VCID2 presents inconsistencies due to occasional *in situ* station position on stripe edges (invalid data zones). Landsat-8/OLI TIRS1 and TIRS2 bands are known to suffer from sensor malfunctions since early 2013.Black line: *in situ* data, Blue line: Satellite data.

Figure 43 depicts the pH over the sampling station pixels against the pH values as derived following the methods described in Chapter 7.5.5.

In the case of Landsat-5/TM data, the pH values appear to deviate no more than 1 pH unit, an observation in favor of the equation derived in the aforementioned chapter. The same limitations with above also apply for this parameter, which means that when the lake water level was relatively low, the station pixels typically refer to dry land, rendering the parameter calculation equations invalid.

In the case of Landsat-7 SLC OFF, the data appears to be scrambled and misleading. This is because, frequently, every few consecutive satellite images, the scan lines of invalid data cover the sampling station pixels, resulting in invalid measurements. Apart from that, the deviations could also be attributed to shortcomings of the derived parameter model equation. In the case of Landsat-8, the temporal overlap between the *in situ* and the satellite image derived data is even smaller in duration, primarily because the Landsat-8 mission is very recent in comparison to the data available from the sampling stations. Also, the inconsistency of the data could be, too, attributed to the fact the water level of the lake was lower, often forcing the calculation to take place over very shallow waters.

It is also possible that, because the original equations were developed using Landsat-5 data, discrepancies arise from slight differences in the corresponding sensors of Landsat-7 and Landsat-8 satellites. Apart from all the above, a peak in pH value, around 9.3, was observed in the middle of 2011, which was followed by a continuous subsequent drop, reaching a locally minimum pH value of around 8.2 in the middle of 2012, slightly increasing and varying smoothly from then on.

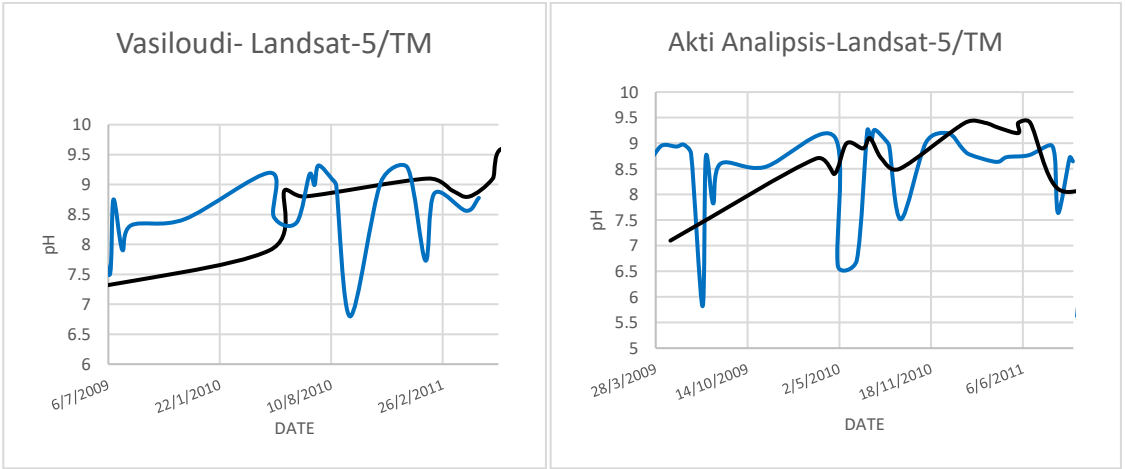

Vasiloudi station was not included in the water mask

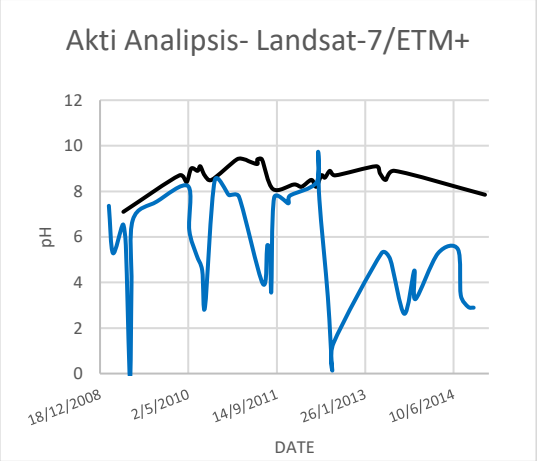


There were no available *in situ* data

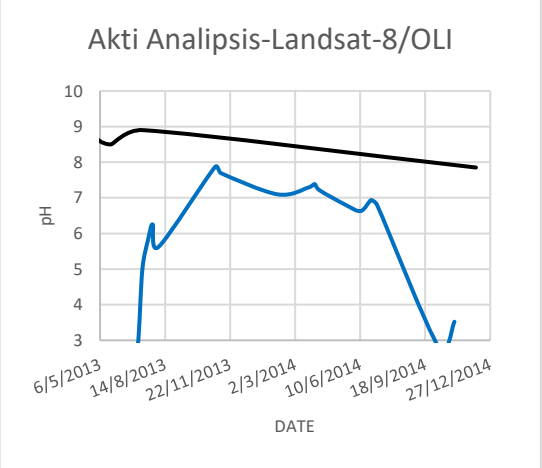


**Figure 43.** pH variations over the two sampling stations (Vasiloudi, Akti Analipsis) in pairs of time-series (2009-2014) from *in situ* data and data derived from suitable radiometric calibration of the thermal bands of the Landsat satellites. Black line: *in situ* data, Blue line: satellite data

Figure 44 depicts the values of Conductivity taken from the sampling stations against the values derived following the methods of Chapter 7.5.6. Apart from a small occurrence of jumps over the satellite data time-series, there is a fair consistency between the two data sources in the case of Landsat-5 time-series. In the cases of Landsat-7 and Landsat-8 the two time-series are increasingly discrepant, which further corroborates the suspicion of the satellite sensor specificities in the equation model for conductivity, as it once again performs better in the case of Landsat-5 data. It should be stated once again at this point that the satellite-derived equations for the parameter calculations are relatively simplistic and are only expected to be able to provide results with a fairly rough level of accuracy.

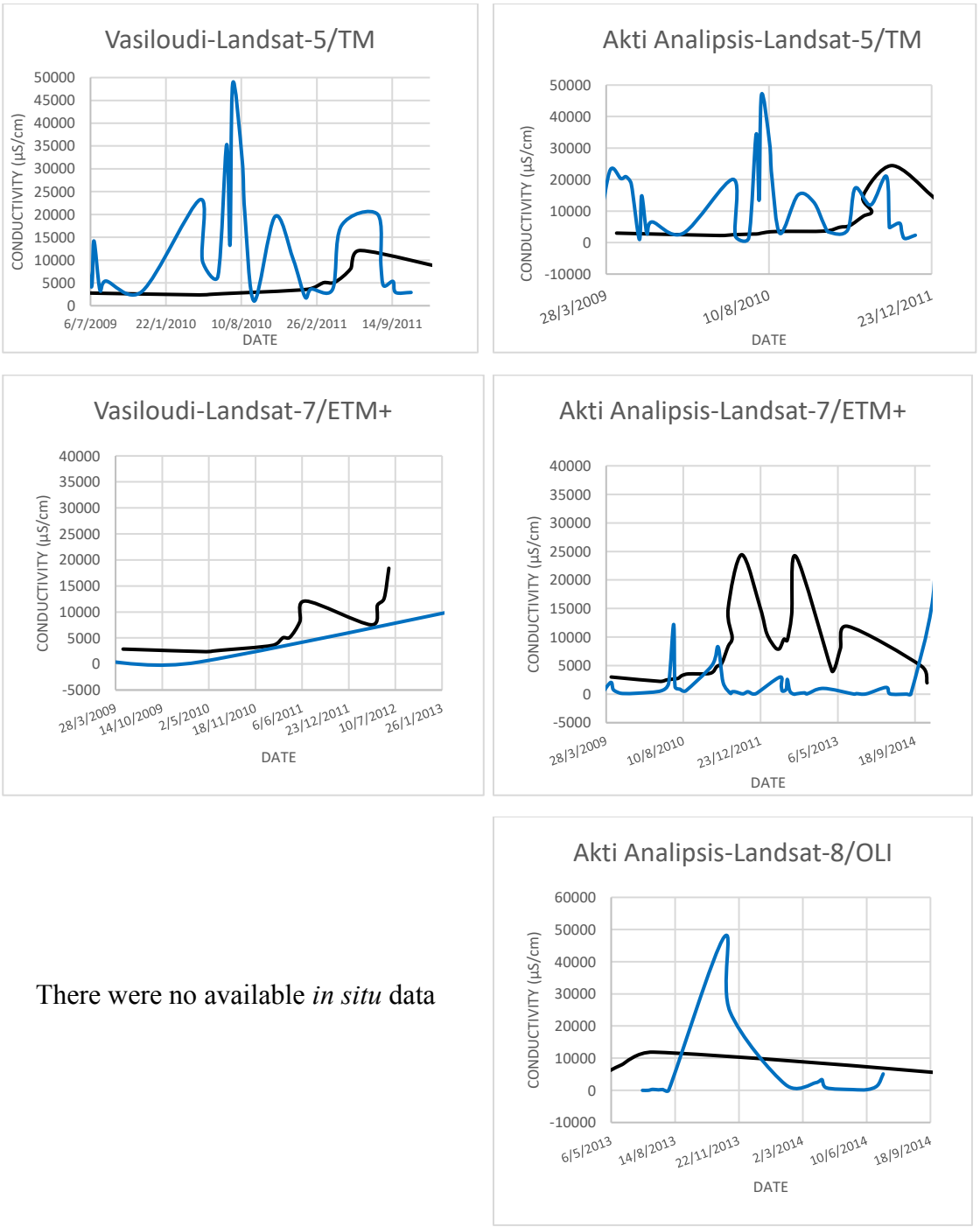


There were no available *in situ* data

**Figure 44.** Conductivity variations over the two sampling stations (Vasiloudi, Akti Analipsis) in pairs of time-series (2009-2014) from *in situ* data and data derived from suitable radiometric calibration of the thermal bands of the Landsat satellites. Black line: *in situ* data, Blue line: satellite data

Figure 45 below depicts the Secchi Disk Depth time-series on the approximate deepest point of the lake from *in situ* data, provided by Michaloudi et al.(2012) against satellite-derived data. In all cases, the satellite-derived SDD equation model seems to systematically over-estimate the SDD value in comparison to the *in situ* data. This is, in part, due to the fact that the SDD equation of Chapter 6.6.2 utilizes a blue/green band reflectance ratio, which has been shown to strongly correlate with depth in relatively

clear water (Stumpf et al. 2003). As a result, the equation is mathematically expected to produce larger values over deeper positions, as, in this case, the deepest point of the lake, when the water is relatively clear. Since the green band reflectance is used, lake coverage from aquatic vegetation is expected to alter the result towards the right direction, since the presence of aquatic vegetation means higher turbidity, higher green reflectance (the denominator in the equation) and, therefore, lower estimated SDD values. Apart from that, the mismatch between the time-series values could possibly be related to inaccurate location of the *in situ* sampling station, since the original paper does not clearly provide accurate position data.

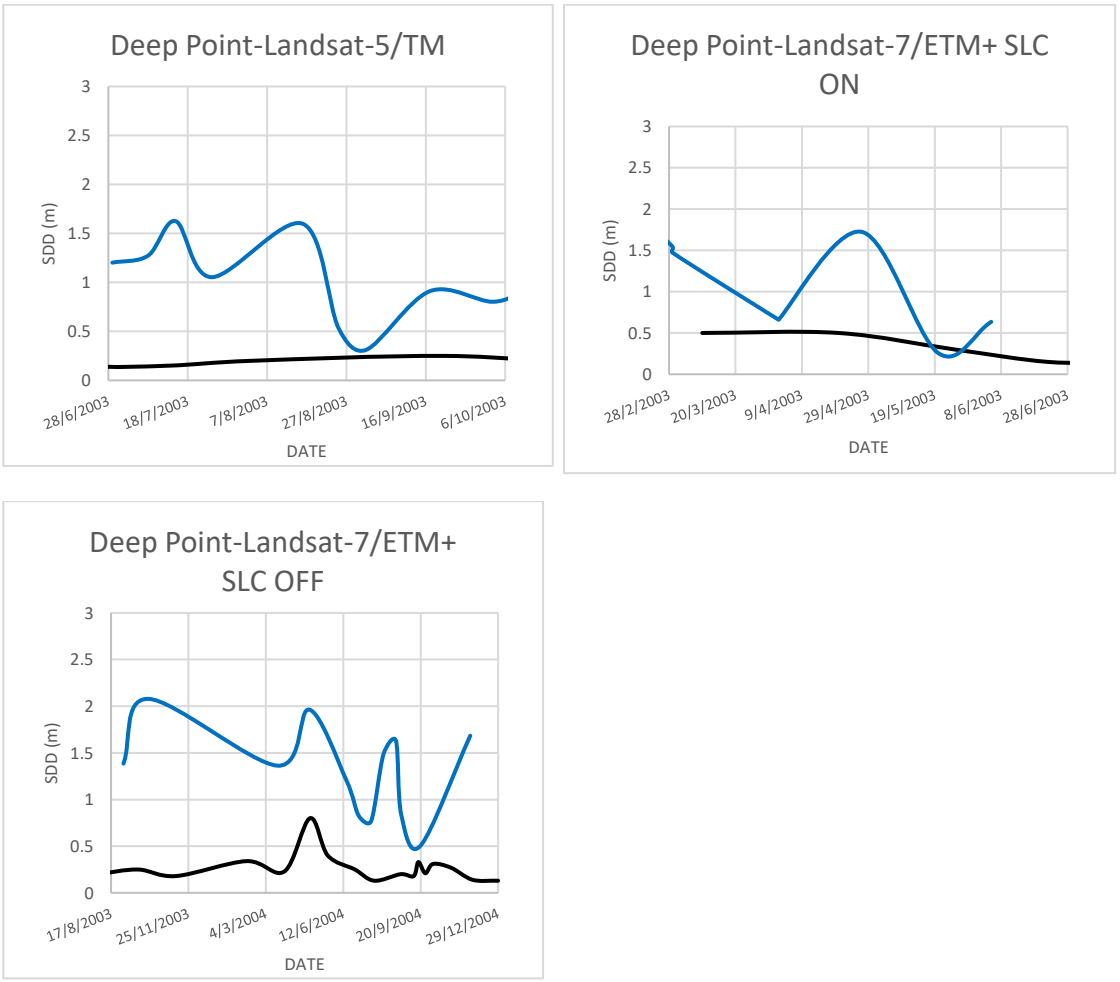


**Figure 45.** SDD variations over the deepest point of Koronia in pairs of time-series from *in situ* data (Michaloudi et al. 2012) and data derived from suitable radiometric calibration of the thermal bands of the Landsat satellites. Black line: *in situ* data, Blue line: satellite data

## 9.4 **Satellite data validation using satellite sensor calibration information**

The analysis of the Chapter 9.3 aims primarily to assist in assessing the reliability of the derived results. This refers to the validity of the results with respect to the actual values, namely their proximity to the corresponding values for the parameters under

determination, which are regarded as “most accurate”, provided they originate, in turn, from a highly reliable measurement system and methodology. The accuracy of the results is, instead, a measure of how good the accordance is between different sessions of measurements for the same parameter, under the same conditions. In other words, the accuracy measures how well repeated measurements of the same parameter under identical conditions are distributed around their overall average. Accuracy is typically expressed in statistical contexts in terms of the standard deviations of the measured values.

The accuracy of results obtained from satellite data is immediately related to the accuracy of the satellite data, as well as the mathematical model used to derive each parameter. According to the law of covariance propagation (Ku 1996, Clifford 1973), the standard deviation of a parameter derived from one or more variables by virtue of a concise mathematical formula is estimated using the mathematical derivatives of the variables and their standard deviation values. Therefore, a measure of the precision of the originally used satellite data is necessary. The precision of satellite data is estimated by means of calibration of the collected data by the satellite using a number of different techniques. Among these techniques, on-board instruments are frequently depended upon, such as internal calibrators, and more extensive analyses are carried out using either vicarious data of trusted precision and reliability, or satellite data of large areas with specific, relatively constant optical properties, such as deserts. A common option was, in the case of Landsat-5/TM satellite data, to use as external vicarious data for the calibration those collected by the Landsat-7/ETM+ satellite sensor.

The outcome of the calibration procedures is an estimate of the percentage precision of the measured satellite data, i.e. the radiance, or the final reflectance value. Extensive research indicated that limited post-launch calibration analyses have been carried out, which provide mixed, but adequately concordant information. The differences may be attributed to the different time periods of the datasets used for the calibration as the instruments on the satellites wear out with time and the quality of the data slowly degrades. This is especially true for the Landsat-5/TM satellite, which is well known for the fact that it operated well beyond the initially predicted lifespan of three years (Barsi et al. 2007). In the following, the precision has only been evaluated using the Landsat-5 TM data, due to the variable accuracy of the sensors of the different satellites. The data of the satellite missions have been calibrated using all of the above methods, and, after a review of the literature (Markham & Helder 2012), the adopted standard deviation values for the Landsat-5/TM satellite data were taken to be equal to 5% of the derived reflectance values for all bands except for the thermal band, which was taken to be equal to 2% of the measured radiance value.

In order to assess the precision of the results, a resolution comparison scheme was adopted. Instead of evaluating and presenting the derived standard deviation of the results, the ratio of the derived standard deviation to the overall standard deviation of the value distribution over the lake was calculated. The latter was judged to be a more directly evident measure of the suitability of each algorithm for the derived results,

which would be far easier to interpret. Specifically, for each satellite image, two values were estimated. The standard deviation of the derived satellite precision of a parameter (henceforth called sigma of that parameter) was calculated using the law of covariance propagation on the algorithm equation for the parameter in question, utilizing a reflectance standard deviation value at 5% of the satellite reflectance value at each pixel for all bands except for the thermal band, for which the radiance standard deviation was taken to be 2% of the radiance value at each pixel. This reflects the fact that the temperature was determined on a more accurate basis than the rest of the parameters. The process was carried out for every single satellite image, which means that the parameter sigma was different at each pixel. Therefore, an overall average for the parameter sigma over the lake was calculated as representative for each satellite image. This value expresses the resolution capability of the satellite instruments in determining the parameter value on a satellite image.

Apart from the above, the standard deviation of the parameter distribution was calculated for each satellite image and parameter. This value expresses the deviation from the average, i.e. the overall variability of the parameter values over the lake. Thus, two values were made available for each satellite image and parameter, the parameter sigma, which is the precision of the parameter determination due to the satellite instrument and algorithm equation, and the parameter standard deviation, which is the variability of the parameter value distribution as measured over the lake. In order for the parameter to be feasibly determined, the parameter sigma value has to be smaller than the deviation of the parameter over the lake, otherwise the difference of the parameter values over the pixels of the lake may just as well be attributed to instrument errors, rather than actual fluctuations of the parameter. For example, when measuring temperatures with an accuracy of ±1$^{o}$C, it would seem incongruous to attempt to interpret a distribution of measured temperatures that appears to range between 12.5$^{o}$C and 12.9$^{o}$ C. Due to the measurement and derivation precision of ±1$^{o}$C, these temperatures may just as well be all identical and the deviations owing to observational errors.

In order to present a concise and clear depiction of the aforementioned case, the ratio of the two values (sigma / deviation) for each parameter and satellite image was calculated and plotted for all satellite images and parameters where it was possible to be determined. This ratio expresses how higher or lower the determination precision is from the apparent deviation of the values in a distribution. Naturally, the lower this value, the better the determination of the parameter from a satellite image. It is important to state, however, that this ratio does not express accuracy per se, only the parameter sigma expresses the measurement and parameter derivation accuracy. The reason that this ratio is preferred has to do with the fact that the parameter sigma depends on the initial reflectance or radiance value as measured by the satellite and is determined per pixel. This means that the accuracy differs according to the conditions and the actual parameter values. Furthermore, the accuracy alone cannot be depended upon to judge how trustworthy the results are. Therefore, in order to “uncouple” these accuracy measures

for each satellite image from the conditions and parameter values they are dependent on, the ratio is calculated and used as an absolute measure of algorithm suitability.

The following are plots of the variation of this ratio over the different satellite images according to their date of capture. When the ratio value is equal to 1, meaning that the deviation of the measured value distribution is equal to the parameter sigma (measurement precision), the determination is "borderline" accurate, since the measurement and derivation accuracy (parameter sigma), i.e. the measurement resolution, can marginally discern the deviation of the parameter value distribution. Identically, the parameter sigma should be as low as possible, indicating a small marginal difference between two clearly discernible measurement values and, thus, a high resolution accuracy and, necessarily, lower than the distribution deviation, otherwise, the determined parameter values of the distribution vary on a scale well below the resolution capability of the measurement system and derivation method (equation).

Figure 46 depicts the sigma/deviation ratio for the Temperature, which is derived by the thermal band, a slightly more sensitive and accurate band than the others, with an approximately 2% relative radiance accuracy. Also depicted on the figure is a polynomial best-fit curve over the ratio value time series, in order to clarify the general trend of their variation. In general, it can be noted that the temperature fluctuations over the satellite images are exceedingly often more smaller than the temperature sigma values, i.e. the measurement and derivation resolution of the temperature is not accurate enough to discern the given temperature fluctuations, except for a small time frame between the middle of 2007 and 2010, where the temperature fluctuations are apparently larger and, thus, the variation is more definitive and not possibly owing solely to observation errors. It must be stated that the temperature sigma over the images varies only slightly among the pixels and the overall average for all satellite images and pixels is $1.3^{o}C \pm 0.07^{o}C$. As an example, temperature deviations over the lake that are around $0.5^{o}C$ (a typical average for many satellite images) are too delicate to attribute to actually different pixel temperatures, since the resolution is around $1.3^{o}C$ and anything lower than that can easily be caused by data noise and instrumental measurement and mathematical model shortcomings.

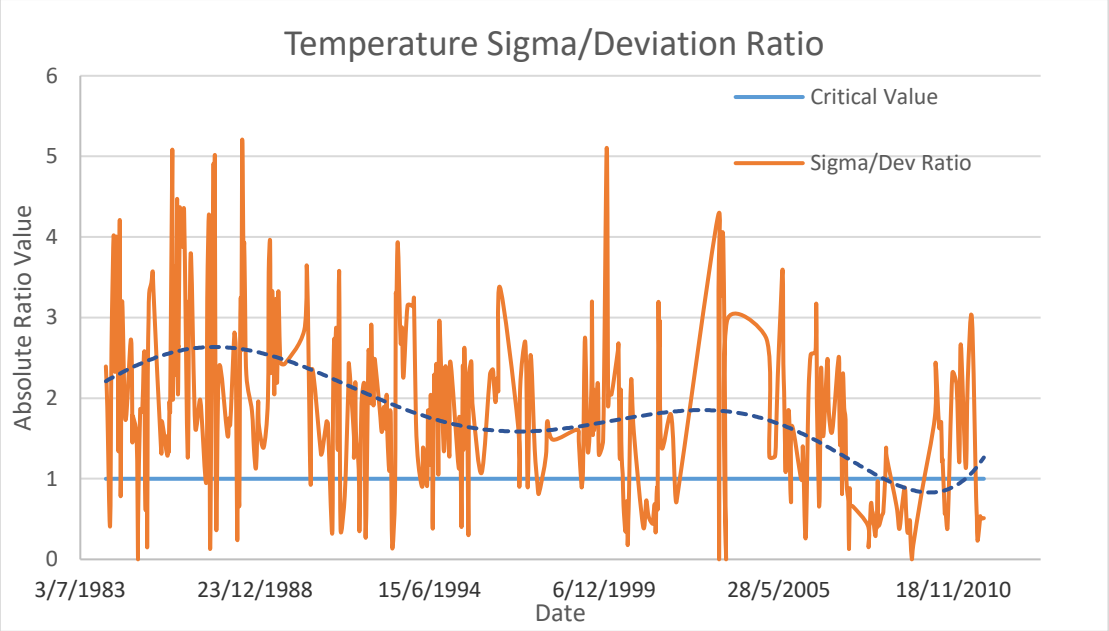


**Figure 46.** The determination ratio for temperature from data of Landsat-5/TM.

The Figure 47 below depicts the sigma/deviation ratio for the Secchi Disk Depth determination, along with a polynomial best-fit curve to capture the main trend of the variation. It can be clearly noted from this figure as well that the SDD parameter sigma is, in general, larger than the SDD deviation over the lake for almost the entire time period of the Landsat-5 data. This means that the deviations of the SDD value over the lake are not reliably attributable to actual fluctuations of the parameter. It should be stated at this point, that this does not render the parameter determination futile, rather it means that one cannot entirely trust the variation of the parameter values over the satellite image. In other words, only the average parameter value can be depended upon to describe the area from a statistical perspective, taking into account the measurement precision and the mathematical model. The average SDD sigma value throughout the satellite images of the lake is 0.656 ± 0.38 m. Taking into account the nature of this parameter, this is not an acceptable average measurement precision for such a shallow lake, especially due to its composition and levels of turbidity, as the SDD value is expected to be lower even than this sigma value at certain areas, and this derivation accuracy is not sensitive enough to capture smaller differences of SDD values between pixels.

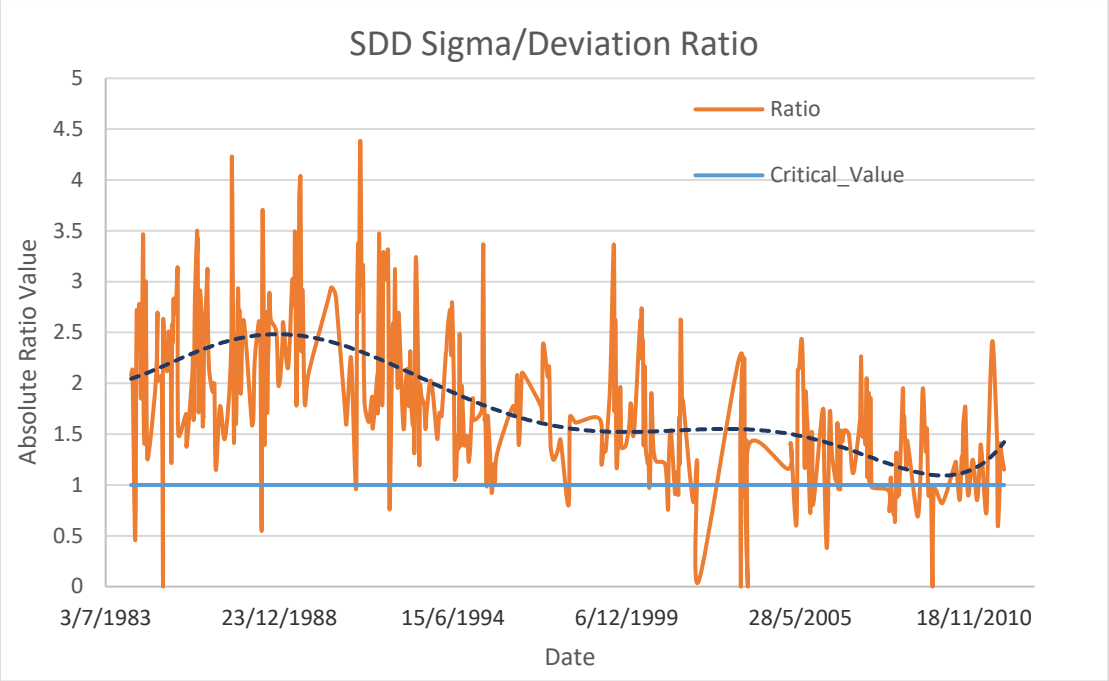


**Figure 47.** Sigma/deviation ratio for the Secchi Disk Depth.

Figure 48 depicts the sigma/deviation ratio for the Chlorophyll *a* parameter, along with a best-fit polynomial line to show the main trend of variation over time. The Chlorophyll *a* parameter overall average sigma value from all satellite image pixel averages, representing the measurement and derivation precision of the parameter, is calculated to be 0.092 ± 0.0245 μg/l. This, as can be noted from Figure 48, is not adequate to capture the variations of the parameter over the lake throughout most of the studied time period. However, after 2000, the determination appears to improve substantially, mainly because the spatial fluctuations of Chlorophyll *a* concentration become more pronounced over the lake pixels. It is noted once again at this point, that when the determination is moderate to bad (ratio values well over the critical value of 1), this is not an overstating of inaccuracy in the measured parameter values. Instead, it means that when comparing pixels with different parameter values on a specific satellite image, the value difference between the pixels cannot be sufficiently substantiated to be actual, but might merely have arisen due to measurement artifacts or data noise.

Because of the fact that a model utilizing DN values is not considered to have a natural interpretation, and also, because there is no physical way to attribute accuracy to DN values other than their inherent scale limitation of being strictly integers, which would pinpoint an accuracy of ±1 DN, the pH parameter was excluded from the accuracy calculations. Another reason for this was the relatively distorting mathematical equation for the calculation of the pH, as presented in Chapter 7. Inherently, this equation provides an overly optimistic accuracy for the pH parameter, in case one considers the aforementioned DN integer precision. In order to calculate a specific precision of the DN values of pixels for a satellite image, it would be necessary to derive it through the radiometric calibration parameters of converting radiance values to DN during the

satellite data acquisition. As this exceedingly complicates the process without adhering to a model as realistic as if using the finally re-retrieved reflectance values, as well as due to all of the aforementioned reasons, it was deemed that the determination ratio would be misleading for the case of the pH.

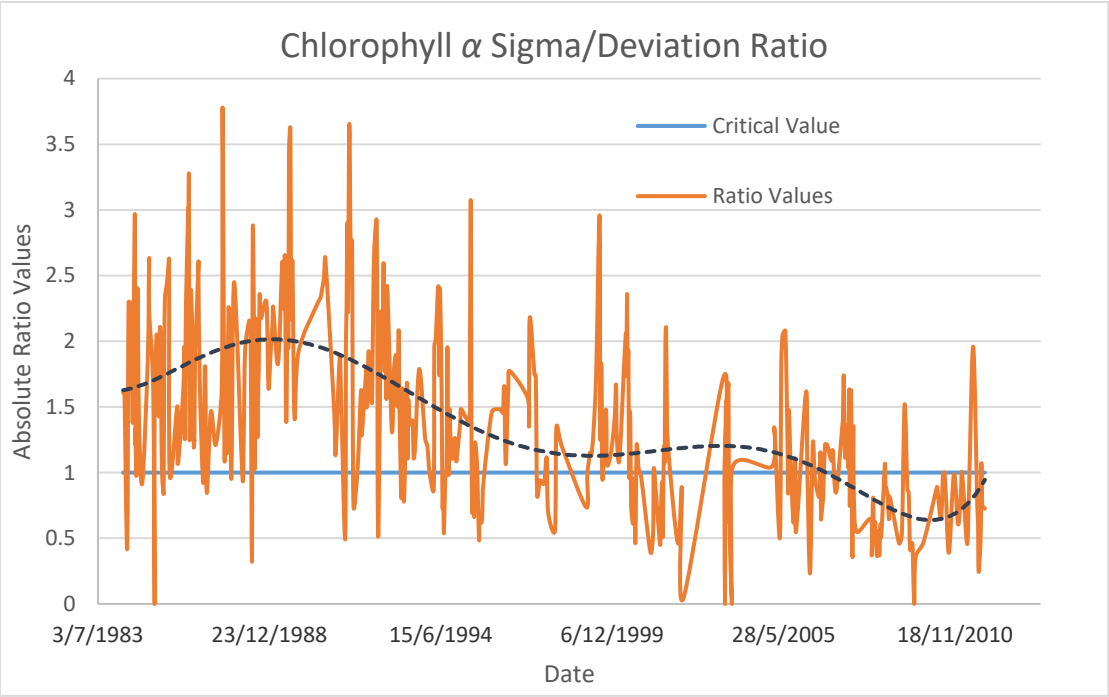


**Figure 48.** Sigma/deviation ratio for the Chlorophyll *a* parameter.

Figure 49, depicts the sigma/deviation ratio of the Electrical Conductivity parameter, along with a polynomial best-fit curve to reveal the main trend of the ratio over time. In this case, the parameter derivation accuracy appears to be adequate enough to capture the exhibited variations over the lake for most of the time period. The determination quality appears to degrade between 2000-2002 and 2005-2007 because the Electrical Conductivity parameter presented smaller deviations in its distribution over the lake. The derivation sigma for the Electrical Conductivity parameter was, on average for all pixels and satellite images, found to be equal to 813.6 ± 428.56 μS/cm.

As a final comment, the results of this subchapter are meant to be interpreted with special care; in the above, it was overstated, that the ratio values do not assess the accuracy of the satellite data, rather their level of accuracy with respect to the parameter distribution variability, since the focus of this study revolves around evaluating the suitability and reliability of the specific data at hand and not assessing the overall accuracy of the satellite data for the derivation of parameters in general. As such, an unfavorable relation does not necessarily speak against the accuracy of the derived parameters, and a favorable relation does not necessarily support the accuracy quality. The accuracy can only be judged by the average sigma values provided above and, with reservation, as always, these values are only meaningful when interpreted under clear

and comprehensible circumstances of determination and well-defined respective precision requirements.

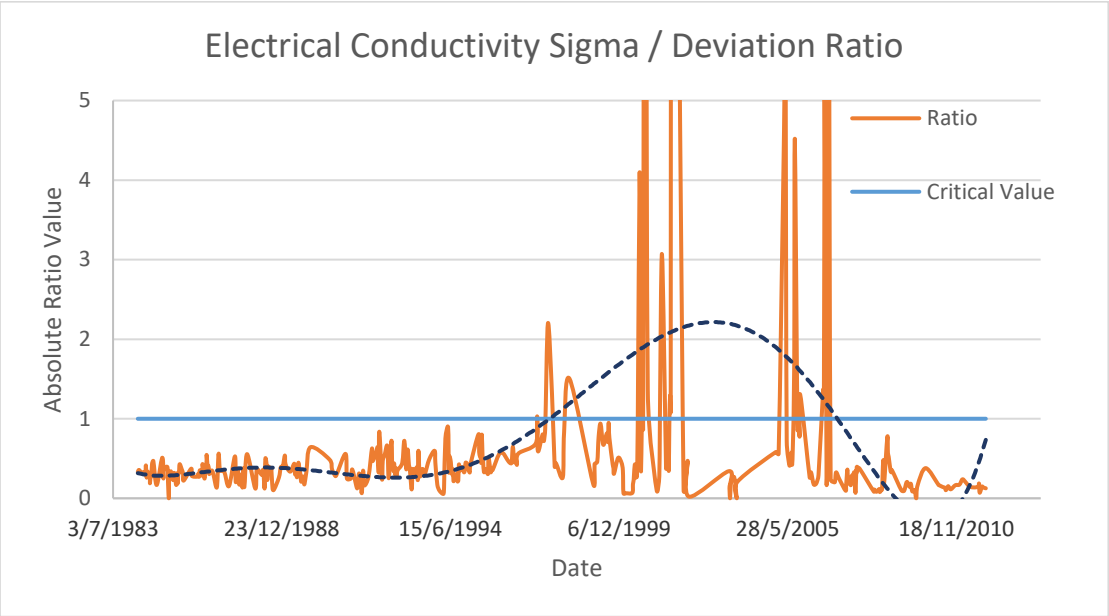


**Figure 49.** Sigma/deviation ratio of the Electrical Conductivity parameter.

## 9.5 **Temperature**

Water surface temperature is the result of the energy balance at the water surface and heat transport mechanisms within the water body. Therefore, knowledge of it is required to characterize processes at the water surface. Figures 50-53 present the average temperature time-series of Lake Koronia from satellite image derived data over a period of about 30 years. The seasonal pattern is clearly visible on the charts, with peak temperatures occurring during the summer seasons and minimums in winter seasons.

The temperature of the lake's water presented wide fluctuations over the course of the years, with values in the expected range, from a few degrees under 0 ºC up to 25 ºC, or even 30 ºC. Climatic factors, including air temperature, cloud cover, and solar radiation, in addition to geomorphometric factors, such as lake surface area and depth, influence surface water temperatures in lake Koronia. It is important to observe a slightly increasing trend in temperature, especially in the later years, which may be a weak indication of the effects of the reduction, up to 90%, of lake Koronia water volume (Mylopoulos et al. 2007). Shallower lakes tend to warm more rapidly with higher surface water temperatures compared to deep lakes that have greater heat storage capacities (Oswald & Rouse 2004). A simultaneous monitoring of climatic forcing variables and geomorphometric factors of lake Koronia, which are the most important in driving changes in water temperature, and an extensive analysis might be necessary in order to infer causality with more certainty.

A comparison of the Temperature values with data from Bobori (2001) shows a relatively fair accuracy, well within the limits of one standard deviation. In specific, the temperature from 5 stations in a period of two full years (of irregular observations), namely 1989 and 1990, from Bobori (2001) results in an average Temperature value of 16.90 ± 8.2 ºC, whereas the corresponding overall average of the lake in the same time period in the current study results in a value of 14.78 ± 8.1 ºC.

Furthermore, an investigation of Temperature data from Michaloudi et al. (2012) also reveals a fair accordance. An indicative example from Michaloudi et al. (2012) shows an average Temperature value of 24.1 ºC in August and September 2003. The Temperature data of the present study resulted in an average Temperature value of 21.84 ± 2.35 ºC during the same period.

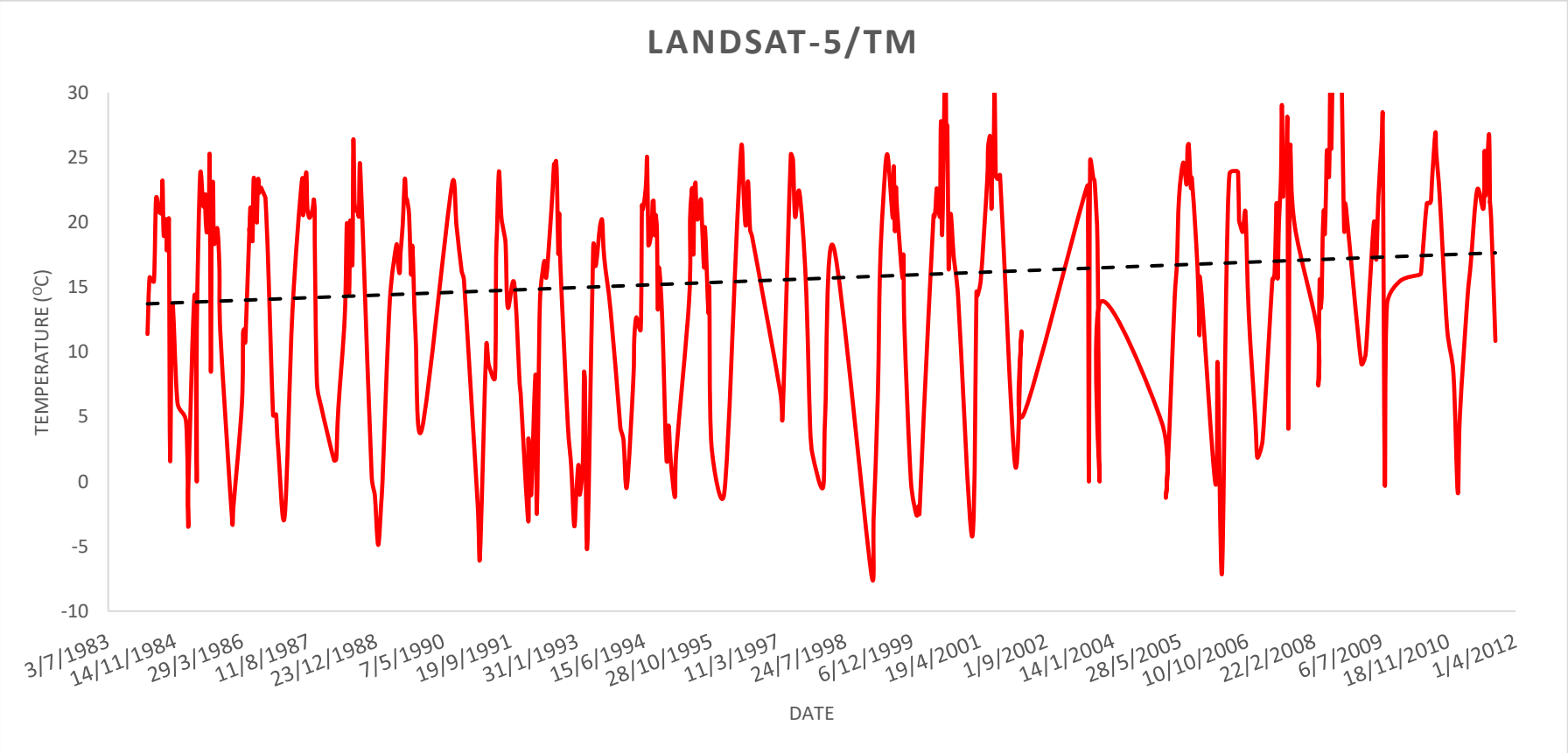


**Figure 50.** The average water Temperature of Lake Koronia derived from Landsat-5/TM images (1984-2011).

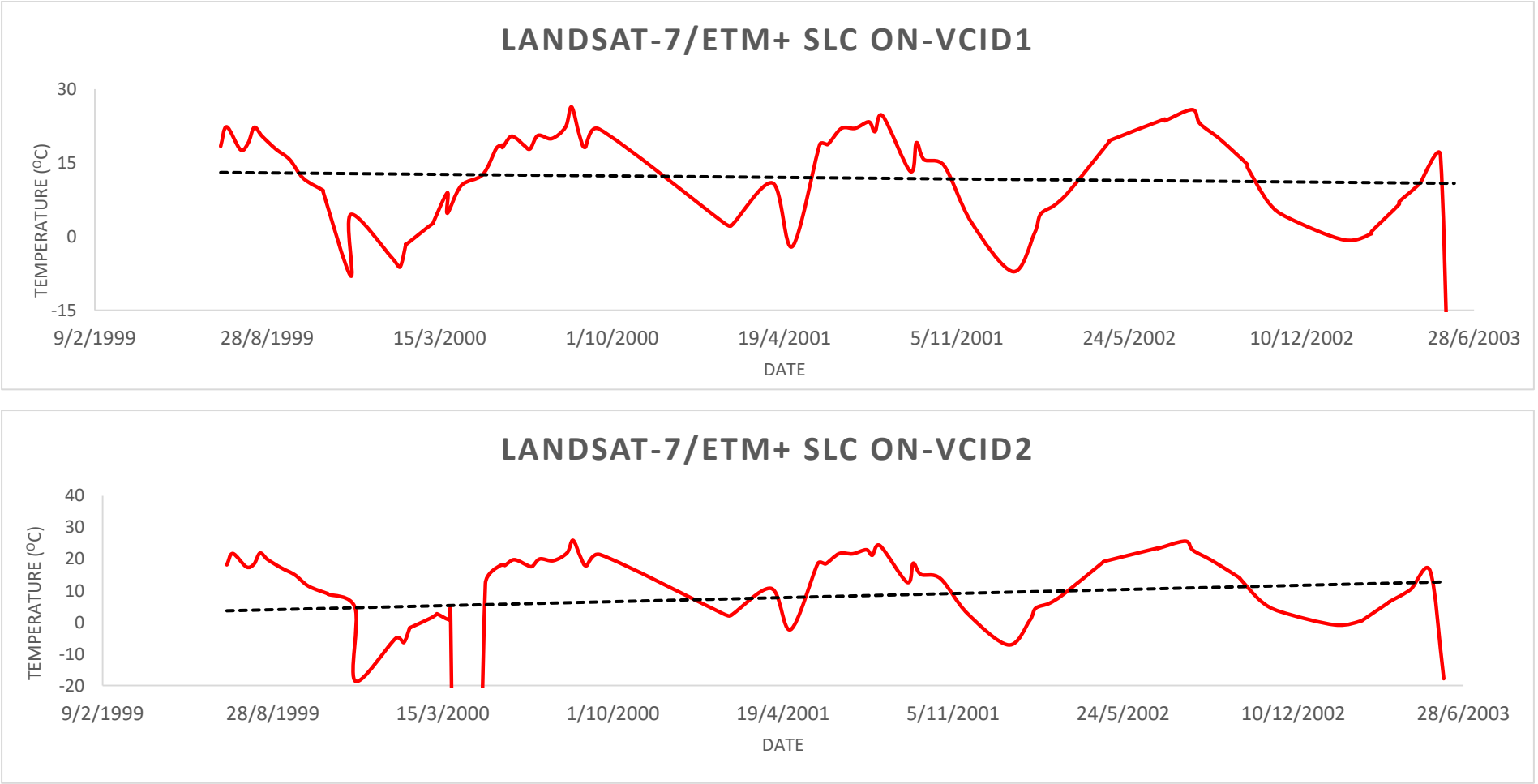


**Figure 51.** The average water Temperature of Lake Koronia derived from Landsat-7/ETM+ SLC ON (VCID1 & 2) images (1999-2003).

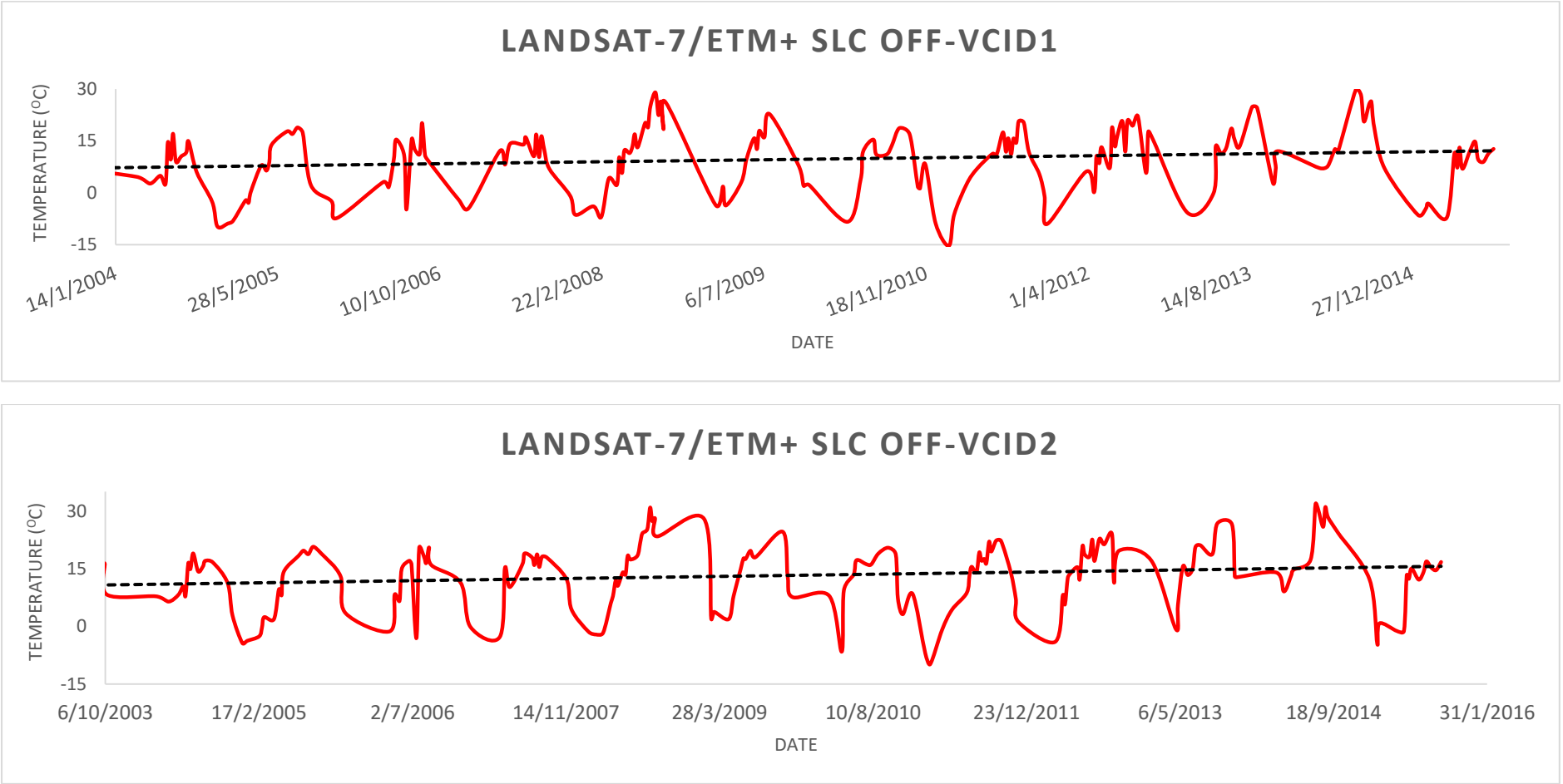


**Figure 52.** The average water Temperature of Lake Koronia derived from Landsat-7/ETM+ SLC OFF (VCID1 & 2) images (2003-2015).

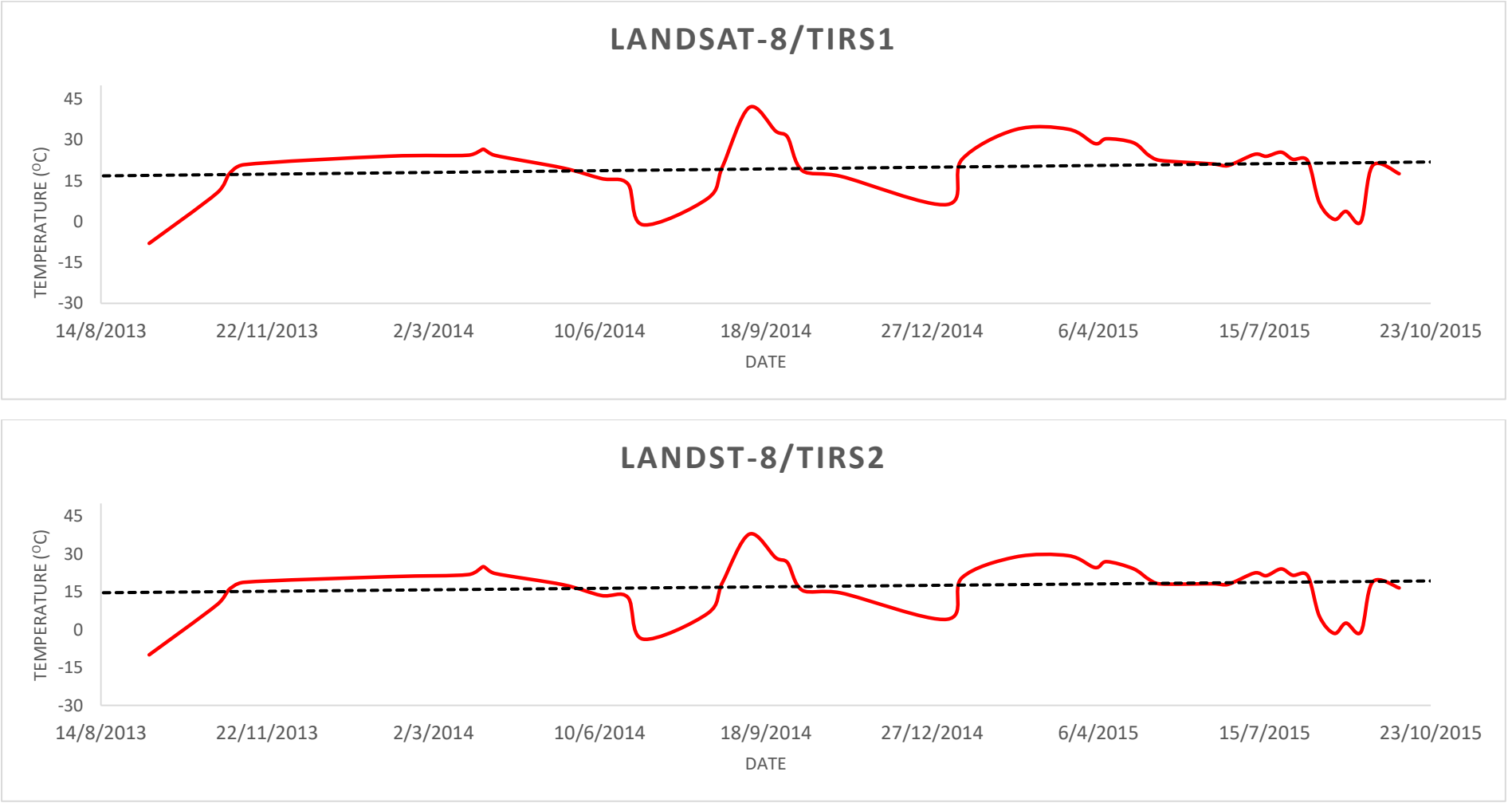


**Figure 53.** The average water Temperature of Lake Koronia derived from Landsat-8/TIRS images (2013-2016).

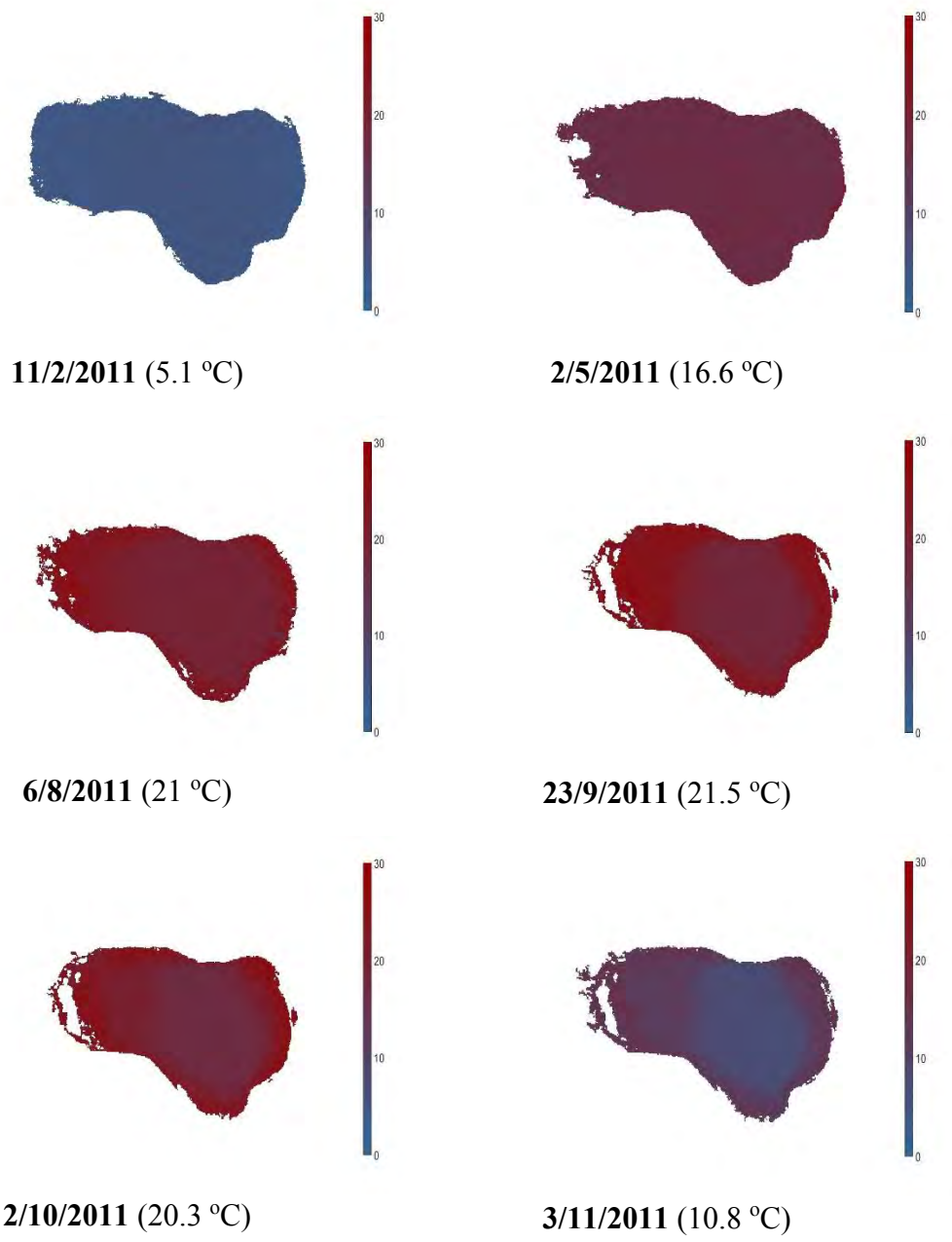


**Figure 54.** Seasonal spatial variation of water Temperature and the average Temperature values of water surface of Lake Koronia in 2011.

As mentioned in Chapter 2.2, Lake Koronia is a shallow polymictic lake. Polymictic lakes occur in regions of low seasonal temperature variations, subject to rapidly alternating winds and often with large daily temperature variations (Thomas et al. 1996). These lakes are not deep enough to form a hypolimnion (Boehrer & Schultze 2008). The entire lake behaves like an epilimnion, which is mixed by sporadic strong wind events over the year or even on a daily basis in response to a strong daily temperature cycle. The wind produces turbulence and currents at the water surface that mix the shallow water.The surface of Lake Koronia shows a pronounced temperature

cycle over the year. Figure 54 depicts the seasonal variation of water Temperature of Lake Koronia in 2011. Several processes contribute to heat transfer through the lake surface: solar radiation, long-wave radiation of atmosphere and surface waters, sensible heat exchange, and heat flux connected with evaporation and precipitation.

## 9.6 **Secchi Disk Depth**

The SDD is valued as a useful and informal visual index of the trophic activity of a lake (Preisendorfer 1986). As mentioned in Chapter 7.3, light attenuation in water is attributable to four factors: water molecules, dissolved yellow pigments, photosynthesizing biota and inanimate particulate matter. As a result, SDD provides a readily understood and quite useful record of the growth and decay of aquatic plant life in lakes. It is also useful in tracking visually the movements of suspended detritus and the migration of sediment influxes from tributary streams and rivers.

Figures55-58 depict the overall average of Secchi Disk Depth time-series from satellite-derived data. In all cases, the values appear to vary from very low (less than 0.5 m) to about 2.5 m on an average higher, excluding some characteristic jumps in the various time-series. The same comments as those of the previous subchapter apply in those cases as well. Counterintuitively, there are some specific time periods, when the SDD values become negative in the time-series. This can be attributed to a possible flaw of the used model, or, as mentioned earlier, a strong deviation of certain characteristics of the lake from the normally expected condition, i.e. intense aquatic vegetation coverage, very low water levels and other factors, which have a strong tendency to alter the resulting profile of the parameter.

There are several factors that can cause systematic shifts in the SDD measurements (Preisendorfer 1986, Borkman & Smayda 1998): the amount of attenuating material; optical state of the water surface; reflected luminance of the sky; reflectance of the body of water; disk reflectance; diameter of the disk; altitude of the sun; immediate height of the observer over the surface of the water; adaptation luminance; and shadowing. All these factors represent possible sources of error in comparing SDD measurements.

A comparison of the SDD values with data from Bobori (2001) shows a relatively fair accuracy, well within the limits of one standard deviation. In specific, the SSD from 5 stations in a period of two full years (of irregular observations), namely 1989 and 1990, from Bobori (2001) results in an average SSD value of 0.36±0.1 m, whereas the corresponding overall average of the lake in the same time period in the current study results in a value of 1.22 ± 0.5 m.

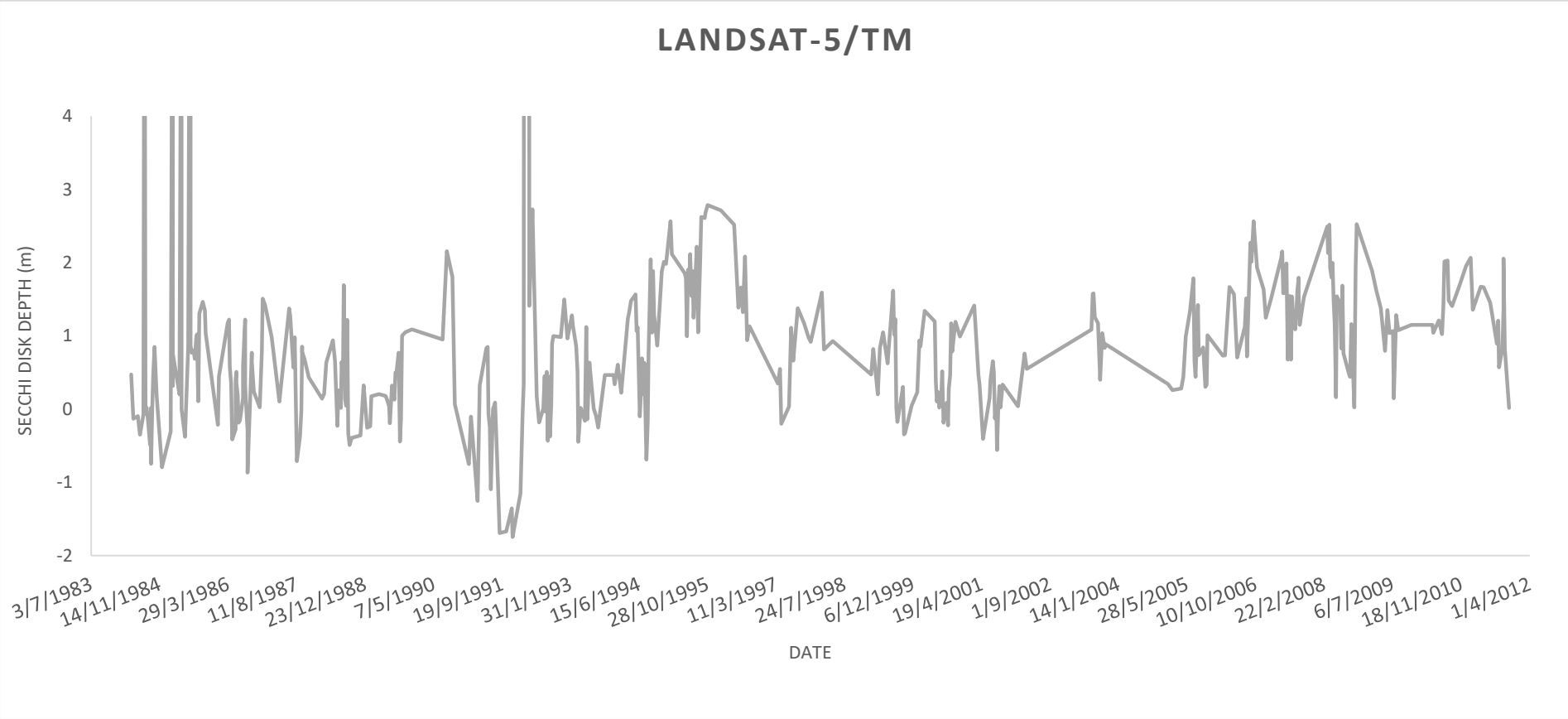


**Figure 55.** The average Secchi Disk Depth of Lake Koronia derived from Landsat-5/TM images (1984-2011).

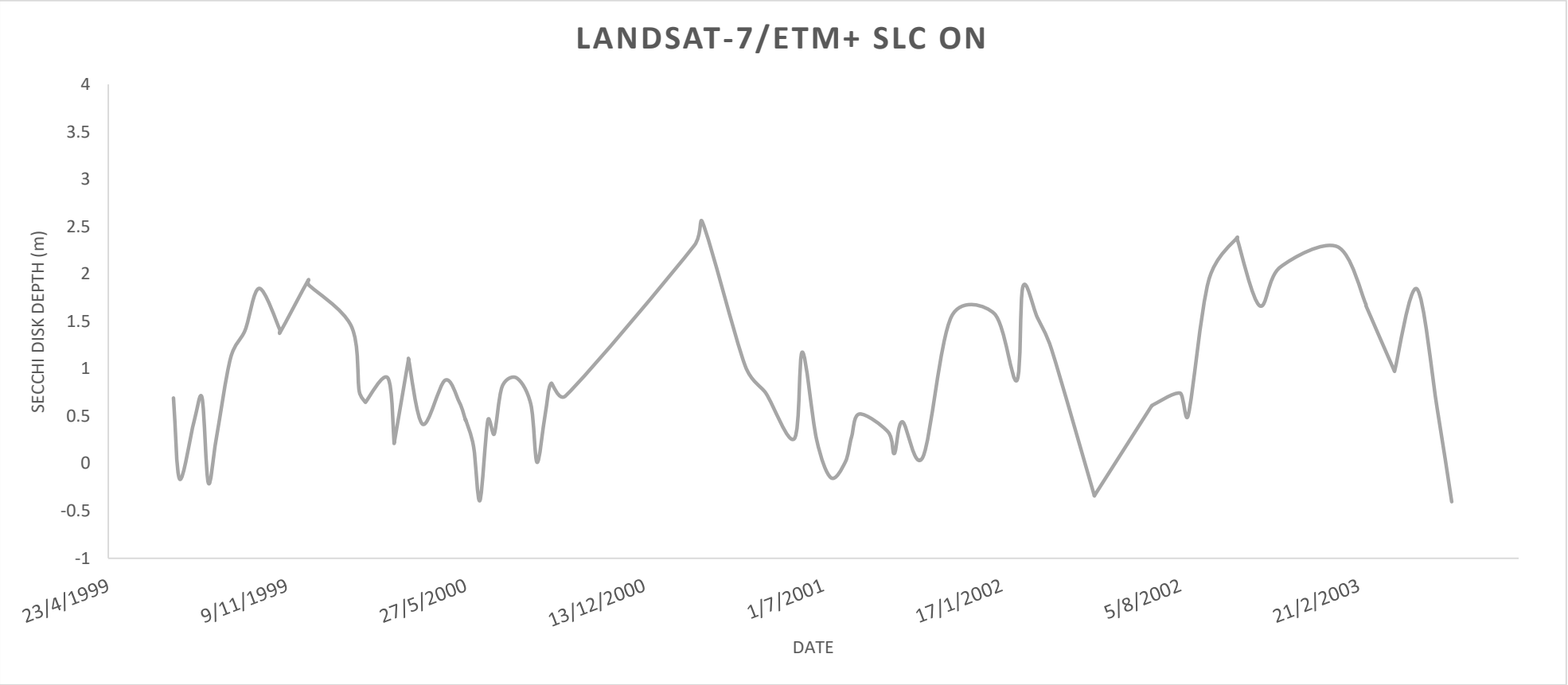


**Figure 56.** The average Secchi Disk Depth of Lake Koronia derived from Landsat-7/ETM+ SLC ON images (1999-2003).

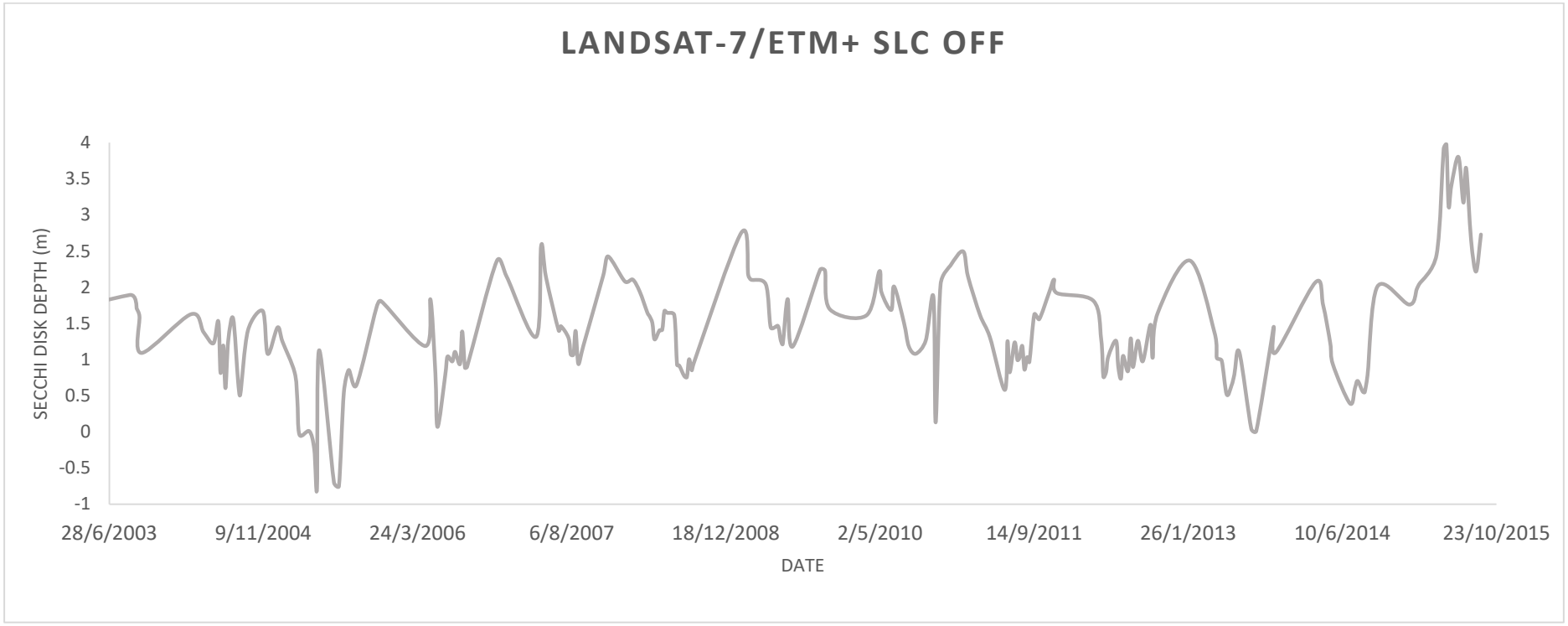


**Figure 57.** The average Secchi Disk Depth of Lake Koronia derived from Landsat-7/ETM+ SLC OFF images (2003-2015).

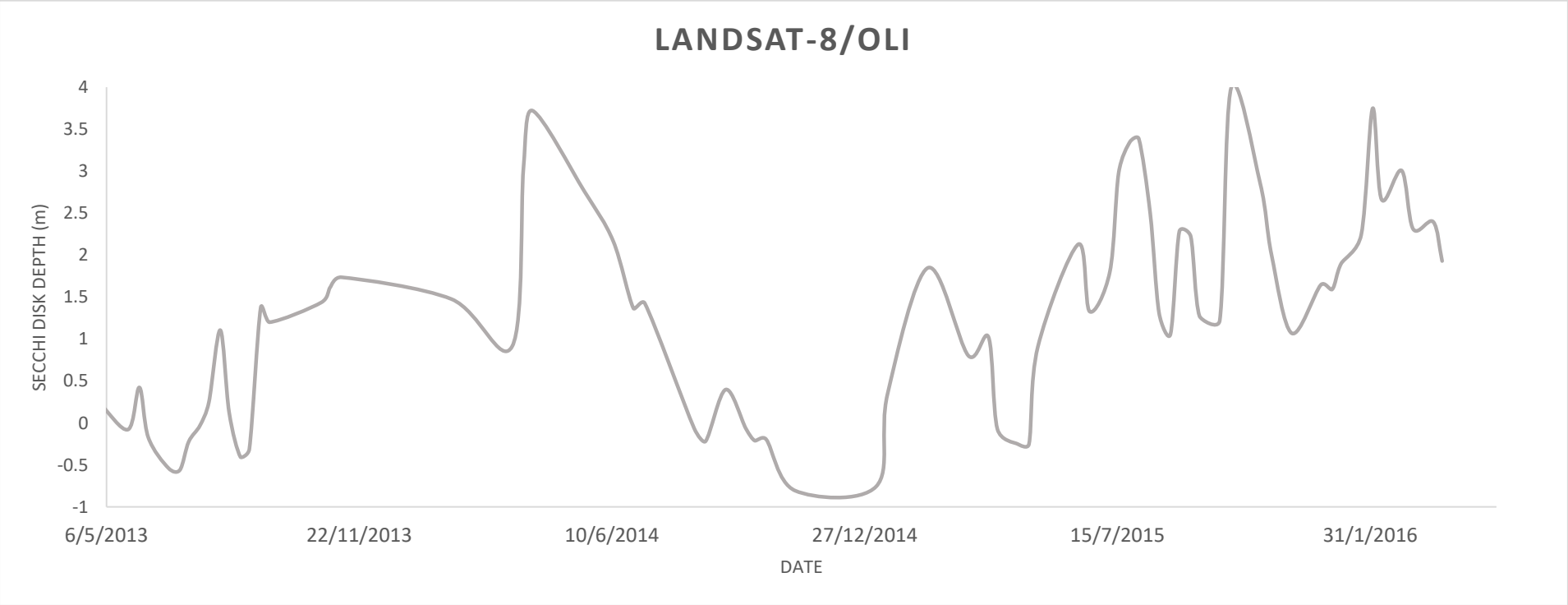


**Figure 58.** The average Secchi Disk Depth of Lake Koronia derived from Landsat-8/OLI images (2013-2016).

## 9.7 **Chlorophyll a**

Figures 59-62 depict the time-series of the overall average of Chlorophyll *α* concentration over the lake. Similar comments with the previous subchapters apply in these cases as well. According to Dall'Olmo & Gitelson (2005) the remote estimation of Chl*a* concentration may be affected by the variability of ecophysiological parameters, such as the Chl*a* fluorescence quantum yield and the Chl*a* specific absorption coefficient. The parametrization of the specific absorption coefficient of Chl*a* and the fluorescence quantum yield requires *a priori* knowledge of many different variables such as cell size distribution, intracellular pigment distribution, temperature and nutrient concentrations.

It is important to observe that the Chl*α* concentrations vary over a scale of 2 or slightly higher, which is to say that the local maxima are almost double, if not more, in value, than the neighboring minima most of the time. This corresponds to at least twice as much vegetation activity within or over the water. A seasonal pattern is also observed, with increase of Chl*α* during the warmer seasons, which was to expect, as the intensification of vegetation activity (blooming) is a natural consequence of warmer, sunnier weather conditions.

The Chl*a* concentration peak during the period 2004-2005 (Figure 59, Point A) can be related with an extremely dense bloom of the haptophyte *P. parvum* was observed in Lake Koronia in August–September 2004 (Moustaka-Gouni et al. 2004). In July 2009, prior to the dry out of the lake in the fall of 2009, phytoplankton biomass was relatively low and dominated by diatoms (in terms of biomass). Re- filling of the lake in the spring of 2010 ultimately led to a resurgence of phytoplankton biomass, with a succession of blooms dominated by different species (Zalidis et al. 2014). This can explain the Chl*a* concentration peak during the year 2010 (Figure 59, Point B).

Chl*a* concentration is commonly used to represent the density of the algal population in a lake. Free-floating algae (phytoplankton) are the primary food producers in the food chain. Moderate concentration of algae is necessary for a biologically productive, healthy lake; however, excessive concentrations (algal blooms) are undesirable and can have profound effects on the water quality. The accelerated production of algae in a lake is generally the result of excess nutrients– in particular, phosphorus. The depth at which light can penetrate a lake diminishes with more algae in a lake. Thus the greater the value of Chl*a* and phosphorus, the lower the value of SDD (Fuller & Minnerick 2007). The measurements of SDD and Chl*a* derived from Landsat5/TM images reveal a fair accordance to this statement. Although the measurements derived from Landsat-7/ETM+ and Landsat-8/OLI images show that the greater the Chl*a* concentration, the greater the SDD. This mismatch may be due to the specification of the algorithms for Landsat-5 images.

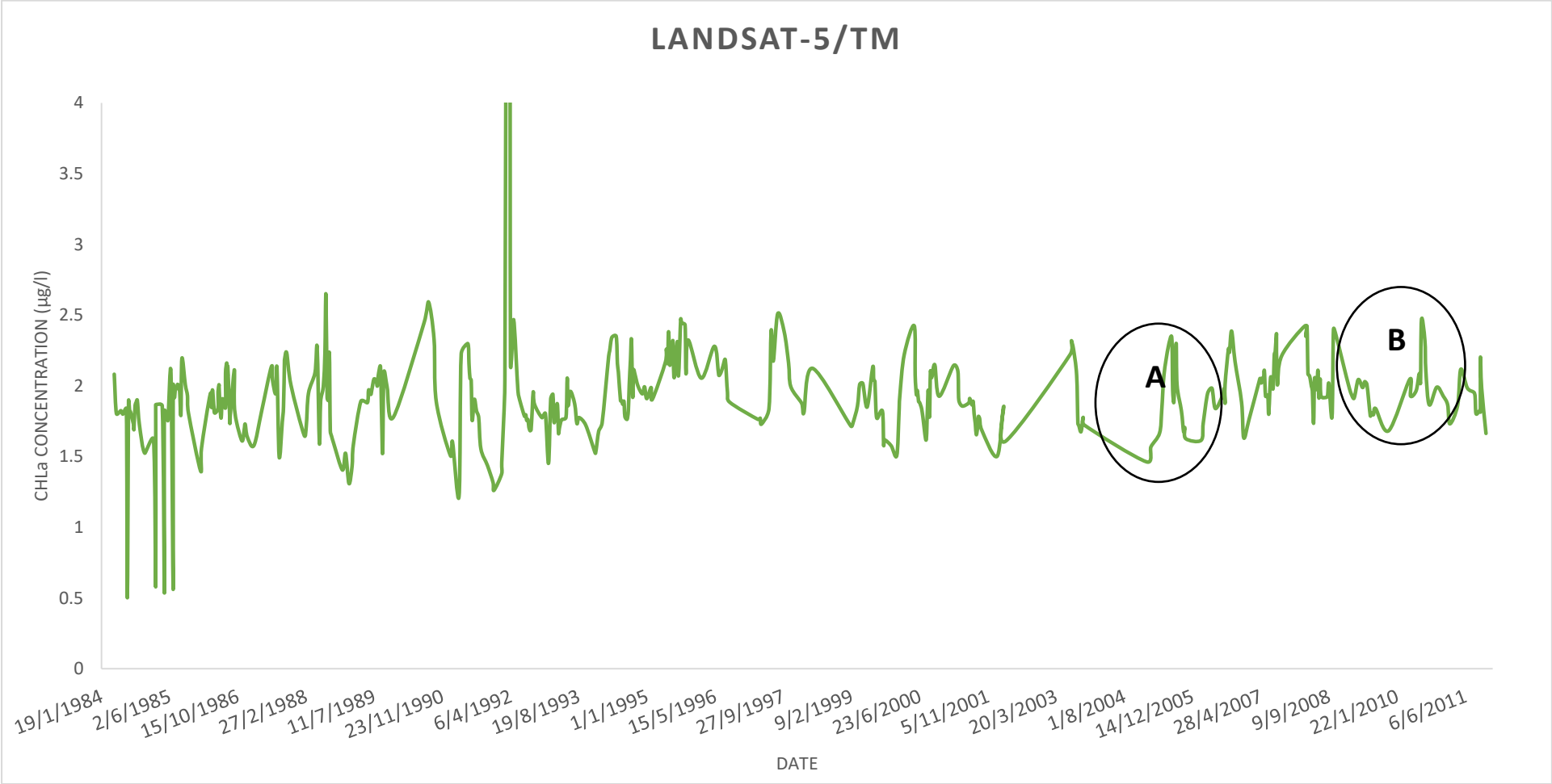


**Figure 59.** The average Chl*a* concentration of Lake Koronia derived from Landsat-5/TM images (1984-2011).

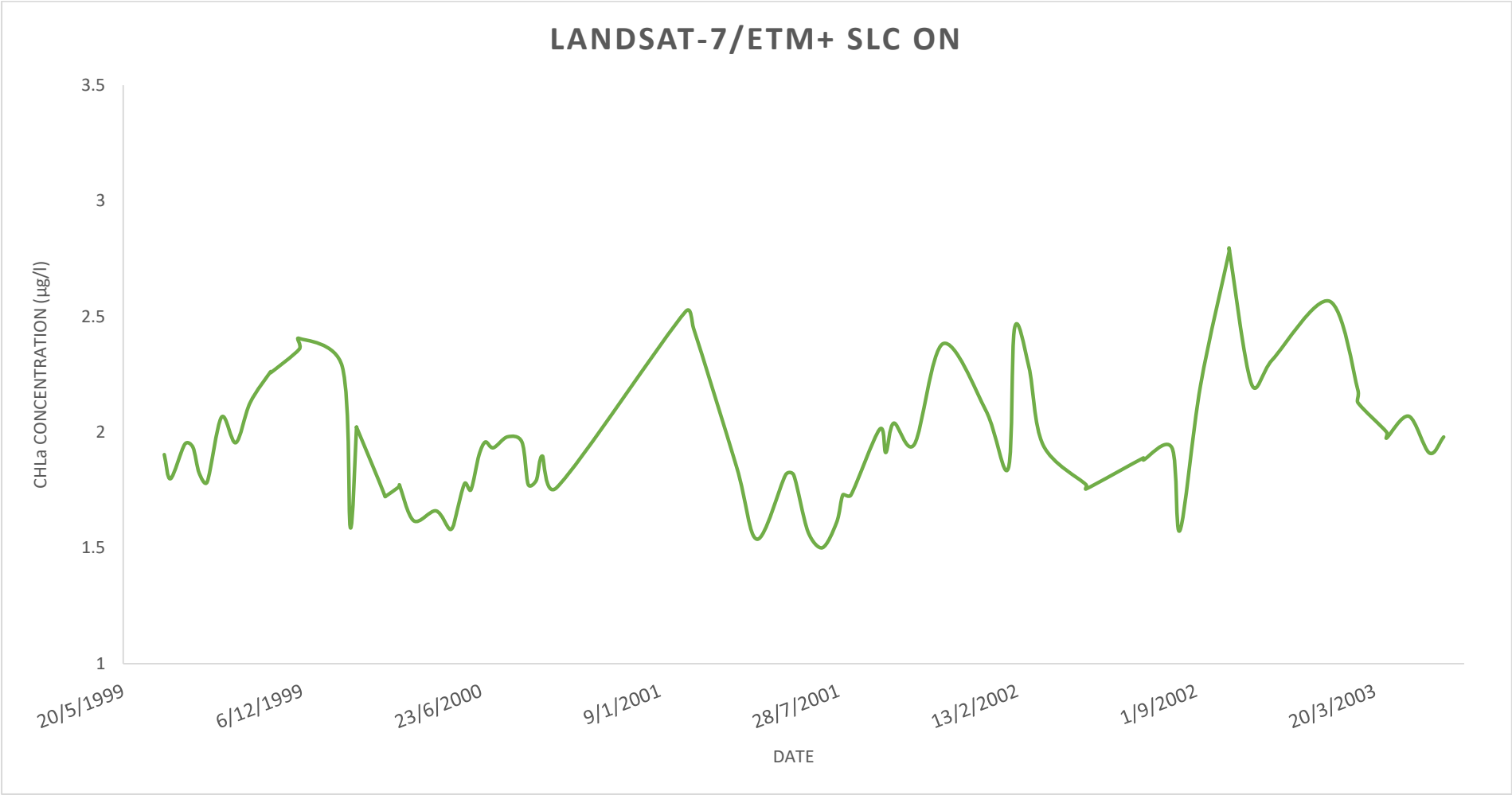


**Figure 60.** The average Chl*a* concentration of Lake Koronia derived from Landsat-7/ETM+ SLC ON images (1999-2003).

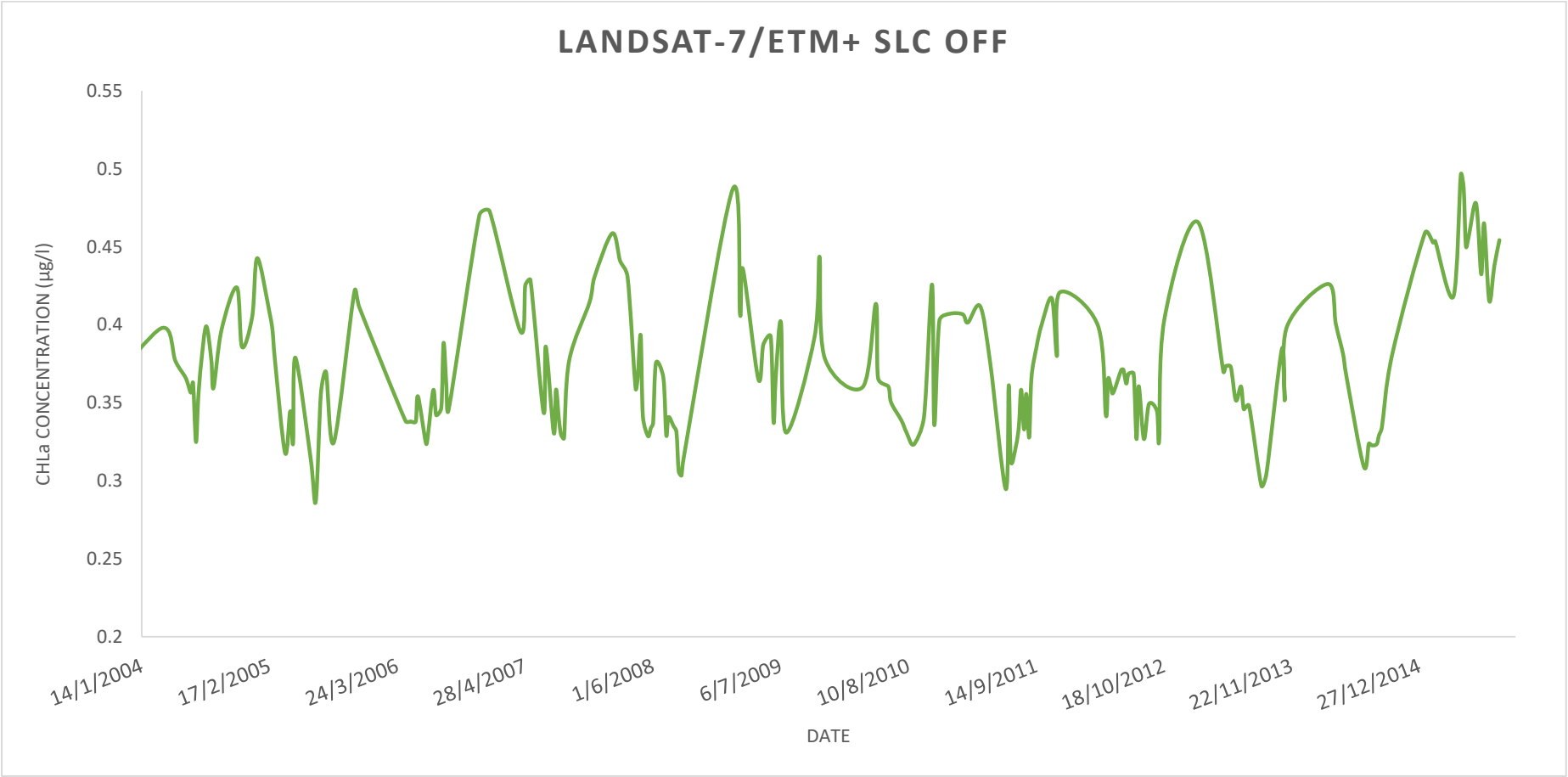


**Figure 61.** The average Chl*a* concentration of Lake Koronia derived from Landsat-7/ETM+ SLC OFF images (2003-2015).

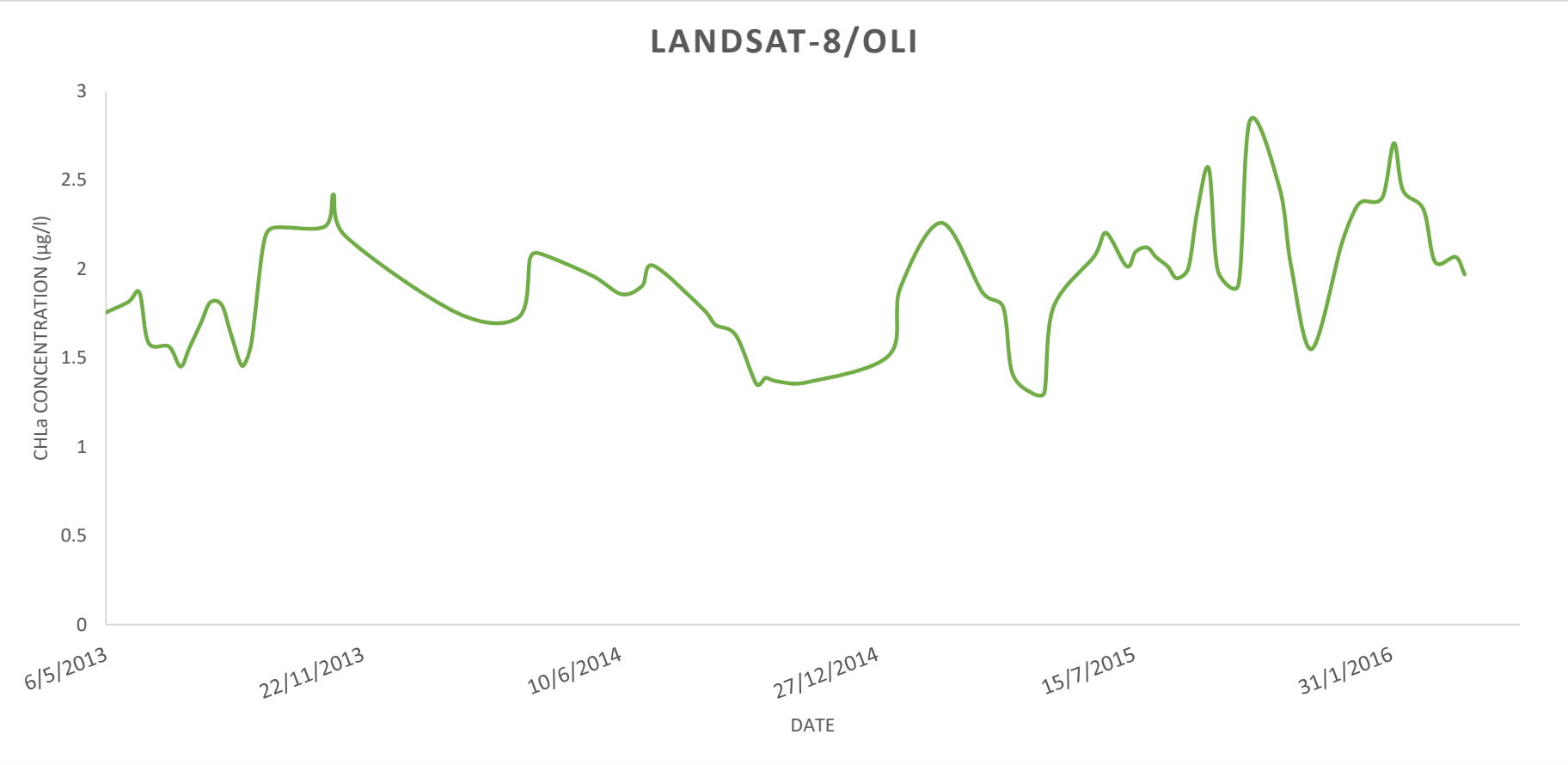


**Figure 62.** The average Chl*a* concentration of Lake Koronia derived from Landsat-8/OLI images (2013-2016).

## 9.8 **Lake Coverage**

The Figures 63-66 depict the time-series of the lake pixel coverage as classified following the methods presented in Chapter 7.5.4 into water, SAV, Macrophytes and Cyanobacterial blooms. The data are presented in percentage of pixels of each class with respect to the total of the lake pixels. In general, a strong temporal variation in the 4 categories is apparent from all charts. There are extended time periods, during which the lake was increasingly covered with either Macrophytes, or Cyanobacterial blooms. An interesting observation is that pixel Macrophytes and Cyanobacteria never appear to covary. This contravariance between the two coverage types can be explained as the two organism species are antagonistic in nature. In the later years, the lake appears to have relatively clear water, with a notable exception between approximately August, 2014 to May, 2015, when there was an increase in Macrophytes coverage and Submerged Aquatic Vegetation. Similar observations can be made from the charts for earlier time periods.

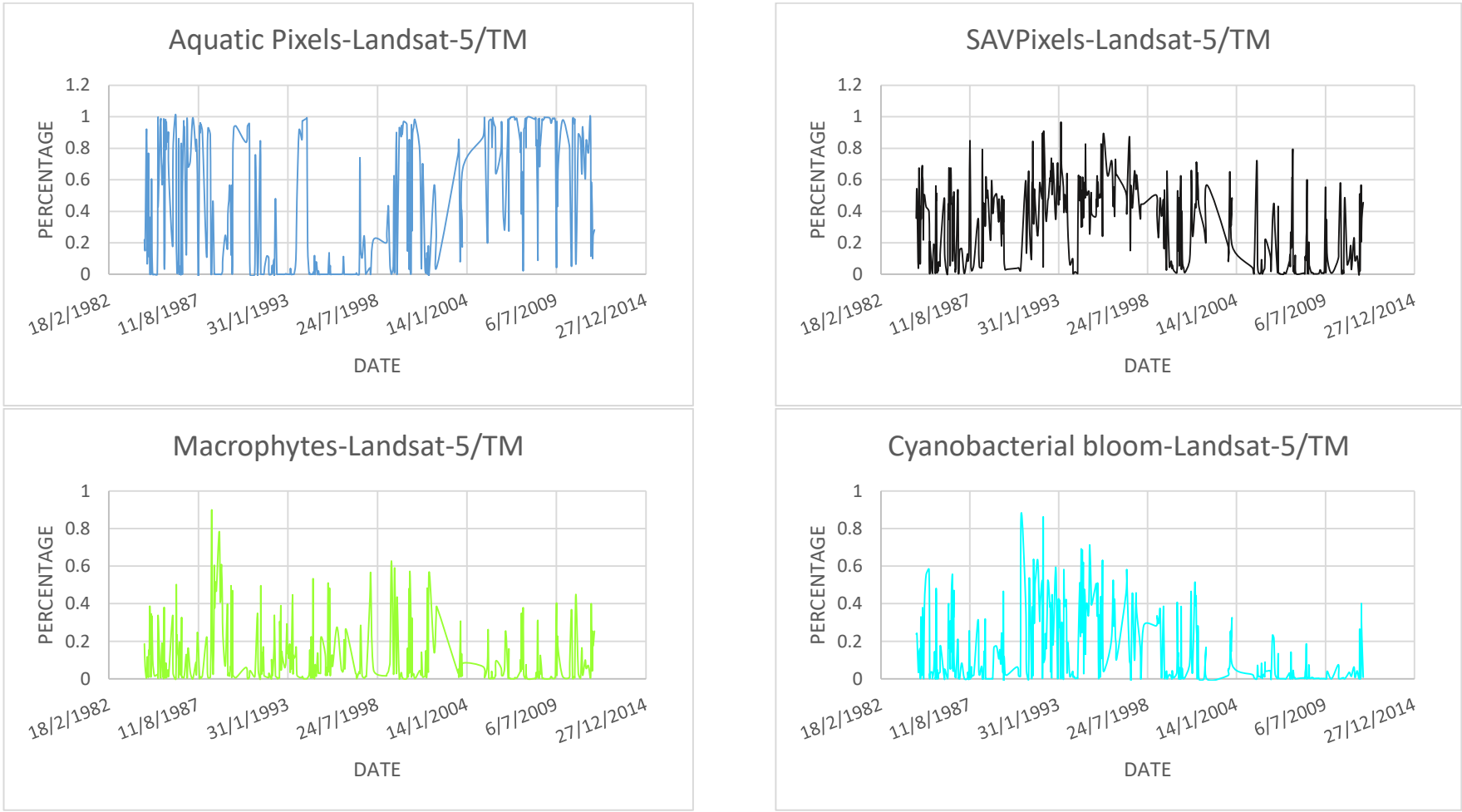


**Figure 63.** The percentages of various coverage types (water, Submerged Aquatic Vegetation, Macrophytes, Cyanobacterial Blooms) of Lake Koronia surface derived from Landsat-5/TM images (1984-2011).

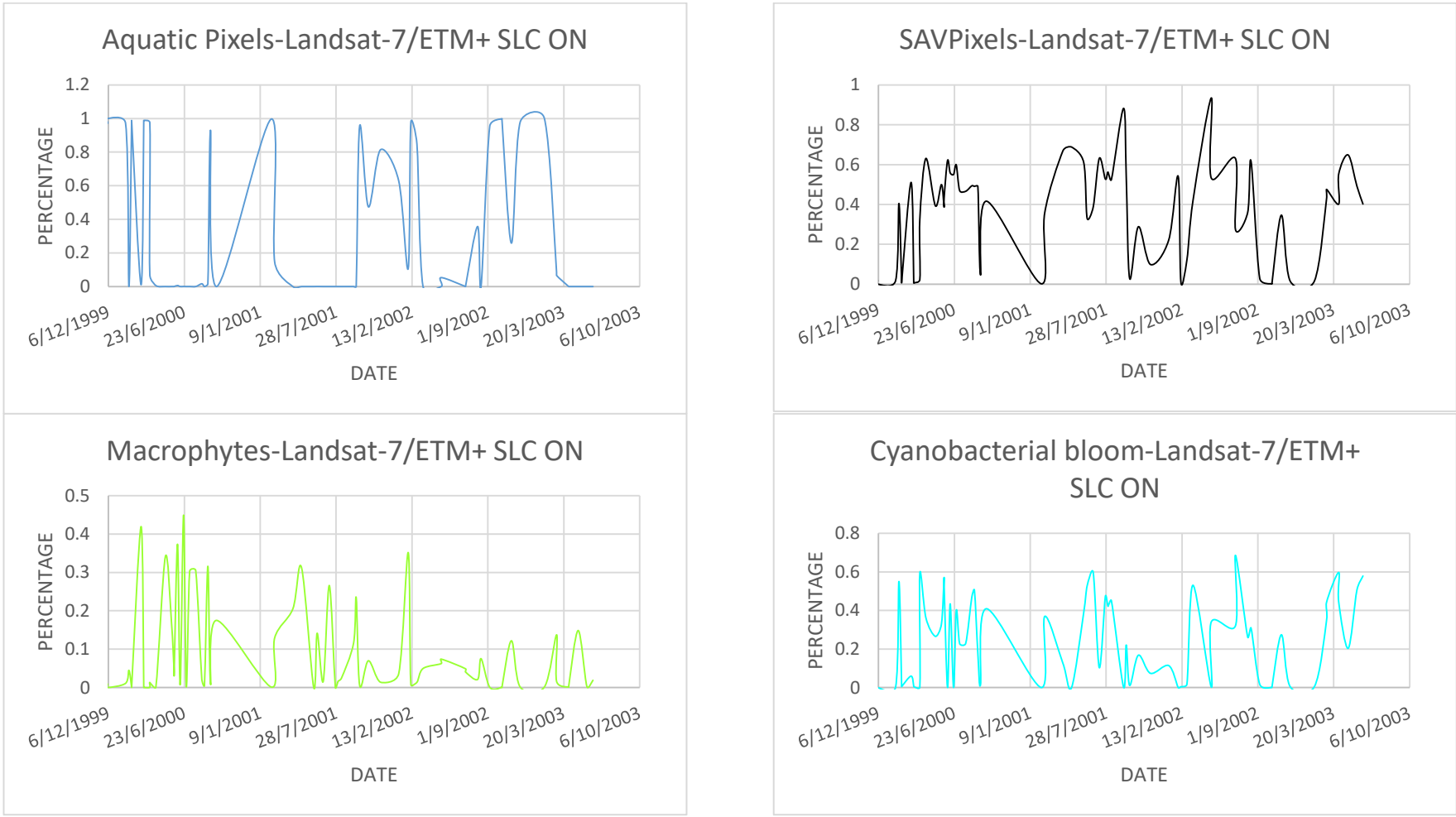


**Figure 64.** The percentages of various coverage types (water, Submerged Aquatic Vegetation, Macrophytes, Cyanobacterial Blooms) of Lake Koronia surface derived from Landsat-7/ETM+ SLC ON images (1999-2003).

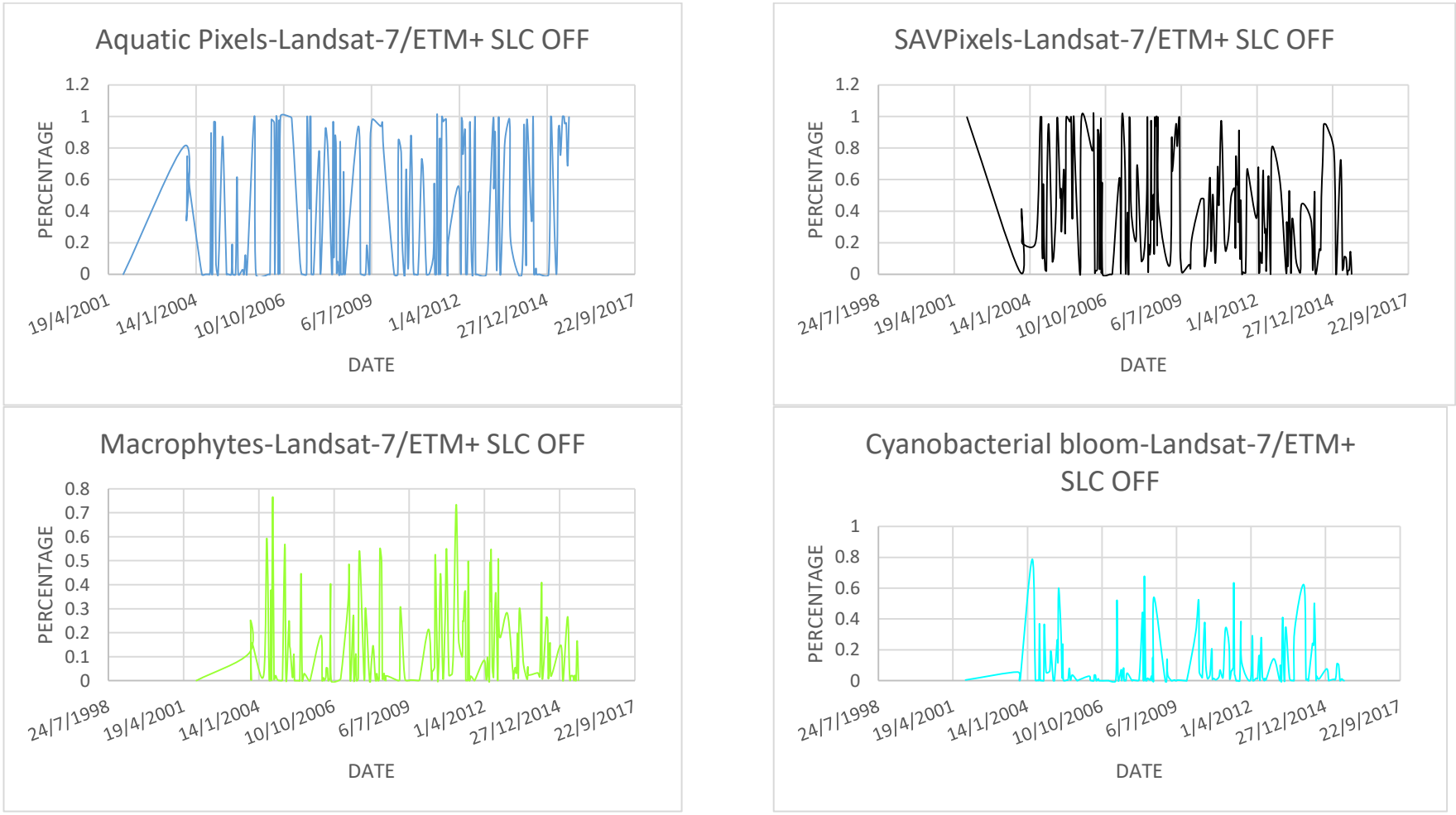


**Figure 65.** The percentages of various coverage types (water, Submerged Aquatic Vegetation, Macrophytes, Cyanobacterial Blooms) of Lake Koronia surface derived from Landsat-7/ETM+ SLC OFF images (2003-2015).

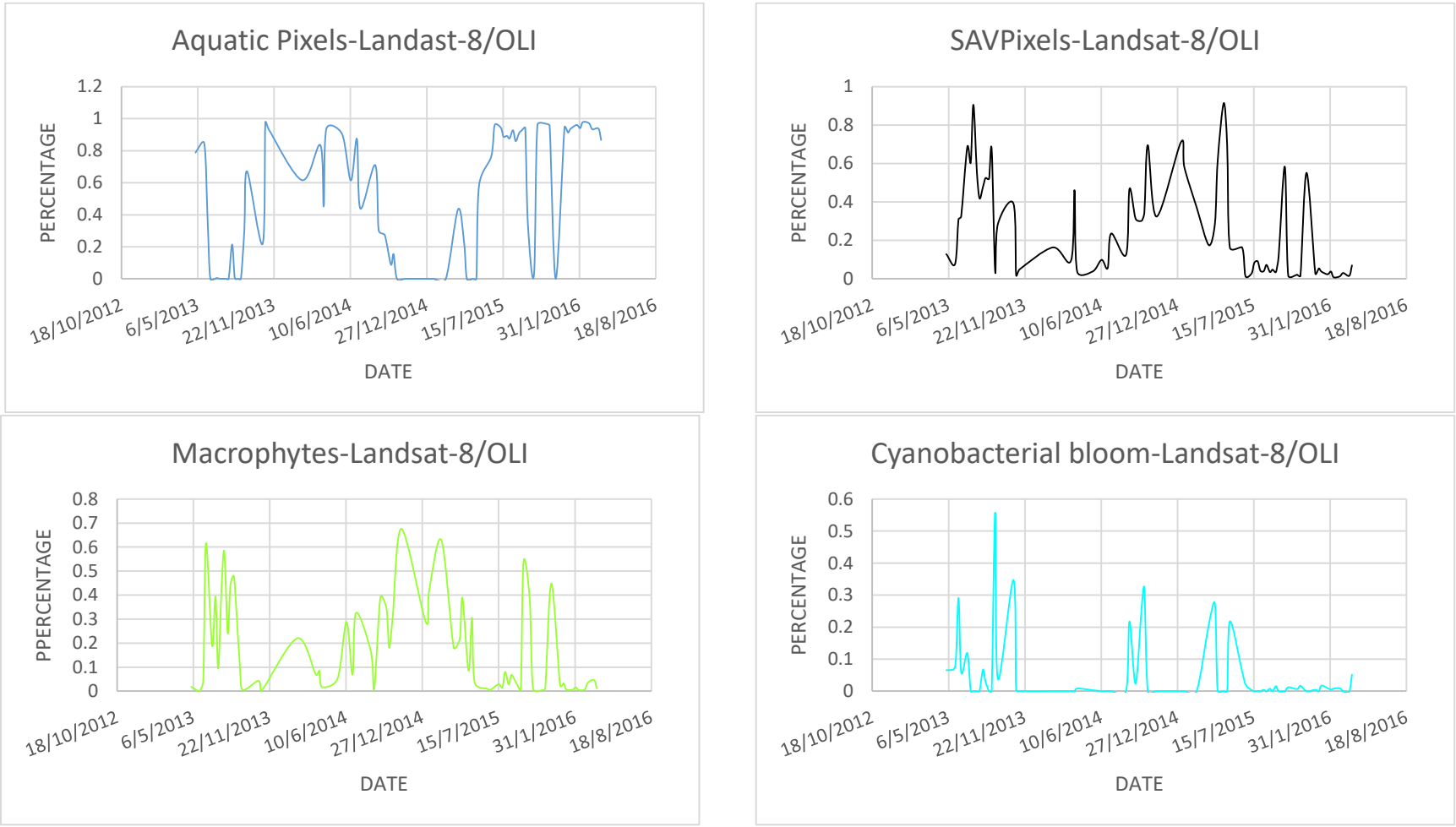


**Figure 66.** The percentages of various coverage types (water, Submerged Aquatic Vegetation, Macrophytes, Cyanobacterial Blooms) of Lake Koronia surface derived from Landsat-8/OLI images (2013-2016).

Figure 67 depicts maps of the distribution of the various coverage types over the lake on 6 distinct dates. All types of cases are depicted, in which the lake is either almost entirely clear, or variably covered with submerged aquatic vegetation and Macrophytes piled in layers (probably due to corresponding winds and streams), or covered with diffused Macrophytes, or a mix of Macrophytes and cyanobacterial blooms in variable proportions and dominance.

24/3/1991

9/7/1995

11/9/1995

28/4/1998

5/8/1999

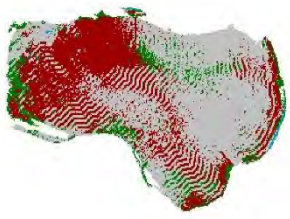

8/8/2006

**Figure 67.** Examples of lake Koronia coverage. Green: Macrophytes, Red: Cyanobacterial blooms, Grey: Submerged vegetation, Blue:Water

## 9.9 **pH**

Figures 68-71 depict the time-series of satellite-derived average pH values of Lake Koronia. The same comments as with the previous subchapters apply. It is easy to distinguish an overall drop in pH in the case of Landsat-5 data over the period of approximately mid-1988 until the early 1990. Similar periods can be seen in Landsat-8 data. It is important to note once again, that the Landsat-8 data appear to be out of place, with relatively unrealistic pH values. This observation once again validates the suspicion that the pH equation favors data from the Landsat-5 satellite. Although Landsat-7 SLC-ON derived data also appear realistic in relation to well-known *in situ* data over the area, data derived from Landsat-7 SLC-OFF images appear to produce distorted pH values. This can be attributed to both the Scan Line Corrector malfunction (as the designated point pixels may contain invalid data in many cases) and the presumed higher "affinity" of the equation model to Landsat-5 data.

Elevated pH values arise when the photosynthetic activity is very high (Scheffer 2004).Three major processes that affect the pH are photosynthesis, respiration, and nitrogen assimilation. The effects of photosynthesis and respiration on the pH depend largely on the carbonate–bicarbonate–carbon dioxide equilibrium (Lampert & Sommer 2007).

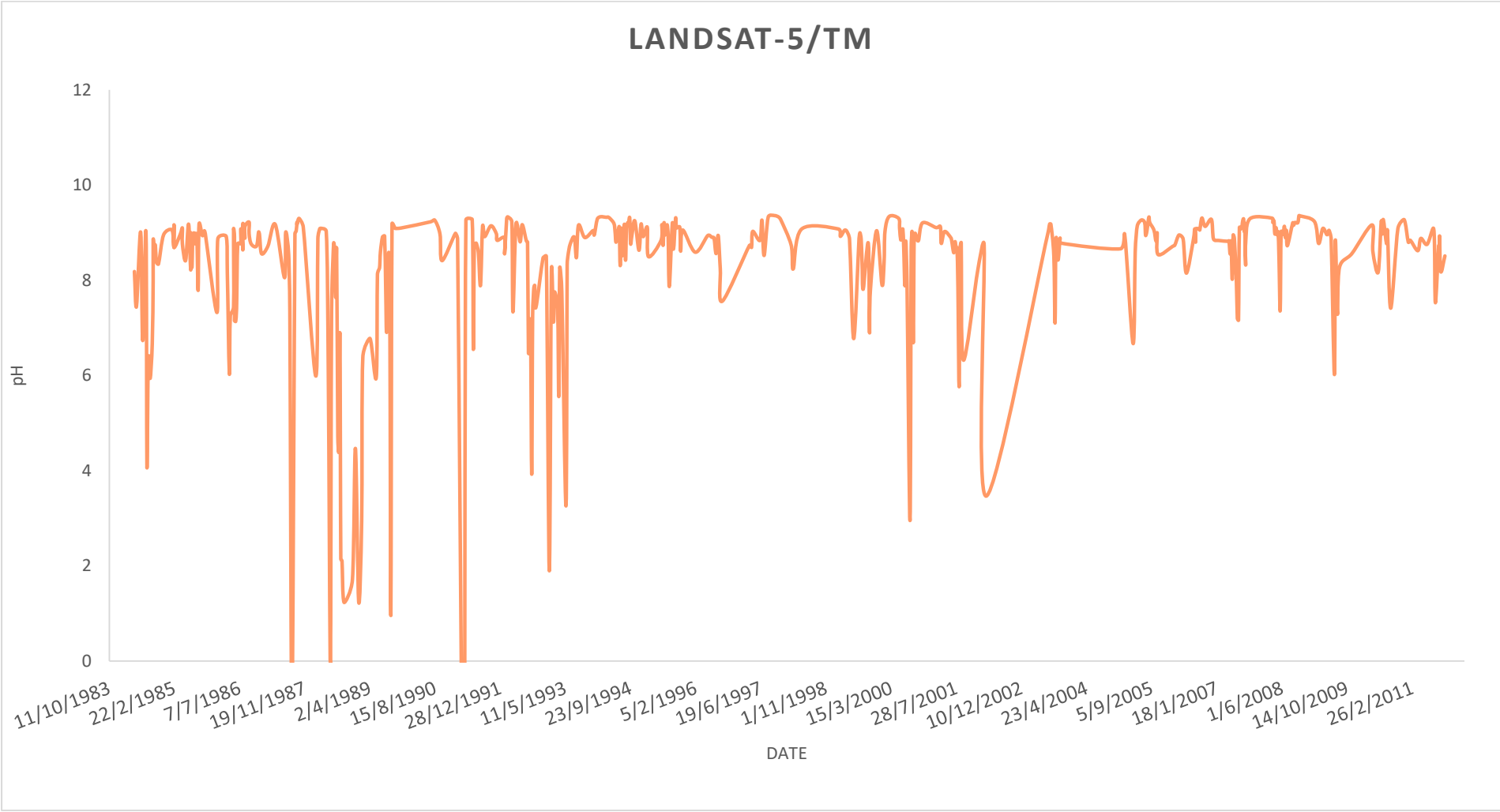


**Figure 68.** The average pH values of Lake Koronia derived from Landsat-5TM images (1984-2011).

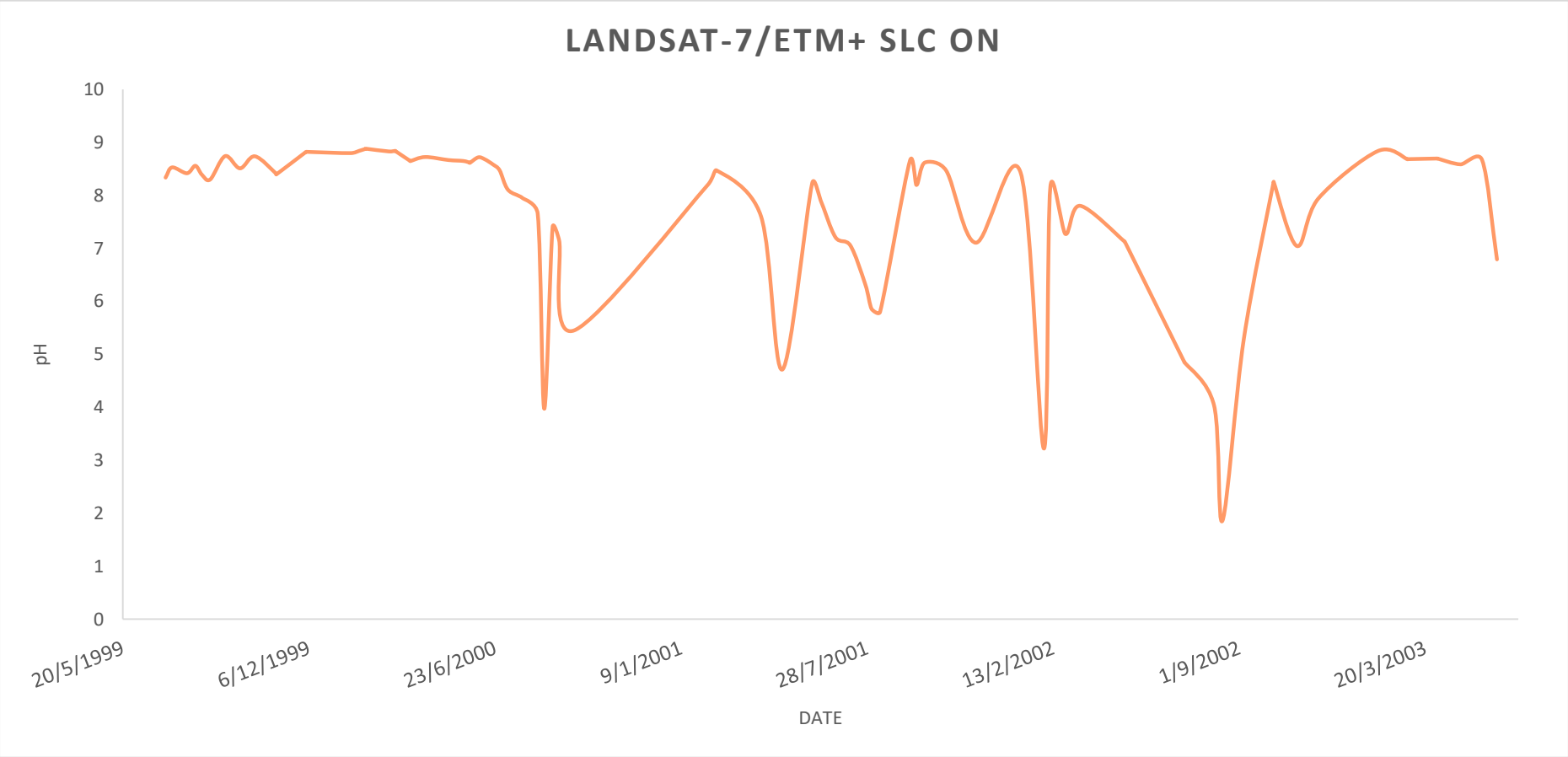


**Figure 69.** The average pH values of Lake Koronia derived from Landsat-7/ETM+ SLC ON images (1999-2003).

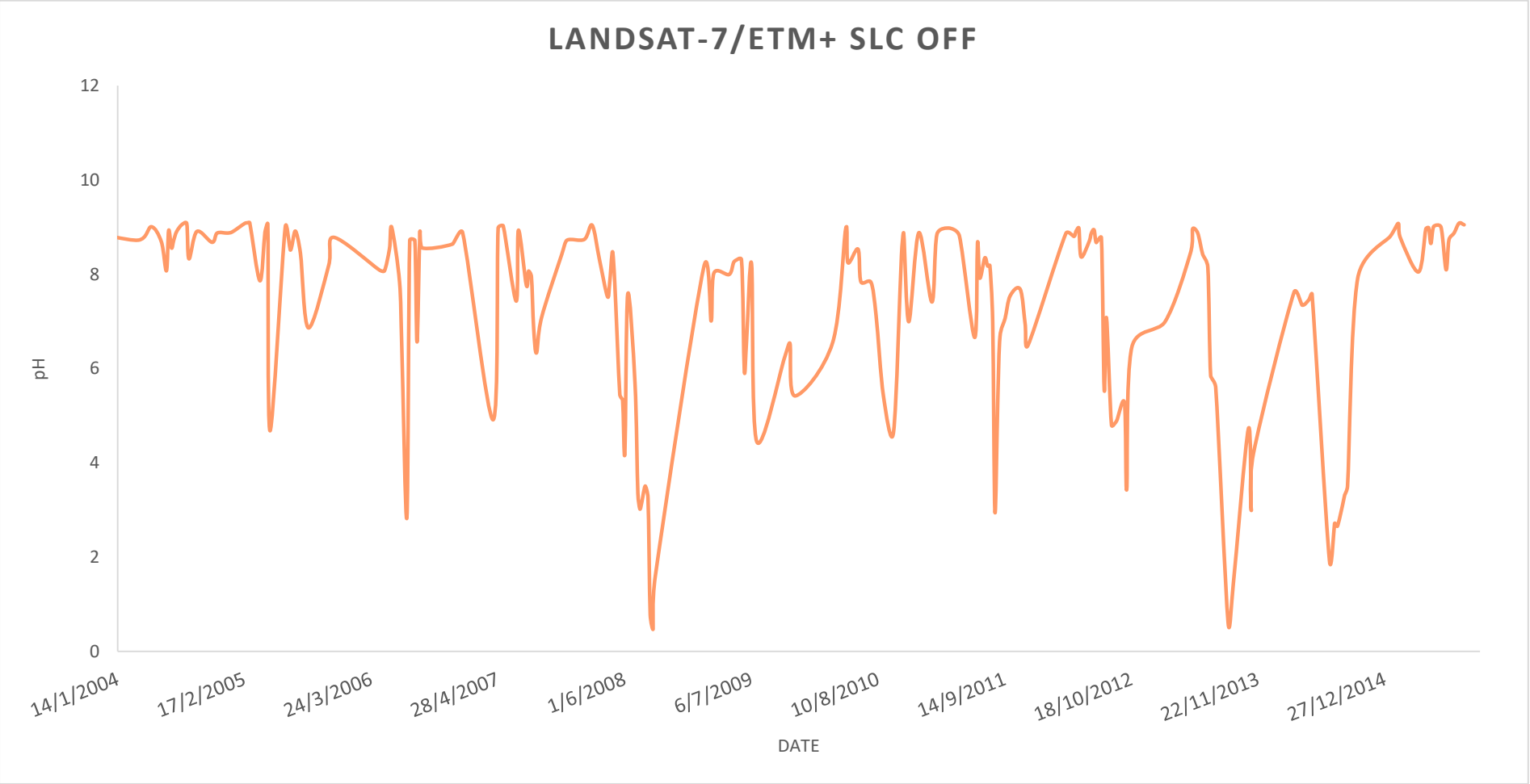


**Figure 70.** The average pH values of Lake Koronia derived from Landsat-7/ETM+ SLC OFF images (2003-2015).

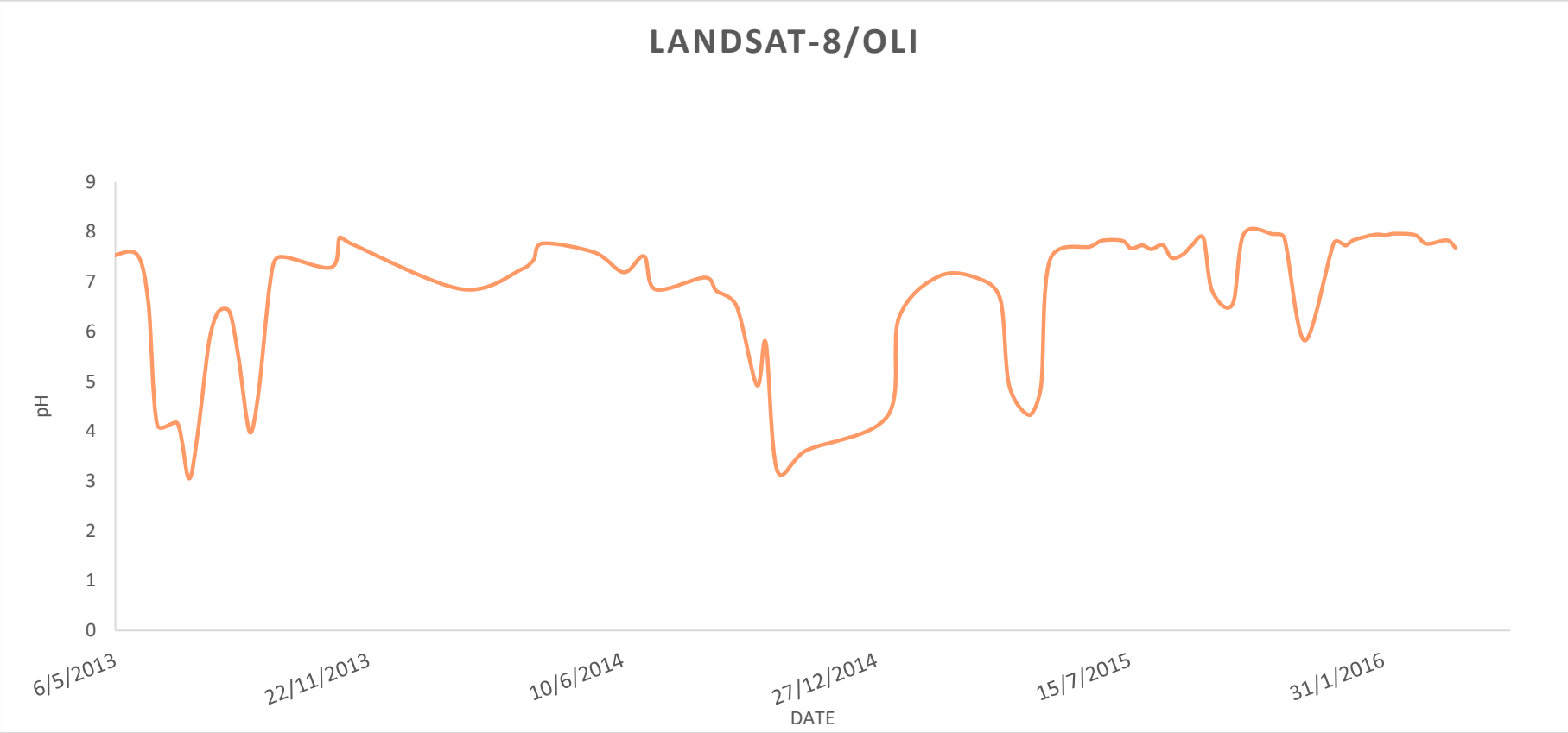


**Figure 71.** The average pH values of Lake Koronia derived from Landsat-8/OLI images (2013-2016).

## 9.10 **Conductivity**

Figures 72-75 depict the time-series of satellite-derived average Conductivity values of Lake Koronia. Monthly values for electrical conductivity from July 2009 through July 2010 ranged from 2600μS/cm to 20000μS/cm. Before 1993, values were relatively stable at 1300μS/cm, while after that they increased exponentially to more than 6000μS/cm and a maximum of 7700 μS/cm (Zalidis et al. 2014). According to Michaloudi et al. (2012) the water Conductivity in 2003-2004 ranged from about 4000 μS/cm to 10000 μS/cm. This measurements differ from the satellite measurements. Conductivity is not directly related with the optical properties of the lake water and presents a very high degree of complexity as to how all the different ions contribute to the final Conductivity values.

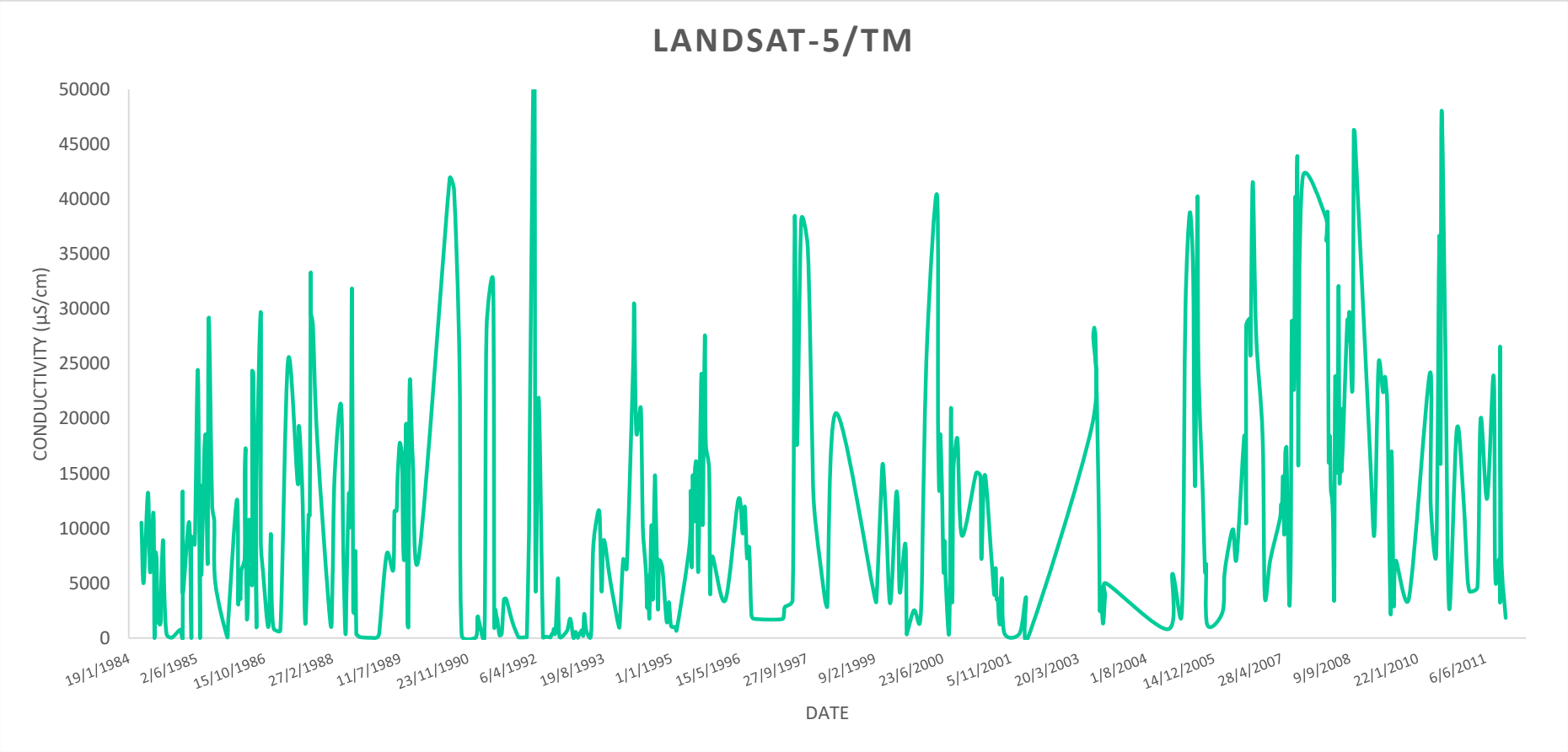


**Figure 72.** The average Conductivity of Lake Koronia derived from Landsat-5/TM images (1984-2011).

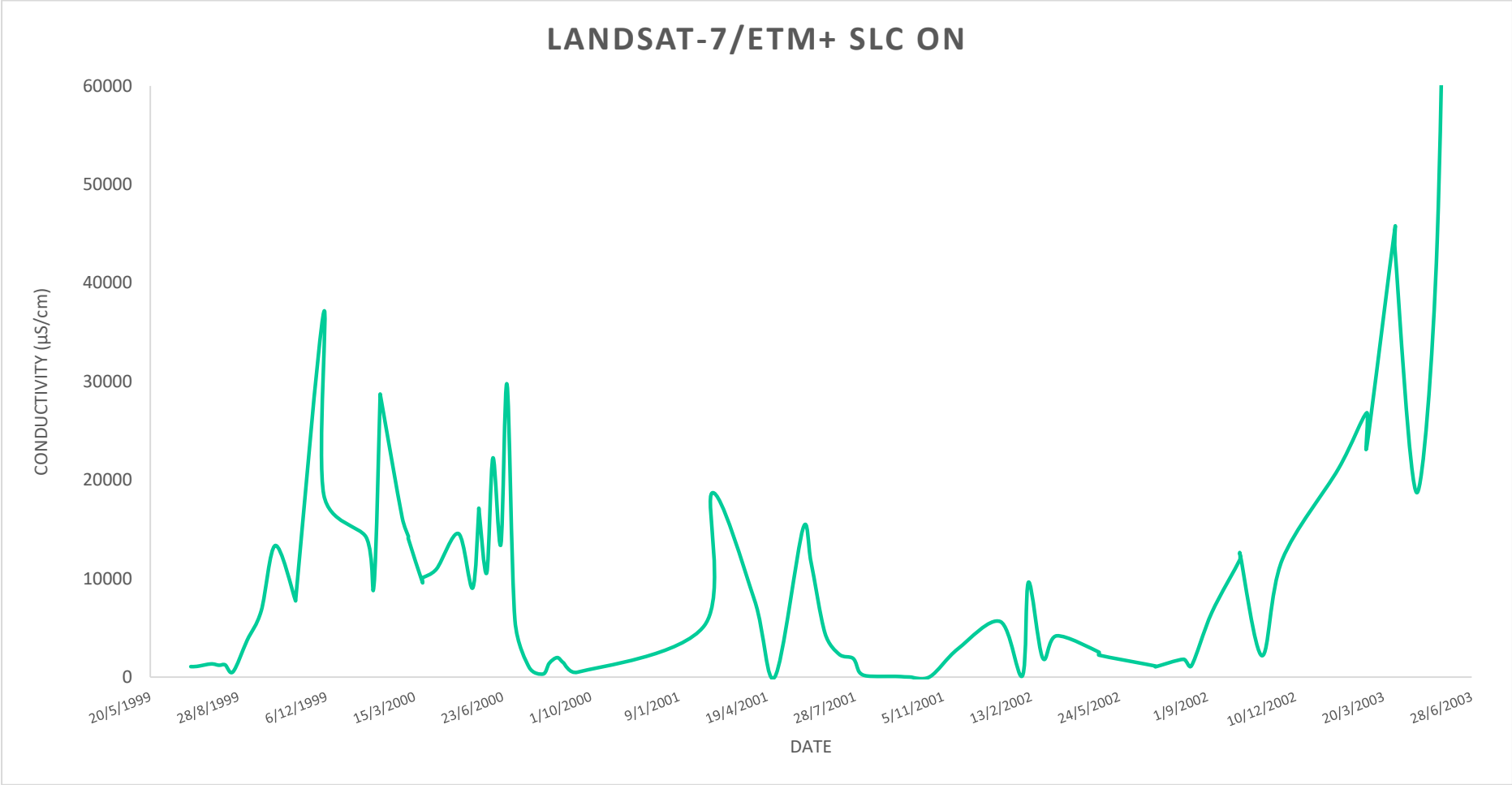


**Figure 73.** The average Conductivity values of Lake Koronia derived from Landsat-7/ETM+ SLC ON images (1999-2003).

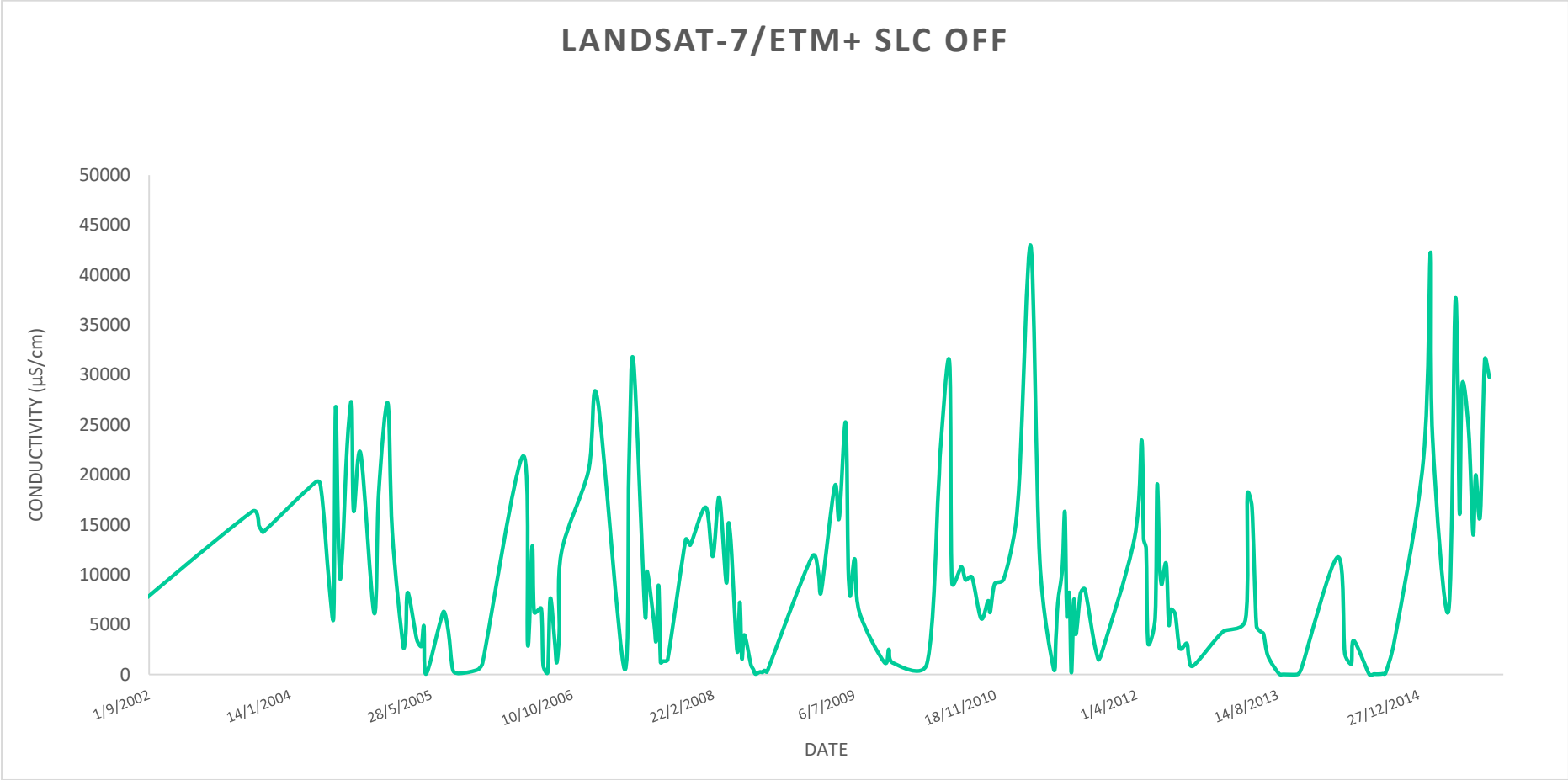


**Figure 74.** The average Conductivity values of Lake Koronia derived from Landsat-7/ETM+ SLC OFF images (2003-2015).

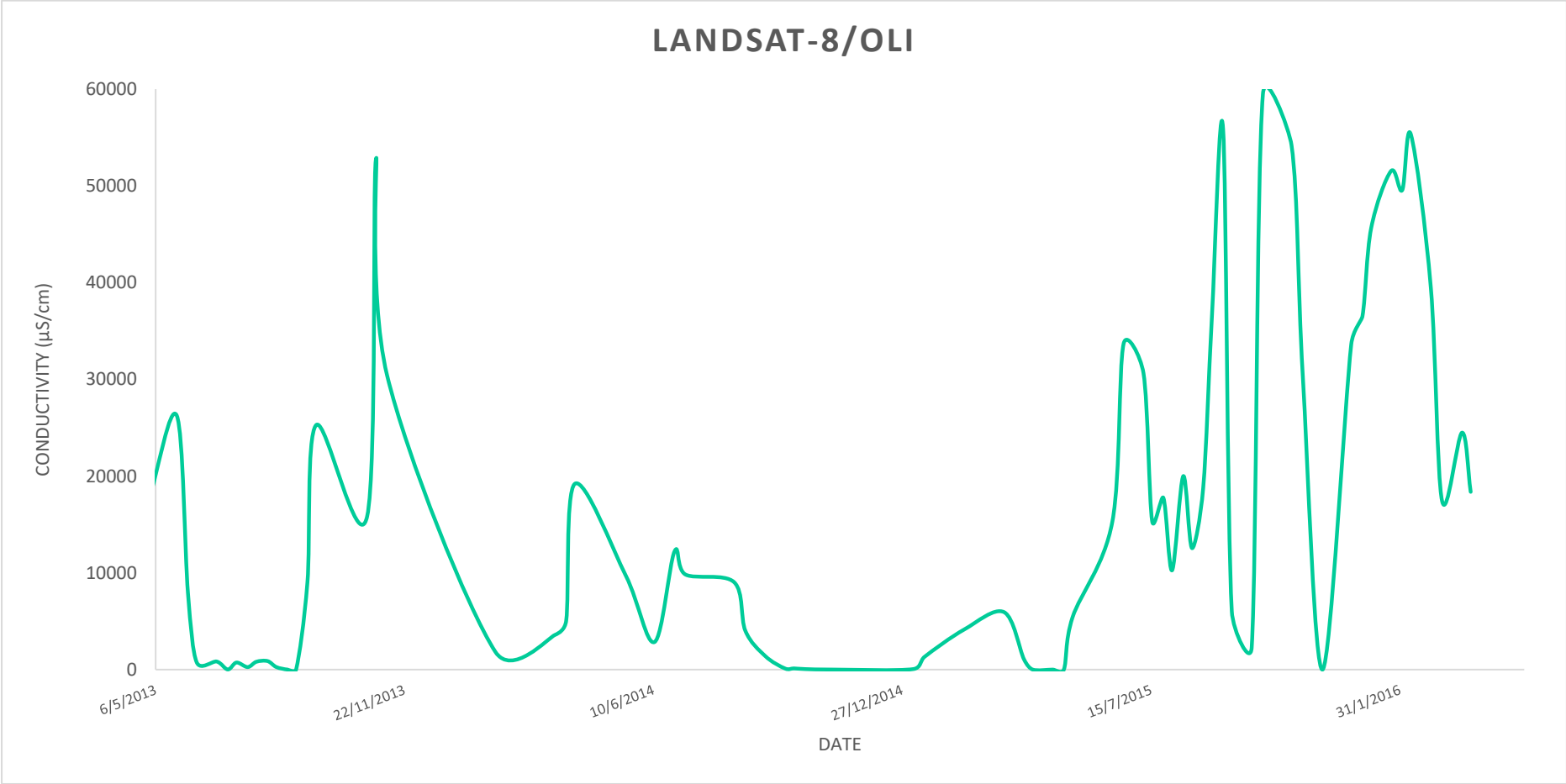


**Figure 75.** The average Conductivity values of Lake Koronia derived from Landsat-8/OLI images (2013-2016).

## 9.11 Water Depth

Figure 76-78 depict the data for the fitting of the log-ratio bathymetric model. The data plotted are logarithmic ratios (X-axis) against depth values over pixels (Y-axis). The data pairs used for the fit about 50000, which is a very large amount of data for this kind of statistical calculations. Although this can strongly bias the data, it appears on the plot that there is an even balancing-out of relative outliers. The expected trend is effectively captured and the resulting equation can be seen on the plot.

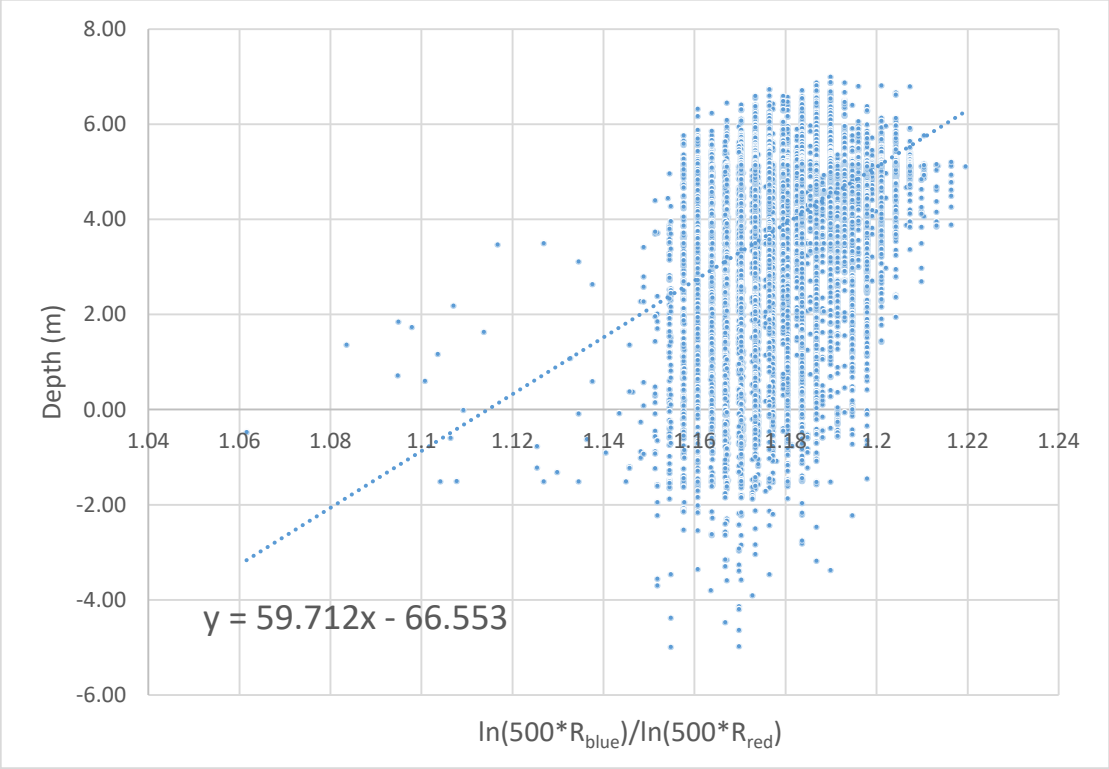


**Figure 76.** Water Depth model of Lake Koronia (22/5/1986).

Figure 77 depicts the application of the derived bathymetric model over the lake at a later date, but still relatively close to the date of the satellite image used to estimate the model. In time, it is expected that the bottom of the lake undergoes significant changes in its morphology, due mass (and biomass) deposition and other reasons. This fact alone is enough to render the bathymetric model valid for a limited time period spanning the temporal proximity of the date of retrieval of the data used for the model fitting. The result appears to provide a bathymetric map of the lake with a fairly satisfactory accuracy, as seen in comparison to the lake bottom DEM used for the extraction of the model, from Chapter 7.5.7.

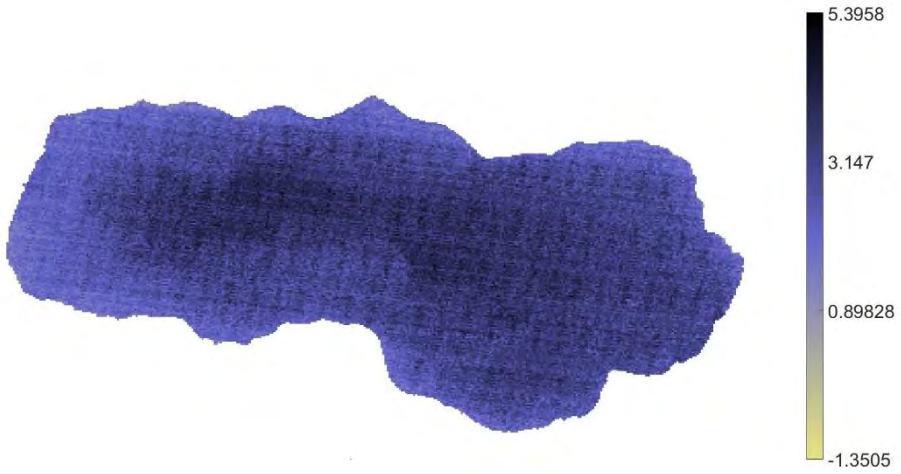


**Figure 77.** Lake Koronia Depth (m) (30/7/1988).

Figure 78 depicts the error map of the extracted bathymetric model referred to in the previous two figures. The values of the lake pixels are calculated as the differences between the pixel 'actual' depth (from the DEM) and the depth calculated using the equation extracted from the log-ratio fitted model. It is encouraging to observe the fair accuracy of the model, as well as the very important pattern of higher errors close to the shores. The latter observation was expected and provides a validation of the model and is attributed to the much smaller difference in electromagnetic radiation attenuation between the two different wavelength bands of blue and red when the 'travelled' water column thickness is smaller. When light travels a larger distance in water, the much higher absorbance of the red band wavelengths in comparison to blue absorbance, due to much faster exponential attenuation of red radiation, creates much more acute differences in the distribution of ratio values, resulting in a higher sensitivity for the model. In simple words, the model can capture a depth difference of 0.5 m between two points much more accurately in deeper waters than in shallower. Furthermore, in shallow waters, the recorded reflectance values are also significantly altered by the optical properties of the bottom of the lake.

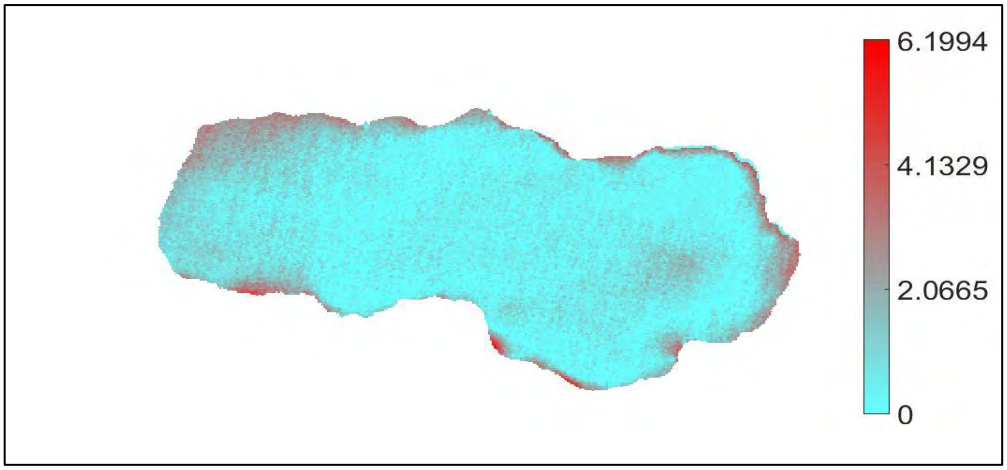


**Figure 78.** The residuals (m) of the lake depth model of 22/5/1986 compared against the bathymetry derived from the used DEM of **Figure 34**.

## 9.12 **Sentinel-2**

Figure 79 depicts the average concentration of Chl*a* (μg/l) and the average values of Conductivity (μS/cm), SDD (m) and pH of Lake Koronia. In addition, it presents the spatial variation of these parameters along Lake Koronia.

According to Figure 79 the greater the concentration of Chl*a*, the lower the value of SDD. The Conductivity values derived from Sentinel-2 are very low and do not correspond to the *in situ* measurements.

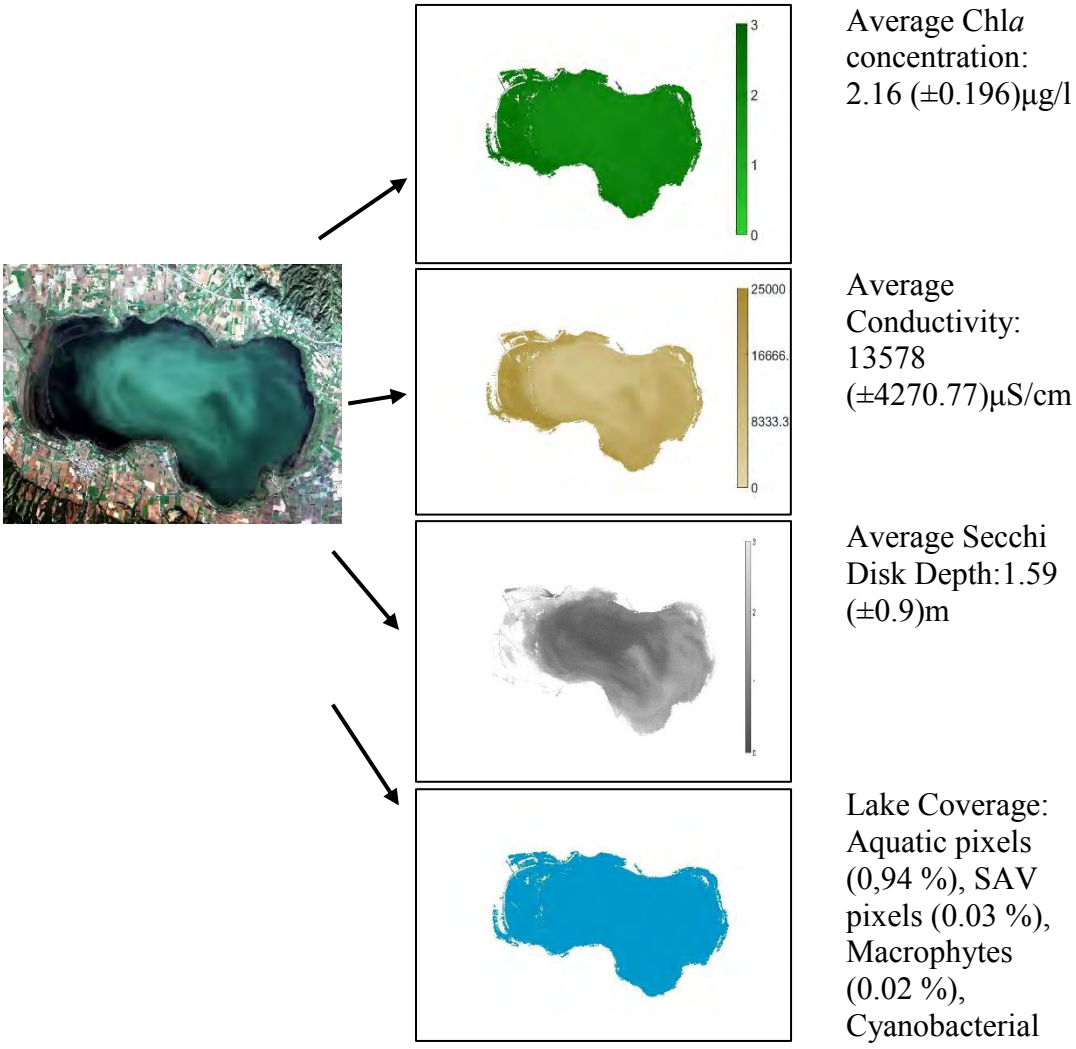


**Figure 79.** The average values of Chl*a*, SDD, Conductivity of Lake Koronia and the corresponding colormaps, derived from a Sentinel-2 image (16/11/2015).

# 10. CONCLUSIONS

## 10.1 Model Assessment and Feasibility of Parameter Calculation

Prior to presenting the conclusions of this study, it ought to be noted that the mathematical foundations underlying the mechanics of the models adopted, do not bear the same integrity in all cases of parameters, and a similar observation can be made for the physical foundations to an even higher degree. It is nevertheless important to be cautiously optimistic in view of the vast availability and potential of satellite data. Apart from the physics behind the studied parameters, moderation should also guide the statistical interpretations, in the sense that there is not always a clear and definitive meaning behind an apparent correlation. Therefore, the results of this study are in no way conclusive, and extensive cross-validation is necessary prior to adopting a model for wider application.

In this context, the notion of feasibility as used henceforth, refers to the physical possibility of exploiting the satellite imagery data to obtain a deterministic relation between the optical properties of water and a specific parameter. It is clear that this cannot always be the case. Whenever this is not the case, a relation may still be obtainable but is nevertheless not expected to carry a deterministic meaning, rather it may be valid for purely statistical reasons. Such relations are not expected to be reliable in the long term, in contrast to deterministic ones for feasible parameters. Empirical models specific for the calculation of feasible quality parameters have long term use, while empirical models related with not feasible parameters should be calibrated/validated using *in situ* measurements when the optical properties of the lake change.**Water Temperature** can be considered as a **feasible** parameter, as it is related with thermal radiation

It is impossible to estimate the reflectance of an object (the Secchi Disk) in its absence. What is more, the definition of the **Secchi Disk Depth** refers to the liminal visual detection by the human eye specifically, a fact that further complicates the effectiveness of the measurement approach, as it is even more complex to model the intricate functionality of a human eye. Therefore, water transparency expressed in terms of SDD is not only subjective, but also impossible to capture with a sensor detecting reflectance of water. The reason for this is that, in any wavelength, the actually measured reflectance is the cumulative effect of reflectance values of every layer of water (of arbitrarily small thickness) along a water column of a given surface area. There is no way to distinguish the layer (depth) from which on the contribution to the total reflectance becomes negligible (yet another subjective notion). Band combination does not improve the physical model either. All this explains, in part, why the satellite-derived SDD parameter time-series is inconsistent with the in-situ data. Therefore, in this case, only a statistical correlation can be exploited to capture the general variation trend of SDD and this parameter is considered **not feasible** hereby. According to Preisendorfer (1986), statistical links exist between the inherent optical properties of the water and the SDD measurements, using light measuring equipment. Such

experimental endeavors are progressively frustrating because, in time, the statistical links may weaken as the natural hydrosol undergoes its seasonal and inter- annual changes. These changes, while tending to be periodic, are always perturbed to some extent by random climatic and man- made events. Additionally, two lakes can have the same SDD, but differ markedly in light attenuation if the relative importance of scattering differs. For instance, a lake in which turbidity is mainly caused by suspended clay particles (which scatter rather than absorb), will have a lower light attenuation than a lake with the same SDD in which the turbidity is mainly due to phytoplankton (Scheffer 2004).

**Chlorophyll *α*** concentration is a very distinct characteristic of aquatic vegetation coverage. As a result, the parameter is very specific to that and is naturally correlated with it. The natural properties of chlorophyll $\alpha$ have been extensively studied and its connection to electromagnetic radiation is supported by an explicit scientific consensus. It is directly related to the reflectance of the green band wavelengths, which is the reason it can be effectively determined through reflectance values from satellite image data. Therefore, this parameter is hereby considered **feasible**.

**pH** is a very important parameter in the determination of water condition and quality. A deviation of the pH of water from its neutral value in a natural system is always brought about by the existence of one or more substances, acidic or basic in chemical nature. Each substance may have a specific light absorption spectrum, different to that of another one. Should the spectra have a high degree of overlap, the results on optical properties and reflectance of the various wavelengths are expected to be cumulative, creating a specific optical signature determinable by reflectance. However, this is not always the case. Therefore, the cumulative optical signature will necessarily depend on the concentrations of the strongest of acids or bases that are dissolved in the water and, simultaneously, have dominant EMR absorbance spectra (strong absorption or reflection at various wavelengths). EMR absorbance spectra of such substances may have very diverse presentations. As a result, a significant problem is that the water in natural systems is only slightly acidic or alkaline, which means that small changes in pH may be associated with large changes in optical properties. This renders pH determination a rather precarious methodology. In a simple example, two acid substances with very different absorption spectra might, in suitable concentrations, alter pH in the exact same way in a water solution. Any model “trained” to identify the pH based on EMR reflectance of water in the setting of one substance will fail when the pH change is due to the other substance, due to much different reflectance values. Therefore, pH is hereby considered **not feasible** as a satellite-image derivable parameter. It must be mentioned, however, that there are cases of natural water bodies that are affected by, more-or-less, the same substances over relatively medium-sized time periods of up to a few decades. Therefore, it must be made clear that relatively small pH variations can actually be effectively captured by a model exploiting the reflectance properties of water, as long as the dissolved substance profile does not change significantly in composition.

The physical parameter of **Conductivity** is readily connected to the existence, concentration, and, more important, the type of ions within the water from dissolved electrolytes. Simply put, lighter ions move faster, whereas heavier ones tend to move slower. The type and mobility of ions in water depend primarily on the dissolved substances (e.g. element ions from salts), apart from the pH-related ions from acids or bases ($H^+$, $OH^-$). For similar reasons with those mentioned above for the pH parameter calculation, every single dissolved element or acid/base will cause a specific change in the absorption spectrum of the water, together with a specific apparent behavior with respect to the Conductivity. It is natural that more than one different combinations of dissolved elements/acids/bases may result in the same behavior with respect to Conductivity, since the overall effect is cumulative but presents a very high degree of complexity as to how all the different ions contribute to the final Conductivity values. Therefore, two or more absorption spectrum signatures for the studied water volume may provide the same Conductivity values. Exactly like the pH case above, a model trained to detect Conductivity values in a water volume with a given profile of dissolved elements/acids/bases in varying proportions may be able to detect variations of Conductivity relatively accurately, as long as the profile does not change significantly. Although this is the case in large water bodies, at least within a reasonable time period, for all the aforementioned reasons, Conductivity is considered **not feasible** as a parameter in this study.

The **Lake Coverage** from various types of aquatic vegetation and organisms is based on justified scientific evidence. In this sense, the physical basis is connected to the natural pigmentation from molecules residing within the various different organisms, such as chlorophyll in aquatic vegetation or phycobiliproteins, such as phycocyanin and phycoerythrin in cyanobacteria. The light absorbance spectra of these pigments are well documented and reflectance in the suitable wavelengths, as well as various band combinations, correlate well with the concentration of vegetation or cyanobacteria. Thus, the physical mechanism is clear and the lake coverage is hereby considered a **feasible** determination.

The model fitting of **Water Depth** on reflectance data is based on the different properties of the absorption spectrum of clear water in different wavelengths. A very important problem arising in this calculation is the maximum depth that can be captured from a model, and the prerequisite that the water be clear. These two facts need to be suitably verified to an adequate degree in order for the model to be able to provide bathymetric data of usable accuracy. Since the mechanics of the model are very vividly explained and consolidated in (Stumpf et al. 2003), the approximation of bathymetric from satellite-image derived data is hereby considered a **feasible** process with trustworthy results. It must be stated in this point as well that a bathymetric model of whichever, relatively shallow overall, water body is only valid as long as the water remains relatively clear and the surface of the bottom is not heavily affected and deformed. Furthermore, it is clear from the fact that the final model is a single linear equation that acute simplification of reality occurs in the end product (the equation of

the log-ratio model). As a result, the model should only be considered a preliminary compaction of bathymetric information, valid for a few years or even decades in the case of clear water and relatively undeformable lakebed.

**Sentinel-2**

In order to guarantee the availability of satellite data and avoid any gap in data availability that would affect the on-going monitoring programs, the Copernicus initiative supports a new generation of environmental Earth Observation missions, the so-called Sentinel missions. ESA's forthcoming Sentinel-2 and Sentinel-3 satellites aim to improve the old generation of satellite sensors by providing superspectral imagery of high spatial and temporal resolution. Seninel-2 is equipped with additional new bands for improved parameter retrieval. Easy access to the Sentnel-2 data archives and the standardized processing tools foster the advances in lake water quality monitoring. Sentinel-2 satellites offer a comprehensive spatial and temporal coverage and new technical capabilities. The potential synergistic use of Sentinel images jointly with data of other related missions, such as Landsat missions, offer the opportunity for development of new scientific applications, related with the water quality monitoring. The development of sensor-specific calibration/validation procedures and statistical approaches will result in a more accurate calculation of lake QE. Sentinel-2 observations should join forces with in situ lake monitoring in order to understand complex interactions between physical and bio-geochemical lake processes. In addition, Sentinel-2 data may facilitate the understanding of the complex interactions between the atmosphere and lake water.

## 10.2 The profile of Lake Koronia

Lake Koronia has a highly dynamic character, which reflects the highly variable hydrologic conditions. This leads to rapid changes in physical and chemical conditions in the lake water column. The regular dry out and re-filling of the lake creates an extreme state of flux which prevents the establishment of stable states observed in more typical lakes (Reynolds 2006). Extreme hydrologic variability also makes it difficult to predict future trends in the QE values and complicates the development of management strategies that may lead to a healthy and sustainable ecosystem.

The values of the various QE determined in this study by analyzing satellite image data of (Landsat-5/TM, -7/ETM+, -8/OLI) are relatively close to reality for the feasible parameters in general, and clearly appear to follow the patterns of their actual variations in time. In the case of non-feasible parameters, short-term periods of accordance between satellite-derived and *in situ* data have been sporadically observed, although general variation trends are missed in the long term. All parameter models perform more accurately on average, rather than in a point-wise (pixel) approach, mostly because of the inconsistencies in image clarity over specific fixed pixels, which invalidate intermediate images of a timeline and, therefore, values of a time-series. It is natural that, as lake ecosystems have integral evolutionary characteristics, parameters

(QE) are also interdependent and not fully independent of each other. For a deeper understanding, a more extensive statistical correlation analysis between different time-series would be of utmost importance in order to monitor the co-evolution and discover highly-specific relevant trends in covariation. In order to provide a more functional satellite-data facility for the monitoring of, including but not limited to, Lake Koronia, a larger volume of *in situ* measurement data with high consistency would be necessary in order to formulate new models and algorithms based on data extracted from satellite images.In that case Manegement Authority of Lakes Koronia-Volvi will be able to have multiple QE measurements with only a few *in situ* mesurements.

## 10.3 The usefulness of remote sensing approach

Lake water quality monitoring aims at the generation of accurate data, which reflect the actual status of the water body. It is acknowledged that simply generating good data is not enough to meet the objectives. These data should be presented in a manner that aids the understanding of the spatial and temporal patterns in water quality, taking into consideration the natural processes and characteristics of the lake, and that allows the detection of the consequences of human activities. As a result, the researcher will be provided with the understanding that is necessary to meet the objectives behind the lake monitoring program. Coupled with advanced processing methods and improved sensor capabilities, recent years have seen increasing development in remote sensing of the quality parameters of inland and coastal waters. Unless a water body is sufficiently instrumented by *in situ* sensors, remote sensing is one satisfactory method to detect the status of inland waters. Remote sensing technology provides an emerging capability that can significantly augment or even replace traditional *in situ* methods but the field is relatively new, especially in addressing optically complex waters.

The image processing procedures, which were detailed in Chapter 5, were used/developed for Lake Koronia, but with appropriate modifications to reflect the optical properties and pre-existing geographic information, these procedures should work equally well for other lakes. In case of empirical approach, algorithms related with the optical properties of each lake should be evaluated and calibrated/validated with lake reference field data. Field data must be collected as close to the satellite overpass date as possible and taking account the adequate temporal and spatial coverage of the study area. Consequently, only the mathematical expressions, which relate the QE with the optical properties of each water body, vary through the image processing procedure.

Another key-point is that using the, at the time quite long (over 40 years in the present study), archive of appropriate satellite imagery, several parameters and their historical evolution may be retrieved, even in absence of any other data. Satellite images enable change detection of previously unmeasured or unmonitored water bodies. In fact, in many cases, satellite images may be the only source of information on past

conditions, awaiting to be exploited and this extends to a plethora of other applications beyond water quality.

The estimation of lake QE using satellite images may lead to the calculation of outlying values (values that fall outside the usual distribution). In the present study, the decrease of the measurement accuracy was, mainly, caused by:

- ✓ Atmospheric effects
- ✓ Sensor accuracy: <5%
- ✓ Sensor failure (e.g. TIRS)
- ✓ Models evaluated in other lakes
- ✓ Unclear relationship between parameter and optical properties of the water
- ✓ Use of DN values in estimating QE
- ✓ Low water level of lake Koronia

Additionally, genuine outlying values do occur, however, and may be important indicators of changes in water quality.

The adopted remote sensing approach for can be used for successful measure of the QE values or trend, regardless of their feasibility. Surface measurements of water reflectivity will be useful for the correction of the atmospheric effects. Also, the evaluation of algorithms specific for the optical properties of Lake Koronia will result in more accurate satellite calculations.

The objectives of Lake Koronia monitoring programs, which include the ultimate intention of regulation or control of water quality, cannot be accomplished, based, exclusively, on the long term water quality data and the derived statistics. It is relatively easy to collect QE measurements by remote sensing techniques and report the degree of deterioration or improvement of the water quality at a particular image. However, it is far more complicated to explain exactly why those changes have occurred and to suggest actions for management. The derived water quality data should be combined with supporting information (e.g. land use changes, waste discharges) and interpreted in a way that specifically addresses the objectives of the end-user of the information.

The long term QE database, which was derived in the present study using Landsat images, contributes to:

- ✓ The identification of areas under serious threat by water pollution, both presently and over the past decades.
- ✓ The regular monitoring of water quality, which is a crucial part of identifying any existing problems, or any issues that could emerge in the future.
- ✓ The designing and development pollution of prevention and management strategies.
- ✓ The determination of whether or not pollution regulations are being complied with.
- ✓ The raise of awareness of the importance of water quality degradation for local development.
- ✓ The identification of policy options that can be replicated and scaled-up to protect or restore water quality.

- ✓ The detection of any changes or trends that appear in water bodies over a period of time.

## 10.4 General conclusions

This study attempts to monitor water quality parameters using satellite images and suitable models from the available scientific literature. A number of parameters are successfully extracted from satellite images, including Temperature, SDD, Chlα, pH, Conductivity, Lake Coverage and Water Depth, following proposed techniques from a wide range of published papers. Furthermore, aquatic vegetation classification was successfully attempted with promising results. The degree of reliability of these results should be taken with caution. As concluded by scrutinizing the content of the corresponding articles in literature, the primary concern is to capture possible trends and correlations between a parameter and variations in one or more bands or mathematical band combinations from satellite images of the Landsat satellite missions. It appears that the TOA reflectance (or surface reflectance after suitable atmospheric corrections) is not the only favored measurement for the modeling, as a significant number of papers make extensive use of DN values from raw satellite images.

Although a number of models, such as those applied for the estimation of pH from Landsat-5 satellite images, appear to provide realistic results, it must be noted that there is an irregular intrinsic scaling between DN values from different bands. This can be ascertained by closely following the radiometric calibration procedure, during which DN values are converted to radiances using a predesignated linear transformation, with different coefficients for each band, as given in the satellite image accompanying metadata files. Apart from that, the fact that DN values are used for reasons of 'digital convenience' (numbers packed in 8-bit values) further complicates things. Because DN values of a band are rescaled and compacted in integer values, the DN pixel value distribution over a specific band does not accurately reflect the actual variation of the optical properties for the various land covers, as does true TOA- or surface reflectance value distribution. Because the transformation between DN and radiance values is linear, this turns out to be a minor problem when fitting linear models of parameters on DN values. However, the final statistical coefficients cannot be physically interpreted. It is, of course, clear, that the scaling difference between DN values and radiance values becomes a problem when fitting a nonlinear model on DN values, rather than radiances.

By definition, DN values do not directly correspond to a physical quantity and being favorable when probing for a realistic correlation between pixel values from a specific band of a satellite image and the values of a specific parameter appears rather counterintuitive to the researcher/end user to the author. The statistical basis is even further distorted, when the correlation model involves more than one band from DN pixel values, because DN pixel values follow different scaling for different bands. In spite of all that, however, a number of research articles use DN values, probably because they are easier to access, without having to follow a number of cumbersome preprocessing steps. The corresponding models appear to capture the relation between

the DN values and certain parameters with satisfactory accuracy. It is important to state that the equations of these models do not have clear natural interpretations, rather they reflect the covariations presented in the data used. On the other hand, models based on reflectance values, such as the aquatic vegetation classification, are more realistic and exhibit a straightforward dependence on certain natural properties of the parameters involved. It can be stated, for example, that the TOA- (or surface) reflectance of a specific piece of land cover (within a pixel) with respect to EMR of a specific wavelength (e.g. TIRS, or VCID bands) is directly associated with some natural properties (correspondingly, the average temperature) of the same piece of land.

In general, a number of different models are employed, most of which are linear, exponential, or utilize ratios of band pixel values. In some cases, logarithms are used instead of the original reflectance values, possibly to remove exponential trends or scale-down the degree of variation of the values involved. Overall, a wide range of documented cases and modelling attempts were traced down, referenced and used to extract a number of important parameters. The resulting time-series appear to correlate well with in-situ data on average, or, generally, provide realistic results (in the case of absence of in-situ data for validation). This is a very important observation, as satellite data are easy to access and also becoming increasingly easy to manipulate and extract information from, potentially providing large volumes of information spanning long temporal ranges to assist in any scientific discipline, in the frame of which this information may be of use and importance.

The successful retrieval of water quality information from Landsat data depends on the quality of *in situ* measurements that will be used for data calibration/validation. The *in situ* samples collected should be as fully representative as possible of the whole site to be characterized and all precautions should be taken to ensure, as far as possible, that the samples do not undergo any changes in the interval between sampling and analysis. Before any sampling program is devised, it is very important to define the lake structure and to establish the objectives since these are the major factors in determining the position of sampling sites, frequency of sampling, duration of sampling, sampling procedures, subsequent treatment of samples, and analytical requirements. Extensive field data are required in order to enable an accurate comparison of satellite data with actual ground data. One of the very first problems is the spatial divergence between the *in situ* measurements and the satellite remotely sensed data. In order to solve this problem it was suggested to realize limnological transects, where possible, instead of point stations. Another problem is the temporal congruity among all the in situ measurements. Sampling *in situ* is a long process and a time gap of several hours may exist between sampling stations. On the contrary, the remotely sensed data collection is instantaneous. A partial solution for the problem was pointed and consisted in organizing more boat-stations, displaced at different locations, and again sampling transects. The recording of some additional, complementary to the *in situ*, data, such as weather conditions and wind speed may be useful for the interpretation of the results derived from satellite data.

The utilization of the computer graphics capabilities in providing graphical user interfaces is of high importance. One of the products of the methodology that was followed in this master thesis was an unified processing environment presented as a Graphical User Interface (GUI). This GUI is a powerful and versatile means of communication between a user and a computer. The use of GUI may result in the reduction of the cost and the time for the calculation of lake QE using satellite images, even by non-specialists in Earth Observation from Space and image processing techniques. In addition, it contributes to the improvement of the quality and reliability of the satellite measurements, as it ensures that the followed process is the same every time. The GUI provides a user with the basic tools of satellite image pre-processing and QE calculation process.

## 11. REFERENCES


Alexandridis, T.K., et al., 2007. Remote sensing and GIS techniques for selecting a sustainable scenario for Lake Koronia, Greece. *Environmental Management*, 39(2), pp.278–290.

Atazadeh, I., 2011. *Biomass and remote sensing of biomass*, Niksa Mandic.

Azab, A.M., 2012. *Integrating GIS , remote sensing and mathematical modelling for surface water quality management in irrigated watersheds*, CRC Press/Balkema.

Baban, S.M.J., 1993. Detecting and evaluating the influence of water depth, volume and altitude on the variations in the surface temperature of lakes using Landsat imagery. *International Journal of Remote Sensing*, 14(15), pp.2747–2758.

Bakker, W. et al., 2009. *Principles of Remote Sensing* 4th edi. K. Tempfli et al., eds., The International Institute for Geo-Information Science and Earth Observation (ITC).

Barret, J., & Mansell, A.L., 1960. Ultra-violet absorption spectra of the molecules $H_2O$, HDO and $D_2O$, *Nature*, 187(4732), pp.138–138.

Barsi, J., Markham, B., Helder, D., & Chander, G., 2007. Radiometric calibration status of Landsat-7 and Landsat-5 - art. no. 67441F, Proceedings of SPIE - The International Society for Optical Engineering

Bierwirth, P.N., Lee, T.J., & Burne, R.V, 1993. Shallow sea-floor reflectance and water depth derived by unmixing multispectral imagery. *Photogrammetric Engineering and Remote Sensing*, 59(3), pp.331–338.

Blackwell, II. R., 1946. Contrast thresholds of the human eye. *J. Opt. Sot. Am*., 36, pp. 624- 643.

Bobori, D., 2001. Temporal and spatial variability of physicochemical parameters and nutrients in Lake Koronia (Greece). *BIOS*, 6, pp.9–18.

Boehrer, B., & Schultze, M., 2008. Stratification of Lakes. *Reviews of Geophysics*, 46, pp.1–27.

Borkman, D.G., & Smayda, T.J., 1998. Long-term trends in water clarity revealed by Secchi-disk measurements in lower Narragansett Bay. *ICES Journal of Marine Science: Journal du Conseil*, 55(4), pp.668–679.

Bricaud, A., Morel. A. & Prieur. L. 1983. Optical efficiency factors of some phytoplankters. *Limnology and Oceanography*, 28(5), pp. 816-832.

Brivio, P.A., Giardino, C. & Zilioli, E., 2001. Determination of chlorophyll concentration changes in Lake Garda using an image-based radiative transfer code for Landsat TM images. *International Journal of Remote Sensing*, 22, pp.487–502.

Butt, M., & Nazeer, M., 2015. Landsat ETM+ Secchi Disc Transparency (SDT) retrievals for Rawal Lake, Pakistan. *Advances in Space Research*, 56, pp.1428–1440.

Campbell, J., 2002. *Introduction to Remote Sensing*. 3rd ed., The Guilford Press.

Carlson, R., 1977. A Trophic State Index for Lakes. *Limnology and Oceanography* 22, pp.361–369.

Caselles, V., Rubio, E., Coll, C., & Valor, E., 1998. Thermal Band Selection for the PRISM Instrument: 3. Optimal Band Configurations. *J. Geophys. Res. Atmos*., 103,pp. 17057–17067.

Chander, G., & Markham, B., 2003. Revised Landsat-5 TM Radiometrie Calibration Procedures and Postcalibration Dynamic Ranges. *IEEE Transactions on Geoscience and Remote Sensing*, 41(11), pp.2674–2677.

Chaplin, M., 2006. Water Structure and Behavior; Molecular Vibration and Absorption, London South Bank Univ. (http://www.lsbu.ac.uk/water/vibrat.html).

Chen, J. & Quan, W., 2012. Using Landsat/TM imagery to estimate nitrogen and phosphorus concentration in Taihu Lake, China. *IEEE Journal of Selected Topics in Applied Earth Observations and Remote Sensing*, 5(1), pp.273–280.

Cho, H.J., 2007. Depth-variant spectral characteristics of submersed aquatic vegetation detected by Landsat 7 ETM +. *International Journal of Remote Sensing*, 28(7), pp.1455–1467.

Cohen, W.B., & Goward, S.N., 2004. Landsat's Role in Ecological Applications of Remote Sensing. *BioScience*, 54(6), pp.535–545.

Clifford, A.A., 1973. *Multivariate error analysis: a handbook of error propagation and calculation in many-parameter systems*. John Wiley & Sons.

Collett, L.J., Goulevitch, B.M., & Danaher, T.J., 1997. SLATS Radiometric Correction: A semi-automated, multi-stage process for the standardisation of temporal and spatial radiometric differences, Queensland Department of Natural Resources.

Colwell, R.N., 1966. Determining the prevalence of certain cereal crop diseases by means of aerial photography. *Hilgardia*, 26 (5), pp. 223-286.

Council Directive 76/464/EEC on pollution caused by certain dangerous substances discharged into the aquatic environment of the Community.

Council, E.P., 2000. Directive 2000/60/EC of the European Parliament and of the Council of 23 October 2000 establishing a framework for Community action in the field of water policy. *Official Journal of the European Parliament*, pp.1–72.

Dall'Olmo, G. & Gitelson, A., 2005. Effect of bio-optical parameter variability and uncertainties in reflectance measurements on the remote estimation of chlorophyll-a concentration in turbid productive waters: experimental results. *Applied Optics*, 44(3), pp.412–422.

Danbara, T.T., 2014. *Deriving Water Quality Indicators of Lake Tana , Ethiopia, From Landsat-8*. Faculty of Geo-Information Science and Earth Observation of the University of Twente.

Dekker, A.G., & Seyhan, E., 1988. The Remote Sensing Loosdrecht Lakes project. *International Journal of Remote Sensing*, 9(10-11), pp.1761–1773.

Dekker, A.G., & Peters, S.W.M., 1993. The use of the Thematic Mapper for the

analysis of eutrophic lakes: a case study in the Netherlands. *International Journal of Remote Sensing*, 14(5), pp.799–821.

Dekker, A.G., 1993. *Detection of optical water quality parameters for eutrophic waters by high resolution remote sensing*. Proefschrift Vrije Universiteit Amsterdam.

Dekker, A.G., et al., 2001. Imaging Spectrometry of Water. In D. van der M. Freek & S. M. Jong, eds. *Imaging Spectrometry*. pp. 307–359.

Dewidar, K., Khedr, A.A., & Dewidar, K., 2005. Remote Sensing of Water Quality for Burullus Remote Sensing of Water Quality for Burullus Lake, Egypt. *Geocarto International*, 20(3), pp.43–49.

Doxani, G., et al., 2012. Shallow-Water Bathymetry Over Variable Bottom Types Using Multispectral Worldview-2 Image. In *ISPRS - International Archives of the Photogrammetry, Remote Sensing and Spatial Information Sciences*. pp. 159–164.

Du, Y., et al., 2016. Water Bodies' Mapping from Sentinel-2 Imagery with Modified Normalized Difference Water Index at 10-m Spatial Resolution Produced by Sharpening the SWIR Band. *Remote Sensing*, 8, pp.354–373. Available at: http://www.mdpi.com/2072-4292/8/4/354.

Duntley, S.Q., 1952. The visibility of sub- merged objects.Final Rept., Visibility Lab., Mass. Inst. Tech. 74

Eisenberg, D., & Kauzmann, W., 1969. *The Structure and Properties of Water*, Oxford University Press, London.

Elachi, C. & Zyl, J., 2006. *Introduction to the physics and techniques of remote sensing* Second edi. J. A. Kong, ed., John Wiley & Sons, INC.

Ewing, G.C, & McAlister, E.D., 1960. On the thermal boundary layer of the Ocean. *Science*, 131, pp.1374-1376.

Fuller, L.M., & Minnerick, R.J., 2007. Predicting Water Quality by Relating Secchi-Disk Transparency and Chlorophyll a Measurements to Satellite Imagery for Michigan Inland Lakes, August 2002. Scientific Investigations Report 2004-5086. *USGS*.

Furby, S.L., & Campbell, N.A., 2001. Calibrating images from different dates to "like-value" digital counts. *Remote Sensing of Environment*, 77(2), pp.186–196.

Fyfe, S.K., 2003. Spatial and temporal variation in spectral reflectance: Are seagrass species spectrally distinct? *Limnol. Oceanogr.*, 48(1, part2), pp.464–479.

Gege, P., 2004. The water color simulator WASI: An integrating software tool for analysis and simulation of optical in situ spectra. *Computers and Geosciences*, 30, pp.523–532.

Gege, P., 2014. WASI-2D: A software tool for regionally optimized analysis of imaging spectrometer data from deep and shallow waters. *Computers and Geosciences*, 62, pp.208–215. Available at: http://dx.doi.org/10.1016/j.cageo.2013.07.022.

Giardino, C. et al., 2001. Detecting chlorophyll, Secchi disk depth and surface

temperature in a sub-alpine lake using Landsat imagery. *Science of the Total Environment*, 268, pp.19–29.

Giardino, C., et al., 2007. Assessment of water quality in Lake Garda (Italy) using Hyperion. *Remote Sensing of Environment*, 109(2), pp.183–195.

Giardino, C. et al., 2012. BOMBER : A tool for estimating water quality and bottom properties from remote sensing images. *Computers and Geosciences*, 45, pp.313–318.

Gitelson, A., M., et al., 1994. The use of high spectral resolution radiometer data for detection of low chlorophyll concentrations in Lake Kinneret.*Journal of Plankton Research*, 16, pp.993–1002.

Gitelson, A., Mayo, M., Yacobi, Y.Z., Paroarov, A., & Berman, T., 1994. The use of high spectral resolution radiometer data for detection of low chlorophyll concentrations in Lake Kinneret, *Journal of Plankton Research*, 16, pp.993–1002.

Goel, P.K., 2011. *Water Pollution: Causes, Effects and Control*. 2nd ed., New Age International Publishers.

Gordon, H. R., & Morel, A.Y., 1983. Remote assessment of ocean colour for interpretation of satellite visible imagery: A review. New York: Springer-Verlag.

Greenwood, N.N. & Earnshaw, A., 1997. *Chemistry of the Elements*, 2nd ed., Butterworth-Heinemann, Oxford.

Guidance document no.7 2003. Common implementation strategy for the water framework directive (2000/60/EC): Monitoring under the Water Framework Directive. Office for Official Publications of the European Communities, Produced by Working Group 2.7 - Monitoring.

Han, L, & Jordan, K.J., 2005. Estimating and mapping chlorophyll- a concentration in Pensacola Bay, Florida using Landsat ETM+ data. *International Journal of Remote Sensing*, 26(23), pp.5245–5254.

Hansen, M.C., & Loveland, T.R., 2012.A review of large area monitoring of land cover change using Landsat data. *Remote sensing of Environment*, 122, pp.66-74.

Harrison, R., 2001. *Pollution: Causes, Effects and Control*. 4th ed., Royal Society of Chemistry.

Hathout, S., 1985, The use of enhanced Landsat imagery for mapping lake depth. *Journal of Environmental Management*, 20, pp.253-261.

Hellenic Military Geographical Service: Topographic maps, on a scale 1:50000 [Thermi (1970, 1982)].

Hogenboom, H. J. & Dekker, A., 1999. Report: Inversion: assessment of water composition from spectral reflectance. A feasibility study to the use of matrix inversion method. Delft, Report of the Netherlands Remote Sensing Board (BCRS), pp. 98-15.

Ingram, K., Knapp, E. & Robinson, J.W., 1981. Change detection technique development for improved urbanized area delineation, technical memorandum CSCITM-81/6087, Computer Sciences Corporation, Silver Springs, Maryland,

U.S.A

Irons, J.R, & Loveland, T.R., 2013. Eight Landsat satellite becomes operational. *Photogrammetric Engineering and Remote Sensing*, 79, pp.398-401.

Janca, A., Tereszchuk, K., Bernath, P.F., Zobov, N.F., Shirin, S.V., Polyansky, O.L., & Tennyson, J., 2003. Emission spectrum of hot HDO below 4000 $cm^{-1}$, *J. Mol. Spectrosc.*, 219,pp. 132–135.

Jassby, A.D., et al., 1999. Origins and scale dependence of temporal variability in the transparency of Lake Tahoe, California-Nevada. *Limnology and Oceanography*, 44(2), pp.282–294.

Jerlov N.G., 1976. Marine optics. 2nd ed.,Elservier, Amsterdam

Ji, L., Zhang, L., & Wylie, B., 2009. Analysis of Dynamic Thresholds for the Normalized Difference Water Index. *Photogrammetric Engineering & Remote Sensing*, 75(11), pp.1307-1317.

Kaiserli, A., Voutsa, D., & Samara, C., 2002. Phosphorus fractionation in lake sediments - Lakes Volvi and Koronia, N. Greece. *Chemosphere*, 46(8), pp.1147-1155.

Khattab, M.F.O., & Merkel, B.J., 2014. Application of Landsat 5 and Landsat 7 images data for water quality mapping in Mosul Dam Lake, Northern Iraq. *Arabian Journal of Geosciences*, 7(9), pp.3557–3573.

Kingsford, R.T., Thomas,R. F. Wong, P. S. & Knowles, E. 1997. GIS database for wetlands of the Murray Darling Basin, final report of the Murray Darling basin commission. National Parks and Wildlife Service, Sydney, Australia.

Kirk, J.T.O.,1980. Spectral absorption properties of natural waters: contribution of the soluble and particulate functions of light absorption in some inland waters of south- eastern Australia, *Austr. J. Mar. Freshwater Res.*, 31, pp.287-296.

Kirk, J.T.O., 1994. *Light and Photosynthesis in Aquatic Ecosystems*. Cambridge University Press, New York, NY, USA

Kirk, J.T.O., 2013. *Light and Photosynthesis in Aquatic Ecosystems* 3rd ed., Cambridge University Press.

Kishino, M., Okami, N., Takahashi, M. & Ichimura, S. 1986. Light utiliza- tion efficiency and quantum yield of phytoplankton in a thermally stratified sea. *Limnol. Oceanogr*., 31, pp.557–66.

Kloiber, S. M., Brezonik, P.L., Olmanson, L.G. & Bauer, B. E. 2002. A procedure for regional water clarity assessment using Landsat multispectral data. *Remote Sens. Environ*., 82(1), pp.38-47.

Knight, P., Karavokyris, G., & Anelixi Agrisystems, 1999. Environmental Rehabilitation of Lake Koronia, Greece (European Commission, Directorate General XVI).

Kolokytha, E., 2014. Agricultural development in lake koronia . The role of the water footprint of major crops in combating climate change. In *3rd IAHR Europe Congress, Book of Proceedings, 2014, Porto - Portugal.* pp. 237–250.

Kotchenova, S., Vermote, E., Matarrese, R., & Klemm, F., Jr., 2006. Validation of a

vector version of the 6S radiative transfer code for atmospheric correction of satellite data. Part I: Path radiance. *Applied Optics*, 45,pp. 6762–6774.

Koussouris, T.S., Bertakos, T.I. & Diapoulis, A.C., 1992. Background trophic state of Greek lakes. Fresenius Environ. Bull. 1, pp. 96–101.

Ku, H.H., 1966. Notes on the use of propagation of error formulas. Journal of Research of the National Bureau of Standards. Section C: Engineering and Instrumentation, 70C, No. 4.

Kungolos, A. et al., 1998. Water quality and toxicity assessment in Koronia lake-Greece. *Fresenius Environmental Bulletin,* 7, pp.615-622.

Kutser, T., 2004. Quantitative detection of chlorophyll in cyanobacterial blooms by satellite remote sensing. *Limnology and Oceanography*, 49, pp.2179–2189.

Kutser, T., Vahtma, E. & Martin, G., 2006. Assessing suitability of multispectral satellites for mapping benthic macroalgal cover in turbid coastal waters by means of model simulations. *Estuarine, Coastal and Shelf Science*, 67, pp.521–529.

Kutser, T., Metsamaa, L. & Dekker, A.G., 2008. Influence of the vertical distribution of cyanobacteria in the water column on the remote sensing signal. *Estuarine, Coastal and Shelf Science*, 78, pp.649–654.

Kutser, T., 2009. Passive optical remote sensing of cyanobacteria and other intense phytoplankton blooms in coastal and inland waters. *International Journal of Remote Sensing*, 30(17), pp.4401-4425.

Lal, R., 1994. *Soil Erosion.* Soil and Water Conservation Society, Ankeny, Iowa, pp. 340.

Lamaro, A.A., et al., 2013. Water surface temperature estimation from Landsat 7 ETM+ thermal infrared data using the generalized single-channel method: Case study of Embalse del Río Tercero (Córdoba, Argentina). *Advances in Space Research*, 51, pp.492–500.

Lampert, W., & Sommer, U., 2007. *Limnoecology:The ecology of lakes and streams* 2nd ed., Oxford University Press.

Lathrop, R.G.J., & Lillesand, T.M., 1989. Monitoring water quality and river plume transport in Green Bay, Lake Michigan with SPOT-l imagery. *Photogramm. Eng. and Rem. Sens*., 55(3), pp.349- 354.

Lathrop, R.G.J. & Lillesand, T.M., 1986. Use of Thematic Mapper data to assess water quality in Green Bay and central Lake Michigan. *Photogramm. Eng. Remote Sens.,* 52, pp.671–680.

Law 1739/87. Management of water resources and other provisions (Official Gazette A 201/19-20.11.1987).

Law 3199/2003. Protection and management of water-Compliance with Directive 2000/60 / EC of the European Parliament and of the Council of 23 October 2000. Government Gazette 280 / A / 12.9.2003 (in Greek).

Lewis, P. et al., 2012. An Earth Observation Land Data assimilation system (EO-LDAS). *Remote Sensing of Environment*, 120, pp.219-235.

Li, F. et al., 2004. Deriving land surface temperature from Landsat 5 and 7 during SMEX02/SMACEX. *Remote Sensing of Environment*, 92(4), pp.521–534.

Li, R. & Liu, J., 2002. Wetland vegetation biomass estimation and mapping from Landsat ETM data: a case study of Poyang Lake. *Journal of Geographical Sciences*, 12(1), pp.35–41.

Lindell, T. et al., 1999. *Manual for monitoring european lakes using remote sensing techniques*, European Communities.

Lyzenga, D.R., & Polcyn, F.C., 1979. *Water Depth Information From Landsat Digital Data*, Research Institute of Michigan Prepared for: Defense Mapping Agency Hydrographic/Topographic Center Washington.

Lyzenga, D.R., 1978. Passive Remote-Sensing Techniques for Mapping Water Depth and Bottom Features. *Applied Optics*, 17(3), pp.379–383.

Ma, R., & Dai, J., 2005. Investigation of chlorophyll--a and total suspended matter concentrations using Landsat ETM and field spectral measurement in Taihu Lake, China. *International Journal of Remote Sensing*, 26(13), pp.2779–2795.

Ma, R. et al., 2008. Detecting Aquatic Vegetation Changes in Taihu Lake, China Using Multi-temporal Satellite Imagery. *Sensors*, 8, pp.3988–4005.

Mahiny, A.S., & Turner, B.J., 2007. A comparison of four common atmospheric correction methods. *Photogrammetric Engineering & Remote Sensing*, 73(4), pp.361–368.

Malthus, T.J. et al., 2013. Inland water quality monitoring in Australia. In *IGARSS*. pp.2872–2875.

Manakou, V., Kungolos, A., & Beriatos, E., 2008. Hazards that threaten Greek wetlands: the case of Lake Koronia. In *Risk Analysis VI*. 10th International Conference on Risk Analysis and Hazard Mitigation: WIT Press, Southampton, UK (Cephalonia, Greece), pp. 3–10.

Markham, B., & Helder, D., 2012. Forty-Year Calibrated Record of Earth-Surface Reflected Radiance from Landsat: A Review. *Remote Sens. Environ.*, 122, pp.30–40

Masek, J.G. et al., 2013. LEDAPS Calibration, Reflectance, Atmospheric Correction Preprocessing Code, Version 2. Model product. Available on-line [http://daac.ornl.gov] from Oak Ridge National Laboratory Distributed Active Archive Center, Oak Ridge, Tennessee, U.S.A.

Masuda, K., Takashima, T., & Takayama, Y., 1988. Emissivity of pure and sea waters for the model sea surface in the infrared window regions. *Remote Sensing of the Environment,* 24, pp. 313-332.

Mather, P., 2004. *Computer Processing of Remotely-Sensed Images:An Introduction* Third edit., John Wiley & Sons Ltd.

McAlister, E.D., & McLeish, W., 1969. Heat transfer in the top millimeter of the ocean. *Journal of Geophysical Research*, 74, pp.3408-3414.

McFeeters, S.K., 1996. The use of the Normalized Difference Water Index (NDWI) in the delineation of open water features. *International Journal of Remote Sensing*,

17(7), pp.1425–1432.

Michaloudi, E. et al., 2009. Plankton community structure during an ecosystem disruptive algal bloom of Prymnesium parvum. *Journal of Plankton Research*, 31(3), pp.301–309.

Michaloudi, E. et al., 2012. Plankton Succession in the Temporary Lake Koronia after Intermittent Dry-Out. *International Review of Hydrobiology*, 97(5), pp.405–419.

Mitraki, C., Crisman, T.L., & Zalidis, G., 2004. Lake Koronia, Greece: Shift from autotrophy to heterotrophy with cultural eutrophication and progressive water-level reduction. *Limnologica*, 34, pp.110–116.

Mittenzwey, K.H. et al., 1992. Determination of Chlorophyll-a of Inland Waters on the Basis of Spectral Reflectance. *Limnology and Oceanography*, 37(1), pp.147–149.

Mobed, J.J., Hemmingsen, S.L., Autry, J.L., & McGown, L.B., 1996. Fluorescence characterisation of IHSS humic substances: total luminescence spectra with absorbance correction. *Environ. Sci. Technol*., 30(10), pp.3061–3066.

Morel, A. & Prieur, L., 1977. Analysis of variations in ocean color. *Limnology and Oceanography*, 22, pp.709–722.

Morel, A. & Gordon, H.R.1980. Report of the working group on water color. *Boundary-Layer Meteorol*. 18, pp.343-355.

Mouratidis, A., Briole, P. & Katsambalos, K., 2010. SRTM 3″ DEM (versions 1, 2, 3, 4) validation by means of extensive kinematic GPS measurements: a case study from North Greece. *International Journal of Remote Sensing*, 31(23), pp.6205–6222.

Mourkides, G. et al., 1978. Lakes of northern Greece. I. State of eutrophication. Scientific Annuals of the Faculty of Agriculture, Aristotle University of Thessaloniki.

Moustaka-Gouni, M. et al., 2004.The coincidence of a Prymnesium parvum bloom and the mass kill of birds and fish in Lake Koronia. *Harmful Algae News*, 26, pp. 1–2.

Moustaka-Gouni, M. et al., 2012. Plankton changes as critical processes for restoration plans of lakes Kastoria and Koronia. *European Water*, 40, pp.43–51.

Mushtaq, F., Ghosh, M. & Lala, N., 2016. Remote Estimation of Water Quality Parameters of Himalayan Lake (Kashmir) using Landsat 8 OLI Imagery Title : Remote Estimation of Water Quality Parameters of Himalayan Lake. *Geocarto International,* DOI: 10.1080/10106049.2016.1140818

Mylopoulos, N. et al., 2007. Integrated water management plans for the restoration of lake Koronia, Greece. *Water International*, 32(5), pp.720–738.

National Aeronautics and Space Administration, 1999. *Landsat 7 Science Data Users Handbook*

Nemani, R. et al. 2009. Monitoring and forecasting ecosystem dynamics using the Terrestial Observation and Prediction System (TOPS). *Remote Sensing of Environment*, 113, pp.109-110.

Njoku, E., 2014. Encyclopedia of remote sensing, pp.957.

Nobel, P. S., 2005. Physicochemical and Environmental Plant Physiology. New York: Academic Press.

Olmanson, L.G., Bauer, M.E., & Brezonik, P.L., 2008. A 20-year Landsat water clarity census of Minnesota's 10,000 lakes. *Remote Sensing of Environment*, 112, pp.4086–4097.

Oswald, C. J. & Rouse, W. R., 2004. Thermal characteristics and energy balance of various-size Canadian Shield lakes in the Mackenzie River Basin. *J. Hydrometeorol.*, 5, pp.129–144.

Oyama, Y., Matsushita, B., & Fukushima, T., 2015. Distinguishing surface cyanobacterial blooms and aquatic macrophytes using Landsat/TM and ETM+ shortwave infrared bands. *Remote Sensing of Environment*, 157, pp.35–47.

Papakonstantinou, A. & Katirtjoglou, K. 1995. Proposals for the restoration of hydrodynamics in Lake Koronia, Greece. Greek Geological Institute (IGME). Thessaloniki, Greece.

Papakonstantinou, A., Chatzikyrkou, A. & Kalousi, E. 1996. Study of surface and groundwater quality in the Prefecture of Thessaloniki. Greek Geological Institute (IGME). Thessaloniki, Greece.

Paris, J.F., 1992. Remote sensing applications for freshwater systems. In Global Climate Change and Freshwater Ecosystems, edited by P. Firth and S. G. Fisher (New York: Springer-Verlag).

Patel-Sorrentino, N., Mounier, S., & Benaim, J.Y., 2002. Excitation–e- mission fluorescence matrix to study pH influence on organic matter fluorescence in the Amazon Basin rivers.*Water Res.*, 36 (10), pp.2571–2581.

Pattanaik, A., Sahu, K. & Bhutiyani, M.R., 2015. Estimation of Shallow Water Bathymetry Using IRS-Multispectral Imagery of Odisha Coast, India. *Aquatic Procedia*, 4(0), pp.173–181.

Paulson, C.A., & Parker, T.W., 1972. Cooling of a water surface by evaporation, radiation and heat transfer. Journal of Geophysical Research, 77, pp.491-495.

Petaloti, C. et al., 2004. Nutrient dynamics in shallow lakes of Northern Greece. *Environmental science and pollution research international*, 11(1), pp.11–17.

Philpot, W.D., 1989. Bathymetric mapping with passive multispectral imagery. *Applied optics*, 28(8), pp.1569–1578.

Preisendorfer, W., 1986. Secchi disk science: Visual optics of natural waters. *Limnology and Oceanography*, 31(5), pp.909–926.

Psilovikos, A., 1977. Paleogeographic evolution of the Megdonia Basin. PhD, Aristotle University of Thessaloniki, Greece (in Greek).

Quevauviller, P. et al., 2008. *The Water Framework Directive: Ecological and Chemical Status Monitoring*. 1st ed.,Wiley & Sons.

Reis, S., & Yilmaz, H.M., 2008. Temporal monitoring of water level changes in Seyfe lake using remote sensing. Hydrolog. Proc. Published online in Wiley InterScience

Reynolds, C. S., 1993. Scales of disturbance and their role in plankton ecology.*Hydrobiologia*, 249, pp.157-172.

Richards, J.A. & Jia, X., 2006. *Remote Sensing Digital Image Analysis: An Introduction* 4th editio., Springer-Verlag Berlin Heidelberg.

Ritchie, J.C., Cooper, C.M. & Schiebe, F.R., 1990. The relationship of MSS and TM digital data with suspended sediments, chlorophyll, and temperature in Moon Lake, Mississippi. *Remote Sensing of Environment*, 33, pp.137–148.

Ritchie, J.C., Zimba, P. V & Everitt, J.H., 2003. Remote Sensing Techniques to Assess Water Quality. *Photogrammetric Engineering Remote Sensing*, 69(6), pp.695–704.

Rollin, E.M., Steven, M.D. &Mather, P., 1985. Atmospheric corrections for remote sensing : proceedings of a remote sensing workshop on "Atmospheric Corrections", University of Nottingham, Department of Geography, University of Nottingham.

Rose, R. et al., 2015. Ten ways remote sensing can contribute to conservation. *Conservation Biology*, 29(2), pp.350–359.

Roy, D.P. et al., 2014. Landsat-8: Science and product vision for terrestrial global change research. *Remote Sensing of Environment*, 145, pp.154–172.

Rundquist, D., Lawson, M., Queen, L. & Cerveny, R., 1987. The Relationship between the Timing of Summer-Season Rainfall Events and Lake-Surface Area. *Water Resources Bulletin*, 23, pp. 493–508.

Sahu, A., 2014. Identification and mapping of the water-logged areas in Purba Medinipur part of Keleghai river basin, India: RS and GIS methods. *International Journal of Advanced Geosciences*, 2(2), pp.59–65.

Schalles, J.F., Schiebe, F.R., Starks, P.J. & Troeger, W.W., 1997. *Estimation of algal and suspended sediment loads (singly and combined) using hyperspectral sensors and integrated meso- cosm experiments,* Fourth International Conference on Re- mote Sensing for Marine and Coastal Environments, 17–19 March, Orlando, Florida (University of Michigan Press, Ann Arbor, Michigan), pp. 111–120.

Scheffer, M., 2004. *Ecology of shallow lakes* 1st ed. M. B. Usher, ed., Springer Netherlands.

Schneider, K. & Mauser, W., 1996. Processing and accuracy of Landsat Thematic Mapper data for lake surface temperature measurement. *International Journal of Remote Sensing*, 17(11), pp.2027–2041.

Schott, J.R., 1989. Image processing of Thermal Infrared images. *Photogrammetric Engineering and Remote Sensing*, 55, pp.1311-1321.

Schowengerdt, R., 2007. *Remote sensing:Models and Methods for Image Processing* Third edit., Department of Electrical and Computer Engineering, College of Optical Sciences, and Office of Arid Lands Studies University of Arizona Tucson, Arizona: Elsevier.

Senesi, N., 1990. Molecular and quantitative aspects of the chemistry of fulvic acid and its interactions with metal ions and organic chemicals. Part II. The

fluorescence spectroscopy approach. *Anal. Chim. Acta*, 232, pp.77–106.

Shaw, J.H., 1970. Determination of the Earth's surface temperature from remote spectral radiance observation near 2600 $cm^{-1}$. *Journal of Atmospheric Science*, 27, pp.950-959.

Shifrin K.S., 1988. Physical optics of ocean water, American Institute of Physics, New York

Singh, A., 1989. Review Article: Digital change detection techniques using remotely-sensed data. *International Journal of Remote Sensing*, 10(6), pp.989–1003.

Skoulikidis, N.T., Bertahas, I. & Koussouris, T., 1998. The environmental state of freshwater resources in Greece (rivers and lakes). *Environmental Geology*, 36(1-2), pp.1–17.

Sleeter, B.M. et al. 2012. Scenarios of land use and land cover change in the conterminous United States: Ultilizing the special report on emission scenarios at ecoregional scales. *Global Environment Change*, 22, pp.896-914.

Smith, R.C. & Baker, K.S., 1978. The bio-optical state of ocean waters and remote sensing. *Limnol. Oceanogr*., 23(2), pp.247-259.

Smith, W. & Sandwell, D., 2004. Conventional Bathymetry, Bathymetry from Space, and Geodetic Altimetry. *Oceanography*, 17(1), pp.8–23.

Spencer, R.G.M., Bolton, L. & Baker, A., 2007. Freeze/thaw and pH effects on freshwater dissolved organic matter fluorescence and absorbance properties from a number of UK locations. *Water Research*, 41, pp.2941–2950.

Stramski, D. & Morel. A.. 1990. Optical properties of photosynthetic picoplankton in different physiological states as affected by growth irradiance. Deep Sea Research, 37, pp.245:266.

Stumpf, R.P., Holderied, K. & Sinclair, M., 2003. Determination of water depth with high-resolution satellite imagery over variable bottom types. *Limnol. Oceanogr.*, 48 (1,part 2), pp.547–556.

Swift, T.J. et al., 2006. Water clarity modeling in Lake Tahoe: Linking suspended matter characteristics to Secchi depth. *Aquatic Sciences*, 68, pp.1–15.

Tang, K.K.W. & Pradhan, B., 2015. Converting Digital Number into Bathymetric Depth: A Case Study over Coastal and Shallow Water of Langkawi Island, Malaysia. In *FIG Working Week 2015*. Sofia,Bulgaria, p. 14.

Theologou, I., Patelaki, M. & Karantzalos, K., 2015. Can single empirical algorithms accurately predict inland shallow water quality status from high resolution, multi-sensor, multi-temporal satellite data? In *ISPRS - International Archives of the Photogrammetry, Remote Sensing and Spatial Information Sciences*. pp. 1511–1516.

Thomas, R., Meybeck, M. & Beim, A., 1996. Lakes. In D. Chapman, ed. *Water Quality Assessments:A Guide to Use of Biota, Sediments and Water in Environmental Monitoring*. Published on Behalf of United Nationseducational, Scientific and Cultural Organization World Healthorganization United Nations Environment Programme, pp. 325–371.

Torbick, N. et al., 2013. Mapping inland lake water quality across the Lower Peninsula of Michigan using Landsat TM imagery. *International Journal of Remote Sensing*, 34(21), pp.7607–7624.

Tyler, J. E., 1960. Sea water-water color and transparency, pp. 117-l 18. In McGraw-Hill Encyclopedia of Science and Technology, v. 12. McGraw-Hill, New York.

Tyler, J.E., 1968. The Secchi Disc. *Limnology and Oceanography*, 13(1), pp.1–6.

Tzimopoulos, C. et al., 2005. Water Resources Management in the Watershed of Volvi Lake. In pp. 1–6.

Tzionas, P., Ioannidou, I., A., & Paraskevopoulos, S. (2004). A hierarchical fuzzy decision support system for the environmental rehabilitation of Lake Koronia, Greece. *Environmental Management*, 34(2), pp. 245–260.

USGS, 2016. *Provisional Landsat 8 Surface Reflectance Product*.

Vahtmäe, E., Kutser, T., Martin, G., & Kotta, J. 2006. Feasibility of hyperspectral remote sensing for mapping benthic macroalgal cover in turbid coastal waters. *Remote Sensing of Environment*, 101, pp.342–351.

Vermote, E. F., Tanré, D., Deuzé, J. L., Herman, M. & Morcrette, J. J., 1997. *Second Simulation of Satellite Signal in the Solar Spectrum, 6S: An Overview*. IEEE Transaction on Geoscience and Remote Sensing, 35 (3), pp. 675-686.

Vuglinskiy, V., 2009. *Water level in lakes and reservoirs, water storage,* Version 8.

Wang, F. et al., 2006. Applications of Landsat-5 TM imagery in assessing and mapping water quality in Reelfoot Lake, Tennessee. *International Journal of Remote Sensing*, 27(23), pp.5269–5283.

Waxter, M.T., 2014. *Analysis of Landsat Satellite Data to Monitor Water Quality Parameters in Tenmile Lake , Oregon*. Portland State University.

Weng, Q., 2011. *Advances in Environmental Remote Sensing:Sensors, Algorithms, and Applications*, Indiana State University, Terre Haute Indiana, U.S.A.: CRC Press.

Wezernak, C.T. & Lyzenga, D.R., 1975. Analysis of Cladophora Distribution in Lake Ontario Using Remote Sensing. *Remote Sensing of Environment*, 4, pp.37–48.

Williams, D. et al., 2003. Preliminary investigation of submarged aquatic vegetation mapping usingyperspectral remote sensing. *Environmental Monitoring and Assessment*, 81, pp.383–392.

Williamson, C.E. et al., 1999. Dissolved organic carbon and nutrients as regulators of lake ecosystems: Resurrection of a more integrated paradigm. *Limnology and Oceanography*, 44(3,part 2), pp.795–803.

Wloczyk, C. et al., 2006. Sea and lake surface temperature retrieval from Landsat thermal data in Northern Germany. *International Journal of Remote Sensing*, 27(12), pp.2489–2502.

Wolberg, G., 1990. Digital Image Warping. Los Alamitos, CA: IEEE Computer Society Press.

Wozniak, B. & Dera, J., 2007. *Light Absorption in Sea Water*, Springer.

Wulder, M.A. et al. 2012. Opening the archive: How free data has enabled science and monitoring promise of Landsat. *Remote Sensing of Environment*, 122, pp.2-10.

Xu, H., 2006. Modification of normalised difference water index (NDWI) to enhance open water features in remotely sensed imagery. *International Journal of Remote Sensing*, 27(14), pp.3025–3033.

Yacobi, Y. Z., Gitelson, A., & Mayo, M., 1995. Remote sensing of chlorophyll in Lake Kinneret using high spectral-resolution radiometer and Landsat TM: Spectral features of reflectance and algorithm development. *Journal of Plankton Research*, 17, pp.2155–2217.

Younos, T. & Parece, T., 2015. *The Handbook of Environmental Chemistry:Advances in Watershed Science and Assessment*, Springer International Publishing Switzerland.

Zalidis, G.C., Takavakoglou, V. & Alexandridis, T., 2004. Revised Restoration Plan of Lake Koronia. Aristotle University of Thessaloniki, Department of Agronomy, Laboratory of Applied Soil Science. Pages 236 + Annexes. In Greek, English Summary

Zalidis, G. et al., 2014. Selection of a proper management strategy for Lake Koronia, Greece, based on monitoring reliable indicators. In *Protection and restoration of the environment XI*. pp. 262–270.

Zanter, K., 2015. Landsat 8 (L8) Data Users Handbook. *Survey, Department of the Interior U.S. Geological*, Version 1., pp.97.

## Internet sources


| | | |
|---|---|---|
| *[ul11]* | The USGS Water Science School | [http://water.usgs.gov/edu/earthwherewater.html] |
| *[url2]* | The Encyclopedia of Earth | [ http://www.eoearth.org/view/article/152861/] |
| *[url3]* | Lakenet | [http://www.lakenet.gr/greecemap.php] |
| *[url4]* | U.S. Geological Survey | [http://www.usgs.gov/] |
| *[url5]* | USGS/Landsat 4 History | [http://landsat.usgs.gov/about_landsat4.php] |
| *[url6]* | USGS/Landsat 5 History | [http://landsat.usgs.gov/about_landsat5.php] |
| *[url7]* | USGS/Landsat 7 History | [http://landsat.usgs.gov/about_landsat7.php] |
| *[url8]* | USGS/Landsat 8 History | [http://landsat.usgs.gov/about_landsat8.php] |
| *[url9]* | Geodata | [http://geodata.gov.gr] |
| *[url10]* | Management Authority Lakes Koronia-Volvi | [http://www.foreaskv.gr/] |
| *[url11]* | USGS/Landsat Missions | [http://landsat.usgs.gov/] |
| *[url12]* | The Landsat Program/NASA | [landsat.gsfc.nasa.gov] |
| *[url13]* | European Environment Agency/Interactive maps/European protected sites | [http://www.eea.europa.eu/data-and-maps/explore-interactive-maps/european-protected-areas-1] |
| *[url14]* | ESA Sentinel Online | [https://earth.esa.int/web/sentinel/user-guides/sentinel-2-msi/resolutions/radiometric] |
| *[url15]* | ESA Sentinel Online | [https://sentinels.copernicus.eu/web/sentinel/missions/sentinel-2/instrument-payload] |
| *[url16]* | ORNL DAAC, NASA | [http://daac.ornl.gov/cgi-bin/dsviewer.pl?ds_id=1146] |
| *[url17]* | USGS | [http://espa.cr.usgs.gov/downloads/auxiliaries/ledaps_auxiliary/ledaps_aux.1978-2014.tar.gz LEDAPS auxiliaries] |
| *[url18]* | GitHub | [https://github.com/USGS-EROS/espa-surface-reflectance/tree/master/not-validated-prototype-l8_sr] |
| *[url19]* | CGIAR-CSI | [http://srtm.csi.cgiar.org/SELECTION/inputCoord.asp] |

| | | |
|---|---|---|
| *[url20]* | NASA | [https://www.google.gr/url?sa=t&rct=j&q=&esrc=s&source=web&cd=1&ved=0ahUKEwirxLDAlMXLAhUJKpoKHXBuBIQQFggaMAA&url=http%3A%2F%2Flandsathandbook.gsfc.nasa.gov%2Fexcel_docs%2Fd.xls&usg=AFQjCNGw60cnGaC46609cU3KkRdGpkUNtw&sig2=M2Vx14bthqLL77gwCW7qLw&bvm=bv.116954456,d.bGs&cad=rja] |
| *[url21]* | Landsat 7 Handbook | [http://landsathandbook.gsfc.nasa.gov/data_prod/prog_sect11_3.html] |
| *[url22]* | NASA-Landsat Science | [http://landsat.gsfc.nasa.gov/?p=11327] |
| *[url23]* | GitHub-fmask | [https://github.com/prs021/fmask] |
| *[url24]* | EOLISA | [https://earth.esa.int/web/guest/eoli] |
| *[url25]* | GLOVIS | [http://glovis.usgs.gov/] |
| *[url26]* | USGS- Landsat Missions | [http://landsat.usgs.gov/thermal_band_on_Landsat_7.php] |
| *[url27]* | Using the USGS Landsat 8 Product | [http://landsat.usgs.gov/Landsat8_Using_Product.php] |
| *[url28]* | ESA Sentinel Online | [https://sentinel.esa.int/web/sentinel/technical-guides/sentinel-2-msi/level-1c/algorithm] |

# Annex I

**Table 1.** Key features of each chemical and physico-chemical quality element for lakes (Guidance document no.7, 2003).

| Aspect/feature | Transparency | Thermal Conditions | Oxygenation Conditions | Salinity | Acidification | Nutrients |
|---|---|---|---|---|---|---|
| **Measured parameters indicative of QE** | Secchi depth, turbidity, colour, TSS | Temperature | DO, TOC, BOD, COD DOC | Conductivity | Alkalinity, pH, ANC | Total P, SRP, Total N, N-NO3, N-NO2, N-NH4 |
| **Relevance of quality element** | Eutrophication, acidification | Hydrological cycle, biological activity | Production, respiration, mineralisation | | Buffering capacity, sensitivity to acidification | Eutrophication |
| **Pressures to which QE responds** | Agricultural, domestic and industrial discharges | Thermal discharges. Water management in reservoirs. | Eutrophication, organic pollution, industrial discharges | Industrial discharges, run-off | Acid rain, industrial discharges | Agricultural, domestic and industrial discharges |
| **Level and sources of variability of QE** | High, influenced by allocthonous and autocthonous material | High, influenced by climate conditions, topography, morphology and waterbody dimensions | Variable, diel changes due to respiration/ photosynthesis | Low-medium, influenced by climatic events | Low-medium, influenced by climatic events | Low-medium, influenced by climatic events |
| **Monitoring considerations** | Seasonal variation | Seasonal variation (mixing and stratification) | Diel variation<br>High gradient in stratified lakes | Seasonal variation | Seasonal variation | Sufficient speciation to enable discrimination (point and diffuse) |
| **Sampling methodology** | *In situ* using Secchi disc<br>TSS: field sample collection followed by laboratory analysis<br>Turbidity: *in situ* turbidimeters, nephelometers<br>Colour: *in situ* comparison to Forel-Ule scale or in lab. | *In situ* using thermistor probes or reversing type Hg thermometer | On-line data acquisition; *in situ* submersible probes; field sample collection followed by laboratory Winkler titration | *In situ* using submersible probes | *In situ* measurement of pH with probe.<br>Sample collection followed by laboratory analysis | Sample collection in the field followed by laboratory analysis |
| **Typical sampling frequency** | Monthly/ quarterly related to the biological elements sampling periodicity. Fortnightly of monthly during growth season in Nordic countries. | Monthly/ quarterly | Depends on morphological characteristics of lake: daily/monthly, or at the end of stratification periods (late winter if ice cover or late summer. | Monthly/ quarterly. Should be measured during snow melt or heavy rainfall events | Monthly/ quarterly. Should be measured during snow melt or heavy rainfall events | Monthly/ quarterly<br>Fortnightly of monthly during growth season in Nordic countries. |
| **Time of year of sampling** | All seasons. | All seasons | All seasons | All seasons | All seasons | All seasons, or mainly during growth season, SRP also measured during late winter in bottom waters |
| **Typical "sample" size** | In-situ observations.<br>Sample collections for chemical analyses (turb, TSS) | Water column profile | Single measurements, water column profiles. 100mL for Winkler titration | In-situ water column profile, integrated epilimnion or single sample from outlet (depending on monitoring purpose) | Single sample from outlet of lake or water column profile | Integrated epilimnion, single samples or water column profile (100-500mL) |
| **Ease of sampling /measurements** | Simple , using *in situ* probes or surface water sample | Simple, using *in situ* probes or water samplers | Simple, using *in situ* submersible probes or sample collection followed by titration | Simple, using *in situ* probe | Simple | Relatively easy, depth sampler need for deep lakes |

**(Continue)**

| Aspect/feature | Transparency | Thermal Conditions | Oxygenation Conditions | Salinity | Acidification | Nutrients |
|---|---|---|---|---|---|---|
| Basis of any comparison of results/quality/stations e.g. reference conditions/best quality | Historical data or data from comparable pristine lakes | Historical data or data from comparable pristine lakes | Historical data or data from comparable pristine lakes | Historical data or data from comparable pristine lakes | Historical data or data from comparable pristine lakes | Statistical methods: MEI index for total phosphorus<br>Historical data or data from comparable pristine lakes |
| Methodology consistent across EU? | No | No | No | No | No | No |
| Current use in monitoring programmes or for classification in EU | Yes | Finland, France, Italy, Norway | Finland, France, Italy, Norway Sweden | Finland, Belgium, France, Italy | Belgium, Finland, France, Italy, Norway, Sweden, UK | Germany, Spain, Finland, France, Italy, Ireland, Netherlands, Norway, Sweden, UK |
| Existing monitoring systems meet requirements of WFD? | No | No | No | No | No | No |
| Existing classification system meets requirements of WFD? | No | No | No | No | No | No |
| ISO/CEN standards | No | No | ISO 5813:1983 DO<br>ISO 5815:1989 $BOD_5$ | Yes | Yes, no standard for ANC | Yes, several ISO standards exist |
| Applicability to lakes | high | High | High | Moderate | High | High |
| Main advantages | • Simple to sample<br>• It is possible the most universally used parameter in limnology: it is a simple and powerful tool for tracking long-term trends | • Simple to measure<br>• Fundamental to understand the hydrological cycle and lake ecology | • Simple to sample and to measure<br>• Extremely useful because it can act as an integrator of the lake health | • Simple to measure<br>• Conductivity is little influenced by anthropogenic inputs. A good correlation was found with the MEI cond and P concentration allowing the determination of natural background (reference) concentrations for P | • Simple to measure<br>• Provides long term trends in acidification<br>• Alkalinity is little influenced by anthropogenic inputs(except in acidified and limed lakes). A good correlation was found with the MEI alk and P concentration allowing the determination of natural background (reference) concentrations for P | • Provide information and long-term information on the trophic state |
| Main disadvantages | • No disadvantages | • May require intensive monitoring for appropriate description of thermal conditions | • May require intensive monitoring following depletion events in stratified lakes | • Does not provide long term information on trends | • None | • Need for standardisation of analytical techniques |

**(Continue)**

| Aspect/feature | Transparency | Thermal Conditions | Oxygenation Conditions | Salinity | Acidification | Nutrients |
|---|---|---|---|---|---|---|
| Conclusions/ recommendations | Easy to monitor. Secchi disc is widely used in limnology for assessing the biological condition of lakes. However, in humic lakes Secchi disc is not useful for assessment of eutrophication.. | Important supporting parameter for interpreting ecological conditions. Seasonal variation, variation with depth and in large lakes horizontal variation should be monitored. | Recommended, and particularly important in deep/stratified lakes and lakes with ice cover. | Important for at characterisation of a lake. For example, it gives an indication of lake mixing processes and of metabolic activity of the lake. | Important for lake characterisation. Acidity is important because it governs the chemical form which metals occur in water body. Alkalinity and Its related variables, pH and conductivity are important classification parameters | Very important indicator for human activity/eutrophication. Total N and P, nitrate and orthophosphate should be monitored as a minimum. Ammonia monitored where concentrations are expected to be problematic e.g. exceedences of limit values over a specific limit. Phosphorus is most often considered to be the nutrient that determines algal production in lakes Thus the focus is mainly on P with regards to lake eutrophication. Nutrients should be monitored not only in water but also in sediments where sediment water interchange processes are expected to be important |

# Annex II

| Satellite/Instrument | ID | Date |
|---|---|---|
| Landsat/5_TM | LT51840321984112ESA00 | 21/4/1984 |
| Landsat/5_TM | LT51840321984128ESA00 | 7/5/1984 |
| Landsat/5_TM | LT51840321984160ESA00 | 8/6/1984 |
| Landsat/5_TM | LT51840321984176ESA00 | 24/6/1984 |
| Landsat/5_TM | LT51830321984201ESA00 | 19/7/1984 |
| Landsat/5_TM | LT5184032008420850 | 26/7/1984 |
| Landsat/5_TM | LT51830321984217ESA00 | 4/8/1984 |
| Landsat/5_TM | LT51840321984224ESA00 | 11/8/1984 |
| Landsat/5_TM | LT51830321984233ESA00 | 20/8/1984 |
| Landsat/5_TM | LT51830321984249ESA00 | 5/9/1984 |
| Landsat/5_TM | LT51830321984265ESA00 | 12/9/1984 |
| Landsat/5_TM | LT51840321984272ESA00 | 21/9/1984 |
| Landsat/5_TM | LT51830321984281ESA00 | 28/9/1984 |
| Landsat/5_TM | LT51830321984297ESA00 | 7/10/1984 |
| Landsat/5_TM | LT51840321984304ESA00 | 23/10/1984 |
| Landsat/5_TM | LT51840321984336ESA00 | 1/12/1984 |
| Landsat/5_TM | LT51840321985034ESA00 | 3/2/1985 |
| Landsat/5_TM | LT51840321985050AAA04 | 19/2/1985 |
| Landsat/5_TM | LT51840321985050ESA00 | 19/2/1985 |
| Landsat/5_TM | LT51840321985098ESA00 | 8/4/1985 |
| Landsat/5_TM | LT51840321985114ESA00 | 24/4/1985 |
| Landsat/5_TM | LT51830321985139AAA03 | 19/5/1985 |
| Landsat/5_TM | LT51840321985162ESA00 | 11/6/1985 |
| Landsat/5_TM | LT5184032008517850 | 27/6/1985 |
| Landsat/5_TM | LT51830321985187ESA00 | 6/7/1985 |
| Landsat/5_TM | LT51840321985194ESA00 | 13/7/1985 |
| Landsat/5_TM | LT51830321985203ESA00 | 22/7/1985 |
| Landsat/5_TM | LT51840321985210ESA00 | 29/7/1985 |
| Landsat/5_TM | LT51830321985219ESA00 | 7/8/1985 |
| Landsat/5_TM | LT51840321985226ESA00 | 14/8/1985 |
| Landsat/5_TM | LT51830321985235ESA00 | 23/8/1985 |
| Landsat/5_TM | LT51840321985242ESA00 | 30/8/1985 |
| Landsat/5_TM | LT51830321985267ESA00 | 24/9/1985 |
| Landsat/5_TM | LT51830321985283ESA00 | 10/10/1985 |
| Landsat/5_TM | LT51840321985290ESA00 | 17/10/1985 |
| Landsat/5_TM | LT51830321986014ESA00 | 14/1/1986 |
| Landsat/5_TM | LT51840321986021ESA00 | 21/1/1986 |
| Landsat/5_TM | LT51840321986085ESA00 | 26/3/1986 |
| Landsat/5_TM | LT51830321986094ESA00 | 4/4/1986 |
| Landsat/5_TM | LT51840321986101ESA00 | 11/4/1986 |
| Landsat/5_TM | LT51830321986110ESA00 | 20/4/1986 |
| Landsat/5_TM | LT51840321986117ESA00 | 27/4/1986 |
| Landsat/5_TM | LT51830321986142XXX03 | 22/5/1986 |
| Landsat/5_TM | LT51840321986149ESA00 | 29/5/1986 |
| Landsat/5_TM | LT51830321986158ESA00 | 7/6/1986 |
| Landsat/5_TM | LT51840321986165ESA00 | 14/6/1986 |
| Landsat/5_TM | LT51830321986174ESA00 | 23/6/1986 |

| | | |
|---|---|---|
| Landsat/5_TM | LT51840321986197ESA00 | 16/7/1986 |
| Landsat/5_TM | LT51830321986206ESA00 | 25/7/1986 |
| Landsat/5_TM | LT51840321986213XXX02 | 1/8/1986 |
| Landsat/5_TM | LT51830321986222ESA00 | 10/8/1986 |
| Landsat/5_TM | LT51840321986229ESA00 | 17/8/1986 |
| Landsat/5_TM | LT51840321986261ESA00 | 18/9/1986 |
| Landsat/5_TM | LT51840321986277AAA09 | 4/10/1986 |
| Landsat/5_TM | LT51830321986318XXX01 | 14/11/1986 |
| Landsat/5_TM | LT51830321986334ESA00 | 30/11/1986 |
| Landsat/5_TM | LT51840321986341ESA00 | 7/12/1986 |
| Landsat/5_TM | LT51840321986357ESA00 | 23/12/1986 |
| Landsat/5_TM | LT51840321987040ESA00 | 9/2/1987 |
| Landsat/5_TM | LT51830321987097XXX02 | 7/4/1987 |
| Landsat/5_TM | LT51840321987168XXX02 | 17/6/1987 |
| Landsat/5_TM | LT51830321987177XXX02 | 26/6/1987 |
| Landsat/5_TM | LT51840321987200XXX03 | 19/7/1987 |
| Landsat/5_TM | LT51830321987209XXX02 | 28/7/1987 |
| Landsat/5_TM | LT51830321987225XXX02 | 13/8/1987 |
| Landsat/5_TM | LT51840321987248AAA02 | 5/9/1987 |
| Landsat/5_TM | LT51830321987257AAA03 | 14/9/1987 |
| Landsat/5_TM | LT51840321987264ESA00 | 21/9/1987 |
| Landsat/5_TM | LT51840321987280ESA00 | 7/10/1987 |
| Landsat/5_TM | LT51840321987312ESA00 | 8/11/1987 |
| Landsat/5_TM | LT51840321988043ESA00 | 12/2/1988 |
| Landsat/5_TM | LT51840321988059ESA00 | 28/2/1988 |
| Landsat/5_TM | LT51840321988075ESA00 | 15/3/1988 |
| Landsat/5_TM | LT51840321988123ESA00 | 2/5/1988 |
| Landsat/5_TM | LT51840321988139ESA00 | 18/5/1988 |
| Landsat/5_TM | LT51840321988155ESA00 | 3/6/1988 |
| Landsat/5_TM | LT51830321988164ESA00 | 12/6/1988 |
| Landsat/5_TM | LT51830321988180ESA00 | 28/6/1988 |
| Landsat/5_TM | LT51840321988187ESA00 | 5/7/1988 |
| Landsat/5_TM | LT51830321988196ESA00 | 14/7/1988 |
| Landsat/5_TM | LT51840321988203ESA00 | 21/7/1988 |
| Landsat/5_TM | LT51830321988212ESA00 | 30/7/1988 |
| Landsat/5_TM | LT51840321988219ESA00 | 6/8/1988 |
| Landsat/5_TM | LT51830321988228ESA00 | 15/8/1988 |
| Landsat/5_TM | LT51840321988235ESA00 | 22/8/1988 |
| Landsat/5_TM | LT51830321988244ESA00 | 31/8/1988 |
| Landsat/5_TM | LT51830321988260ESA00 | 16/9/1988 |
| Landsat/5_TM | LT51830321988324ESA00 | 19/11/1988 |
| Landsat/5_TM | LT51840321988347ESA00 | 12/12/1988 |
| Landsat/5_TM | LT51830321989006ESA00 | 6/1/1989 |
| Landsat/5_TM | LT51840321989029ESA00 | 29/1/1989 |
| Landsat/5_TM | LT51830321989038ESA00 | 7/2/1989 |
| Landsat/5_TM | LT51840321989093ESA00 | 3/4/1989 |
| Landsat/5_TM | LT51840321989141ESA00 | 21/5/1989 |
| Landsat/5_TM | LT51830321989150ESA00 | 30/5/1989 |

| | | |
|---|---|---|
| Landsat/5_TM | LT51830321989166ESA00 | 15/6/1989 |
| Landsat/5_TM | LT51840321989173ESA00 | 22/6/1989 |
| Landsat/5_TM | LT51840321989189ESA00 | 8/7/1989 |
| Landsat/5_TM | LT51840321989205ESA00 | 24/7/1989 |
| Landsat/5_TM | LT51830321989214ESA00 | 2/8/1989 |
| Landsat/5_TM | LT51840321989221ESA00 | 9/8/1989 |
| Landsat/5_TM | LT51840321989237ESA00 | 25/8/1989 |
| Landsat/5_TM | LT51830321989246ESA00 | 3/9/1989 |
| Landsat/5_TM | LT51840321989253ESA00 | 10/9/1989 |
| Landsat/5_TM | LT51830321989262ESA00 | 19/9/1989 |
| Landsat/5_TM | LT51840321989285ESA00 | 12/10/1989 |
| Landsat/5_TM | LT51840321989333ESA00 | 29/11/1989 |
| Landsat/5_TM | LT51840321990192XXX03 | 11/7/1990 |
| Landsat/5_TM | LT51840321990224XXX03 | 12/8/1990 |
| Landsat/5_TM | LT51830321990265ESA00 | 22/9/1990 |
| Landsat/5_TM | LT51830321990281ESA00 | 8/10/1990 |
| Landsat/5_TM | LT51840321991019ESA00 | 19/1/1991 |
| Landsat/5_TM | LT51840321991035ESA00 | 4/2/1991 |
| Landsat/5_TM | LT51840321991083ESA00 | 24/3/1991 |
| Landsat/5_TM | LT51840321991099ESA00 | 9/4/1991 |
| Landsat/5_TM | LT51840321991147ESA00 | 27/5/1991 |
| Landsat/5_TM | LT51830321991156ESA00 | 5/6/1991 |
| Landsat/5_TM | LT51840321991163ESA00 | 12/6/1991 |
| Landsat/5_TM | LT51830321991172ESA00 | 21/6/1991 |
| Landsat/5_TM | LT51840321991179ESA00 | 28/6/1991 |
| Landsat/5_TM | LT51840321991195ESA00 | 14/7/1991 |
| Landsat/5_TM | LT51840321991211XXX03 | 30/7/1991 |
| Landsat/5_TM | LT51840321991227ESA00 | 15/8/1991 |
| Landsat/5_TM | LT51840321991243ESA00 | 31/8/1991 |
| Landsat/5_TM | LT51840321991291ESA00 | 18/10/1991 |
| Landsat/5_TM | LT51840321991323ESA00 | 28/11/1991 |
| Landsat/5_TM | LT51830321991332ESA00 | 5/12/1991 |
| Landsat/5_TM | LT51840321991339ESA00 | 31/1/1992 |
| Landsat/5_TM | LT51830321992047ESA00 | 16/2/1992 |
| Landsat/5_TM | LT51840321992054ESA00 | 23/2/1992 |
| Landsat/5_TM | LT51840321992086ESA00 | 26/3/1992 |
| Landsat/5_TM | LT51830321992095ESA00 | 4/4/1992 |
| Landsat/5_TM | LT51840321992118ESA00 | 27/4/1992 |
| Landsat/5_TM | LT51840321992150ESA00 | 29/5/1992 |
| Landsat/5_TM | LT51840321992166ESA00 | 14/6/1992 |
| Landsat/5_TM | LT51840321992198ESA00 | 16/7/1992 |
| Landsat/5_TM | LT51830321992207ESA00 | 25/7/1992 |
| Landsat/5_TM | LT51840321992214ESA00 | 1/8/1992 |
| Landsat/5_TM | LT51830321992223ESA00 | 10/8/1992 |
| Landsat/5_TM | LT51840321992230ESA00 | 17/8/1992 |
| Landsat/5_TM | LT51830321992239ESA00 | 26/8/1992 |
| Landsat/5_TM | LT51840321992246ESA00 | 2/9/1992 |
| Landsat/5_TM | LT51830321992255ESA00 | 11/9/1992 |

| | | |
|---|---|---|
| Landsat/5_TM | LT51840321992262ESA00 | 18/9/1992 |
| Landsat/5_TM | LT51830321992271ESA00 | 27/9/1992 |
| Landsat/5_TM | LT51840321992326ESA00 | 21/11/1992 |
| Landsat/5_TM | LT51830321992351ESA00 | 16/12/1992 |
| Landsat/5_TM | LT51840321993008ESA00 | 8/1/1993 |
| Landsat/5_TM | LT51840321993024ESA00 | 24/1/1993 |
| Landsat/5_TM | LT51840321993040ESA00 | 9/2/1993 |
| Landsat/5_TM | LT51830321993049ESA00 | 18/2/1993 |
| Landsat/5_TM | LT51840321993072ESA00 | 13/3/1993 |
| Landsat/5_TM | LT51830321993081ESA00 | 22/3/1993 |
| Landsat/5_TM | LT51840321993088ESA00 | 29/3/1993 |
| Landsat/5_TM | LT51840321993104ESA00 | 14/4/1993 |
| Landsat/5_TM | LT51840321993136ESA00 | 16/5/1993 |
| Landsat/5_TM | LT51830321993145ESA00 | 25/5/1993 |
| Landsat/5_TM | LT51840321993152ESA00_ | 1/6/1993 |
| Landsat/5_TM | LT51840321993168ESA00 | 17/6/1993 |
| Landsat/5_TM | LT51840321993200ESA00 | 19/7/1993 |
| Landsat/5_TM | LT51840321993216ESA00 | 4/8/1993 |
| Landsat/5_TM | LT51840321993232ESA00 | 20/8/1993 |
| Landsat/5_TM | LT51840321993280ESA00 | 7/10/1993 |
| Landsat/5_TM | LT51840321993344ESA00 | 10/12/1993 |
| Landsat/5_TM | LT51830321993353ESA00 | 19/12/1993 |
| Landsat/5_TM | LT51840321994011ESA00 | 11/1/1994 |
| Landsat/5_TM | LT51830321994036ESA00 | 5/2/1994 |
| Landsat/5_TM | LT51830321994084ESA00 | 25/3/1994 |
| Landsat/5_TM | LT51840321994091ESA00 | 1/4/1994 |
| Landsat/5_TM | LT51840321994107ESA00 | 17/4/1994 |
| Landsat/5_TM | LT51840321994139ESA00 | 19/5/1994 |
| Landsat/5_TM | LT51830321994148ESA00 | 28/5/1994 |
| Landsat/5_TM | LT51840321994155ESA00 | 4/6/1994 |
| Landsat/5_TM | LT51840321994171ESA00 | 20/6/1994 |
| Landsat/5_TM | LT51830321994180ESA00 | 29/6/1994 |
| Landsat/5_TM | LT51840321994187ESA00 | 6/7/1994 |
| Landsat/5_TM | LT51830321994196ESA00 | 15/7/1994 |
| Landsat/5_TM | LT51840321994203ESA00 | 22/7/1994 |
| Landsat/5_TM | LT51840321994219ESA00 | 7/8/1994 |
| Landsat/5_TM | LT51830321994228ESA00 | 16/8/1994 |
| Landsat/5_TM | LT51840321994235ESA00 | 23/8/1994 |
| Landsat/5_TM | LT51830321994244ESA00 | 1/9/1994 |
| Landsat/5_TM | LT51840321994251ESA00 | 8/9/1994 |
| Landsat/5_TM | LT51830321994260ESA00 | 17/9/1994 |
| Landsat/5_TM | LT51840321994267ESA00 | 24/9/1994 |
| Landsat/5_TM | LT51830321994276ESA00 | 3/10/1994 |
| Landsat/5_TM | LT51840321994299ESA00 | 26/10/1994 |
| Landsat/5_TM | LT51840321994331ESA00 | 27/11/1994 |
| Landsat/5_TM | LT51840321994347ESA00 | 13/12/1994 |
| Landsat/5_TM | LT51840321994363ESA00 | 29/12/1994 |
| Landsat/5_TM | LT51840321995030ESA00 | 30/1/1995 |

| | | |
|---|---|---|
| Landsat/5_TM | LT51830321995039ESA00 | 8/2/1995 |
| Landsat/5_TM | LT51830321995135ESA00 | 15/5/1995 |
| Landsat/5_TM | LT51840321995142ESA00 | 22/5/1995 |
| Landsat/5_TM | LT51830321995151ESA00 | 31/5/1995 |
| Landsat/5_TM | LT51840321995158ESA00 | 7/6/1995 |
| Landsat/5_TM | LT51830321995167ESA00 | 16/6/1995 |
| Landsat/5_TM | LT51840321995174ESA00 | 23/6/1995 |
| Landsat/5_TM | LT51830321995183ESA00 | 2/7/1995 |
| Landsat/5_TM | LT51840321995190ESA00 | 9/7/1995 |
| Landsat/5_TM | LT51830321995199ESA00 | 18/7/1995 |
| Landsat/5_TM | LT51840321995222ESA00 | 10/8/1995 |
| Landsat/5_TM | LT51830321995231ESA00 | 19/8/1995 |
| Landsat/5_TM | LT51830321995247ESA00 | 4/9/1995 |
| Landsat/5_TM | LT51840321995254ESA00 | 11/9/1995 |
| Landsat/5_TM | LT51830321995279ESA00 | 6/10/1995 |
| Landsat/5_TM | LT51840321995286ESA00 | 13/10/1995 |
| Landsat/5_TM | LT51840321995302ESA00 | 29/10/1995 |
| Landsat/5_TM | LT51840321996033ESA00 | 2/2/1996 |
| Landsat/5_TM | LT51840321996129ESA00 | 8/5/1996 |
| Landsat/5_TM | LT51840321996161ESA00 | 9/6/1996 |
| Landsat/5_TM | LT51840321996177ESA00 | 25/6/1996 |
| Landsat/5_TM | LT51840321996193ESA00 | 11/7/1996 |
| Landsat/5_TM | LT51840321996209ESA00 | 27/7/1996 |
| Landsat/5_TM | LT51840321996225ESA00 | 12/8/1996 |
| Landsat/5_TM | LT51840321996241ESA00 | 28/8/1996 |
| Landsat/5_TM | LT51840321997083ESA00 | 24/3/1997 |
| Landsat/5_TM | LT51840321997099ESA00 | 9/4/1997 |
| Landsat/5_TM | LT51830321997108ESA00 | 18/4/1997 |
| Landsat/5_TM | LT51840321997163ESA00 | 12/6/1997 |
| Landsat/5_TM | LT51840321997179ESA00 | 28/6/1997 |
| Landsat/5_TM | LT51840321997195ESA00 | 14/7/1997 |
| Landsat/5_TM | LT51840321997227ESA00 | 15/8/1997 |
| Landsat/5_TM | LT51840321997275ESA00 | 2/10/1997 |
| Landsat/5_TM | LT51840321997307ESA00 | 3/11/1997 |
| Landsat/5_TM | LT51840321997323ESA00 | 19/11/1997 |
| Landsat/5_TM | LT51840321998038ESA00 | 7/2/1998 |
| Landsat/5_TM | LT51840321998054ESA00 | 23/2/1998 |
| Landsat/5_TM | LT51840321998118ESA00 | 28/4/1998 |
| Landsat/5_TM | LT51830321999034ESA00 | 3/2/1999 |
| Landsat/5_TM | LT51830321999050ESA00 | 19/2/1999 |
| Landsat/5_TM | LT51830321999082ESA00 | 23/3/1999 |
| Landsat/5_TM | LT51830321999098ESA00 | 8/4/1999 |
| Landsat/5_TM | LT51840321999121ESA00 | 1/5/1999 |
| Landsat/5_TM | LT51840321999153ESA00 | 2/6/1999 |
| Landsat/5_TM | LT51830321999194ESA00 | 13/7/1999 |
| Landsat/5_TM | LT51840321999201ESA00 | 20/7/1999 |
| Landsat/5_TM | LT51830321999210ESA00 | 29/7/1999 |
| Landsat/5_TM | LT51840321999217ESA00 | 5/8/1999 |

| | | |
|---|---|---|
| Landsat/5_TM | LT51830321999226ESA00 | 14/8/1999 |
| Landsat/5_TM | LT51840321999265ESA00 | 22/9/1999 |
| Landsat/5_TM | LT51830321999274ESA00 | 1/10/1999 |
| Landsat/5_TM | LT51840321999281ESA00 | 8/10/1999 |
| Landsat/5_TM | LT51840321999329ESA00 | 25/11/1999 |
| Landsat/5_TM | LT51830322000005ESA00 | 5/1/2000 |
| Landsat/5_TM | LT51830322000021ESA00 | 21/1/2000 |
| Landsat/5_TM | LT51840322000028ESA00 | 28/1/2000 |
| Landsat/5_TM | LT51840322000060ESA00 | 29/2/2000 |
| Landsat/5_TM | LT51830322000133ESA00 | 12/5/2000 |
| Landsat/5_TM | LT51840322000140ESA00 | 19/5/2000 |
| Landsat/5_TM | LT51830322000149ESA00 | 28/5/2000 |
| Landsat/5_TM | LT51840322000156ESA00 | 4/6/2000 |
| Landsat/5_TM | LT51830322000165ESA00 | 13/6/2000 |
| Landsat/5_TM | LT51840322000172ESA00 | 20/6/2000 |
| Landsat/5_TM | LT51830322000181ESA00 | 29/6/2000 |
| Landsat/5_TM | LT51840322000188ESA00 | 6/7/2000 |
| Landsat/5_TM | LT51830322000197ESA00 | 15/7/2000 |
| Landsat/5_TM | LT51840322000220ESA00 | 7/8/2000 |
| Landsat/5_TM | LT51830322000229ESA00 | 16/8/2000 |
| Landsat/5_TM | LT51840322000236ESA00 | 23/8/2000 |
| Landsat/5_TM | LT51830322000245ESA00 | 1/9/2000 |
| Landsat/5_TM | LT51840322000252ESA00 | 8/9/2000 |
| Landsat/5_TM | LT51830322000261ESA00 | 17/9/2000 |
| Landsat/5_TM | LT51840322000284ESA00 | 10/10/2000 |
| Landsat/5_TM | LT51840322000316ESA00 | 11/11/2000 |
| Landsat/5_TM | LT51830322001055ESA00 | 24/2/2001 |
| Landsat/5_TM | LT51830322001087ESA00 | 28/3/2001 |
| Landsat/5_TM | LT51840322001094ESA00 | 4/4/2001 |
| Landsat/5_TM | LT51830322001119ESA00 | 29/4/2001 |
| Landsat/5_TM | LT51830322001167ESA00 | 16/6/2001 |
| Landsat/5_TM | LT51840322001174ESA00 | 23/6/2001 |
| Landsat/5_TM | LT51840322001190ESA00 | 9/7/2001 |
| Landsat/5_TM | LT51830322001199ESA00 | 18/7/2001 |
| Landsat/5_TM | LT51840322001206ESA00 | 25/7/2001 |
| Landsat/5_TM | LT51830322001215ESA00 | 3/8/2001 |
| Landsat/5_TM | LT51840322001222ESA00 | 10/8/2001 |
| Landsat/5_TM | LT51830322001231ESA00 | 19/8/2001 |
| Landsat/5_TM | LT51840322001238ESA00 | 26/8/2001 |
| Landsat/5_TM | LT51830322001247ESA00 | 4/9/2001 |
| Landsat/5_TM | LT51830322001263ESA00 | 20/9/2001 |
| Landsat/5_TM | LT51830322002010ESA00 | 10/1/2002 |
| Landsat/5_TM | LT51830322002058ESA00 | 27/2/2002 |
| Landsat/5_TM | LT51830322002074ESA00 | 15/3/2002 |
| Landsat/5_TM | LT51840322003180MTI01 | 29/6/2003 |
| Landsat/5_TM | LT51830322003189MTI01 | 8/7/2003 |
| Landsat/5_TM | LT51840322003196MTI01 | 15/7/2003 |
| Landsat/5_TM | LT51830322003205MTI01 | 24/7/2003 |

| | | |
|---|---|---|
| Landsat/5_TM | LT51840322003228MTI01 | 16/8/2003 |
| Landsat/5_TM | LT51830322003237MTI01 | 25/8/2003 |
| Landsat/5_TM | LT51840322003244MTI01 | 1/9/2003 |
| Landsat/5_TM | LT51840322003260MTI01 | 17/9/2003 |
| Landsat/5_TM | LT51840322003276MTI01 | 3/10/2003 |
| Landsat/5_TM | LT51830322003285MTI01 | 12/10/2003 |
| Landsat/5_TM | LT51840322005009ESA00 | 9/1/2005 |
| Landsat/5_TM | LT51840322005041ESA00 | 10/2/2005 |
| Landsat/5_TM | LT51840322005105ESA00 | 15/4/2005 |
| Landsat/5_TM | LT51840322005121ESA00 | 1/5/2005 |
| Landsat/5_TM | LT51840322005137ESA00 | 17/5/2005 |
| Landsat/5_TM | LT51840322005169ESA00 | 18/6/2005 |
| Landsat/5_TM | LT51830322005194ESA00 | 13/7/2005 |
| Landsat/5_TM | LT51840322005201ESA00 | 20/7/2005 |
| Landsat/5_TM | LT51830322005210ESA00 | 29/7/2005 |
| Landsat/5_TM | LT51830322005226ESA00 | 14/8/2005 |
| Landsat/5_TM | LT51840322005233ESA00 | 21/8/2005 |
| Landsat/5_TM | LT51840322005265ESA00 | 22/9/2005 |
| Landsat/5_TM | LT51840322005281ESA00 | 8/10/2005 |
| Landsat/5_TM | LT51830322005290ESA00 | 17/10/2005 |
| Landsat/5_TM | LT51840322005297ESA00_ | 24/10/2005 |
| Landsat/5_TM | LT51840322006044ESA00 | 13/2/2006 |
| Landsat/5_TM | LT51840322006060ESA00 | 1/3/2006 |
| Landsat/5_TM | LT51840322006092ESA00 | 2/4/2006 |
| Landsat/5_TM | LT51840322006124ESA00 | 4/5/2006 |
| Landsat/5_TM | LT51830322006149MOR00 | 29/5/2006 |
| Landsat/5_TM | LT51840322006204MOR00 | 23/7/2006 |
| Landsat/5_TM | LT51830322006213MOR00 | 1/8/2006 |
| Landsat/5_TM | LT51840322006220MOR00 | 8/8/2006 |
| Landsat/5_TM | LT51840322006220ESA00 | 8/8/2006 |
| Landsat/5_TM | LT51830322006245MOR00 | 2/9/2006 |
| Landsat/5_TM | LT51840322006252MOR00 | 9/9/2006 |
| Landsat/5_TM | LT51840322006268ESA00 | 25/9/2006 |
| Landsat/5_TM | LT51830322006293MOR00 | 20/10/2006 |
| Landsat/5_TM | LT51830322006341ESA00 | 7/12/2006 |
| Landsat/5_TM | LT51830322006357ESA00 | 23/12/2006 |
| Landsat/5_TM | LT51840322007031ESA00 | 31/1/2007 |
| Landsat/5_TM | LT51830322007104ESA00 | 14/4/2007 |
| Landsat/5_TM | LT51840322007111ESA00 | 21/4/2007 |
| Landsat/5_TM | LT51830322007120MOR00 | 30/4/2007 |
| Landsat/5_TM | LT51840322007127MOR00 | 7/5/2007 |
| Landsat/5_TM | LT51830322007136MOR00 | 16/5/2007 |
| Landsat/5_TM | LT51840322007143MOR00 | 23/5/2007 |
| Landsat/5_TM | LT51830322007152MOR00 | 1/6/2007 |
| Landsat/5_TM | LT51830322007168ESA00 | 17/6/2007 |
| Landsat/5_TM | LT51840322007175MOR00 | 24/6/2007 |
| Landsat/5_TM | LT51830322007184MOR00 | 3/7/2007 |
| Landsat/5_TM | LT51840322007191MOR00 | 10/7/2007 |

| | | |
|---|---|---|
| Landsat/5_TM | LT51840322007207MOR00 | 26/7/2007 |
| Landsat/5_TM | LT51830322007200MOR00 | 4/8/2007 |
| Landsat/5_TM | LT51840322007223ESA00 | 11/8/2007 |
| Landsat/5_TM | LT51830322007232MOR00 | 20/8/2007 |
| Landsat/5_TM | LT51830322007216MOR00 | 20/8/2007 |
| Landsat/5_TM | LT51840322007239ESA00 | 27/8/2007 |
| Landsat/5_TM | LT51840322007271MOR00 | 28/9/2007 |
| Landsat/5_TM | LT51830322008075ESA00 | 15/3/2008 |
| Landsat/5_TM | LT51840322008082ESA00 | 22/3/2008 |
| Landsat/5_TM | LT51830322008091ESA00 | 31/3/2008 |
| Landsat/5_TM | LT51840322008098ESA00 | 7/4/2008 |
| Landsat/5_TM | LT51830322008107ESA00 | 16/4/2008 |
| Landsat/5_TM | LT51840322008114ESA00 | 23/4/2008 |
| Landsat/5_TM | LT51830322008123ESA00 | 2/5/2008 |
| Landsat/5_TM | LT51840322008130ESA00 | 9/5/2008 |
| Landsat/5_TM | LT51830322008139ESA00 | 18/5/2008 |
| Landsat/5_TM | LT51840322008146ESA00 | 25/5/2008 |
| Landsat/5_TM | LT51840322008162ESA00 | 10/6/2008 |
| Landsat/5_TM | LT51830322008171ESA00 | 19/6/2008 |
| Landsat/5_TM | LT51840322008178ESA00 | 26/6/2008 |
| Landsat/5_TM | LT51830322008187ESA00 | 5/7/2008 |
| Landsat/5_TM | LT51840322008194ESA00 | 12/7/2008 |
| Landsat/5_TM | LT51830322008235ESA00 | 22/8/2008 |
| Landsat/5_TM | LT51840322008242ESA00 | 29/8/2008 |
| Landsat/5_TM | LT51830322008251ESA00 | 7/9/2008 |
| Landsat/5_TM | LT51840322008274ESA00 | 30/9/2008 |
| Landsat/5_TM | LT51830322008283ESA00 | 9/10/2008 |
| Landsat/5_TM | LT51840322008290ESA00 | 16/10/2008 |
| Landsat/5_TM | LT51840322009036ESA00 | 5/2/2009 |
| Landsat/5_TM | LT51840322009068ESA00 | 9/3/2009 |
| Landsat/5_TM | LT51840322009100ESA00 | 10/4/2009 |
| Landsat/5_TM | LT51840322009132ESA00 | 12/5/2009 |
| Landsat/5_TM | LT51840322009148ESA00 | 28/5/2009 |
| Landsat/5_TM | LT51840322009164MOR00 | 13/6/2009 |
| Landsat/5_TM | LT51830322009189MOR00 | 8/7/2009 |
| Landsat/5_TM | LT51840322009196MOR00 | 15/7/2009 |
| Landsat/5_TM | LT51840322009212MOR00 | 31/7/2009 |
| Landsat/5_TM | LT51840322009228ESA00 | 16/8/2009 |
| Landsat/5_TM | LT51840322009324ESA00 | 20/11/2009 |
| Landsat/5_TM | LT51830322010112ESA00 | 22/4/2010 |
| Landsat/5_TM | LT51840322010119ESA00 | 29/4/2010 |
| Landsat/5_TM | LT51830322010160MOR00 | 9/6/2010 |
| Landsat/5_TM | LT51840322010183MOR00 | 2/7/2010 |
| Landsat/5_TM | LT51830322010192MOR00 | 11/7/2010 |
| Landsat/5_TM | LT51840322010199ESA00 | 18/7/2010 |
| Landsat/5_TM | LT51830322010224MOR00 | 12/8/2010 |
| Landsat/5_TM | LT51840322010231MOR00 | 19/8/2010 |
| Landsat/5_TM | LT51830322010256ESA00 | 13/9/2010 |

| | | |
|---|---|---|
| Landsat/5_TM | LT51840322010311ESA00 | 7/11/2010 |
| Landsat/5_TM | LT51840322010359ESA00 | 25/12/2010 |
| Landsat/5_TM | LT51840322011026ESA00 | 26/1/2011 |
| Landsat/5_TM | LT51840322011042ESA00 | 11/2/2011 |
| Landsat/5_TM | LT51830322011099ESA00 | 9/4/2011 |
| Landsat/5_TM | LT51840322011122ESA00 | 2/5/2011 |
| Landsat/5_TM | LT51840322011170MOR00 | 19/6/2011 |
| Landsat/5_TM | LT51840322011218MOR00 | 6/8/2011 |
| Landsat/5_TM | LT51830322011227MOR00 | 15/8/2011 |
| Landsat/5_TM | LT51840322011234ESA00 | 22/8/2011 |
| Landsat/5_TM | LT51830322011259MOR00 | 16/9/2011 |
| Landsat/5_TM | LT51840322011266MOR00 | 23/9/2011 |
| Landsat/5_TM | LT51830322011275MOR00 | 2/10/2011 |
| Landsat/5_TM | LT51830322011307ESA00 | 3/11/2011 |
| Landsat-7/ETM+ SLC OFF | LE71830322003245ASN01 | 2/9/2003 |
| Landsat-7/ETM+ SLC OFF | LE71830322003277ASN01 | 4/10/2003 |
| Landsat-7/ETM+ SLC OFF | LE71830322004120ASN01 | 29/4/2004 |
| Landsat-7/ETM+ SLC OFF | LE71830322004152ASN01 | 31/5/2004 |
| Landsat-7/ETM+ SLC OFF | LE71830322004168ASN02 | 16/6/2004 |
| Landsat-7/ETM+ SLC OFF | LE71830322004184ASN01 | 2/7/2004 |
| Landsat-7/ETM+ SLC OFF | LE71830322004200ASN01 | 18/7/2004 |
| Landsat-7/ETM+ SLC OFF | LE71830322004216ASN03 | 3/8/2004 |
| Landsat-7/ETM+ SLC OFF | LE71830322004232ASN01 | 19/8/2004 |
| Landsat-7/ETM+ SLC OFF | LE71830322004264ASN01 | 20/9/2004 |
| Landsat-7/ETM+ SLC OFF | LE71830322004312ASN00 | 7/11/2004 |
| Landsat-7/ETM+ SLC OFF | LE71830322004328ASN00 | 23/11/2004 |
| Landsat-7/ETM+ SLC OFF | LE71830322004360ASN00 | 25/12/2004 |
| Landsat-7/ETM+ SLC OFF | LE71830322005010ASN00 | 10/1/2005 |
| Landsat-7/ETM+ SLC OFF | LE71830322005058ASN00 | 27/2/2005 |
| Landsat-7/ETM+ SLC OFF | LE71830322005122ASN00 | 2/5/2005 |
| Landsat-7/ETM+ SLC OFF | LE71830322005250ASN00 | 7/9/2005 |
| Landsat-7/ETM+ SLC OFF | LE71830322005314ASN00 | 10/11/2005 |
| Landsat-7/ETM+ SLC OFF | LE71830322005330ASN00 | 26/11/2005 |
| Landsat-7/ETM+ SLC OFF | LE71830322006109ASN00 | 19/4/2006 |
| Landsat-7/ETM+ SLC OFF | LE71830322006125ASN00 | 5/5/2006 |
| Landsat-7/ETM+ SLC OFF | LE71830322006141ASN00 | 21/5/2006 |
| Landsat-7/ETM+ SLC OFF | LE71830322006173ASN00 | 22/6/2006 |
| Landsat-7/ETM+ SLC OFF | LE71830322006205ASN00 | 24/7/2006 |
| Landsat-7/ETM+ SLC OFF | LE71830322006221ASN00 | 9/8/2006 |
| Landsat-7/ETM+ SLC OFF | LE71830322006237ASN00 | 25/8/2006 |
| Landsat-7/ETM+ SLC OFF | LE71830322007176ASN00 | 25/6/2007 |
| Landsat-7/ETM+ SLC OFF | LE71830322007208ASN00 | 27/7/2007 |
| Landsat-7/ETM+ SLC OFF | LE71830322007224ASN00 | 12/8/2007 |
| Landsat-7/ETM+ SLC OFF | LE71830322007240EDC00 | 28/8/2007 |
| Landsat-7/ETM+ SLC OFF | LE71830322007256ASN00 | 13/9/2007 |
| Landsat-7/ETM+ SLC OFF | LE71830322007320ASN00 | 16/11/2007 |
| Landsat-7/ETM+ SLC OFF | LE71830322007336ASN00 | 2/12/2007 |
| Landsat-7/ETM+ SLC OFF | LE71830322008051ASN00 | 20/2/2008 |

| | | |
|---|---|---|
| Landsat-7/ETM+ SLC OFF | LE71830322008099ASN00 | 8/4/2008 |
| Landsat-7/ETM+ SLC OFF | LE71830322008115ASN01 | 24/4/2008 |
| Landsat-7/ETM+ SLC OFF | LE71830322008147ASN00 | 26/5/2008 |
| Landsat-7/ETM+ SLC OFF | LE71830322008163ASN00 | 11/6/2008 |
| Landsat-7/ETM+ SLC OFF | LE71830322008195ASN00 | 13/7/2008 |
| Landsat-7/ETM+ SLC OFF | LE71830322008227ASN00 | 14/8/2008 |
| Landsat-7/ETM+ SLC OFF | LE71830322008243ASN00 | 30/8/2008 |
| Landsat-7/ETM+ SLC OFF | LE71830322009037ASN00 | 6/2/2009 |
| Landsat-7/ETM+ SLC OFF | LE71830322009069ASN00 | 10/3/2009 |
| Landsat-7/ETM+ SLC OFF | LE71830322009117ASN00 | 27/4/2009 |
| Landsat-7/ETM+ SLC OFF | LE71830322009133ASN00 | 13/5/2009 |
| Landsat-7/ETM+ SLC OFF | LE71830322009165ASN01 | 14/6/2009 |
| Landsat-7/ETM+ SLC OFF | LE71830322009293ASN00 | 20/10/2009 |
| Landsat-7/ETM+ SLC OFF | LE71830322009309ASN00 | 5/11/2009 |
| Landsat-7/ETM+ SLC OFF | LE71830322009325ASN01 | 21/11/2009 |
| Landsat-7/ETM+ SLC OFF | LE71830322010120ASN00 | 30/4/2010 |
| Landsat-7/ETM+ SLC OFF | LE71830322010168ASN00 | 17/6/2010 |
| Landsat-7/ETM+ SLC OFF | LE71830322010200ASN00 | 19/7/2010 |
| Landsat-7/ETM+ SLC OFF | LE71830322010216ASN00 | 4/8/2010 |
| Landsat-7/ETM+ SLC OFF | LE71830322010296ASN00 | 23/10/2010 |
| Landsat-7/ETM+ SLC OFF | LE71830322011027ASN00 | 27/1/2011 |
| Landsat-7/ETM+ SLC OFF | LE71830322011043ASN00 | 12/2/2011 |
| Landsat-7/ETM+ SLC OFF | LE71830322011171ASN00 | 20/6/2011 |
| Landsat-7/ETM+ SLC OFF | LE71830322011203ASN00 | 22/7/2011 |
| Landsat-7/ETM+ SLC OFF | LE71830322011219ASN00 | 7/8/2011 |
| Landsat-7/ETM+ SLC OFF | LE71830322011235ASN00 | 23/8/2011 |
| Landsat-7/ETM+ SLC OFF | LE71830322011331ASN00 | 27/11/2011 |
| Landsat-7/ETM+ SLC OFF | LE71830322012110ASN00 | 19/4/2012 |
| Landsat-7/ETM+ SLC OFF | LE71830322012126ASN00 | 5/5/2012 |
| Landsat-7/ETM+ SLC OFF | LE71830322012158ASN00 | 6/6/2012 |
| Landsat-7/ETM+ SLC OFF | LE71830322012174ASN00 | 22/6/2012 |
| Landsat-7/ETM+ SLC OFF | LE71830322012206ASN00 | 24/7/2012 |
| Landsat-7/ETM+ SLC OFF | LE71830322012270ASN00 | 26/9/2012 |
| Landsat-7/ETM+ SLC OFF | LE71830322013032ASN00 | 1/2/2013 |
| Landsat-7/ETM+ SLC OFF | LE71830322013112ASN00 | 22/4/2013 |
| Landsat-7/ETM+ SLC OFF | LE71830322013176ASN00 | 25/6/2013 |
| Landsat-7/ETM+ SLC OFF | LE71830322013192ASN00 | 11/7/2013 |
| Landsat-7/ETM+ SLC OFF | LE71830322013304ASN00 | 31/10/2013 |
| Landsat-7/ETM+ SLC OFF | LE71830322014099ASN00 | 9/4/2014 |
| Landsat-7/ETM+ SLC OFF | LE71830322014131ASN00 | 11/5/2014 |
| Landsat-7/ETM+ SLC OFF | LE71830322014211ASN00 | 30/7/2014 |
| Landsat-7/ETM+ SLC OFF | LE71830322014227ASN00 | 15/8/2014 |
| Landsat-7/ETM+ SLC OFF | LE71830322014243ASN00 | 31/8/2014 |
| Landsat-7/ETM+ SLC OFF | LE71830322014275SG100 | 2/10/2014 |
| Landsat-7/ETM+ SLC OFF | LE71830322015038ASN00 | 7/2/2015 |
| Landsat-7/ETM+ SLC OFF | LE71830322015102NSG00 | 12/4/2015 |
| Landsat-7/ETM+ SLC OFF | LE71830322015134NSG00 | 14/5/2015 |
| Landsat-7/ETM+ SLC OFF | LE71830322015150NSG00 | 30/5/2015 |

| | | |
|---|---|---|
| Landsat-7/ETM+ SLC OFF | LE71830322015166NSG00 | 17/7/2015 |
| Landsat-7/ETM+ SLC OFF | LE71830322015214ASN00 | 2/8/2015 |
| Landsat-7/ETM+ SLC OFF | LE71830322015230NSG00 | 18/8/2015 |
| Landsat-7/ETM+ SLC OFF | LE71830322015246NSG00 | 3/9/2015 |
| Landsat-7/ETM+ SLC OFF | LE71840322001278SGS00 | 5/10/2001 |
| Landsat-7/ETM+ SLC OFF | LE71840322003268ASN01 | 25/9/2003 |
| Landsat-7/ETM+ SLC OFF | LE71840322003284ASN01 | 11/10/2003 |
| Landsat-7/ETM+ SLC OFF | LE71840322004079ASN02 | 19/3/2004 |
| Landsat-7/ETM+ SLC OFF | LE71840322004175ASN01 | 23/6/2004 |
| Landsat-7/ETM+ SLC OFF | LE71840322004191ASN01 | 9/7/2004 |
| Landsat-7/ETM+ SLC OFF | LE71840322004239ASN01 | 26/8/2004 |
| Landsat-7/ETM+ SLC OFF | LE71840322005049ASN00 | 18/2/2005 |
| Landsat-7/ETM+ SLC OFF | LE71840322005065ASN00 | 6/3/2005 |
| Landsat-7/ETM+ SLC OFF | LE71840322005097ASN00 | 7/4/2005 |
| Landsat-7/ETM+ SLC OFF | LE71840322005113ASN00 | 23/4/2005 |
| Landsat-7/ETM+ SLC OFF | LE71840322005129ASN00 | 9/5/2005 |
| Landsat-7/ETM+ SLC OFF | LE71840322005177ASN00 | 26/6/2005 |
| Landsat-7/ETM+ SLC OFF | LE71840322005193ASN00 | 12/7/2005 |
| Landsat-7/ETM+ SLC OFF | LE71840322005209ASN00 | 28/7/2005 |
| Landsat-7/ETM+ SLC OFF | LE71840322005225ASN00 | 13/8/2005 |
| Landsat-7/ETM+ SLC OFF | LE71840322006148ASN00 | 28/5/2006 |
| Landsat-7/ETM+ SLC OFF | LE71840322006180ASN00 | 29/6/2006 |
| Landsat-7/ETM+ SLC OFF | LE71840322006196ASN00 | 15/7/2006 |
| Landsat-7/ETM+ SLC OFF | LE71840322006228ASN00 | 16/8/2006 |
| Landsat-7/ETM+ SLC OFF | LE71840322006244ASN00 | 1/9/2006 |
| Landsat-7/ETM+ SLC OFF | LE71840322006340ASN00 | 6/12/2006 |
| Landsat-7/ETM+ SLC OFF | LE71840322007007ASN00 | 7/1/2007 |
| Landsat-7/ETM+ SLC OFF | LE71840322007103ASN00 | 13/4/2007 |
| Landsat-7/ETM+ SLC OFF | LE71840322007119ASN00 | 29/4/2007 |
| Landsat-7/ETM+ SLC OFF | LE71840322007135ASN00 | 15/5/2007 |
| Landsat-7/ETM+ SLC OFF | LE71840322007183ASN00 | 2/7/2007 |
| Landsat-7/ETM+ SLC OFF | LE71840322007215ASN00 | 3/8/2007 |
| Landsat-7/ETM+ SLC OFF | LE71840322007231ASN00 | 19/8/2007 |
| Landsat-7/ETM+ SLC OFF | LE71840322008026ASN00 | 26/1/2008 |
| Landsat-7/ETM+ SLC OFF | LE71840322008074ASN00 | 14/3/2008 |
| Landsat-7/ETM+ SLC OFF | LE71840322008106ASN00 | 15/4/2008 |
| Landsat-7/ETM+ SLC OFF | LE71840322008122ASN00 | 1/5/2008 |
| Landsat-7/ETM+ SLC OFF | LE71840322008138ASN00 | 17/5/2008 |
| Landsat-7/ETM+ SLC OFF | LE71840322008154ASN00 | 2/6/2008 |
| Landsat-7/ETM+ SLC OFF | LE71840322008186ASN00 | 4/7/2008 |
| Landsat-7/ETM+ SLC OFF | LE71840322008202ASN00 | 20/7/2008 |
| Landsat-7/ETM+ SLC OFF | LE71840322008218ASN00 | 5/8/2008 |
| Landsat-7/ETM+ SLC OFF | LE71840322008234ASN00 | 21/8/2008 |
| Landsat-7/ETM+ SLC OFF | LE71840322008250ASN00 | 6/9/2008 |
| Landsat-7/ETM+ SLC OFF | LE71840322009060ASN00 | 1/3/2009 |
| Landsat-7/ETM+ SLC OFF | LE71840322009156ASN00 | 5/6/2009 |
| Landsat-7/ETM+ SLC OFF | LE71840322009172ASN00 | 21/6/2009 |
| Landsat-7/ETM+ SLC OFF | LE71840322009188ASN00 | 7/7/2009 |

| | | |
|---|---|---|
| Landsat-7/ETM+ SLC OFF | LE71840322009204ASN00 | 23/7/2009 |
| Landsat-7/ETM+ SLC OFF | LE71840322010079ASN00 | 20/3/2010 |
| Landsat-7/ETM+ SLC OFF | LE71840322010127ASN00 | 7/5/2010 |
| Landsat-7/ETM+ SLC OFF | LE71840322010159ASN00 | 8/6/2010 |
| Landsat-7/ETM+ SLC OFF | LE71840322010239ASN00 | 27/8/2010 |
| Landsat-7/ETM+ SLC OFF | LE71840322010271EDC00 | 28/9/2010 |
| Landsat-7/ETM+ SLC OFF | LE71840322010303ASN00 | 30/10/2010 |
| Landsat-7/ETM+ SLC OFF | LE71840322010319ASN00 | 15/11/2010 |
| Landsat-7/ETM+ SLC OFF | LE71840322010351ASN00 | 17/12/2010 |
| Landsat-7/ETM+ SLC OFF | LE71840322011082ASN00 | 23/3/2011 |
| Landsat-7/ETM+ SLC OFF | LE71840322011114ASN00 | 24/4/2011 |
| Landsat-7/ETM+ SLC OFF | LE71840322011162ASN00 | 11/6/2011 |
| Landsat-7/ETM+ SLC OFF | LE71840322011178ASN00 | 27/6/2011 |
| Landsat-7/ETM+ SLC OFF | LE71840322011194ASN00 | 13/7/2011 |
| Landsat-7/ETM+ SLC OFF | LE71840322011210ASN00 | 29/7/2011 |
| Landsat-7/ETM+ SLC OFF | LE71840322011226ASN00 | 14/8/2011 |
| Landsat-7/ETM+ SLC OFF | LE71840322011242ASN00 | 30/8/2011 |
| Landsat-7/ETM+ SLC OFF | LE71840322011258ASN01 | 15/9/2011 |
| Landsat-7/ETM+ SLC OFF | LE71840322011274ASN00 | 1/10/2011 |
| Landsat-7/ETM+ SLC OFF | LE71840322011306ASN00 | 2/11/2011 |
| Landsat-7/ETM+ SLC OFF | LE71840322011322ASN00 | 18/11/2011 |
| Landsat-7/ETM+ SLC OFF | LE71840322012085ASN00 | 25/3/2012 |
| Landsat-7/ETM+ SLC OFF | LE71840322012117ASN00 | 26/4/2012 |
| Landsat-7/ETM+ SLC OFF | LE71840322012133ASN00 | 12/5/2012 |
| Landsat-7/ETM+ SLC OFF | LE71840322012165ASN00 | 13/6/2012 |
| Landsat-7/ETM+ SLC OFF | LE71840322012181ASN00 | 29/6/2012 |
| Landsat-7/ETM+ SLC OFF | LE71840322012197ASN00 | 15/7/2012 |
| Landsat-7/ETM+ SLC OFF | LE71840322012213ASN00 | 31/7/2012 |
| Landsat-7/ETM+ SLC OFF | LE71840322012229ASN00 | 16/8/2012 |
| Landsat-7/ETM+ SLC OFF | LE71840322012245ASN00 | 1/9/2012 |
| Landsat-7/ETM+ SLC OFF | LE71840322012277ASN00 | 3/10/2012 |
| Landsat-7/ETM+ SLC OFF | LE71840322012293ASN00 | 19/10/2012 |
| Landsat-7/ETM+ SLC OFF | LE71840322013119ASN00 | 29/4/2013 |
| Landsat-7/ETM+ SLC OFF | LE71840322013135ASN00 | 15/5/2013 |
| Landsat-7/ETM+ SLC OFF | LE71840322013151ASN00 | 31/5/2013 |
| Landsat-7/ETM+ SLC OFF | LE71840322013167ASN00 | 16/6/2013 |
| Landsat-7/ETM+ SLC OFF | LE71840322013231ASN00 | 19/8/2013 |
| Landsat-7/ETM+ SLC OFF | LE71840322013247ASN00 | 4/9/2013 |
| Landsat-7/ETM+ SLC OFF | LE71840322013295ASN00 | 22/10/2013 |
| Landsat-7/ETM+ SLC OFF | LE71840322013311ASN00 | 7/11/2013 |
| Landsat-7/ETM+ SLC OFF | LE71840322014074ASN00 | 15/3/2014 |
| Landsat-7/ETM+ SLC OFF | LE71840322014122ASN00 | 2/5/2014 |
| Landsat-7/ETM+ SLC OFF | LE71840322014186ASN00 | 5/7/2014 |
| Landsat-7/ETM+ SLC OFF | LE71840322014202ASN00 | 21/7/2014 |
| Landsat-7/ETM+ SLC OFF | LE71840322014234ASN00 | 22/8/2014 |
| Landsat-7/ETM+ SLC OFF | LE71840322015013SG100 | 13/1/2015 |
| Landsat-7/ETM+ SLC OFF | LE71840322015045ASN00 | 14/2/2015 |
| Landsat-7/ETM+ SLC OFF | LE71840322015125NSG00 | 5/5/2015 |

| | | |
|---|---|---|
| Landsat-7/ETM+ SLC OFF | LE71840322015141SG100 | 21/5/2015 |
| Landsat-7/ETM+ SLC OFF | LE71840322015173NSG00 | 22/6/2015 |
| Landsat-7/ETM+ SLC OFF | LE71840322015189SG100 | 8/7/2015 |
| Landsat-7/ETM+ SLC ON | LE71830321999186EDC00 | 5/7/1999 |
| Landsat-7/ETM+ SLC ON | LE71830321999218ESA00 | 6/8/1999 |
| Landsat-7/ETM+ SLC ON | LE71830321999234ESA00 | 22/8/1999 |
| Landsat-7/ETM+ SLC ON | LE71830321999250ESA00 | 7/9/1999 |
| Landsat-7/ETM+ SLC ON | LE71830321999266ESA00 | 23/9/1999 |
| Landsat-7/ETM+ SLC ON | LE71830321999282ESA00 | 9/10/1999 |
| Landsat-7/ETM+ SLC ON | LE71830322000029ESA00 | 29/1/2000 |
| Landsat-7/ETM+ SLC ON | LE71830322000061ESA00 | 1/3/2000 |
| Landsat-7/ETM+ SLC ON | LE71830322000125ESA00 | 4/5/2000 |
| Landsat-7/ETM+ SLC ON | LE71830322000141ESA00 | 20/5/2000 |
| Landsat-7/ETM+ SLC ON | LE71830322000157ESA00 | 5/6/2000 |
| Landsat-7/ETM+ SLC ON | LE71830322000173ESA00 | 21/6/2000 |
| Landsat-7/ETM+ SLC ON | LE71830322000189ESA00 | 7/7/2000 |
| Landsat-7/ETM+ SLC ON | LE71830322000205ESA00 | 23/7/2000 |
| Landsat-7/ETM+ SLC ON | LE71830322000221ESA00 | 8/8/2000 |
| Landsat-7/ETM+ SLC ON | LE71830322000237EDC00 | 24/8/2000 |
| Landsat-7/ETM+ SLC ON | LE71830322001047SGS00 | 16/2/2001 |
| Landsat-7/ETM+ SLC ON | LE71830322001095EDC00 | 5/4/2001 |
| Landsat-7/ETM+ SLC ON | LE71830322001159ESA00 | 8/6/2001 |
| Landsat-7/ETM+ SLC ON | LE71830322001175ESA00 | 24/6/2001 |
| Landsat-7/ETM+ SLC ON | LE71830322001191ESA00 | 10/7/2001 |
| Landsat-7/ETM+ SLC ON | LE71830322001207ESA00 | 26/7/2001 |
| Landsat-7/ETM+ SLC ON | LE71830322001223ESA00 | 11/8/2001 |
| Landsat-7/ETM+ SLC ON | LE71830322001255ESA00 | 12/9/2001 |
| Landsat-7/ETM+ SLC ON | LE71830322001271ESA00 | 28/9/2001 |
| Landsat-7/ETM+ SLC ON | LE71830322002034SGS01 | 3/2/2002 |
| Landsat-7/ETM+ SLC ON | LE71830322002226EDC00 | 14/8/2002 |
| Landsat-7/ETM+ SLC ON | LE71830322002306SGS00 | 2/11/2002 |
| Landsat-7/ETM+ SLC ON | LE71830322003117ESA00 | 27/4/2003 |
| Landsat-7/ETM+ SLC ON | LE71840321999193ESA00 | 12/7/1999 |
| Landsat-7/ETM+ SLC ON | LE71840321999209EDC00 | 28/7/1999 |
| Landsat-7/ETM+ SLC ON | LE71840321999225ESA00 | 13/8/1999 |
| Landsat-7/ETM+ SLC ON | LE71840321999305ESA00 | 1/11/1999 |
| Landsat-7/ETM+ SLC ON | LE71840321999337SGS00 | 3/12/1999 |
| Landsat-7/ETM+ SLC ON | LE71840322000020ESA00 | 20/1/2000 |
| Landsat-7/ETM+ SLC ON | LE71840322000036ESA00 | 5/2/2000 |
| Landsat-7/ETM+ SLC ON | LE71840322000068SGS00 | 8/3/2000 |
| Landsat-7/ETM+ SLC ON | LE71840322000084ESA00 | 24/3/2000 |
| Landsat-7/ETM+ SLC ON | LE71840322000100ESA00 | 9/4/2000 |
| Landsat-7/ETM+ SLC ON | LE71840322000148EDC00 | 27/5/2000 |
| Landsat-7/ETM+ SLC ON | LE71840322000164ESA00 | 12/6/2000 |
| Landsat-7/ETM+ SLC ON | LE71840322000180EDC00 | 28/6/2000 |
| Landsat-7/ETM+ SLC ON | LE71840322000228ESA00 | 15/8/2000 |
| Landsat-7/ETM+ SLC ON | LE71840322000244ESA00 | 31/8/2000 |
| Landsat-7/ETM+ SLC ON | LE71840322000260ESA00 | 16/9/2000 |

| | | |
|---|---|---|
| Landsat-7/ETM+ SLC ON | LE71840322001038SGS00 | 7/2/2001 |
| Landsat-7/ETM+ SLC ON | LE71840322001118ESA00 | 28/4/2001 |
| Landsat-7/ETM+ SLC ON | LE71840322001150SGS00 | 30/5/2001 |
| Landsat-7/ETM+ SLC ON | LE71840322001214SGS00 | 2/8/2001 |
| Landsat-7/ETM+ SLC ON | LE71840322001262ESA00 | 19/9/2001 |
| Landsat-7/ETM+ SLC ON | LE71840322001294ESA00 | 21/10/2001 |
| Landsat-7/ETM+ SLC ON | LE71840322001326SGS00 | 22/11/2001 |
| Landsat-7/ETM+ SLC ON | LE71840322002009SGS00 | 9/1/2002 |
| Landsat-7/ETM+ SLC ON | LE71840322002041SGS00 | 10/2/2002 |
| Landsat-7/ETM+ SLC ON | LE71840322002057ESA00 | 26/2/2002 |
| Landsat-7/ETM+ SLC ON | LE71840322002073ESA00 | 14/3/2002 |
| Landsat-7/ETM+ SLC ON | LE71840322002121ESA00 | 1/5/2002 |
| Landsat-7/ETM+ SLC ON | LE71840322002185EDC00 | 4/7/2002 |
| Landsat-7/ETM+ SLC ON | LE71840322002217SGS00 | 5/8/2002 |
| Landsat-7/ETM+ SLC ON | LE71840322002249ESA00 | 6/9/2002 |
| Landsat-7/ETM+ SLC ON | LE71840322002281ESA00 | 8/10/2002 |
| Landsat-7/ETM+ SLC ON | LE71840322002329ESA00 | 25/11/2002 |
| Landsat-7/ETM+ SLC ON | LE71840322003028SGS00 | 28/1/2003 |
| Landsat-7/ETM+ SLC ON | LE71840322003060ESA00 | 1/3/2003 |
| Landsat-7/ETM+ SLC ON | LE71840322003092ESA00 | 2/4/2003 |
| Landsat-7/ETM+ SLC ON | LE71840322003140ASN00 | 20/5/2003 |
| Landsat-7/ETM+ SLC ON | LE71840322003156ESA00 | 5/6/2003 |
| LANDSAT-8/OLI&TIRS | LC81830322013120LGN01 | 30/4/2013 |
| LANDSAT-8/OLI&TIRS | LC81840322013143LGN03 | 23/5/2013 |
| LANDSAT-8/OLI&TIRS | LC81830322013152LGN00 | 1/6/2013 |
| LANDSAT-8/OLI&TIRS | LC81840322013159LGN00 | 8/6/2013 |
| LANDSAT-8/OLI&TIRS | LC81840322013175LGN00 | 24/6/2013 |
| LANDSAT-8/OLI&TIRS | LC81830322013184LGN00 | 3/7/2013 |
| LANDSAT-8/OLI&TIRS | LC81840322013191LGN00 | 10/7/2013 |
| LANDSAT-8/OLI&TIRS | LC81830322013200LGN00 | 19/7/2013 |
| LANDSAT-8/OLI&TIRS | LC81840322013207LGN00 | 26/7/2013 |
| LANDSAT-8/OLI&TIRS | LC81830322013216LGN00 | 4/8/2013 |
| LANDSAT-8/OLI&TIRS | LC81840322013223LGN00 | 11/8/2013 |
| LANDSAT-8/OLI&TIRS | LC81830322013232LGN00 | 20/8/2013 |
| LANDSAT-8/OLI&TIRS | LC81840322013239LGN00 | 27/8/2013 |
| LANDSAT-8/OLI&TIRS | LC81830322013248LGN00 | 5/9/2013 |
| LANDSAT-8/OLI&TIRS | LC81840322013255LGN00 | 12/9/2013 |
| LANDSAT-8/OLI&TIRS | LC81830322013296LGN00 | 23/10/2013 |
| LANDSAT-8/OLI&TIRS | LC81840322013303LGN00 | 30/10/2013 |
| LANDSAT-8/OLI&TIRS | LC81830322013312LGN00 | 8/11/2013 |
| LANDSAT-8/OLI&TIRS | LC81840322014034LGN00 | 3/2/2014 |
| LANDSAT-8/OLI&TIRS | LC81840322014082LGN00 | 23/3/2014 |
| LANDSAT-8/OLI&TIRS | LC81830322014091LGN00 | 1/4/2014 |
| LANDSAT-8/OLI&TIRS | LC81840322014098LGN00 | 8/4/2014 |
| LANDSAT-8/OLI&TIRS | LC81830322014139LGN00 | 19/5/2014 |
| LANDSAT-8/OLI&TIRS | LC81840322014162LGN00 | 11/6/2014 |
| LANDSAT-8/OLI&TIRS | LC81840322014178LGN00 | 27/6/2014 |
| LANDSAT-8/OLI&TIRS | LC81830322014187LGN00 | 6/7/2014 |

| | | |
|---|---|---|
| LANDSAT-8/OLI&TIRS | LC81840322014226LGN00 | 14/8/2014 |
| LANDSAT-8/OLI&TIRS | LC81830322014235LGN00 | 23/8/2014 |
| LANDSAT-8/OLI&TIRS | LC81830322014251LGN00 | 8/9/2014 |
| LANDSAT-8/OLI&TIRS | LC81830322014267LGN00 | 24/9/2014 |
| LANDSAT-8/OLI&TIRS | LC81840322014274LGN00 | 1/10/2014 |
| LANDSAT-8/OLI&TIRS | LC81830322014283LGN00 | 10/10/2014 |
| LANDSAT-8/OLI&TIRS | LC81840322014306LGN00 | 2/11/2014 |
| LANDSAT-8/OLI&TIRS | LC81840322015005LGN00 | 5/1/2015 |
| LANDSAT-8/OLI&TIRS | LC81830322015014LGN00 | 14/1/2015 |
| LANDSAT-8/OLI&TIRS | LC81830322015046LGN00 | 15/2/2015 |
| LANDSAT-8/OLI&TIRS | LC81830322015078LGN00 | 19/3/2015 |
| LANDSAT-8/OLI&TIRS | LC81830322015094LGN00 | 4/4/2015 |
| LANDSAT-8/OLI&TIRS | LC81840322015101LGN00 | 11/4/2015 |
| LANDSAT-8/OLI&TIRS | LC81840322015117LGN00 | 27/4/2015 |
| LANDSAT-8/OLI&TIRS | LC81830322015126LGN00 | 6/5/2015 |
| LANDSAT-8/OLI&TIRS | LC81840322015133LGN00 | 13/5/2015 |
| LANDSAT-8/OLI&TIRS | LC81840322015165LGN00 | 14/6/2015 |
| LANDSAT-8/OLI&TIRS | LC81830322015174LGN00 | 23/6/2015 |
| LANDSAT-8/OLI&TIRS | LC81830322015190LGN00 | 9/7/2015 |
| LANDSAT-8/OLI&TIRS | LC81840322015197LGN00 | 16/7/2015 |
| LANDSAT-8/OLI&TIRS | LC81830322015206LGN00 | 25/7/2015 |
| LANDSAT-8/OLI&TIRS | LC81840322015213LGN00 | 1/8/2015 |
| LANDSAT-8/OLI&TIRS | LC81830322015222LGN00 | 10/8/2015 |
| LANDSAT-8/OLI&TIRS | LC81840322015229LGN00 | 17/8/2015 |
| LANDSAT-8/OLI&TIRS | LC81830322015238LGN00 | 26/8/2015 |
| LANDSAT-8/OLI&TIRS | LC81840322015245LGN00 | 2/9/2015 |
| LANDSAT-8/OLI&TIRS | LC81830322015254LGN00 | 11/9/2015 |
| LANDSAT-8/OLI&TIRS | LC81840322015261LGN00 | 18/9/2015 |
| LANDSAT-8/OLI&TIRS | LC81840322015277LGN00 | 4/10/2015 |
| LANDSAT-8/OLI&TIRS | LC81830322015286LGN00 | 13/10/2015 |
| LANDSAT-8/OLI&TIRS | LC81840322015309LGN00 | 5/11/2015 |
| LANDSAT-8/OLI&TIRS | LC81830322015318LGN00 | 14/11/2015 |
| LANDSAT-8/OLI&TIRS | LC81830322015334LGN00 | 30/11/2015 |
| LANDSAT-8/OLI&TIRS | LC81840322015357LGN00 | 23/12/2015 |
| LANDSAT-8/OLI&TIRS | LC81830322016001LGN00 | 1/1/2016 |
| LANDSAT-8/OLI&TIRS | LC81840322016008LGN00 | 8/1/2016 |
| LANDSAT-8/OLI&TIRS | LC81840322016024LGN00 | 24/1/2016 |
| LANDSAT-8/OLI&TIRS | LC81830322016033LGN00 | 2/2/2016 |
| LANDSAT-8/OLI&TIRS | LC81840322016040LGN00 | 9/2/2016 |
| LANDSAT-8/OLI&TIRS | LC81840322016056LGN00 | 25/2/2016 |
| LANDSAT-8/OLI&TIRS | LC81830322016065LGN00 | 5/3/2016 |
| LANDSAT-8/OLI&TIRS | LC81830322016081LGN00 | 21/3/2016 |
| LANDSAT-8/OLI&TIRS | LC81840322016088LGN00 | 28/3/2016 |